The role of platelet glycoprotein V in thrombosis and hemostasis: *in vitro* and *in vivo* studies in mice

• • •

Die Rolle des Thrombozytenrezeptors Glykoprotein V in Thrombose und Hämostase: *in vitro* und *in vivo* Studien in Mäusen

Doctoral thesis for a doctoral degree
at the Graduate School of Life Sciences,
Julius-Maximilians-Universität Würzburg,
Section Biomedicine

submitted by

Sarah Margaretha Beck

from Würzburg

Würzburg, 2018

Submitted on:

Members of the Promotionskomitee:

Chairperson:	**Prof. Dr. Manfred Gessler**
Primary Supervisor:	**Prof. Dr. Bernhard Nieswandt**
Supervisor (Second):	**Prof. Dr. Guido Stoll**
Supervisor (Third):	**Prof. Dr. Johan W. M. Heemskerk**
Date of Public Defense:	_____
Date of receipt of Certificates:	_____

Table of Contents

Summary

Cardio- and cerebrovascular diseases (CVDs), such as myocardial infarction and ischemic stroke, are the leading cause of death worldwide, caused by overshooting platelet activation and subsequent thrombus formation. However, at sites of vascular injury this tightly-regulated, multistep process is critical to limit blood loss and to prevent bleeding. Anti-platelet agents, such as aspirin or clopidogrel, have been proven to be beneficial in prevention of CVDs, but are associated with an elevated bleeding risk and therefore are often contraindicative.

In recent years, the (hem)ITAM-bearing receptors GPVI and CLEC-2 have been identified as critical regulators of platelet activation and thrombus formation, rendering them promising targets for novel anti-platelet drugs. Yet, they are also involved in a plethora of (patho)physiological processes. Consequently, interference with the (hem)ITAM signaling cascade may lead to severe side-effects. In this context, GPV has previously been identified as a mediator of thrombotic and hemostatic function, while its mode of action remains elusive. Therefore, this thesis focused on the function of GPV in thrombotic and hemostatic processes.

Extensive characterization of GPV-deficient mice as well as generation and analysis of anti-GPV antibodies and mice with a mutation rendering GPV uncleavable by thrombin (*Gp5*$^{Kin/Kin}$) revealed an unexpected role of GPV as a central modulator of platelet activation and thrombus formation. *Gp5*$^{-/-}$ as well as *Gp5*$^{Kin/Kin}$ mice restored the thrombotic and hemostatic defect in the absence of both (hem)ITAM receptors. The in-house generated monoclonal anti-GPV antibodies 89F12 and 5G2 were found to reproduce the knockout phenotype and extended the thrombus-modulatory role of GPV beyond (hem)ITAM receptors, pointing to a critical role of thrombin-cleaved soluble GPV (sGPV). Surprisingly, recombinant sGPV had a strong antithrombotic effect in *in vivo* thrombosis models as well as in *in vitro* flow adhesion assays using human or murine blood, without affecting hemostasis. These data establish GPV as a key player in platelet physiology. Although data gained from studies using genetically modified mice cannot always directly be transferred to humans, the findings presented in this thesis may serve as basis for the generation of novel treatment options for bleeding complications (anti-GPV antibodies) and thrombotic diseases (sGPV) with a good safety profile. The newly generated humanized GPV mouse provides a valuable tool to study human GPV *in vivo*.

A second part of this thesis focused on the analysis of protein kinase C (PKC) ι/λ. PKC family of serine/threonine kinases is involved in several physiological processes regulating platelet activation. However, little is known about atypical PKC isoforms and particularly PKCι/λ has never been studied before in platelets. Therefore, platelet- and megakaryocyte-specific PKCι/λ knockout mice were used to assess its role in platelet function *in vitro* and *in vivo*. Surprisingly, PKCι/λ was found to be dispensable for platelet function in thrombosis and hemostasis.

Zusammenfassung

Kardio- und zerebrovaskuläre Krankheiten, wie Myokardinfarkt und ischämischer Schlaganfall, sind die häufigste Todesursache weltweit und werden durch überschießende Thrombozyten-Aktivierung und anschließende Thrombusbildung verursacht. Andererseits ist Thrombusbildung nach Gefäßverletzungen ein eng regulierter, mehrstufiger Prozess, der wichtig ist, um Blutverlust zu begrenzen und Blutungen zu verhindern.

Thrombozytenaggregationshemmer, wie Aspirin oder Clopidogrel, haben sich in der Prävention von kardiovaskulären Krankheiten als nützlich erwiesen, erhöhen aber gleichzeitig das Blutungsrisiko und sind deshalb oft kontraindikativ.

In den letzten Jahren wurden die (hem)ITAM-gekoppelten Rezeptoren GPVI und CLEC-2 als wichtige Regulatoren der Thrombozytenaktivierung und Thrombusbildung identifiziert, was sie zu vielversprechenden Angriffspunkten in der Entwicklung neuartiger Thrombozyten-aggregationshemmer macht. Beide Rezeptoren sind jedoch an einer Vielzahl von weiteren (patho)physiologischen Prozessen beteiligt, was vermuten lässt, dass eine Interferenz mit der (hem)ITAM Signalkaskade unter Umständen starke Nebenwirkungen hervorrufen kann. Im Zusammenhang mit Untersuchungen zu (hem)ITAM Rezeptoren wurde GPV als wichtiger Mediator thrombotischer und hämostatischer Prozesse identifiziert. Die Wirkungsweise von GPV blieb bislang jedoch unklar. Studien zur physiologischen Rolle von GPV in Thrombose und Hämostase standen daher im Fokus dieser Thesis.

Die intensive Charakterisierung von GPV-defizienten Mäusen sowie die Generierung und Analyse von anti-GPV Antikörpern und von Mäusen mit einer Mutation, aufgrund derer GPV nicht mehr von Thrombin geschnitten werden kann (*Gp5*$^{Kin/Kin}$), deckten eine unerwartete Rolle von GPV als Regulator der Thrombozytenaktivierung und Thrombusbildung auf. *Gp5*$^{-/-}$ und *Gp5*$^{Kin/Kin}$ Mäuse konnten den Verlust der (hem)ITAM Rezeptoren GPVI und CLEC-2 in Thrombose und Hämostase kompensieren. Die eigens generierten monoklonalen anti-GPV Antikörper 89F12 und 5G2 reproduzierten den GPV-knockout Phänotyp und erweiterten die Thrombus-modulierende Rolle von GPV über (hem)ITAM Rezeptoren hinaus. Zusammengenommen weisen die Ergebnisse auf eine wichtige Rolle des Thrombin-geschnittenen, löslichen GPV (sGPV) hin. Überraschenderweise hat rekombinantes sGPV einen starken antithrombotischen Effekt in Thrombosemodellen *in vivo* und *in vitro* unter Flussbedingungen in humanem und murinem Blut, ohne die hämostatische Funktion zu beeinflussen. Diese Daten etablieren GPV als wichtigen Akteur in der Thrombozyten-Physiologie. Obwohl Daten aus Studien mit genetisch veränderten Mäusen nicht direkt auf den Menschen übertragbar sind, können die in dieser Arbeit präsentierten Ergebnisse als Grundlage für die Entwicklung neuer Behandlungsmöglichkeiten mit gutem Sicherheitsprofil

bei Blutungskomplikationen (anti-GPV Antikörper) und bei thrombotischen Erkrankungen (sGPV) dienen. Eine neu generierte humanisierte GPV Maus bietet zudem ein wertvolles Werkzeug, um humanes GPV *in vivo* zu untersuchen.

Der zweite Teil der Thesis konzentrierte sich auf die Proteinkinase (PKC) ι/λ. Die Familie der PKC aus den Serin/Threonin Kinasen ist an einer Reihe physiologischer Prozesse beteiligt, die Thrombozytenaktivierung regulieren. Zur Rolle atypischer PKC Isoformen in thrombozytären Prozessen ist jedoch wenig bekannt und insbesondere zur Rolle von PKCι/λ in Thrombozyten lagen bisher keine Untersuchungen vor. Diese wurde daher in Thrombozyten- und Megakaryozyten-spezifischen PKCι/λ-knockout Mäusen *in vitro* und *in vivo* untersucht. Überraschenderweise zeigte sich, dass die atypische PKC Isoform PKCι/λ im Gegensatz zu vielen anderen Isoformen für die Thrombozytenfunktion bei Thrombose und Hämostase entbehrlich ist.

1 Introduction

Platelet activation and subsequent thrombus formation at sites of vascular injury is critical to prevent bleeding. However, under pathophysiological conditions it may as well cause life-threatening diseases, such as *myocardial infarction* (MI) and ischemic stroke [1]. *Cardiovascular diseases* (CVD) are the leading cause of death worldwide with more than 17 million people dying each year, accounting for more than 30% of all global deaths [2, 3]. In Germany, more than 200.000 first-ever and 70.000 recurrent strokes occur per year with a higher risk for men than for women [4], leading to serious disability and persistent comorbidity [5]. Smoking, unhealthy diet, physical inactivity and harmful use of alcohol, which may lead to elevated blood pressure and glucose levels, overweight and obesity risk, are amongst the risk factors for developing a CVD. Consequently, anti-platelet treatment is a common strategy to prevent coronary syndromes and secondary stroke [6]. Restoration of blood flow after MI or ischemic stroke is critical, e.g. by rt-PA (*recombinant tissue plasminogen activator*) treatment or mechanical thrombectomy [6], but despite successful recanalization, most patients still develop large infarcts (ischemia/reperfusion injury) [7-9]. Despite extensive research efforts in recent years that identified platelet adhesion and degranulation rather than platelet aggregate formation as important mediators of infarct progression, the pathomechanisms underlying this pathology are still incompletely understood, thus limiting therapeutic options in clinics.

1.1 Platelets

Blood platelets are anucleate discoid-shaped cells with a diameter of 3-4 µm in humans and 1-2 µm in mice [10]. They are the smallest and second most abundant cell type in the blood. Platelets are constantly produced by their bone-marrow resident precursors, the *megakaryocytes* (MKs), to maintain a normal range of circulating platelets of 150-400 x 10^3/µl in humans and ~1000 x 10^3/µl in mice [11]. The average life span is 10 days in humans and 5 days in mice [12]. Platelets are constantly replenished and thus provide an exemplary system to study hematopoiesis. Resident macrophages in the reticuloendothelial system of the spleen and liver clear aged, pre-activated or dysfunctional platelets from the circulation [13].

The mechanism of platelet production from MKs is not fully understood. *Thrombopoietin* (TPO) is the primary regulator of MK differentiation and platelet production [14]. According to a current concept, MKs form protrusions, so called proplatelets, which consist of platelet-sized swellings, and release them into the bone marrow sinusoids, where they are further fragmented into platelets likely through the shear force in the blood stream [15]. This model of thrombopoiesis is now further supported by recent findings from studies using intravital two-photon microscopy

[16, 17]. Since platelets lack a nucleus, *de novo* protein synthesis is limited to the MK-derived mRNA content and translational machinery [18].

Most platelets never undergo adhesion before they are removed from the circulation. The pivotal primary hemostatic function of platelets is only retrieved when they come into contact with components of the exposed *extracellular matrix* (ECM) upon vascular injury, which induces their deceleration, activation, adhesion and aggregation resulting in formation of a stable hemostatic plug. This thrombus seals the vessel lesion, minimizes blood loss and prevents infections. However, under pathological conditions (e.g. rupture of an atherosclerotic plaque), uncontrolled platelet aggregation may lead to formation of an occlusive thrombus resulting in vessel occlusion and infarction of vital organs [19]. Therefore, platelet activation is tightly regulated by a complex interplay between activatory and inhibitory mechanisms as well as release of soluble mediators and inactivation of receptors to ensure controlled spatial and temporal responses [20, 21].

Besides their role in thrombosis and hemostasis, platelets are also critically involved in several other (patho)physiological processes, such as embryonic development, wound repair, infection, maintenance of vascular integrity, especially in the context of inflammation as well as cancer metastasis [22-24].

Platelets harbor numerous organelles, such as glycogen stores, mitochondria and peroxisomes, and contain a highly organized actin-based cytoskeletal network and a peripheral band of microtubule coils, the surface-connected *open canalicular system* (OCS) consisting of plasma invaginations and the *dense tubular system* (DTS). The OCS serves as membrane reservoir, allowing surface area increase upon platelet activation and shape change. The DTS, which is derived from the residual *endoplasmatic reticulum* (ER), is thought to be a Ca^{2+}-reservoir [25]. Platelets possess three different types of granula: α- and dense granula and lysosomes [26]. α-granula are the most abundant granules in platelets and store adhesive proteins (e.g. fibrinogen, fibronectin, thrombospondin and *von Willebrand factor* (vWF)), coagulation factors and inhibitors of the coagulation cascade (e.g. plasminogen, FV, FXII), chemokines (e.g. PF4), growth factors (e.g. *platelet-derived growth factor* (PDGF)) and glycoproteins (e.g. αIIbβ3). Dense granula are smaller, less abundant and contain second wave mediators and inorganic molecules, such as *adenosine diphosphate* (ADP), *adenosine triphosphate* (ATP), *thromboxane A2* (TxA_2), serotonin (5-HT), Ca^{2+}, polyphosphates and catecholamines. Lysosomes store enzymes required for the degradation of proteins, lipids, and carbohydrates [27-29].

1.2 Platelet activation and thrombus formation

Platelet adhesion and subsequent thrombus formation at sites of vascular injury is a tightly-regulated, multistep process and can be divided into three main steps (Figure 1-1): (I) tethering and adhesion, (II) activation/granule release and (III) aggregation and thrombus growth.

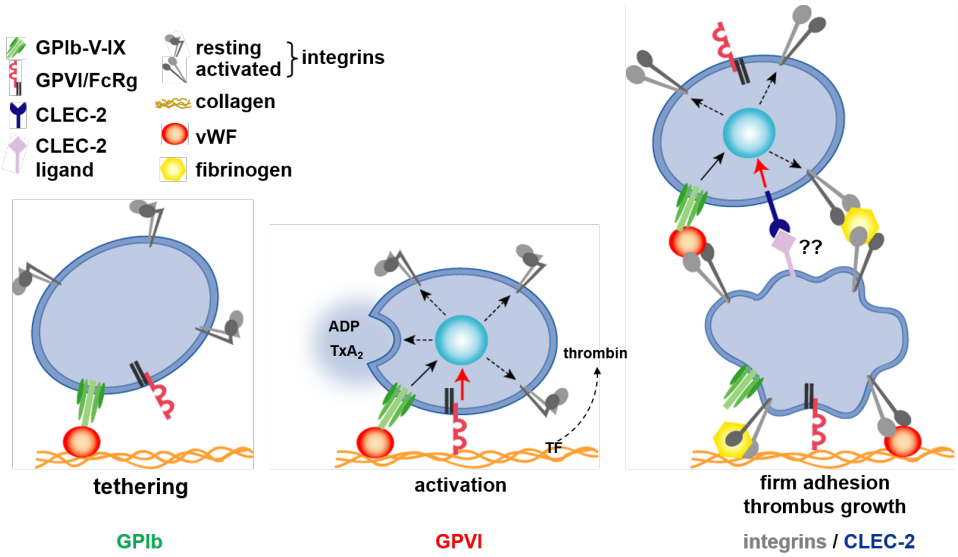

Figure 1-1: Model for platelet adhesion to the ECM and subsequent thrombus formation. Upon vascular injury, components of the *extracellular matrix* (ECM) become exposed and under high shear, platelets tether by interaction of GPIb with collagen-bound vWF. This enables binding of GPVI to collagen, leading to intracellular signaling and release of second wave mediators, like ADP and TxA_2. In parallel, exposed *tissue factor* (TF) triggers thrombin generation, which contributes to platelet activation and *phosphatidylserine exposure* (PS). Finally, these cellular events trigger the conversion of integrins to a high-affinity state, which mediate firm platelet adhesion resulting in thrombus growth. The growing thrombus is stabilized through CLEC-2 (C-type lectin-like receptor 2), however the vascular ligand of CLEC-2 remains elusive. Taken from Nieswandt *et al.,* 2011 [19].

Tethering of platelets occurs under intermediate or high shear forces (1,000-10,000 s^{-1}), which are predominantly found in arterioles or stenosed arteries. During the first step, platelets come into contact with the exposed ECM, which comprises macromolecules such as fibronectin, collagens and laminin [20]. Initial adhesion of platelets to the exposed ECM is mainly mediated by interaction of collagen-bound vWF and the adhesive receptor complex *glycoprotein* (GP) Ib-V-IX (tethering) [30-32]. However, GPIbα-vWF interactions are only transient and too weak to mediate firm platelet adhesion, but rather decelerate and recruit platelets from the blood stream, which is reflected by ‘rolling’ of platelets. [33]. This GPIbα-vWF interaction enables binding of collagen to GPVI, the central activating platelet collagen receptor [34]. GPVI-collagen interaction induces a powerful intracellular signaling cascade (see 1.3), leading to platelet activation and culminating in an increase in intracellular calcium levels ($[Ca^{2+}]_i$), surface

exposure of negatively charged procoagulant *phosphatidylserine* (PS), cytoskeletal rearrangements and mobilization of α- and dense granula. This results in the release of second wave mediators (ADP, ATP, TxA_2) [19, 35]. Simultaneously, exposed *tissue factor* (TF) triggers thrombin generation (extrinsic coagulation pathway) (see 1.7). These soluble agonists, together with locally produced thrombin, contribute to firm platelet activation by stimulation of *G protein-coupled receptors* (GPCRs) [36]. Finally, firm platelet adhesion and aggregation is mediated by a conformational change of integrins (most importantly α2β1 and αIIbβ3) from a low (inactive) affinity to a high (active) affinity state through extra- and intracellular signaling events (inside-out signaling) [34, 37]. Activated α2β1 mediates direct binding to collagen and laminin, whereas αIIbβ3 binds to collagen via vWF (outside-in signaling) [38, 39]. Finally, binding of αIIbβ3 to fibrinogen bridges adjacent platelets, leading to incorporation of activated platelets into the growing thrombus [40, 41].

Binding of αIIbβ3 to ECM components finally leads to firm platelet adhesion. In addition, binding of high-affinity β1- and β3-integrins to their ligands supports subsequent thrombus formation: α2β1 integrin binds to collagen, α5β1 integrin to fibronectin, α6β1 integrin to laminin, αvβ3 integrin to vitronectin and αIIbβ3 integrin to fibrinogen and vWF [37, 42].

1.3 Platelet signaling

Platelet activation can occur through two major signaling pathways, depending on the initial stimulus (Figure 1-2): signaling via GPCR (1.3.1) or the (hem)*immunoreceptor tyrosine-based activation motif* (ITAM)-bearing receptors (1.3.2). Both signaling pathways culminate in activation of phospholipase C (PLC) isoforms, leading to hydrolysis of *phosphatidylinositol-4,5-bisphosphate* (PIP_2) to *inositol-3,4,5-trisphosphate* (IP_3) and *diacylglycerol* (DAG) [40]. Binding of IP_3 to its receptor on the ER membrane induces Ca^{2+} release from its intracellular store leading to a decrease in Ca^{2+} store content and an opening of the Ca^{2+} channels in the plasma membrane. This process is called store-operated Ca^{2+} entry (SOCE) and is mediated by STIM1 (*stromal interaction molecule 1*) and Orai1 (*Ca^{2+} release-activated calcium channel protein 1*) [43].

Activation of platelets also results in rearrangement of the actin and tubulin cytoskeleton, leading to formation of membrane protrusions, such as filopodia and lamellipodia [44].

1.3.1 G protein-coupled receptor signaling in platelets

Soluble mediators, like ADP, TxA_2, and thrombin stimulate receptors that couple to heterotrimeric G proteins. ADP binds to $P2Y_1$ and $P2Y_{12}$ receptors that activate G_q and G_i, respectively. TxA_2 stimulates the TxA_2 receptor (TP) activating G_q whereas thrombin signals through *protease-activated receptors* (PAR) 1/4 on human or PAR3/4 on mouse platelets, mainly activating G_q and $G_{12/13}$ [36, 45-48]. Signaling through GPCR induces generation of TxA2 and release of ADP and ATP and thereby amplifies platelet activation.

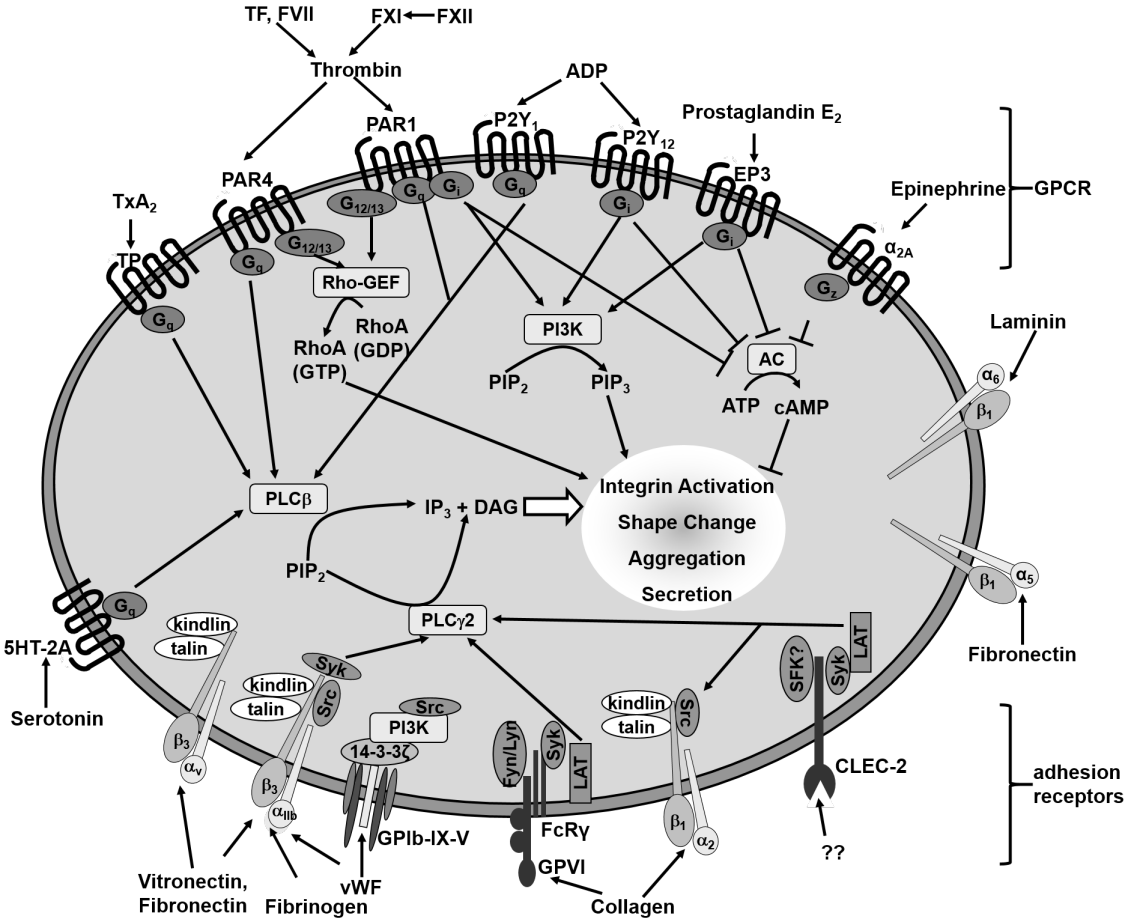

Figure 1-2: Major signaling pathways in platelets. Soluble agonists, including ADP, TxA_2, and thrombin, activate G protein-coupled receptors. G_q proteins stimulate PLCβ, while $G_{12/13}$ trigger Rho activation and G_i and G_z inhibit the *adenylyl cyclase* (AC). Stimulation of adhesion receptors, such as GPVI and CLEC-2 results in PLCγ2 activation. Both signaling pathways culminate in integrin activation, platelet shape change, aggregation and secretion. TxA_2 thromboxane A_2; TP, thromboxane receptor; TF, tissue factor; ADP, adenosine diphosphate; PAR, protease-activated receptor; Rho-GEF, Rho guanine nucleotide exchange factor; PI3K, phosphoinositide-3-kinase; PIP_2, phosphatidylinositol-4,5-bisphosphate; PIP_3, phosphatidylinositol-3,4,5-trisphosphate; IP_3, inositol-3,4,5-trisphosphate; DAG, diacylglycerol. Modified from Stegner *et al.,* 2011 [40].

Stimulation of G_q activates PLCβ isoforms, inducing hydrolysis of PIP_2 to IP_3 and DAG, which leads to an increase of cytoplasmic Ca^{2+} concentrations, activation of PKC and consequently to integrin activation and granule secretion [49].

Activation of G_i through $P2Y_{12}$ inhibits *adenylyl cyclase* (AC) activity and activates *phosphatidylinositide 3-kinase* (PI3K), which in turn hydrolyses PIP_2 to PIP_3 culminating in activation of multiple downstream effects, such as Akt signaling [50]. Finally, this leads to integrin activation. G_z, a subtype of G_i, is stimulated via the epinephrine receptor (α_{2a}) and inhibits AC activity. However, activation of G_z is not sufficient to induce platelet activation. In contrast, activation of $G_{12/13}$ stimulates Rho *guanine nucleotide-exchange factors* (GEFs). Rho-GEFs stimulate the exchange of GDP to GTP, leading to activation of GTPases of the Rho family, including RhoA [36, 40]. In addition, RhoA is activated by G_q [51, 52].

1.3.2 (Hem)immunoreceptor tyrosine-based activation motif signaling in platelets

The second major signaling pathway is initiated by the GPVI-Fc receptor γ chain (FcRγ-chain) complex or by the *C-type lectin-like receptor 2* (CLEC-2) and requires phosphorylation of critical tyrosine residues in the ITAM or hemITAM, respectively. An ITAM is a highly conserved sequence of four *amino acids* (aa) ($YxxL/Ix_{(6-12)}YxxL/I$), which is repeated twice in the cytoplasmic tail of several hematopoietic *immunoglobulin* (Ig) receptors, among those are Fc receptors (FcR) and C-type lectin-like receptors [53]. Human platelets express three ITAM-bearing receptors, FcγRIIA, GPVI and the hemITAM receptor CLEC-2, murine platelets only express GPVI and CLEC-2. The FcRγ-chain contains the ITAM motif and thereby serves as the signal transducing subunit of the GPVI/FcRγ-chain. Cross-linking of the central activatory platelet receptor GPVI with collagen induces a downstream signaling cascade: Src family kinases Fyn and Lyn phosphorylate the ITAM-bearing FcRγ-chain, which in turn leads to recruitment and activation of the *spleen tyrosine kinase* (Syk). The downstream signaling cascade involves a large number of adaptor and effector proteins, such as the *linker for activated T cells* (LAT), the *Src-homology* (*SH) 2 domain-containing leukocyte protein of 76 kDa* (SLP-76) and the *growth factor receptor-bound protein 2* (Grb2), ultimately culminating in activation of effector enzymes, such as PI3K and PLCγ2, leading to the aforementioned hydrolysis of PIP_2 to IP_3 and DAG and release of intracellular Ca^{2+} via IP_3 binding to its receptor [35, 54, 55]. The hemITAM receptor CLEC-2 utilizes similar activation pathways, involving Src family kinases and Syk leading to activation of PLCγ2 [56, 57].

1.4 The (hem)ITAM receptors GPVI and CLEC-2

1.4.1 GPVI

GPVI, the central activating collagen receptor, is exclusively expressed on platelets and MKs and belongs to the Ig superfamily of surface receptors [58]. It is non-covalently associated with the disulphide-homodimeric FcRγ-chain via a salt bridge. The FcRγ-chain represents the signaling subunit of the complex, since it contains the ITAM, and cross-linking by ligands leads to ITAM-dependent signaling (see 1.3.2) [34, 59]. The FcRγ-chain is critically required for expression of GPVI and signal transduction downstream of GPVI (Figure 1-3) [60].

The cytosolic tail of GPVI has been shown to associate with calmodulin [61]. Disruption of calmodulin binding causes downregulation of GPVI from the platelet surface [62]. Besides this, the Src kinases Fyn and Lyn bind to the proline-rich sequence in the cytosolic tail [63].

GPVI is the major collagen receptor on human and mouse platelets. It specifically recognizes and binds to GPO repeats (glycine, proline, hydroxyproline) in the collagen sequence [34]. Powerful GPVI activation can also be triggered by non-physiological ligands: the synthetically GPO-rich *collagen-related peptide* (CRP) and convulxin, a C-type lectin from the venom of the rattlesnake *Crotalus durissus terrificus* [64]. Recently, a novel extracellular GPVI ligand was identified – the ectodomain of GPVI interacts with immobilized fibrin and thereby promotes thrombin generation and thrombus stabilization [65, 66].

In vivo administration of monoclonal rat anti-GPVI antibodies (JAQ1, 2, 3) leads to specific and irreversible downregulation of GPVI from circulating platelets (“immunodepletion”), resulting in a persistent “knock-out like” phenotype for up to two weeks and is accompanied by a transient thrombocytopenia [67, 68]. The process underlying the antibody-induced GPVI depletion *in vivo* is still incompletely understood, however, there is recent evidence that the FcγRIIb expressed on liver sinusoidal endothelial cells is critically involved in this process [69]. It was shown that two distinct pathways exist regulating the prevalence of GPVI on the platelet surface: internalization and ectodomain shedding by *a disintegrin and metalloproteinases* (ADAMs) [54, 67, 70, 71].

During the past years, GPVI has emerged as a potential anti-platelet target [35, 54, 72]. Data from GPVI-deficient mice, antibody-induced GPVI depletion or GPVI blockade demonstrated in *in vivo* models a profound protection from thrombosis [73], ischemia reperfusion injury after myocardial infarction [74] and ischemic stroke [73, 75] with only a mild effect on hemostasis [76].

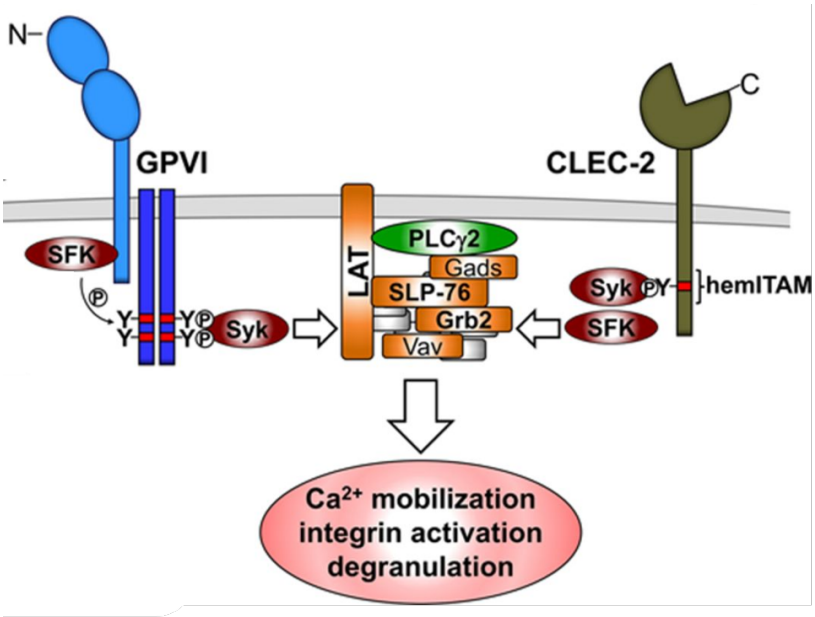

Figure 1-3: (hem)ITAM signaling in platelets. GPVI is non-covalently associated with the ITAM-bearing FcRγ-chain. Ligand-induced crosslinking of GPVI initiates phosphorylation of the ITAM by SFKs leading to receptor activation, which in turn leads to recruitment and activation of Syk. The hemITAM motif contained in CLEC-2 is phosphorylated by Syk. Syk and SFKs regulate a downstream signaling cascade similar to that found in GPVI, involving many adaptor and effector proteins, such as LAT, SLP-76 and Grb2. Finally, PLCγ2 is activated leading to Ca^{2+} mobilization, integrin activation and granule secretion. SFK, Src family kinases; Syk, spleen tyrosine kinase; LAT, linker for activated T cells; Grb2, growth factor receptor-bound protein 2; Gads, Grb2-related adapter downstream of Shc; SLP-76, SH2-containing leukocyte protein 76; PLCγ2; phospholipase C γ2. Modified from Stegner *et al.,* 2014 [54].

1.4.2 CLEC-2

The type II transmembrane protein CLEC-2 is the second (hem)ITAM containing receptor expressed on mouse platelets. It is highly expressed on MKs and platelets and at low levels on some immune cells [55, 77]. Downstream signaling of CLEC-2 is induced by phosphorylation of a single conserved YxxL motif in its cytoplasmic tail (Figure 1-3). The only known physiological ligand of CLEC-2, the transmembrane protein podoplanin, is not expressed in the vasculature under healthy conditions and is not known to be involved in primary hemostasis [78, 79]. Therefore, a yet unidentified ligand of CLEC-2 has been proposed which should be exposed or released upon vascular injury or on growing thrombi and contributes to CLEC-2-dependent thrombus stabilization [80]. The snake venom rhodocytin is a non-physiological agonist mediating powerful platelet activation via CLEC-2 [81].

Since a constitutive knockout of CLEC-2 results in embryonic or perinatal lethality [82-84], function of CLEC-2 was primarily investigated using a MK- and platelet-specific knockout mouse or in mice where CLEC-2 has been depleted using a monoclonal rat anti-CLEC-2 antibody (INU1). Like described for JAQ1-mediated GPVI-depletion, CLEC-2 is depleted from the platelet surface after injection of INU1, resulting in a knockout-like phenotype. This

immunodepletion is accompanied by a severe thrombocytopenia for up to 48 h after antibody injection and a loss of the receptor for > 5 days [75, 80], which is to a large extent Syk-independent. The receptor downregulation is, however, mediated through *Src family kinases* (SFK)-triggered receptor internalization [56] and results in the complete loss of the receptor from the platelet surface and therefore its signaling in platelets. Several studies indicate, that CLEC-2 is a major platelet activatory surface receptor known to contribute to both embryonic development and hemostasis [82, 85]. Lack of CLEC-2 leads to protection from occlusive thrombus formation. While single deficiency of CLEC-2 results only in a moderate increase in bleeding times, deficiency of both (hem)ITAM receptors reveals a functional redundant role in hemostasis as well as in maintenance of vascular integrity [75, 86, 87]. Besides this, CLEC-2 is required for lymphatic development including blood/lymph vessel separation during embryogenesis, maintenance of the integrity of high endothelial venules, development of lymph nodes and in patho-physiological processes such as tumor metastasis [88-93].

Recent studies by our group identified a signaling-independent role of CLEC-2 in *in vivo* hemostasis and thrombus stability, but a signaling-dependent role of CLEC-2 in lymphatic development [94].

1.5 PKCι

The protein kinase C family belongs to the family of serine/threonine kinases. Mammalian PKCs are encoded by nine different genes and consist of 12 isoforms, which are classified into three subtypes based on their structural differences. A highly conserved carboxyterminal kinase domain is linked via a hinge region to a more variable amino-terminal regulatory domain, which contains a conserved pseudosubstrate domain [95]. PKCα, β and γ belong to conventional (c) PKCs and are activated in a DAG- and Ca^{2+}-dependent manner. Novel (n) PKCs δ, ε, η and θ are DAG-dependent, but Ca^{2+}-independent, since their C2-like domain lacks the ability to bind Ca^{2+}, but rather serves as a phosphotyrosine binding motif. The atypical (a) PKCs ι (also known as λ) and ζ are activated independent of DAG- and Ca^{2+}. They totally lack a C2 domain and the C1-domain is insensitive for DAG. Like all PKC isoforms, aPKCs can respond to PS [96]. PKC isoforms are important mediators of shape change, release of intracellularly stored granules, and spreading on immobilized ligands upon platelet activation [97, 98]. In particular, conventional and novel PKC isoforms were previously identified as important mediators of central platelet signaling pathways with distinct functions in platelet granule release (PKCα, ε, δ, θ) [97, 99, 100], thromboxane synthesis (PKCδ, θ, η) [101-103], spreading [97, 99, 104] and thrombus formation [97].

However, the role of aPKCs in platelet function remains elusive. aPKCs are mostly known for their role in immune cell responses and cell polarization. It has been shown that aPKCs are allosterically activated in a DAG- and Ca^{2+}-independent manner by interacting with the small Rho GTPases Cdc42 and Rac1 (Figure 1-4) [95, 105, 106]. RhoA, Cdc42 and Rac1 are essential for cytoskeletal rearrangements [107]. Previous studies confirmed that Cdc42 and Rac1 play a crucial role in shape change during platelet spreading and for adhesion to exposed ECM molecules. Consequently, lack of these GTPases results in impaired filopodia and lamellipodia formation, respectively [108-112].

PKCι mediates cell polarization. It forms a complex with Par3/Par6 which then associates with cell junctions and is important for apical membrane development [113]. Furthermore, Welchman *et al.* described a role of PKCι in immune cell responses and cell migration *in vivo* in *C. elegans* [114]. aPKCs are considered to be located downstream of PDPK1 and PI3K as direct binding of PIP_3 has been proven [115], and thereby to promote cell survival in glioblastoma cells [116]. Lack of functional PKCι/λ results in embryonic lethality [117, 118], showing the importance of aPKCs in development. Using conditional knockout mice, it has been shown that deficiency of aPKCζ specifically in immune cells leads to a defective immune response and compromised NF-κB signaling concomitant with a reduced number of mature B cells as well as impaired T cell differentiation [119, 120]. Studies with PKCι/λ-deficient T cells showed similar results [121].

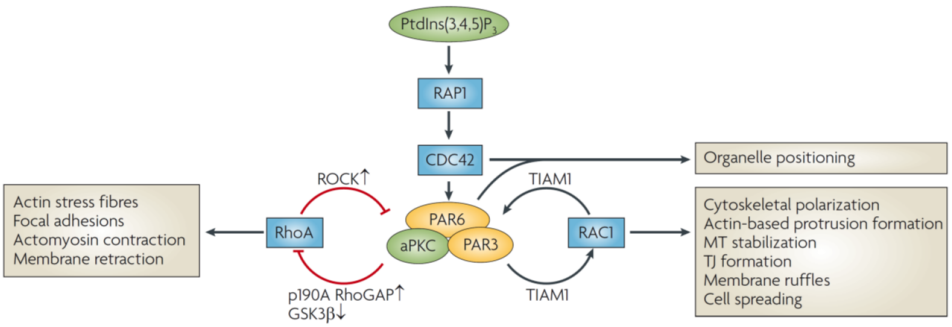

Figure 1-4: Simplified schematic crosstalk between aPKCs and the small GTPases RhoA, Rac1 and Cdc42 during cell polarization. External signals trigger PIP_3 production, which in turn activates Cdc42 and aPKC leading to formation of the Par3/Par6/aPKC complex. TIAM1 (*T cell-lymphoma invasion and metastasis-1*)-PAR3 interaction in turn induces Rac1 activation via aPKC. Formation of the Par3/Par6/aPKC complex is crucial for regulation of small GTPases during cell polarization. PIP_3, phosphatidylinositol-3,4,5-trisphosphate; RAP1, Ras-like protein 1; ROCK, Rho-associated coiled-coil-containing protein kinase; GSK3β, glycogen synthase kinase 3β. Taken from Iden *et al.,* 2008 [106].

A recent study by our group showed that MK polarization and transendothelial platelet biogenesis is modulated by the small GTPases Cdc42 and RhoA. While Cdc42 together with

PI3K triggers cell polarization via GPIb, RhoA counteracts this process. Here, loss of PKCι/λ mimicked the absence of Cdc42, indicating that PKCι/λ functions downstream of this GTPase in GPIb-signaling [122]. Likewise, PKCι/λ has been identified as a downstream mediator of Cdc42-triggered processes in endothelial cells [106, 123].

1.6 The GPIb-V-IX Complex

The multifunctional hetero-oligomeric membrane receptor complex GPIb-V-IX is an adhesion receptor on the platelet surface and critically involved in hemostasis, thrombosis, cancer metastasis and inflammation [124-127]. The complex is highly abundant with approximately 25.000 copies per platelet [128] and consists of four transmembrane subunits: GPIbα (CD42b), GPIbβ (CD42c), GPIX (CD42a) and GPV (CD42d) in a ratio of 1:2:1:0.5 (Figure 1-5) [129] or 1:2:1:1 (R. Li, personal communication). They all belong to the *leucine-rich repeat* (LRR) protein superfamily [130]. GPIbα and GPIbβ are disulfide-linked and tightly complexed with GPIX by interacting with their transmembrane domains and GPIbβ-GPIX are disulfide-linked with their extracellular domains [131-133]. GPV is non-covalently attached to the complex, with the transmembrane domains of GPIbα and GPV forming close contacts [134]. GPIb and GPIX are required for expression of GPV on the platelet surface [135, 136]. However, in contrast to GPIb and GPIX, GPV is not necessary for expression of the GPIb-GPIX complex on the platelet surface [137]. Structural details of the GPIb-V-IX complex association still require further elucidation, since there are also recent reports indicating that some complexes could be free of GPV on the platelet surface and instead interact with GPVI, FcγRIIa and apolipoprotein E receptor 2 [138-140].

Lack of functional GPIb-V-IX complexes on the platelet surface is the cause of the *Bernard-Soulier syndrome* (BSS), a rare congenital bleeding disorder, emphasizing the importance of the receptor complex. BSS patients exhibit a mild thrombocytopenia accompanied by giant platelets and MKs resulting in massively prolonged bleeding times [130, 141, 142]. Mutations from BSS patients map to GPIbα, GPIbβ or GPIX genes, indicating that mutations in any of the three subunits can abolish expression of the whole complex [130, 133]. Lack of GPIbα or GPIbβ in mice reproduces a BSS phenotype [124, 143]. However, no patient with a mutation in the *GP5* gene has been observed so far. A possible explanation could be that lack of GPV is lethal or the absence of GPV does not cause any clinical symptoms. The latter is more likely, since mice lacking GPV are viable and do not exhibit a BSS, have normal platelet counts and display an unaltered vWF binding activity in platelets [144, 145].

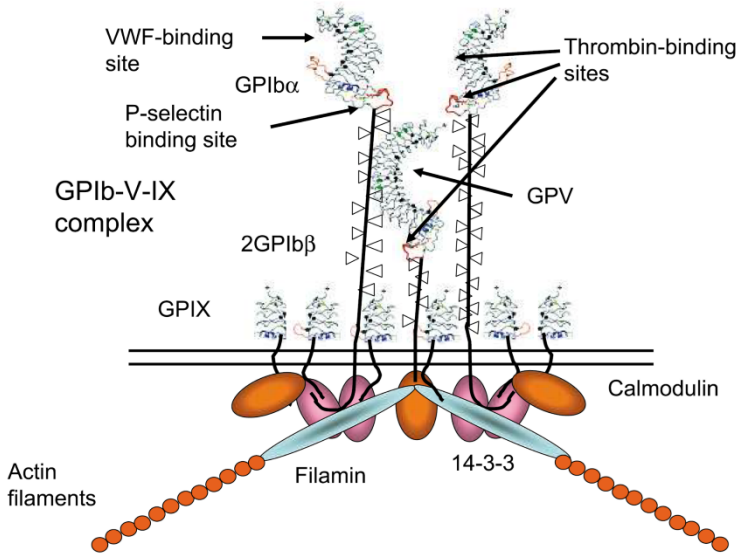

Figure 1-5: Schematic model of the GPIb-V-IX complex. The GPIb-V-IX complex is composed of four different transmembrane polypeptides: GPIbα, GPIbβ, GPV and GPIX in a stoichiometry of 1:2:1:0.5. GPV is non-covalently associated with the GPIb-IX complex. Two GPIbβ subunits form one disulfide bond each to one GPIbα subunit. Each member of the complex contains leucine-rich repeats in the extra-cellular domain. GPIbα and GPV are highly glycosylated. Many extracellular ligands bind to the GPIb-V-IX complex, most of them to GPIbα. Displayed are the three binding sites for the most prominent ligands. The cytoplasmic domains of the single subunits interact with a number of proteins, including calmodulin, filamin and 14-3-3ζ. Modified from Clemetson, 2007 [146].

1.6.1 GPIb-Signaling

The GPIb-V-IX complex plays a significant role in initial platelet adhesion to the injured vessel wall, especially under conditions of high shear flow by binding of GPIbα to vWF [30, 147, 148]. This can also elicit intracellular signals downstream of GPIb, leading to stable platelet adhesion, shape change and thrombus formation [147]. Besides this, multiple ligands involved in platelet adhesion and coagulation bind to GPIbα (e.g. thrombin, P-selectin, Mac-1, β2 integrins, thrombospondin and coagulation factors FXI, FXII, high molecular weight kininogen) [149-155]. In addition, a number of snake venom toxins, e.g. botrocetin, bind to GPIbα [156]. Furthermore, the GPIb-V-IX complex is associated with the signaling protein 14-3-3ζ via GPV and GPIbα, with filamin and PI3K via GPIbα and with the actin-binding protein [44, 157-161]. Binding of 14-3-3ζ requires a C-terminal sequence in the cytoplasmic domain of GPIbα, which is important in vWF-induced GPIb-IX signaling and in regulating the vWF binding function of GPIb [162, 163]. Calmodulin binds to all receptor subunits, except for GPIX, however the only known function of calmodulin binding is the prevention of receptor downregulation by ADAM17-mediated shedding [164, 165].

Besides the pivotal role of GPIb-V-IX in platelet adhesion, an additional role of GPIb at extremely high shear rates (> 10.000 s^{-1}), such as found in stenosed arteries, has been

identified. Rapid changes in blood flow causing shear-microgradients guide initial adhesion and aggregation of discoid platelets and represent a general feature of thrombus development, most likely through a shear-regulated GPIb-dependent mechanism, but independently of integrin αIIbβ3 activation [166-168].

It has been assumed for long time, that ligand-binding to the receptor complex generates transmembrane signaling finally leading to Ca^{2+} mobilization, cytoskeletal rearrangements and ultimately integrin αIIbβ3 activation implicating a signal-transducing role of the GPIb-V-IX complex [146, 169]. However, GPIb-V-IX signaling is rather weak compared to GPVI or GPCR-dependent signaling. Despite this, GPIb-V-IX signaling is difficult to study, since GPIb does not interact with its main ligand vWF under static conditions, but instead requires high shear conditions [170]. Ristocetin can induce GPIb-vWF interactions on human [171] and botrocetin on both, mouse and human platelets [172] under static conditions, causing GPIb-specific signaling events [173-175]. Nevertheless, several molecules were proposed to mediate GPIb-dependent signaling [147, 176, 177]. It was described that vWF binding to GPIb induces activation of the ITAM-containing receptor FcγRIIa [139] and the immune receptor associated FcRγ-chain [178], but other studies did not confirm these observations [179]. Besides this, SFK and PI3K are proposed to participate in GPIb-signaling [161, 180]. ADAP *(adhesion and degranulation promoting adapter protein)* has been shown to mediate αIIbβ3-integrin activation downstream of GPIb-V-IX upon vWF binding [181].

Studies using mice with a mutated extracellular domain of GPIbα or an inhibitory anti-GPIbα antibody, which blocks the vWF-binding site (p0p/B), demonstrated the physiological relevance of GPIbα-vWF interactions for thrombus formation under high shear flow conditions. In the absence of functional GPIb, mice were protected from arterial occlusive thrombus formation [127, 182] as well as in a model of ischemic brain infarction, since platelet tethering to the injured vessel wall was abrogated. These observations together with the fact that both prophylactic and therapeutical administration of anti-GPIbα Fab fragments profoundly protect mice from secondary infarct growth, suggested the GPIb-vWF interaction as a suitable pharmacologic target for prevention and treatment of ischemic stroke [183-186].

1.6.2 GPV

The *GP5* gene is located on chromosome 3q29 in humans and on chromosome 16B2 in mice and has a simple structure: unlike most genes that comprise multiple exons the entire coding sequence of GPV is contained in its second exon [187]. Both, *GP1b* and *GP9* genes exhibit a similar exon and intron distribution [188-190]. Human and murine GPV share a nucleotide sequence homology of 80% translating into 70% homology of the amino acid sequence [128].

GPV is a type I transmembrane protein with a short C-terminal intracellular domain of 16 aa, which does not contain potential phosphorylation sites [191]. It is followed by a transmembrane domain of 25 aa, important for the correct complex assembly by interacting with GPIbα, and a long extracellular domain.

Like GPIb and GPIX, GPV belongs to the leucine rich protein superfamily and contains 15 LRR [192, 193]. Its expression is restricted to the megakaryocyte-platelet lineage and GPV is highly abundant on platelets (approximately 12.0000 copies/cell) [128, 194, 195]. GPV is the only subunit of the GPIb-V-IX complex not required for the correct expression of the complex [196]. In fact, it was shown that expression of GPV on the surface of transfected cells is enhanced in the presence of the other subunits [159] and GPV was proposed to strengthen the interaction with vWF under high shear conditions [197]. *In vitro* properties and structure of GPV were investigated through development of antibodies and recombinant proteins, by cloning of genes coding for human, rat and mouse GPV [128, 187, 191, 193-195, 198].

GPV is highly glycosylated (7 potential N-glycosylation sites) and has a molecular weight of 82 kDa. Besides cleavage by elastase (releasing a 73 kDa fragment), ADAMs and calpain (releasing the entire extracellular domain), GPV is cleaved by thrombin at nM concentrations releasing a 69 kDa soluble fragment [128, 187], which leads to elevated plasma levels of the soluble protein. Therefore, GPV was proposed as biomarker for *in vivo* platelet activation after thrombotic events, such as myocardial infarction and stroke [199-203] and to follow platelet storage for transfusion [198, 204], but high plasma levels of GPV may also be caused by high doses of aspirin [205].

Gp5$^{-/-}$ mice were generated and described by two independent groups [144, 145]. GPV-deficient mice did not suffer from a BSS-like phenotype. Besides this, overall platelet function was grossly normal in the absence of GPV except for a slight hyperresponsiveness towards intermediate and low thrombin concentrations [135, 145], which was confirmed by later studies using *Gp5*$^{-/-}$ mice backcrossed on a C57Bl/6 background [206]. The hyperreactivity of GPV-deficient platelets upon thrombin stimulation is rather due to lack of GPV as a thrombin substrate, rendering more thrombin available to activate platelets via PAR receptors [145, 207, 208]. While one mouse strain showed shortened tail bleeding times, accelerated thrombus formation and increased embolization in the absence of GPV [145, 209], the second mouse strain had unaltered tail bleeding times and a decreased tendency to form arterial occlusive thrombi [135, 144], which was ascribed to a role of GPV in collagen signaling and established GPV as a collagen receptor [135]. The role of GPV as collagen receptor was regarded to be negligible for platelet function [34, 146].

Nevertheless, mice double-deficient for the major collagen receptor GPVI and GPV were previously generated in our laboratory and analyzed in *in vivo* thrombosis and hemostasis models expecting an even more severe phenotype than in GPVI-single deficient mice [73]. Surprisingly, these studies revealed an unexpected role of GPV as modulator of thrombus formation *in vivo*, which contrasts previous findings that GPV is only of minor relevance for arterial thrombus formation [206]. Strikingly, the thrombotic defects in the absence of the platelet-activating collagen receptor GPVI could be reversed by lack of GPV leading to occlusion times comparable to WT mice (Figure 1-6) [210]. Moreover, *Gp5*$^{-/-}$ mice restored hemostatic function in the absence of GPVI and prevented the protective effect of GPVI-deficiency in a model of ischemic stroke [210], establishing GPV as a key modulator of thrombosis and hemostasis *in vivo*. However, the function of GPV and the mechanism underlying the compensatory effect of GPV-deficiency remain extensively elusive and were studied in detail in this thesis.

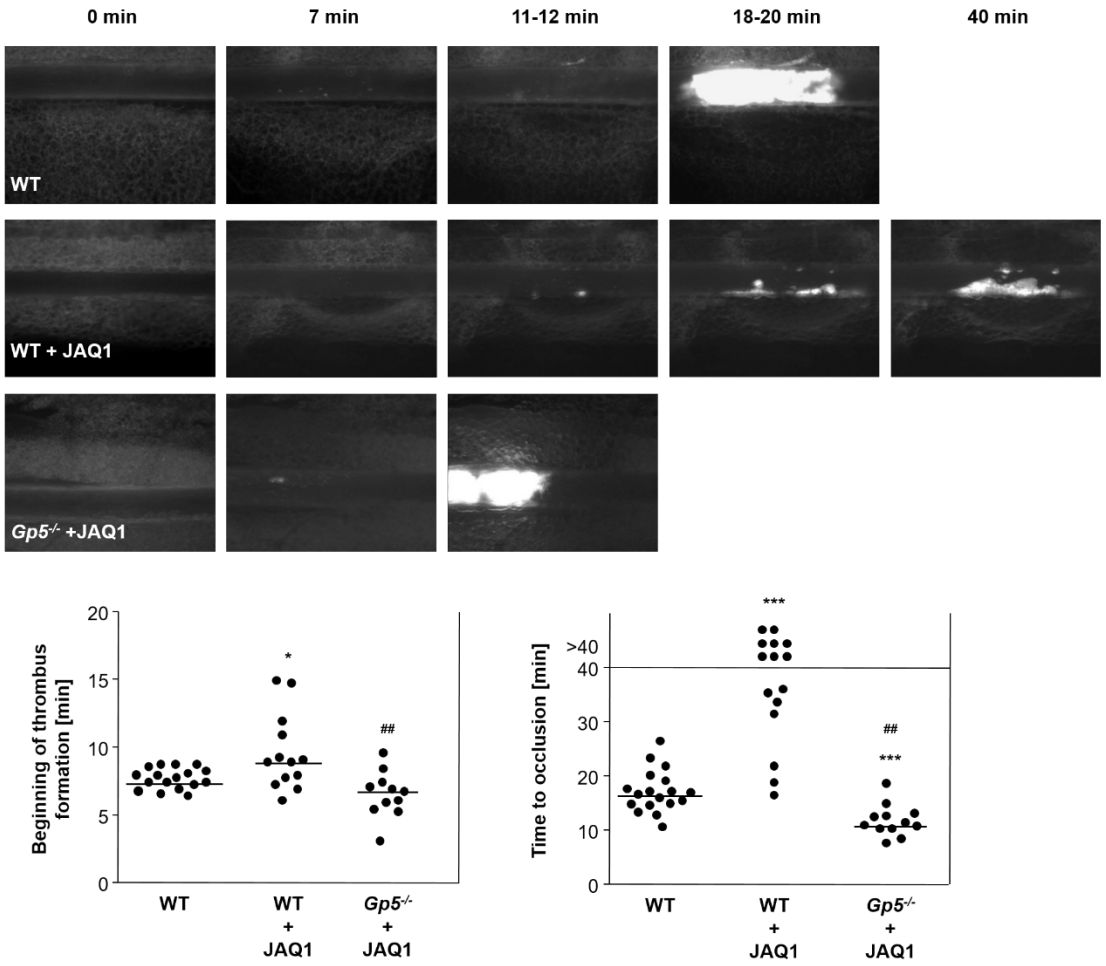

Figure 1-6: GPV-deficiency restores occlusive thrombus formation in GPVI-deficient mice. Mesenteric arterioles were injured with 20% $FeCl_3$ and adhesion as well as thrombus formation of fluorescently-labeled platelets were monitored by intravital microscopy. Each dot represents one vessel, horizontal lines indicate the median. * p<0.05; ** p<0.01; *** p<0.001 as compared to untreated WT mice. # p<0.05; ## p<0.01 as compared to JAQ1-treated WT mice. Modified from Stegner, 2011 [210].

1.7 Coagulation cascade and thrombin generation

Vascular injury triggers rapid activation of the coagulation cascade ultimately leading to thrombin generation, fibrin formation and formation of a fibrin- and platelet-rich clot. Blood coagulation can be initiated by two distinct pathways (Figure 1-7): the extrinsic and intrinsic coagulation pathway. Both pathways consist of a sequence of tightly regulated activation steps of plasma serine proteases and cofactors culminating in generation of thrombin and subsequently fibrin formation. Most of these steps depend on Ca^{2+} and take place on a phospholipid surface [211].

The extrinsic coagulation pathway is initiated when locally exposed TF, expressed by cells within the vessel wall and adjacent tissue or on cell-derived microparticles, comes into contact with *activated coagulation factor* VII (FVIIa), which in turn catalyzes the activation of traces of FX and FIX [212]. FX and FIX amplify TF-bound FVII activation in a feedback signal leading to thrombin generation. Thrombin cleaves FVIII and FV to FVIIIa and FVa, respectively. FIXa can bind to FVIIIa. This efficiently propagates coagulation by formation of the prothrombinase complex (FXa-FVa), which subsequently cleaves prothrombin (FII) to thrombin [213]. The generated thrombin will activate further platelets. In parallel, the coagulation cascade is promoted by PS exposure on activated platelets (procoagulant platelets), which enhances assembly and activity of two major coagulation complexes [214-216].

The intrinsic coagulation pathway is initiated when FXII (Hageman factor) becomes autoactivated on negatively charged surfaces (contact activation), such as polyphosphates (polyP) released from dense granules in platelets or extracellular RNA [217, 218]. Surface bound FXIIa activates FXI followed by successive activation of FIX (forming the tenase complex by binding to FVIIIa on PS-exposing cells) and FX. FXa/FVa produce sufficient amounts of thrombin [219]. Furthermore, it activates the complement cascade by activation of C1 esterases and converts prekallikrein into plasma kallikrein.

The locally produced thrombin enhances platelet activation by cleavage and activation of PARs [45, 48, 207], which in turn initiates an intracellular signaling cascade [36]. Thrombin finally cleaves fibrinogen to fibrin [219, 220]. Despite requirement for PARs, platelets react poorly to low doses of thrombin in the absence of the GPIb-V-IX complex [155].

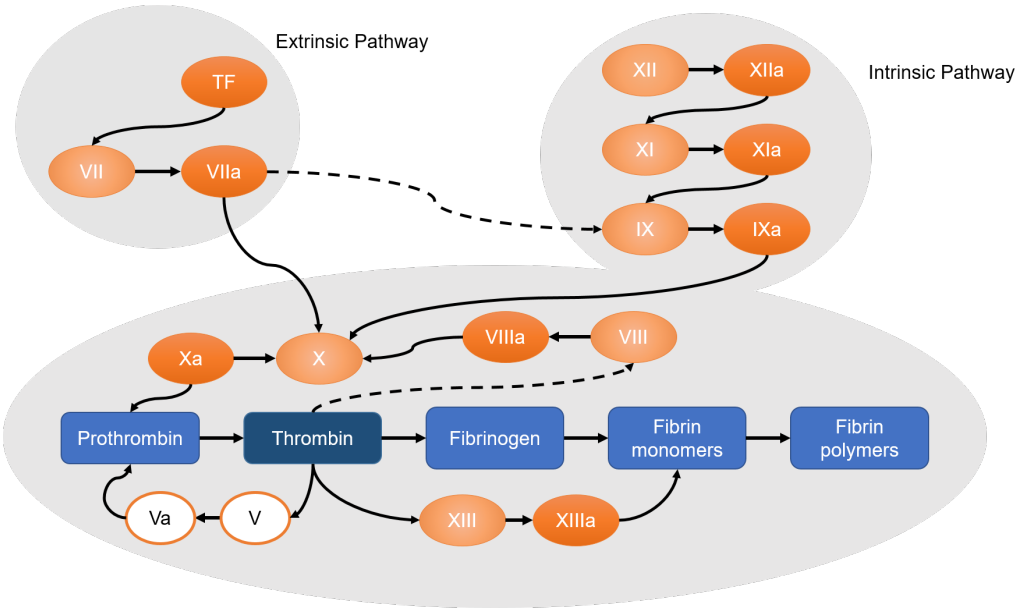

Figure 1-7: Schematic overview of the classical coagulation cascade. The extrinsic coagulation pathway is initiated by exposure of tissue factor (TF) at sites of vascular injury which activates FVII followed by activation of FX and FIX. The intrinsic pathway gets initiated by activation of FXII, which in turn activates FXI and FIX, leading to FX activation. Both pathways culminate in the conversion of prothrombin to thrombin, which is the key protease in the coagulation system. It activates multiple proteases and cofactors, stimulates further platelet activation and finally, cleaves fibrinogen to fibrin.

1.8 Aim of the study

The major collagen receptor GPVI has been previously recognized as an essential regulator of hemostasis and thrombo-inflammatory brain infarction and emerged as a promising antithrombotic target.

An unexpected role of GPV as mediator of *in vivo* thrombus formation, hemostasis and thrombo-inflammatory brain infarction was previously shown by our group. Lack of GPV restored thrombus formation and hemostasis in the absence of GPVI and prevented protection of GPVI-deficient mice in a model of ischemic brain infarction. However, the mechanism underlying these compensatory processes remained elusive. Therefore, the aim of this thesis was to unravel the mechanisms underlying the function of GPV in physiology and pathology. For this, GPV-deficient mice were further characterized. In addition, a mouse with a mutation rendering GPV uncleavable by thrombin was generated and the *in vivo* relevance of the thrombin cleavage site was studied in thrombosis and hemostasis.

The results of the first part of this thesis point to a regulatory role of the cleaved (soluble) GPV in thrombus formation and hemostasis. During thrombus formation, sGPV is released in the plasma upon platelet activation in the presence of thrombin. In a second part of the thesis, the

effect of soluble murine and human GPV on *in vitro* and *in vivo* thrombus formation was analyzed.

Besides this, the protein kinase C (PKC) family is involved in several physiological processes regulating platelet activation. Conventional and novel PKCs in platelets were previously shown to distinctively regulate platelet function dependent on the targeted PKC isoform and on the nature and concentration of the stimulus. Atypical PKCι/λ is an important mediator of cell polarity, carcinogenesis, embryonic development and immune cell responses and is known to interact with the small Rho GTPases Rac1 and Cdc42, which are important mediators of various platelet functions. However, the role of aPKCs in platelet physiology remained unknown. Due to the high similarity of aPKC isoforms ι/λ and ζ, it previously was difficult to dissect their distinct functions in platelets. Conditional knockout mice with MK-/platelet-specific deficiency in PKCι/λ were generated and analyzed in *in vitro* and *in vivo* assays in this thesis.

2 Materials and Methods

2.1 Materials

2.1.1 Kits, Reagents and Cell Culture Material

Reagent	Company
3-amino-9-ethylcarbazole (AEC) solution	EUROPA (Cambridge, UK)
2-Methyl-2-butanol	Sigma-Aldrich (Schnelldorf, Germany)
2,2,2-Tribromoethanol	Sigma-Aldrich (Schnelldorf, Germany)
A23187	AppliChem (Darmstadt, Germany)
Acetone	Sigma-Aldrich (Schnelldorf, Germany)
Acetic acid	Roth (Karlsruhe, Germany)
Adenosine diphosphate (ADP)	Sigma-Aldrich (Schnelldorf, Germany)
Adenosine triphosphate (ATP)	Fermentas (St. Leon-Rot, Germany)
Albumin Fraction V, endotoxin tested (Bovine Serum Albumin, BSA)	Roth (Karlsruhe, Germany)
Agarose	Roth (Karlsruhe, Germany)
Alexa Fluor 488 reactive dye	Molecular Probes (Karlsruhe, Germany)
Alexa Fluor 647 reactive dye	Molecular Probes (Karlsruhe, Germany)
Ammonium persulfate (APS)	Roth (Karlsruhe, Germany)
Anti-Flag® M2 affinity gel	Sigma-Aldrich (Schnelldorf, Germany)
Dylight 488-labeled annexin-A5	In-house generated
Apyrase (grade III)	Sigma-Aldrich (Schnelldorf, Germany)
Aquatex®	Merck Millipore (Darmstadt, Germany)
Aspirin	Bayer (Wuppertal, Germany)
ATP Standard	Chrono-log (Lemgo, Germany)
β-mercaptoethanol	Roth (Karlsruhe, Germany)
Bis(sulfosuccinimidyl)suberate (BS^3)	Life Technologies (Darmstadt, Germany)
Blocking solution	Candor Bioscience (Wangen, Germany)
BlueStar plus prestained protein marker	Nippon Genetics (Düren, Germany)
Bromophenol blue	Sigma-Aldrich (Schnelldorf, Germany)
Calcium chloride	Roth (Karlsruhe, Germany)
Carbonate-bicarbonate buffer capsules	Sigma-Aldrich (Schnelldorf, Germany)
Cell clean	Sysmex Europe (Norderstedt, Germany)
Chloroform	AppliChem (Darmstadt, Germany)
Collagen-related peptide (CRP)	provided by S.P Watson (University of Birmingham, UK)

Convulxin	Axxora (Lörrach, Germany)
Coomassie brilliant blue	Sigma-Aldrich (Schnelldorf, Germany)
3,3'-dihexyloxacarbocyanine iodide ($DiOC_6$)	Enzo Life (Lörrach, Germany)
Deoxynucleotide triphosphate (dNTP) mix (10 mM)	Life Technologies (Darmstadt, Germany)
Dimethyl sulfoxide (DMSO)	Roth (Karlsruhe, Germany)
Disodium hydrogen phosphate (Na_2HPO_4)	Roth (Karlsruhe, Germany)
Dorbene	Pfizer (Karlsruhe, Germany)
Dulbecco's phosphate buffered saline (PBS)	Sigma-Aldrich (Schnelldorf, Germany)
Dylight 488	Pierce (Rockford, IL, USA)
Ethylenediaminetetraacetic acid (EDTA)	AppliChem (Darmstadt, Germany)
Ethylene glycol tetraacetic acid (EGTA)	Roth (Karlsruhe, Germany)
Ethanol	Roth (Karlsruhe, Germany)
Fentanyl	Janssen-Cilag (Neuss, Germany)
Fetal calf serum (FCS)	Perbio (Bonn, Germany)
Fibronectin	Sigma-Aldrich (Schnelldorf, Germany)
Flag peptide	Sigma-Aldrich (Schnelldorf, Germany)
Flumazenil	Delta Select (Pfullingen, Germany)
Fluorescein-5-isothiocyanate (FITC)	Molecular Probes (Karlsruhe, Germany)
Forene® (Isoflurane)	Abott (Wiesbaden, Germany)
Freund's Adjuvant complete	Sigma-Aldrich (Schnelldorf, Germany)
Freund's Adjuvant incomplete	Sigma-Aldrich (Schnelldorf, Germany)
GeneRuler DNA Ladder Mix	Life Technologies (Darmstadt, Germany)
Glucose	Roth (Karlsruhe, Germany)
Glycerol	Roth (Karlsruhe, Germany)
Glycine	AppliChem (Darmstadt, Germany)
Ham's F12 medium	Gibco (Karlsruhe, Germany)
Hypoxanthine, aminopterin, thymidine (HAT) Media Supplement (50x)	Sigma-Aldrich (Schnelldorf, Germany)
N-2-Hydroxyethylpiperazine-N'-2-ethanesulfonic acid (HEPES)	Roth (Karlsruhe, Germany)
High molecular weight heparin	Sigma-Aldrich (Schnelldorf, Germany)
Horm Collagen type I	Nycomed (Munich, Germany)
Human fibrinogen (#F3879)	Sigma-Aldrich (Schnelldorf, Germany)
Human fibrinogen (#F4883)	Sigma-Aldrich (Schnelldorf, Germany)
Human recombinant tissue factor	Innovin® Siemens (Erlangen, Germany)
Immunolon® 2HB 96-well U bottom	Life Technologies (Darmstadt, Germany)

Indomethacin	Sigma-Aldrich (Schnelldorf, Germany)
Integrilin	GlaxoSmithKline (Munich, Germany)
Iron-III-chloride hexahydrate ($FeCl_3$ x $6H_2O$)	Roth (Karlsruhe, Germany)
Isopropanol	Roth (Karlsruhe, Germany)
Low cross buffer	Candor Biosciences (Wangen, Germany)
Magnesium chloride ($MgCl_2$)	Roth (Karlsruhe, Germany)
Membrane amersham hybond 0.45 µM *polyvinylidene difluoride* (PVDF)	VWR (Darmstadt, Germany)
Methanol	Roth (Karlsruhe, Germany)
Midazolam	Roche (Grenzach-Wyhlen, Germany)
Midori Green™ Advanced DNA stain	Nippon Genetics Europe (Düren, Germany)
Naloxon	Delta Select (Pfullingen, Germany)
Nonidet P-40 (NP-40)	Roche Diagnostics (Mannheim, Germany)
N Protein Standard SL	Siemens Healthcare Diagnostics Products GmbH (Marburg, Germany)
NuPAGE® Novex® 4-12% Bis-Tris Gels, 1 mm, 10 well, 15 well	Life Technologies (Darmstadt, Germany)
PageRuler® prestained protein ladder	Fermentas (St. Leon-Rot, Germany)
Paraformaldehyde (PFA)	Roth (Karlsruhe, Germany)
Penicillin/Streptomycin	Gibco (Karlsruhe, Germany)
Phenol/chloroform/isoamyl alcohol	Roth (Karlsruhe, Germany)
Phenylmehtylsulfonyl fluoride (PMSF)	Sigma-Aldrich (Schnelldorf, Germany)
Polyethylene glycol 1500	Sigma-Aldrich (Schnelldorf, Germany)
Potassium chloride (KCl_2)	Roth (Karlsruhe, Germany)
Powdered milk, blotting grade, fat free	Roth (Karlsruhe, Germany)
Prostacyclin (PGI_2)	Sigma-Aldrich (Schnelldorf, Germany)
Protease inhibitor cocktail	Sigma-Aldrich (Schnelldorf, Germany)
Proteinase K, recombinant, PCR grade (20 mg/ml)	Life Technologies (Darmstadt, Germany)
Protein G sepharose	Amersham (Freiburg, Germany)
Puromycin	Life Technologies (Darmstadt, Germany)
R-phycoerythrin (PE)	EUROPA (Cambridge, UK)
Rhodocytin	provided by J. Eble (University of Münster, Münster, Germany)
Roswell Park Memorial Institute (RPMI) 1640 medium	Gibco (Karlsruhe, Germany)

Rotiphorese® Gel 30 acrylamide	Roth (Karlsruhe, Germany)
SKF solution for Horm collagen	Takeda (Linz, Austria)
Sodium azide (NaN_3)	Sigma-Aldrich (Schnelldorf, Germany)
Sodium chloride (NaCl)	AppliChem (Darmstadt, Germany)
Sodium citrate	AppliChem (Darmstadt, Germany)
Sodium dihydrogen phosphate monohydrate ($NaH_2PO_4 \times H_2O$)	Roth (Karlsruhe, Germany)
Sodium dodecyl sulphate (SDS)	Roth (Karlsruhe, Germany)
Sodium hydroxide (NaOH)	AppliChem (Darmstadt, Germany)
Sodium orthovanadate (Na_3VO_4)	Sigma-Aldrich (Schnelldorf, Germany)
Spectra™ multicolor high range protein ladder	Life Technologies (Darmstadt, Germany)
Stop solution OSFA	Siemens Healthcare (Erlangen, Germany)
Sulphuric acid	Roth (Karlsruhe, Germany)
10x Taq Buffer (+KCl, -$MgCl_2$)	Life Technologies (Darmstadt, Germany)
Taq DNA polymerase (# EP0282)	Life Technologies (Darmstadt, Germany)
2,3,5-triphenyltetrazolium (TTC)	Sigma-Aldrich (Schnelldorf, Germany)
3,3',5,5'-Tetramethylbenzidine (TMB)	EUROPA (Cambridge, UK)
Tetramethylethylendiamine (TEMED)	Roth (Karlsruhe, Germany)
Thrombin from human plasma	Roche Diagnostics (Mannheim, Germany)
Thrombin from human plasma	Sigma-Aldrich (Schnelldorf, Germany)
Thrombin calibrator	Stago (Paris, France)
Tissue-Tek®	Sakura (Alphen aan den Rijn, The Netherlands)
Tris(hydroxymethyl)-aminomethane (TRIS) ultra	Roth (Karlsruhe, Germany)
TRIS/HCl	Roth (Karlsruhe, Germany)
Triton X-100	Sigma-Aldrich (Schnelldorf, Germany)
TRIzol®	Life Technologies (Darmstadt, Germany)
0.05% Trypsin-EDTA	Gibco (Karlsruhe, Germany)
Tween 20®	Roth (Karlsruhe, Germany)
U46619	Alexis Biochemicals (San Diego, USA)
Western Lightning Plus-ECL, enhanced chemiluminescence substrate	PerkinElmer (Waltham, MA, USA)
Z-Gly-Gly-Arg-AMC-HCL	Bachem (Bubendorf, Switzerland)

All enzymes were purchased from Life Technologies (Darmstadt, Germany) or New England Biolabs (NEB, Ipswich, MA, USA). Primers were purchased from Metabion (Planegg-Martinsried, Germany) or MWG-Eurofins (Ebersberg, Germany). *Annexin V* (Anxa5) was generously provided by Jonathan F. Tait (Medical Center Washington, USA) and conjugated in our laboratory. Recombinant P-selectin was previously generated and purified by Dr. David Stegner in our laboratory.

Soluble human GPV was kindly provided by CSL Behring (Marburg, Germany) or Prof. Renhao Li (Emory University, Atlanta, USA).

All non-listed standard reagents were purchased from AppliChem (Darmstadt, Germany), Roth (Karlsruhe, Germany) or Sigma-Aldrich (Schnelldorf, Germany).

2.1.2 Cell lines

CHO-GPV-EX-Flag	Genecopoeia (Rockville, USA)
SP2/0 AG14 myeloma cells	DMSZ (Braunschweig, Germany)

2.1.3 Material for purification of smGPV

Äkta pure	GE Healthcare (Chicago, USA)
Unicorn 7 (software)	GE Healthcare (Chicago, USA)
Superdex 200 Increase 10/300 GL	GE Healthcare (Chicago, USA)
Superdex 200 Increase 5/150GL	GE Healthcare (Chicago, USA)
Superdex 75 Increase	GE Healthcare (Chicago, USA)
HiTrap Capto ion exchange selection kit	GE Healthcare (Chicago, USA)
HiTrap Q FF anion exchange chromatography column	GE Healthcare (Chicago, USA)

2.1.4 Antibodies

2.1.4.1 Purchased primary and secondary antibodies

Antibodies	**Source**
Donkey anti-rat IgG FITC (# 112095068)	Jackson ImmunoResearch (West Grove, PA, USA)

Donkey anti-rabbit IgG HRP, MinX (# 711035152)	Jackson ImmunoResearch (West Grove, PA, USA)
Donkey anti-rat IgG HRP (# 712035153)	Jackson ImmunoResearch (West Grove, PA, USA)
Goat anti-human albumin IgG	Biomol (Hamburg, Germany)
Goat anti-human albumin IgG HRP	Biomol (Hamburg, Germany)
Goat anti-mouse IgG HRP, MinX	Dianova (Hamburg, Germany)
Goat anti-rabbit IgG HRP (# 7074)	Cell Signaling (Danvers, MA; USA)
Hamster anti-mouse/rat CD29 (β1-Integrin)-FITC (clone HMβ1-1) (# 102206)	BioLegend (Fell, Germany)
Mouse anti-Flag® HRP	Sigma-Aldrich (Schnelldorf, Germany)
Mouse anti-Flag® M2	Sigma-Aldrich (Schnelldorf, Germany)
Mouse anti-human GPV (sc271662)	Santa Cruz (Dallas, USA)
Platelet depletion antibody (# R300)	Emfret Analytics (Eibelstadt, Germany)
Polyclonal rabbit anti-human vWF (# A0082)	DAKO (Hamburg, Germany)
Rabbit anti-actin (# A2066)	Sigma-Aldrich (Schnelldorf, Germany)
Rabbit anti-GAPDH (# 9545)	Sigma-Aldrich (Schnelldorf, Germany)
Rabbit anti-human albumin (EPSISR1)	Abcam (Cambridge, UK)
Rabbit anti-human albumin (EPSISR3)	Abcam (Cambridge, UK)
Rabbit anti-mouse IgG FITC	DAKO (Hamburg, Germany)
Rabbit anti-mouse IgG HRP (# P026002-2)	DAKO (Hamburg, Germany)
Rabbit anti-sheep IgG HRP	Dianova (Hamburg, Germany)
Rat anti-mouse tubulin (MAB1864)	Chemicon (Hofheim, Germany)
Sheep anti-mouse GPV	R&D Systems (Wiesbaden, Germany)

2.1.4.2 In-house generated monoclonal antibodies

Antibody	Clone	Isotype	Antigen	Described in
BAR-1	25B11	IgG1	α5 integrin	[221]
ULF3	96H10	IgG2b	CD9	unpublished
DOM2	89F12	IgG2a	mGPV	[222]
DOM1	89H11	IgG1	mGPV	[222]
	85H5	IgG1	mGPV	unpublished
	93H12	IgG2a	mGPV	unpublished
	5G2	IgG1/2a	mGPV	unpublished

	10C10	IgG1	hGPV	unpublished
EDL1	57B10	IgG2a	β3 integrin	[222]
INU1	11E9	IgG1	CLEC-2	[80]
JAQ1	98A3	IgG2a	GPVI	[67]
JER1	10B6	IgG2a	CD84	[223]
JON/A	4H5	IgG2b	GPIIb/IIIa	[224]
JON6	14A3	IgG2b	GPIIb/IIIa	unpublished
LEN1	12C6	IgG1	α2 integrin	[60]
LEN/B	23C11	IgG2b	α2 integrin	[225]
p0p/B	57E12	IgG2a	GPIb	[182]
p0p1	3G6	IgG1	GPIbβ	[226]
p0p4	15E2	IgG2b	GPIb	[222]
p0p6	56F8	IgG1	GPIX	[222]
ULF1	97H1	IgG2a	CD9	[222]
WUG1.9	5C8	IgG1	P-selectin	unpublished

2.1.5 Buffer solutions and media

If not stated otherwise, all buffers were prepared in deionized water obtained from a MilliQ Water Purification System (Millipore, Schwalbach, Germany), pH was adjusted with HCl or NaOH.

Binding buffer (for smGPV purification), pH 7.3

NaCl	150 mM
HEPES	30 mM
Glycerol	10%
NP-40	0.1%
Protease inhibitor cocktail	1:100

Blocking solution for Western blot

BSA or fat-free dry milk	5%
in TBS-T	

Blocking buffer for ELISA

BSA or fat-free dry milk	5%
in PBS	

CHO-GPV-EX growth medium

FCS	1%
Ham's F12 medium	99%
Puromycin	7 µg/ml

CHO-GPV-EX purification medium

RPMI1640	
Puromycin	7 µg/ml

Coating buffer (ELISA), pH 9.0

$NaHCO_3$	50 mM

Coomassie staining solution

Acetic acid	10%
Methanol	40%
Coomassie brilliant blue	0.01%

Coomassie destaining solution

Acetic acid	10%
Methanol	40%

Feeder cell Medium

RPMI	

Freezing medium (CHO-GPV-EX cells)

FCS	50%
Ham's F12 medium	40%
DMSO	10%

Fluorescent thrombin substrate buffer (thrombin generation assay)

Z-GGR-AMC	2.5 mM
HEPES	20 mM
NaCl	140 mM
$CaCl_2$	200 mM
BSA	6%

HBS buffer, pH 7.6

HEPES	50 mM
NaCl	150 mM

***Immunoprecipitation* (IP) buffer, pH 8.0**

TRIS	15 mM
NaCl	155 mM
EDTA	1 mM
NaN_3	0.005%
NP-40	1%
Protease inhibitor cocktail	1%

HAT Medium

FCS	10%
Penicillin/Streptomycin	1%
HAT (50x)	1x

Laemmli sodium dodecyl sulfate (SDS) sample buffer (4x)

TRIS/HCl, pH 6.8	200 mM
Glycerol	40%
SDS	8%
Bromophenol blue (3',3'',5',5''-tetrabromophenolsulfonphthalein)	0.04%
β-mercaptoethanol (for reducing conditions)	20%

Laemmli running buffer for SDS-PAGE

TRIS	0.25 M
Glycine	1.92 M
SDS	35 mM

Loading dye solution (6x) for analysis of PCR products

Tris buffer (150 mM)	33%
Glycerol	60%
Bromophenol blue (3',3'',5',5''-tetrabromophenolsulfonphthalein)	0.04%

Lysis buffer (for DNA isolation), pH 7.2

TRIS base	100 mM
EDTA	5 mM
NaCl	200 mM
SDS	0.2%
Proteinase K (to be added directly before use)	100 µg/ml

MES buffer, pH 6.0

MES	50 mM
NaCl	50 mM

***3-(N-morpholino) propanesulfonic acid* (MOPS) buffer (20x)**

MOPS	1 M
TRIS base	1 M
SDS	69.3 mM
EDTA	20.5 mM

PHEM buffer, pH 6.8

PIPES	100 mM
HEPES	5.25 mM
EGTA	10 mM
$MgCl_2$	20 mM
NP-40	0.1%

PFA	1%

***Phosphate buffered saline* (PBS), pH 7.14**

NaCl	137 mM
KCl	2.7 mM
KH_2PO_4	1.5 mM
Na_2HPO_4 x 2 H_2O	8 mM

***Platelet rich plasma* (PRP) reagent (Thrombin generation assay)**

HEPES	20 mM
NaCl	140 mM
BSA	0.5%
Tissue factor (TF)	3 pM

***Red blood cell* (RBC) buffer, pH 7.4**

HEPES	10 mM
NaCl	140 mM
Glucose	5 mM

Separating gel buffer (Western Blot), pH 8.8

TRIS/HCl	1.5 M

Sodium citrate, pH 7.0

Sodium citrate	0.129 M

Stacking gel buffer (Western Blot), pH 6.8

TRIS/HCl	0.5 M

Stripping buffer (“mild”), pH 2.0

SDS	1%
Glycine	25 mM
in HCl/PBS	

TAE buffer, 50x, pH 8.0

TRIS	0.2 M
Acetic acid	5.7%

EDTA (0.5 M, pH 8.0)	10%
TBS-T (Wash buffer for Western Blot), pH 7.2	
Tween 20	0.1%
in TBS	
Transfer buffer (semi-dry blot)	
TRIS ultra	48 mM
Glycine	39 mM
Methanol	20%
TE buffer, pH 8.0	
TRIS base	10 mM
EDTA	1 mM
***Tris-buffered saline* (TBS), pH 7.3**	
NaCl	137 mM
TRIS/HCl	20 mM
Tyrode's buffer, pH 7.4	
NaCl	137 mM
KCl	2.7 mM
$NaHCO_3$	12 mM
NaH_2PO_4	0.43 mM
$CaCl_2$	0, 1 or 2 mM
$MgCl_2$	1 mM
HEPES	5 mM
BSA (to be added directly before use)	0.35%
Glucose (to be added directly before use)	0.1%
Wash buffer (for ELISA), pH 7.2	
NaCl	300 mM
Tween-20	0.05%
in PBS	

Wash buffer (for smGPV purification), pH 7.3

NaCl	150 mM
HEPES	30 mM
Glycerol	10%
NP-40	0.1%
Triton-X100	0.1%

2.1.6 Animals

Specific-pathogen free female mice (NMRI Ex-Breeder, C57Bl/6J) and rats (Wistar) were obtained from Charles River (Sulzfeld, Germany) or Janvier (Le Genest-Saint-Isle, France).

2.1.6.1 Genetically modified mice

Gp5$^{-/-}$ mice [144] were kindly provided by Prof. François Lanza (Inserm-Université de Strasbourg, Strasbourg, France). *Gp5*$^{Kin/Kin}$ mice, which carry a point mutation in the thrombin cleavage site of GPV, and *Gp5*$^{hGp5/hGp5}$ mice, where the murine extracellular domain is replaced by the human extracellular domain of GPV, were generated as described (see Figure 3-16 and Figure 3-26). *Gp5*$^{Kin/Kin}$ and *Gp5*$^{hGp5/hGp5}$ mice were intercrossed with Flip-positive mice to delete the Neo-cassette. *Gp5*$^{Kin/Kin}$ mice were initially on a mixed Sv129/C57Bl/6J background and backcrossed to C57Bl/6J background. *Gp5*$^{-/-}$ and *Gp6*$^{-/-}$ mice were intercrossed by Dr. David Stegner to obtain double-deficient mice.

Gp6$^{-/-}$ mice were generated by Dr. Markus Bender in the laboratory as described previously [73]. *Clec1b*$^{fl/fl}$ mice [85] were kindly provided by Prof. Steve P. Watson (University of Birmingham, Birmingham, UK). *Syk*$^{fl/fl}$ mice [56] were kindly provided by Prof. Friedemann Kiefer (Max-Planck-Insitute for Molecular Biomedicine, Münster, Germany). *RhoA*$^{fl/fl}$ [227] and *Cdc42*$^{fl/fl}$ [228] mice were kindly provided by Prof. Cord Brakebusch (University of Copenhagen, Copenhagen, Denmark). *Prkci*$^{fl/fl}$ mice [118] were kindly provided by PD Michael Leitges (PKC Research Consult, Köln, Germany). To generate MK-/platelet-specific knockout mice, the floxed mice were intercrossed with mice carrying the Cre recombinase under control of the Pf4 (platelet factor) promoter. *Talin*$^{fl/fl,Pf4\text{-}Cre}$ [229], *Gp1ba-tg* [124] and Munc13-4 knockout (*Unc13d*$^{-/-}$) [230] mice were described previously.

All animal studies were approved by the District Government of Lower Franconia (Bezirksregierung Unterfranken, Würzburg, Germany).

2.2 Methods

2.2.1 Production of monoclonal antibodies

2.2.1.1 Immunization of mice

To generate mouse anti-GPV antibodies, *Gp5*$^{-/-}$ mice, 8 weeks of age, were immunized with either of the following antigens: washed WT (wildtype) mouse platelets, purified recombinant soluble murine GPV (smGPV) or immunoprecipitate from WT platelet lysates using 89H11 to generate a mouse anti-mouse antibody or with purified soluble human GPV (shGPV) to generate a mouse anti-human GPV antibody. For this, 0.5 x 10^9 washed mouse platelets (resting state, resuspended in sterile PBS) were used per mouse for each immunization. Alternatively, immunoprecipitate from WT platelet lysates with 89H11 was used (lysate from 0.5 x 10^9 washed mouse platelets, pull-down with 5 µg/ml 89H11 and 50 µl protein G sepharose per mouse). In addition, 50 µg/mouse purified smGPV was used for immunization. The antigen was solved in Freund's adjuvans (Freund's adjuvans complete for the first immunization and Freund's adjuvans incomplete for all following immunizations). The antigen was injected subcutaneously (s. c.) under isoflurane anesthesia. The immunization was repeated at least 5 times at an interval of 3-4 weeks.

2.2.1.2 Immunization of rats

To generate rat anti-GPV antibodies, three female WISTAR rats, 6 weeks of age, were repeatedly immunized with 100 µg shGPV/rat, which was kindly provided by CSL Behring (Marburg, Germany). The antigen was solved in Freund's adjuvans complete for the first immunization and Freund's adjuvans incomplete for all following immunizations and injected subcutaneously (s. c.) under isoflurane anesthesia. The immunization was repeated at least 5 times at an interval of 3-4 weeks.

2.2.1.3 Preparation of feeder cells

NMRI ex-breeder mice were used for preparation of feeder cells. 1 ml sterile prewarmed PBS was injected intraperitoneally per mouse. Migrated immune cells (= feeder cells, mostly macrophages) were collected 10-16 h after PBS injection. Mice were decapitated and the peritoneum exposed without damaging. To collect feeder cells, 12 ml feeder cell medium was injected into the peritoneum and withdrawn again without injuring the intestines. The medium containing immune cells was filled up to 50 ml using feeder cell medium. 100 µl/well were seeded into a 96-well plate and checked for contamination after two days.

2.2.1.4 Generation of hybridoma cells

The mouse or rat spleen was removed under sterile conditions and filtered through a 100 µm cell strainer to obtain a single cell suspension. The spleen cell suspension was washed twice by centrifugation at 900 rpm for 5 min using feeder cell medium. After the last washing step, the pellet was resuspended in 5 ml feeder cell medium. Meanwhile, mouse myeloma cells (Ag14, 10^8 cells per fusion) were collected, mixed with the washed splenic cells and again washed twice using feeder cell medium at 900 rpm for 5 min. The supernatant was removed carefully and 1 ml polyethylene glycol (PEG) 1500, warmed up to 37°C, was added drop-wise over a time of 2 min. This was followed by a slow addition of 10 ml feeder cell medium (37°C) over a time of 10 min. The fused spleen/Ag14 cells were filled up to 50 ml with HAT medium to select only the fused hybridoma cells which solely survive in this medium. 100 µl/well were seeded onto the feeder cells. 10 and 15 96-well plates were seeded per fused mouse and rat spleen, respectively. The cells were grown at 37°C, 5% CO_2.

2.2.1.5 Screening of hybridoma clones by flow cytometry

To detect hybridoma clones producing monoclonal antibodies (mAbs) against the desired antigen (mGPV, hGPV), hybridoma supernatant was tested by flow cytometry. 80 µl hybridoma supernatant was incubated with 50 µl diluted washed blood for 15 min at RT. WT and *Gp5*$^{-/-}$ blood was used to screen for anti-mouse GPV antibodies, WT and *Gp5*$^{hGp5/hGp5}$ blood to screen for anti-human GPV antibodies. For washing, 1 ml PBS was added and the samples centrifuged at 1800 rpm for 5 min. After discarding the supernatant, the samples were incubated with 50 µl 1:35 diluted rabbit anti-mouse FITC (for antibodies generated in mice) or donkey anti-rat FITC (for antibodies generated in rats) for 15 min at RT in the dark. Afterwards, the reaction was stopped with 500 µl PBS and the samples analyzed on a FACS Calibur (Becton Dickinson, Heidelberg, Germany).

2.2.1.6 Subcloning and large-scale production of antibodies

Positive hybridoma clones were subcloned twice and allowed to adapt to FCS-free medium (RPMI) in tissue culture flasks (T175). Positive hybridoma clones that stably expressed desired monoclonal anti-GPV antibodies were cultured at 37°C and 5% CO_2 until 4 l of medium containing the secreted antibody was collected. The medium was sterile filtered and approximately 13 mg antibody was purified from the medium via affinity chromatography using an immobilized protein G column. Bound antibodies were eluted from the column using elution

buffer and collected into supplied neutralization buffer to prevent precipitation of the antibody. Eluted antibodies were dialyzed against PBS *over night* (o/n) at 4°C.

2.2.2 CHO-GPV-EX-Flag cell line

2.2.2.1 Generation of the stable CHO-GPV-EX-Flag cell line

The extracellular domain of murine GPV was cloned into the Mm02808-M13 plasmid.

Construction of the EX-Mm02808-M13 plasmid (blue = signaling peptide):

ATGCTAAGAAGCGCCCTGCTGTCCGCGGTGCTCGCACTCTTGCGTGCCCAACCTTTTCCCTGCCCCAA
AACCTGCAAGTGTGTGGTCCGCGATGCCGCGCAGTGCTCGGGCGGCAGCGTGGCTCACATCGCTGAGC
TAGGTCTGCCTACGAACCTCACACACATCCTGCTCTTCCGAATGGACCAGGGCATATTGCGGAACCAC
AGCTTCAGCGGCATGACAGTCCTTCAGCGCCTGATGCTCTCAGATAGCCACATTTCCGCCATCGACCC
CGGCACCTTCAATGACCTGGTAAAACTGAAAACCCTCAGGTTGACGCGCAACAAAATCTCTCGTCTTC
CACGTGCGATCCTGGATAAGATGGTACTCTTGGAACAGCTGTTCTTGGACCACAATGCACTAAGGGAC
CTTGATCAAAACCTGTTTCAGCAACTGCGTAACCTTCAGGAGCTCGGTTTGAACCAGAATCAGCTCTC
TTTTCTTCCTGCTAACCTTTTCTCGAGCCTGAGAGAACTGAAGTTGTTGGATTTATCGCGAAACAACC
TGACCCACCTGCCCAAGGGACTGCTTGGGGCTCAAGTTAAGCTTGAGAAACTGCTGCTCTATTCAAAC
CAGCTCACGTCTGTGGATTCGGGGCTGCTGAGCAACCTGGGCGCCCTGACTGAGCTGCGGCTGGAGCG
GAATCACCTCCGCTCCGTAGCCCCGGGTGCCTTCGACCGCCTCGGAAACCTGAGCTCCTTGACTCTAT
CCGGAAACCTCCTGGAGTCTCTGCCGCCCGCGCTCTTCCTTCACGTGAGCAGCGTGTCTCGGCTGACT
CTGTTCGAGAACCCCCTGGAGGAGCTCCCGGACGTGTTGTTCGGGGAGATGGCCGGCCTGCGGGAGCT
GTGGCTGAACGGCACCCACCTGAGCACGCTGCCCGCCGCTGCCTTCCGCAACCTGAGCGGCTTGCAGA
CGCTGGGGCTGACGCGGAACCCGCGCCTGAGCGCGCTCCCGCGCGGCGTGTTCCAGGGCCTACGGGAG
CTGCGCGTGCTCGCGCTGCACACCAACGCCCTGGCGGAGCTGCGGGACGACGCGCTGCGCGGCCTCGG
GCACCTGCGCCAGGTGTCGCTGCGCCACAACCGGCTGCGGGCCCTGCCCCGCACGCTCTTCCGCAACC
TCAGCAGCCTCGAGAGCGTGCAGCTAGAGCACAACCAGCTGGAGACGCTGCCAGGAGACGTGTTCGCG
GCTCTGCCCCAGCTGACCCAGGTCCTGCTGGGTCACAACCCCTGGCTCTGCGACTGTGGCCTGTGGCC
CTTCCTCCAGTGGCTGCGGCATCACCCGGACATCCTGGGCCGAGACGAGCCCCCGCAGTGCCGTGGCC
CGGAGCCACGCGCCAGCCTGTCGTTCTGGGAGCTGCTGCAGGGTGACCCGTGGTGCCCGGATCCTCGC
AGCCTGCCTCTCGACCCTCCAACCGAAAATGCTCTGGAAGCCCCGGTTCCGTCCTGGCTGCCTAACAG
CTGGCAGTCCCAGACGTGGGCCCAGCTGGTGGCCAGGGGTGAAAGTCCCAATAACAGG-Flag tag
(DYKDDDDK)

To guarantee a stable cell pool, the extracellular domain of GPV was cloned from the CS-Mm02808-M13 into the pEZ-Mm02808-Lv203 vector and stably transfected into *Chinese hamster ovary K1* (CHO-K1) cells using a lentiviral approach. The stable transducted cell pool

was selected using puromycin. The stable cell line expresses the extracellular domain of GPV fused to a Flag-tag (CHO-GPV-EX-Flag). The protein (further referred to as smGPV) is secreted into the cell culture supernatant.

2.2.2.2 Cultivation of CHO-GPV-EX cells

Adherent CHO-GPV-EX-Flag cells were initially grown in Ham's F12 medium (containing 10% FCS and 7 µg/ml puromycin) at 37°C, 5% CO_2. The FCS concentration was gradually reduced to a final concentration of 1% FCS. Cells were grown in a monolayer in a T175 polystyrene flask. When cells had grown to 80-90% confluency, they were split into 5 separate tissue culture flasks. For this, cell culture medium was removed and the cells washed with PBS. To detach the cells, they were incubated with 1 ml trypsin/EDTA for 5 min at 37°C. The cells were collected with 10 ml Ham's F12 medium and centrifuged at 900 rpm for 5 min. The pellet was resuspended in 5 ml Ham's F12 medium and transferred to a new culture flask already containing 50 ml culture medium.

2.2.2.3 Freezing and thawing of CHO-GPV-EX cells

CHO-GPV-EX cells were grown until 80-90% confluency, trypsinized as described (2.2.2.2), spun down and the pellet was resuspended in 2 ml ice-cold freezing medium. Cell suspension aliquots of 1 ml in Cryo-tubes were immediately put on dry ice and stored in liquid N_2.

Frozen CHO-GPV-EX cells were shortly thawed at 37°C and resuspended in Ham's F12 growth medium. After centrifugation at 900 rpm for 5 min, the cells were resuspended in fresh Ham's F12 growth medium. Cells were grown in Ham's F12 growth medium in a T75 flask at 37°C, 5% CO_2.

2.2.2.4 Preparation of CHO-GPV-EX cell culture supernatant for protein purification

CHO-GPV-EX cells were grown to confluency and then further incubated for 3-4 weeks at 37°C, 5% CO_2 to maximize protein production and secretion into the cell culture supernatant. After 3-4 weeks, the supernatant was collected, centrifuged at 900 rpm for 5 min and sterile filtered.

2.2.2.5 Purification of smGPV from CHO-GPV-EX cell culture supernatant using anti-Flag M2 affinity gel

300 ml sterile filtered cell culture supernatant was concentrated down to approximately 20 ml using Centricons with a cut-off at 30 kDa and spun down at 3000 rpm for 10 min at 4°C to remove aggregated protein. The supernatant was mixed 1:1 with binding buffer. After washing of 700 µl anti-Flag M2 affinity gel 3 times with 1 ml protein purification wash buffer (2500 rpm for 1 min), the gel was added to the diluted cell culture supernatant and rotated for 90 min at 4°C. The gel was spun down, the supernatant removed and the gel was washed again 3 times with 20 ml wash buffer (3000 rpm for 2 min at 4°C). Following the last washing step, the gel was resuspended in 700 µl wash buffer. The bound GPV protein was competitively eluted with 70 µl 5 mg/ml Flag-peptide for 45 min at 4°C. The sample was spun down for 1 min. The supernatant contained the purified smGPV, which was dialyzed against PBS for at least 24 h at 4°C and stored at -80°C.

2.2.3 Mouse genotyping

2.2.3.1 Mouse genotyping using flow cytometry

Gp5$^{-/-}$ and *Gp6*$^{-/-}$ as well as *Gp5*$^{-/-}$/*Gp6*$^{-/-}$ DKO (double knockout) mice were genotyped using flow cytometry. To determine the surface expression levels of GPV or GPVI, mice were bled from the retro-orbital plexus to 50 µl in 300 µl heparin. 50 µl of the 1:10 diluted whole mouse blood was incubated with FITC-conjugated anti-GPV antibody 89H11 or anti-GPVI antibody JAQ1 for the respective single knockout mice and with both for the *Gp5*$^{-/-}$/*Gp6*$^{-/-}$ DKO mice using saturating antibody concentrations for 15 min at RT. The reaction was stopped with 500 µl PBS and analyzed on a FACSCalibur (Becton Dickinson, Heidelberg, Germany).

2.2.3.2 Isolation of genomic DNA from mouse ears

Ear punches were lysed in 500 µl lysis buffer containing 100 µg/ml Proteinase K. The samples were incubated at 56ºC and constantly shaken o/n at 900 rpm or for 3 h at 14000 rpm (Eppendorf Thermomixer). Phenol/chloroform/isoamyl alcohol mixture (25:24:1) (500 µl) was added to each sample to remove cellular proteins and lipids and, after vigorous shaking, samples were centrifuged at 10000 rpm for 10 min at room temperature (RT) in an Eppendorf 5417R tabletop centrifuge. After centrifugation, the aqueous nucleic acid containing upper phase (approximately 450 µl) was transferred into a new tube containing 500 µl isopropanol to precipitate the DNA/RNA. The samples were vigorously shaken and centrifuged at 14000 rpm for 10 min at 4°C. The resulting DNA pellet was washed and dehydrated with 500 µl 70%

ethanol by centrifugation at 14000 rpm for 10 min at 4°C. The pellet was dried at 37°C and finally solubilized in 50 µl TE buffer at 37°C under shaking conditions (350 rpm). 1-2 µl of DNA was used for a polymerase chain reaction (PCR).

2.2.3.3 Mouse genotyping using PCR

Genotyping was accomplished by PCR using different mixtures of primers and PCR programs as indicated below.

Pipetting scheme for detection of the *Gp5^{Kin}* allele by PCR (25 µl final volume)

1 µl	DNA template
2.5 µl	10x Taq buffer (+ KCl, - $MgCl_2$)
2.5 µl	$MgCl_2$ (stock: 25 mM)
0.4 µl	dNTPs (stock: 10 mM)
1 µl	forward primer (1:10 diluted in H_2O, stock: 100 pM)
1 µl	reverse primer (1:10 diluted in H_2O, stock: 100 pM)
0.25 µl	Taq polymerase (5 U/µl)
15.75 µl	H_2O

Primers to genotype *Gp5$^{Kin/Kin}$* mice:

Gp5^{Kin} fwd: 5’ – TTC ATC TGG AGA AGC CCT GT – 3’

Gp5^{Kin} rev: 5’ – CAC TGG AAA CCA AGC TGT CA – 3’

Resulting band sizes:

WT locus: 197 bp

Floxed locus: 265 bp (after deletion of the Neo-cassette)

Program for *Gp5*$^{Kin/Kin}$ PCR:

96ºC	3 min	
94ºC	0:30 min	35 cycles
60.5ºC	0:30 min	
72ºC	1 min	
72ºC	10 min	
4ºC	∞	

Pipetting scheme for detection of the Gp5^{hGp5} allele by PCR (25 µl final volume)

PCR hGPV (before deletion of the Neo-cassette)

1 µl	DNA template
2.5 µl	10x Dream Taq buffer (+ KCl, - $MgCl_2$)
0.5 µl	$MgCl_2$ (stock: 25 mM)
1 µl	dNTPs (stock: 10 mM)
1 µl	forward primer (1:10 diluted in H_2O, stock: 100 pM)
1 µl	reverse primer (1:10 diluted in H_2O, stock: 100 pM)
0.13 µl	Dream Taq polymerase (0.5 U/ml)
17.87 µl	H_2O

Primers for genotyping of *Gp5*^{hGp5} mice:

GPV-FRT_fwd: 5’ – CTC CTG TGT GTT GTA GCT CG CTC – 3’

GPV-FRT_rev: 5’ – GCT TGT GAA ATG ATG TGG CTG TCA CC – 3’

Resulting band sizes:

mGPV: 222 bp

hGPV: no band (with Neo-cassette still present)

hGPV: 307 bp (after deletion of the Neo-cassette)

Program for *Gp5^{hGp5}* PCR:

95ºC	3 min	
95ºC	0:30 min	35 cycles
59.6ºC	0:30 min	
72ºC	1:00 min	
72ºC	10 min	
4ºC	∞	

PCR hGPV (after deletion of the Neo-cassette)

1 µl	DNA template
2.5 µl	10x Taq buffer (+ KCl, - $MgCl_2$)
2.5 µl	$MgCl_2$ (stock: 25 mM)
1 µl	dNTPs (stock: 10 mM)
1 µl	forward primer (1:10 diluted in H_2O, stock: 100 pM)
1 µl	reverse primer mGPV (1:10 diluted in H_2O, stock: 100 pM)
1 µl	reverse primer hGPV (1:10 diluted in H_2O, stock: 100 pM)
0.5 µl	Taq polymerase (5 U/µl)
14.5 µl	H_2O

Primers for genotyping of *Gp5^{hGp5}* mice:

GPV_TG fwd: 5’ – GAT ATG CTC TGA GCC TG TTT TTG C – 3’

mGPV_ rev: 5’ – CGC AAT ATG CCC TGG TCC ATT CG – 3’

hGPV_ rev: 5’ – CAG GTT CTC CAG ATT CGT GAA GAG ACT G – 3’

Resulting band sizes:

mGPV: 237 bp

hGPV: 556 bp (after deletion of the Neo-cassette)

Program for *Gp5*^{hGp5} PCR:

94ºC	2 min	
94ºC	0:30 min	35 cycles
55ºC	0:30 min	
72ºC	0:30 min	
72ºC	10 min	
4ºC	∞	

Pipetting scheme for the Flip PCR (20 µl final volume)

2 µl	DNA template
2.0 µl	10x Taq buffer (+ KCl, - $MgCl_2$)
2.0 µl	$MgCl_2$ (stock: 25 mM)
0.2 µl	dNTPs (stock: 10 mM)
0.1 µl	oIMR0042 (undiluted, stock: 100 pM) – internal control_f
0.1 µl	oIMR0043 (undiluted, stock: 100 pM) – internal control_r
0.1 µl	oIMR1348 (undiluted, stock: 100 pM)
0.1 µl	oIMR1349 (undiluted, stock: 100 pM)
0.25 µl	Taq polymerase (5 U/µl)
13.125 µl	H_2O

Primers for detection of the Neo-cassette (Flp primer):

oIMR0042 (internal control_f): 5’ – CTA GGC CAC AGA ATT GAA AGA TCT – 3’

oIMR0043 (internal control_r): 5’ – GTA GGT GGA AAT TCTAGCATCATCC – 3’

oIMR1348: 5’ – CAC TGA TAT TGT AAG TAG TTT GC – 3’

oIMR1349: 5’ – CTA GTG CGA AGT AGT GAT CAG G – 3’

Resulting band sizes:

WT locus (internal control): 324 bp

WT locus: no band

hGPV: 725 bp (when the Neo-cassette is not yet removed)

Program for the Flip PCR:

94ºC	5 min	
94ºC	0:30 min	} 35 cycles
58ºC	0:30 min	
72ºC	0:45 min	
72ºC	5 min	
4ºC	∞	

Pipetting scheme to genotype *Prkcι/λ$^{fl/fl}$* mice by PCR (25 µl final volume)

1 µl	DNA template
2.5 µl	10x Taq buffer (+ KCl, - $MgCl_2$)
2.5 µl	$MgCl_2$ (stock: 25 mM)
1 µl	dNTPs (stock: 10 mM)
1 µl	PKCι/λ forward primer (1:10 diluted in H_2O, stock: 100 pM)
1 µl	reverse WT primer (1:10 diluted in H_2O, stock: 100 pM)
1 µl	reverse Ko primer (1:10 diluted in H_2O, stock: 100 pM)
0.25 µl	Taq polymerase (5 U/µl)
14.75 µl	H_2O

Primers to genotype *Prkcι/λ$^{fl/fl}$* mice:

PKCι/λ fwd: 5’ – TTG TGA AAG CGA CTG GAT TG – 3’

WT rev: 5’ – AAT TGT TCA TGT TCA ACA CTG CT – 3’

Ko rev: 5’ – CTT GGG TGG AGA GGC TAT TTC – 3’

Resulting band sizes:

WT locus: 355 bp

Floxed locus: 1000 bp

Program for PKCι/λ PCR:

96ºC	3 min	
94ºC	0:30 min	35 cycles
58ºC	0:30 min	
72ºC	1 min	
72ºC	10 min	
4ºC	∞	

Pipetting scheme for detection of the Pf4-Cre transgene by PCR (25 µl final volume)

1 µl	DNA template
2.5 µl	10x Taq buffer (+ KCl, - $MgCl_2$)
2.5 µl	$MgCl_2$ (stock: 25 mM)
1 µl	dNTPs (stock: 10 mM)
1 µl	forward primer (1:10 diluted in H_2O, stock: 100 pM)
1 µl	reverse primer (1:10 diluted in H_2O, stock: 100 pM)
0.25 µl	Taq polymerase (5 U/µl)
15.75 µl	H_2O

Primers:

Pf4-Cre fwd: 5’ – CCC ATA CAG CAC ACC TTT TG – 3’

Pf4-Cre rev: 5’ – TGC ACA GTC AGC AGG TT – 3’

Resulting band sizes:

WT locus: no band

Pf4-Cre positive: 450 bp

Program for Pf4-Cre PCR:

95ºC	5 min	
95ºC	0:30 min	35 cycles
58ºC	0:30 min	
72ºC	0:45 min	
72ºC	5 min	
4ºC	∞	

2.2.3.4 Agarose gel electrophoresis

1.5% agarose gels were prepared by adding 1.5 g agarose to 100 ml 1x TAE buffer. The agarose in TAE buffer was boiled in a microwave. After all agarose was completely dissolved, the TAE-agarose was allowed to cool down to approximately 60°C before 5 µl Midori green per 100 ml solution was added and the fluid was poured into a tray with a comb. The sleigh was laid in a chamber filled with 1x TAE buffer. 4 µl 6x loading dye solution was added to 20 µl DNA and the samples were loaded into the gel slots, a DNA ladder was loaded on each side of the gel to enable size determination of the PCR products. For size separation, DNA samples were run for 45 min at 120-160 V and UV light was used to detect DNA bands after each run.

2.2.3.5 mRNA isolation, cDNA synthesis and reverse transcriptase PCR (RT-PCR)

Washed platelets were prepared as described (2.2.5.4). Platelets from the same genotype were pooled and resuspended in TRIZOL. In parallel, 100 mg brain tissue was homogenized in TRIZOL. Chloroform was added to extract RNA and precipitated by incubation with isopropanol. mRNA was washed twice in 70% ethanol and resuspended in DEPC H_2O containing RNase inhibitor. cDNA synthesis from platelet and tissue mRNA was performed using super script reverse transcriptase III. RT-PCR primers were designed using Primer-Blast [231].

RT-PCR Primer for *Actb* (β-actin):

5’ TAGCTGCGTTTTACACCCT 3’

5’ TTTGGGGGATGTTTGCTCCA 3’

RT-PCR Primer for *Prkcz* (PKCζ):

5’ AGCAGGAGAGCCAACCTTCTA 3’

5’ TCTACTGGAGGCTCTTGGGA 3’

2.2.4 Biochemistry

2.2.4.1 Immunoblotting (Western Blotting)

For Western blot analysis, 2 x 10^6 platelets were resuspended in 100 µl IP buffer containing 1% NP-40 and protease inhibitors. After incubation for 20 min at 4°C and centrifugation at 14000 rpm for 5 min to remove detergent-insoluble debris, the supernatant was mixed with 4x SDS sample buffer and boiled for 5 min at 95°C. Samples were separated by SDS-PAGE on 10% polyacrylamide gels in Laemmli buffer and transferred onto a PVDF membrane for 1 h with 0.8 mA/cm² using semi-dry transfer systems. To prevent unspecific antibody binding, the membrane was blocked with 5% non-fat dried milk powder or 5% BSA in TBS-T for at least 1 h at RT. Membranes were incubated with the required primary antibody (according to the manufacturers’ instructions or with 5 µg/ml) o/nF at 4°C under gentle shaking. Afterwards, membranes were washed three times with TBS-T for 10 min at RT under shaking conditions. Next, membranes were incubated with appropriate HRP-labeled secondary antibodies for 1 h at RT. After three washing steps, proteins were visualized by ECL with autoradiography films. To re-probe a membrane, blots were incubated in stripping buffer for 30 min at RT, washed thoroughly in TBS-T, blocked and subsequently probed with antibodies. Actin or GAPDH levels were used as loading control.

2.2.4.2 Immunoprecipitation

Platelet lysates were prepared as described (2.2.4.1). Detergent-insoluble debris was removed by centrifugation at 14000 rpm for 10 min and the supernatant was pre-cleared with protein G sepharose for 1 h at 4ºC. Samples were rotated with an anti-GPV antibody (5 µg/sample) pre-coated to protein G sepharose for 1 h at 4ºC. Sepharose beads were pelleted, washed 4 times for 5 min with 1x lysis buffer and used for immunization of mice (2.2.1.1).

2.2.4.3 GPV ELISA

96-well plates (Hartenstein, F-Form) were coated with 50 µl/well 89H11 antibody (30 µg/ml) in carbonate buffer o/n at 4°C, blocked with 5% non-fat dried milk in PBS for 2 h at 37°C and

washed 3 times with wash buffer. Samples were prepared as described (2.2.2.5; 2.2.5.1 and 2.2.5.8), applied to plates, incubated for 1 h at 37°C and washed 3 times with wash buffer (200 µl/well). Plates were incubated with HRP-labeled 89F12 antibody for 1, washed again 3 times with wash buffer and developed using TMB substrate. The reaction was stopped by addition of 0.5 M H_2SO_4. Optical density was measured on a Multiskan Ex device (Thermo Electron Corporation, Braunschweig, Germany). Absorbance was read at 450 nm, the 620 nm filter served as reference wavelength. Plasma samples from *Gp5*$^{-/-}$ mice served as negative controls.

2.2.5 *In vitro* analysis of platelet function

2.2.5.1 Plasma preparation

Mice were bled from the retro-orbital plexus under isoflurane anesthesia. Blood was collected in an Eppendorf tube containing either 100 µl heparin in TBS (20 U/ml, pH 7.3) or 50 µl sodium citrate (0.129 M, pH 7), which was filled up after bleeding to obtain a 1:10 dilution of sodium citrate to blood. Subsequently, the blood was centrifuged at 2800 rpm for 5 min, platelet poor plasma was spun down at 14000 rpm for 5 min. Erythrocyte- and debris-free supernatants were either immediately used for experiments or frozen at -20°C for short-term or at -80°C for long-term storage.

2.2.5.2 Preparation of washed blood

To prepare washed blood, 100 µl blood was drawn from the retro-orbital plexus of anesthetized mice using heparinized capillaries, collected in a tube containing 300 µl heparin in TBS (20 U/ml, pH 7.3) and filled up to 1 ml with 1x PBS. To prepare washed blood and remove all heparin, the samples were spun down at 2800 rpm for 5 min at RT, the supernatant was discarded and the blood pellet was resuspended in 1 ml Ca^{2+}-free Tyrode´s buffer. This washing step was repeated once. Finally, the blood pellet was resuspended in 750 µl Tyrode´s buffer with Ca^{2+}.

2.2.5.3 Purification of red blood cells from whole blood

Fresh blood samples of healthy volunteers were collected in 1:10 volume of acid-citrate-dextrose. Murine blood was collected into 300 µl heparin in TBS (20 U/ml, pH 7.3). To purify *red blood cells* (RBCs), the samples were centrifuged at 900 rpm for 10 min, brake 1 (Heraeus Mulitifuge X3 centrifuge). Erythrocytes were resuspended in red blood cells buffer and washed

6 times by centrifuging at 900 rpm for 10 min, brake 1. RBC count was adjusted to 8 x 10^6 cells/µl using a Sysmex KX-21N Hematology Analyzer.

2.2.5.4 Purification of platelets from whole blood of mice

Mice were bled from the retro-orbital plexus under isoflurane anesthesia. Blood was collected in a tube containing either 300 µl heparin in TBS (20 U/ml, pH 7.3) or 50 µl sodium citrate (0.129 M, pH 7), which was filled up after bleeding to obtain a 1:10 ratio of sodium citrate to blood. Subsequently, the blood was centrifuged at 800 rpm (52 x *g*, in an Eppendorf Centrifuge 5415C) for 5 min. Buffy coat and supernatant were transferred to a new tube and centrifuged again at 800 rpm for 5 min to obtain platelet rich plasma (PRP). To prepare washed platelets, PRP was centrifuged at 2800 rpm (639 x *g*) for 5 min at RT in the presence of apyrase (0.02 U/ml) and *prostacyclin* (PGI_2, 0.1 µg/ml). Then, the pellet was resuspended in 1 ml Ca^{2+}-free Tyrode´s buffer containing apyrase (0.02 U/ml) and PGI_2 (0.1 µg/ml). After a second washing step, the platelet pellet was resuspended, the platelet count was determined using a Sysmex KX-21N Hematology Analyzer and adjusted to the desired final concentration for the following experiment. Platelet suspensions were left to incubate for at least 30 min at 37°C prior to analysis.

2.2.5.5 Purification of platelets from whole blood of humans

Studies on human blood were performed according to the declaration of Helsinki and upon informed consent of blood donors. Fresh blood samples of healthy volunteers were collected in 1:10 volume of acid-citrate-dextrose or in heparin and centrifuged at 900 rpm for 10 min, brake 1 (Heraeus Mulitifuge X3 centrifuge). PRP without any erythrocytes was collected and supplemented with 0.02 U/ml apyrase and PGI_2 (0.1 µg/ml). Platelets were washed twice with Tyrode's buffer without Ca^{2+} by centrifuging at 2800 rpm for 10 min (acceleration 1, brake 3). After adjusting the platelet count to 5 x 10^5 cells/µl, platelets were allowed to rest for 30 min at 37°C.

2.2.5.6 Determination of platelet count and size

For determination of platelet count and size, 50 µl blood was drawn from the retro-orbital plexus of anesthetized mice using heparinized microcapillaries and collected into a 1.5 ml reaction tube containing 300 µl heparin in TBS (20 U/ml, pH 7.3). The heparinized blood was filled up with 650 µl PBS (1:20 dilution) and platelet count and size were determined using a Sysmex KX-21N Hematology Analyzer. Alternatively, 50 µl diluted blood was incubated with

fluorophore-conjugated antibodies directed against platelet-specific surface receptors (e.g. *fluorescein isothiocyanate* (FITC)-conjugated anti-GPIb (15E2) and *phycoerythrin* (PE)-conjugated anti-GPIIb/IIIa (14A3) antibodies) and subsequently analyzed using flow cytometry (FACSCalibur, BD Biosciences, Heidelberg, Germany). *Forward scatter* (FSC) and platelet count per second were determined.

2.2.5.7 Flow Cytometry

Platelets were identified by their forward/side scatter (FSC/SSC) characteristics. For a two-color staining, the following settings were used:

Detectors/Amps:

Parameter	Detector	Voltage
P1	FSC	E01
P2	SSC	380
P3	FL1	650
P3	FL2	580
P5	FL3	150

Threshold:

Parameter	Value
FSC-H	253
SSC-H	52
FL1-H	52
FL2-H	52
FL3-H	52

Compensation:

Parameter	Value
FL1	2.4% of FL2
FL2	7.0% of FL1
FL2	0% of FL3
FL3	0% of FL2

2.2.5.7.1 Determination of platelet surface protein expression

To determine glycoprotein surface expression levels, whole blood was diluted 1:20 with Ca^{2+}-free Tyrode's buffer or PBS and stained with saturating amounts of fluorophore-conjugated antibodies for 10 min at RT in the dark. Samples were analyzed directly after addition of 500 µl PBS on a FACSCalibur.

2.2.5.7.2 Platelet integrin activation and degranulation

To measure platelet integrin activation and platelet degranulation responses, washed blood was resuspended in 750 µl Tyrode's buffer with Ca^{2+} and 50 µl of this suspension was activated with the respective agonists (10-fold concentrated) in the presence of saturating amounts of a 1:1 mixture of PE-coupled JON/A (4H5) and FITC-coupled anti-P-selectin (5C8) antibodies. Samples were incubated for 7 min at 37°C and additionally 7 min at RT. The reaction was stopped by addition of 500 µl PBS and samples were analyzed immediately on a FACSCalibur.

2.2.5.7.3 vWF- and fibronectin-binding

To measure vWF- and fibronectin-binding upon platelet activation, whole blood was diluted 1:20 with Tyrode's buffer with Ca^{2+} and activated with 10 µg/ml CRP or 1 µg/ml CVX in the presence of saturating amounts of FITC-conjugated anti-vWF or FITC-conjugated anti-fibronectin antibodies for 7 min at 37°C and for 7 min at RT in the dark. Samples were analyzed directly after addition of 500 µl PBS on a FACSCalibur.

2.2.5.7.4 Phosphatidylserine exposure

Washed platelets were resuspended to a concentration of 5×10^4 platelets/µl in Tyrode's buffer with 5 mM Ca^{2+} and incubated with the indicated agonists for 15 min at 37°C in the presence of saturating amounts of Dylight 488-coupled annexin-A5 and PE-coupled 4H5 antibodies. Reactions were stopped by addition of 500 µl Tyrode's buffer with 2 mM Ca^{2+}, and samples were immediately analyzed on a FACSCalibur.

2.2.5.8 Shedding of glycoproteins from the platelet surface

Washed platelets were adjusted to a concentration of 1×10^6 platelets/µl in Tyrode's buffer without Ca^{2+}. 60 µl platelet suspension was diluted 1:1 with Tyrode's buffer without Ca^{2+} (for

resting and thrombin-stimulated samples) and with Tyrode's buffer with Ca^{2+} (for NEM (2 mM f.c.)-incubated samples). Stimulation with 0.1 U/ml Thrombin was performed in the presence of 40 µg/ml integrilin and 5 µM EGTA to prevent platelet aggregation. Samples were incubated for 30 min at 37°C. Afterwards, 10 µl platelet suspension was diluted 1:20 with PBS and 50 µl of these samples was incubated with saturating amounts of FITC-conjugated platelet surface antibodies. Samples were analyzed directly after addition of 500 µl PBS on a FACSCalibur.

The residual platelet suspension was pelleted by centrifugation at 2800 rpm for 5 min, the supernatant was again centrifuged at 14000 rpm for 5 min and analyzed in a GPV ELISA.

Experiments were conducted in the presence as well as in the absence of the broad range metalloproteinase inhibitor GM6001 (100 µM f.c.).

2.2.5.9 Aggregometry

50 µl washed platelets (with a concentration of 0.5 x 10^6 platelets/µl) or heparinized PRP was transferred into a cuvette containing 110 µl Tyrode's buffer with 2 mM Ca^{2+}. For all measurements with washed platelets, except those with thrombin as agonist, Tyrode's buffer with 100 µg/ml human fibrinogen was used. To measure aggregation responses, agonists (100-fold concentrated) were added and light transmission was recorded over 10 min on an Apact 4-channel optical aggregation system (APACT, Hamburg, Germany). Before starting a measurement, Tyrode's buffer was set as 100% aggregation and washed platelet suspension or PRP was set as 0% aggregation.

2.2.5.10 Luminometric measurement of ATP release

For determination of ATP release, washed platelets were adjusted to a concentration of 0.5 x 10^6/µl in Tyrode's buffer without Ca^{2+}. 80 µl platelet suspension was mixed with 160 µl Tyrode's buffer supplemented with 2 mM Ca^{2+} and 25 µl CHRONO-LUME and incubated for 2 min at 37°C. Platelets were activated with the indicated agonists under stirring conditions (1000 rpm) at 37°C. Light transmission and luminescence were recorded on a 700 Whole Blood/Optical Lumi-Aggregometer (Chrono-log, Lemgo, Germany) over 10 min. Results were expressed in arbitrary units with buffer representing 100% transmission and washed platelet suspension 0% transmission. ATP release was calculated using an ATP standard. All experiments were performed with AggroLink 8 software (Chrono-log, Lemgo, Germany).

2.2.5.11 Static adhesion on human fibrinogen and vWF

Glass coverslips (24 x 60 mm) were coated with 100 µg human fibrinogen or a polyclonal rabbit anti-human vWF antibody (DAKO, Hamburg, Germany) (1:500 diluted in coating buffer) o/n at 4°C under humid conditions. The coverslips were blocked with 1% BSA/PBS for 1 h at RT. For spreading on vWF, blocked coverslips were incubated with murine WT plasma for 2 h at 37°C to allow binding of vWF from the plasma to the immobilized anti-vWF antibody under humid conditions and blocked with 1% BSA/PBS for 1 h at RT. Coverslips were rinsed with Tyrode's buffer. Washed platelets were adjusted to a concentration of 3 x 10^5 cells/µl in Tyrode's buffer without Ca^{2+}. The platelet suspension (50 µl for early time points and 30 µl for late time points filled up to 100 µl with Tyrode's buffer with Ca^{2+}) were left unstimulated or were stimulated with thrombin (0.01 U/ml) and immediately allowed to spread for the indicated time span. Platelets were fixed with 4% PFA in PBS for 5 min at RT and spreading was monitored with a Zeiss Axiovert 200 inverted microscope (100x/1.4 oil objective; Zeiss, Jena, Germany) using *differential interference contrast* (DIC) microscopy. Representative images were taken and evaluated according to different platelet spreading stages using ImageJ software (NIH, Bethesda, MD, USA).

2.2.5.12 Clot retraction

A sample of 700 µl blood was drawn from the retro-orbital plexus of anesthetized mice using non-heparinized capillaries and collected in a tube containing 70 µl 0.129 M sodium citrate. Platelets were washed and *platelet poor plasma* (PPP) as well as erythrocytes were collected. Washed platelets were adjusted to 3 x 10^5 cells/µl in PPP. 1 µl red blood cells (to contrast the clot) and 20 mM $CaCl_2$ were added to 250 µl of the platelet suspension. Clot retraction was induced by addition of 4 U/ml thrombin and samples were monitored at 37°C under non-stirring conditions. Images were taken after 15 min and then every 30 min for 4 h. After 4 h, the volume of the residual serum fluid in the tube was measured.

2.2.5.13 Thrombin generation assay

Thrombin generation was quantified in citrate-anticoagulated PRP with an adjusted platelet count of 1 x 10^5 platelets/µl. PRP preparations from 2-4 mice with the same genotype were pooled. Platelets were activated with the indicated agonists for 15 min at 37°C. After stimulation, samples (4 vol) were transferred to a polystyrene 96-well plate already containing 1 vol of thrombin calibrator or tissue factor (1 pM f.c.). Coagulation was started by adding 1 vol fluorescent thrombin substrate (2.5 mM Z-GGR-AMC). Thrombin generation was measured

according to the calibrated automated thrombogram method as described previously [232, 233]. Samples were run in duplicates. The Thrombinoscope™ software (version 5.0.0.742, ThrombinoscopeBV, Maastricht, The Netherlands) was used to analyze thrombin generation.

2.2.5.14 Flow adhesion experiments on extracellular matrix proteins

2.2.5.14.1 Flow adhesion on collagen

Coverslips (24 x 60 mm) were coated with fibrillar type I collagen (Horm, 200 µg/ml) o/n at 37°C and blocked with 1% BSA/PBS for 1 h at RT. 700 µl blood was collected into 300 µl heparin (20 U/ml in TBS, pH 7.3). Platelets were labeled with a Dylight 488-conjugated anti-GPIX IgG derivative (0.2 µg/ml, mouse platelets) or with 100 nM $DiOC_6$ (human platelets) for 5 min at 37°C. Two parts of blood were mixed with one part Tyrode's buffer with Ca^{2+} and filled into a 1 ml syringe (for shear rates of 150 s^{-1}, 1000 s^{-1} and 1700 s^{-1}) or a 2 ml syringe (for a shear rate of 3000 s^{-1}). Transparent flow chambers with a slit depth of 50 µm, equipped with the coated coverslips, were connected to the syringe which was filled with diluted whole blood. Perfusion was performed using a pulse-free pump under low or high shear equivalent to a wall shear rate of 150 s^{-1}, 1000 s^{-1}, 1700 s^{-1} or 3000 s^{-1} (10 min at 150 s^{-1}, 2 min at 3000 s^{-1}, otherwise 4 min). During perfusion, platelet adhesion was monitored with a Zeiss Axiovert 200 inverted microscope (40x/0.75 air objective) or a Leica DMI6000B inverted microscope (63x/1.3 glycerol HCX PL APO objective, Type G immersion liquid) and images were recorded every second using a CoolSNAP-EZ camera (Zeiss Axiovert 200) or Leica DFC 360 FX (Leica DMI6000B). Thereafter, coverslips were washed with Tyrode's buffer at the same shear rate and for the same perfusion time. Brightfield and fluorescent images were recorded from at least eight different microscope fields (40x or 63x objective). Image analysis was performed off-line using MetaMorph® software (Visitron, Munich, Germany) or Fiji software (Fiji, open source, released under the GPL). Thrombus formation was depicted as the mean percentage of total area covered by thrombi and as the mean integrated fluorescence intensity.

2.2.5.14.2 Reconstituted collagen flow chamber

Washed human or mouse platelets were prepared as described above (2.2.5.4; 2.2.5.5) and the platelet count was adjusted to 5 x 10^5 platelets/µl in Tyrode's buffer without Ca^{2+}. In the meanwhile, RBCs were washed at least 5 times with RBC buffer at 900 rpm for 10 min. To study thrombus formation in the absence of plasma factors, 700 µl washed platelets (1 x 10^5 cells/µl) were mixed with 500 µl washed RBCs (8 x 10^6 cells/µl), 150 µl fibrinogen (0.25 mg/ml) and 2 mM $CaCl_2$ and incubated with a Dylight 488-conjugated anti-GPIX IgG

derivative (0.2 µg/ml, mouse platelets) or with 100 nM $DiOC_6$ (human platelets) for 5 min at 37°C. Flow adhesion experiments were performed as described above (2.2.5.14.1).

2.2.5.14.3 Flow adhesion on vWF

To study platelet adhesion on vWF under flow conditions, glass cover slips were coated with a polyclonal rabbit anti-human vWF antibody (DAKO, Hamburg, Germany) (1:500 diluted in coating buffer) o/n at 4°C under humid conditions. The coverslips were blocked with 1% BSA/PBS for 1 h at RT. Blocked coverslips were incubated with murine WT plasma for 2 h at 37°C to allow binding of vWF from the plasma to the immobilized anti-vWF antibody. Perfusion experiments were performed as described above (2.2.5.14.1). Cell Profiler software was used to analyze the number of adhered platelets per visual field [234, 235].

2.2.5.14.4 Flow adhesion on P-selectin

To study platelet adhesion on P-selectin, glass coverslips (24 x 60 mm) were coated with recombinant P-selectin (10 µg/ml in carbonate buffer) o/n at 4°C under humid conditions. The coverslips were blocked with 1% BSA/PBS for 1 h at RT. Perfusion experiments were performed as described above. Cell Profiler software was used to analyze the number of adhered platelets per visual field [234, 235].

2.2.5.14.5 Procoagulant activity measurement upon flow adhesion on collagen

To measure procoagulant activity, glass cover slips (24 x 60 mm) were coated with 200 µg/ml fibrillar type I collagen (Horm) o/n at 37°C and blocked with 1% BSA/PBS for 1 h at RT. Flow adhesion experiments were performed as described above (2.2.5.14.1), but the used Tyrode's buffer was supplemented with additional 5 U/ml heparin to prevent coagulation. After blood perfusion, 0.25 µg/ml annexin-A5 Dylight 488 in Tyrode's buffer with Ca^{2+} was rinsed over the adherent platelets. Thereafter, coverslips were washed with Tyrode's buffer with Ca^{2+} and 5 U/ml heparin at the same shear rate for 4 min. Brightfield and fluorescent images were taken from at least 10 different microscopic fields, which were randomly chosen, using a Zeiss Axiovert 200 inverted microscope (40x/0.75 air objective) and analyzed offline using MetaMorph® software (Visitron, Munich, Germany). Procoagulant activity was defined as the ratio of surface coverage of PS-exposing platelets (annexin-A5 Dylight 488 staining of platelets) to the total surface area covered by platelets.

2.2.6 *In vivo* analyses of platelet function

2.2.6.1 Determination of platelet life span

To study platelet clearance from the circulation, mice were injected intravenously with 5 µg of a Dylight 488-conjugated anti-GPIX Ig derivative. The anti-GPIX antibody labeled circulating platelets without interfering with platelet activation *in vitro* or *in vivo* [222]. The antibody concentration applied was sufficient to label only already circulating, but not newly generated platelets. The percentage of labeled platelets was measured 1 h after injection (day 0) and then by daily blood withdrawal (50 µl) on a FACSCalibur.

2.2.6.2 Platelet depletion prior to tail bleeding time assay

Thrombocytopenia was induced by intravenous injection of rat anti-GPIbα antibodies (platelet depletion antibody, 0.14-0.18 µg/g body weight). This low dose of platelet depletion antibody should reduce the platelet count to 5-10% of the initial platelet count. Peripheral platelet count was determined by flow cytometry 16 h after platelet depletion (prior to tail bleeding time experiment).

2.2.6.3 Tail bleeding time assay

Mice were anesthetized by intraperitoneal injection of triple anesthesia (Dormitor 0.5 µg/g, Midazolam 5 µg/g, and Fentanyl 0.05 µg/g body weight) and a 1-mm segment of the tail tip was removed using a scalpel. Tail bleeding was monitored by gently absorbing blood on filter paper at 20 s intervals without directly contacting the wound site. When no blood was observed on the paper, bleeding was determined as ceased. The experiment was manually stopped after 20 min by cauterization.

2.2.6.4 Intravital microscopy of thrombus formation in $FeCl_3$-injured mesenteric arterioles

3-to-4-week-old mice were anesthetized and after a midline incision, the mesentery was exteriorized. Arterioles (35-60 µm diameter) were visualized with a Zeiss Axiovert 200 inverted microscope (10x/0.25 air objective) equipped with a 100-W HBO mercury lamp and a CoolSNAP-EZ camera (Visitron, Munich, Gemany). Digital images were recorded and analyzed off-line using MetaMorph software. Endothelial injury was induced by topical application of a 3 mm^2 filter paper saturated with *ferric chloride* ($FeCl_3$; 20%). Adhesion and

aggregation of fluorescently labeled platelets (Dylight 488-conjugated anti-GPIX IgG derivative) in arterioles was monitored for 40 min or until complete occlusion occurred (blood flow stopped for >1 min).

2.2.6.5 Mechanical injury of the abdominal aorta

To open the abdominal cavity of Avertin-anesthetized mice (10-to-16-week-old), a longitudinal midline incision was performed and the abdominal aorta was exposed. A Doppler ultrasonic flow probe (0.5PSB699, Transonic Systems, Maastricht, The Netherlands) was placed around the vessel and thrombus formation was induced by a single firm compression (20 s) with a forceps upstream of the flow probe. Blood flow was monitored over 30 min or until complete occlusion occurred (blood flow stopped for >5 min).

2.2.6.6 Transient middle cerebral artery occlusion (tMCAO)

Transient middle cerebral artery occlusion (tMCAO) experiments were conducted by Dr. Peter Kraft and Dr. Michael Schuhmann (Department of Neurology, University Hospital Würzburg, Germany) according to the recommendation in mechanism-driven basic stroke research [236]. Focal cerebral ischemia was induced in 8-to-12-week-old mice by a tMCAO as previously described [237]. Briefly, inhalation anesthesia was induced by 2% isoflurane in a 70% N_2/30% O_2 mixture and a servo-controlled heating device was used to record and maintain body temperature during the surgical procedure. Operation time per animal was kept below 15 min. A silicon rubber–coated 6.0 nylon monofilament (6021PK10, Doccol, Redlands, CA, USA) was advanced through the carotid artery up to the origin of the *middle cerebral artery* (MCA) causing MCA infarction. After an occlusion time of 60 min, the filament was withdrawn to allow reperfusion of the MCA territory. The extent of infarction was quantitatively assessed 24 h after reperfusion on *2,3,5-triphenyltetrazolium chloride* (TTC) (2% (w/v) solution) stained brain sections. Global neurological outcome and motor function was evaluated by the Bederson score [238] and the grip test [239], respectively. Planimetric measurements of infarcted areas (ImageJ software, National Institutes of Health, Bethesda, MD, USA) corrected for brain edema [240] and assessment of functional outcome were performed in a blinded fashion by members of the laboratories of Prof. Dr. Guido Stoll (Department of Neurology, University Hospital Würzburg, Germany).

2.2.7 Statistical analysis

Results are presented as mean ± SD from at least three individual experiments per group, unless indicated otherwise. Statistical analysis between two groups was conducted using the Student's t-test, apart from the Fischer's exact test which was applied to assess variance between non-occluded vessels in models of arterial thrombosis or in tail bleeding assays and the Mann-Whitney U test which was used for analysis of Bederson score and grip test after tMCAO. Differences between more than two groups were analyzed with one-way analysis of variance (ANOVA) with Dunnett's T3 as post-hoc test. P-values <0.05 were considered statistically significant with: not significant (ns), $p>0.05$; *, $p<0.05$; **, $p<0.01$; ***, $p<0.001$.

3 Results

3.1 GPV modulates thrombus formation

GPV has been described to bind to collagen and thereby to participate in platelet adhesion and aggregation [135]. Previous studies from our group confirmed that GPV contributes to platelet collagen responses and revealed an unexpected role of the glycoprotein as modulator of thrombus formation and hemostasis – lack of GPV can reverse the hemostatic defect as well as protection from thrombosis and ischemic stroke caused by the absence of the collagen receptors α2 and GPVI (Stegner *et al.*, unpublished). However, the mechanism underlying the thrombus-modulating role of GPV so far remains elusive.

3.1.1 Lack of GPV increases thrombin responsiveness

To further clarify how GPV exerts its compensatory role in *in vivo* thrombus formation and whether these effects can be reproduced in *in vitro* settings, *Gp5*$^{-/-}$ mice [144] were compared to WT (wildtype) controls. Gene targeting of *Gp5* resulted in complete absence of the receptor from the platelet surface. Platelet count, size, life span as well as surface abundance of major platelet glycoproteins were determined. Deficiency of GPV resulted in a slight increase in platelet size (5.6 ± 0.2 fl in WT vs. 6.0 ± 0.2 fl in *Gp5*$^{-/-}$ platelets, *** $p<0.001$ as compared to WT values) without affecting platelet count or life span (data not shown). In addition, GPV-deficient platelets showed overall unaltered glycoprotein expression levels, except for slightly decreased expression of β1, despite unaltered levels of α2 and α5, and a slightly increased CLEC-2 prevalence on the platelet surface, indicating that GPV influences the expression of CLEC-2 by a yet unknown mechanism (data not shown and [210]).

The effect of GPV-deficiency on platelet activation was measured by flow cytometric analyses of agonist-induced αIIbβ3 activation (JON/A-PE which specifically binds to the activated form of αIIbβ3 [224]) and degranulation-dependent P-selectin exposure, which is stored in α-granules under resting conditions. Platelets of *Gp5*$^{-/-}$ mice displayed an overall unaltered agonist-induced integrin activation as well as P-selectin exposure in response to GPCR-coupled agonists, such as ADP, U46619 or thrombin, as well as to (hem)ITAM-dependent agonists (CRP, convulxin and rhodocytin), except for a slight hyperresponsiveness upon stimulation with intermediate thrombin concentrations (Figure 3-1 A and not shown), confirming previous results [145].

Aggregation studies confirmed the hyperreactivity of GPV-deficient platelets at intermediate thrombin concentrations, however upon stimulation with PAR4-activating peptide no

differences were observed (Figure 3-1 B), indicating that the observed thrombin hyperresponsiveness is due to the absence of GPV as PAR-competing thrombin substrate. This also translated into an increased ATP release of GPV-deficient platelets upon thrombin stimulation, whereas ATP release in response to CRP, collagen and U46619 was unaltered, confirming previous results [144].

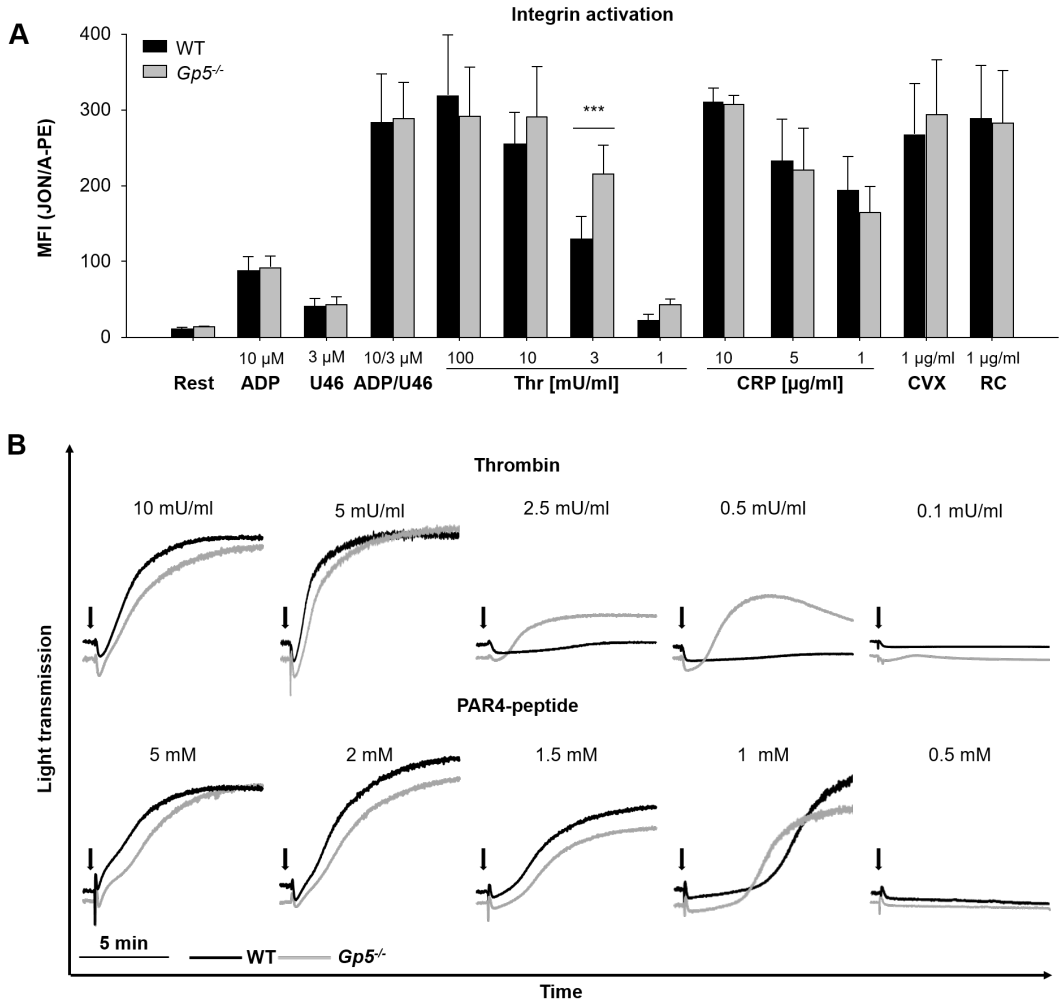

Figure 3-1: Increased thrombin responsiveness of *Gp5*$^{-/-}$ platelets. **(A)** Washed blood was incubated for 15 min with the indicated agonists in the presence of saturating amounts of JON/A-PE (anti-activated αIIbβ3 integrin)**.** Platelets were gated by their *forward and sideward scatter characteristics* (FSC and SSC). Data shown are mean fluorescence intensities (MFI) ± SD (n=4 mice per group; data are representative of three independent experiments). Rest, resting; U46, U46619; Thr, thrombin; CRP, collagen-related peptide; CVX, convulxin; RC, rhodocytin. * p<0.05; ** p<0.01; *** p<0.001 as compared to WT values. **(B)** Washed platelets were stimulated with thrombin or PAR4-peptide and light transmission was recorded on an Apact four-channel aggregometer over 10 min. Representative aggregation curves of at least 4 independent experiments are shown.

3.1.2 GPV is dispensable for thrombus formation on collagen, procoagulant activity and thrombin generation

In vivo, platelet activation occurs in flowing blood on exposed components of the ECM, such as collagen, laminin and fibronectin. Previous studies by our group revealed a thrombus-modulating role of GPV *in vivo*. Flow adhesion experiments on collagen showed that at shear rates of 1000 s^{-1} and 1700 s^{-1}, GPV-deficient platelets formed thrombi to the same extent and with a comparable volume as WT mice (data not shown and [210]), indicating that GPV is dispensable for platelet-collagen interactions *in vitro* under flow.

Sustained platelet activation leads to a marked increase in cytosolic Ca^{2+} concentrations which induce subsequent exposure of procoagulant PS on the platelet surface and result in thrombin generation, thereby promoting coagulation [214, 215].

PS exposure was assessed by annexin-A5 staining, which specifically binds to PS e.g. exposed by procoagulant platelets. GPV was found to be dispensable for PS exposure upon platelet activation with GPCR- and (hem)ITAM-coupled agonists under static conditions as determined by annexin-A5 staining using flow cytometry. In addition, under flow conditions, when heparin-anticoagulated whole blood (to maintain physiological Ca^{2+} and Mg^{2+} concentrations) was perfused over a collagen-coated surface and the adherent platelets were stained with annexin-A5 Dylight 488, the procoagulant index of GPV-deficient platelets was found to be unaltered at a shear rate of 1000 s^{-1} and 1700 s^{-1} (data not shown). This is in line with a previous report and indicates that GPV is dispensable for procoagulant activity [210, 241].

Surface-exposed PS triggers procoagulant activity of platelets and propagates coagulation by facilitating assembly and activation of the tenase and prothrombinase complex [216, 242]. This in turn leads to thrombin generation. In line with an unaltered PS exposure, thrombin generation, as assessed by the calibrated automated thrombogram method, was indistinguishable between WT and *Gp5*$^{-/-}$ mice regarding maximum thrombin peak concentration, time to start of thrombin generation as well as time to peak concentration (Figure 3-2).

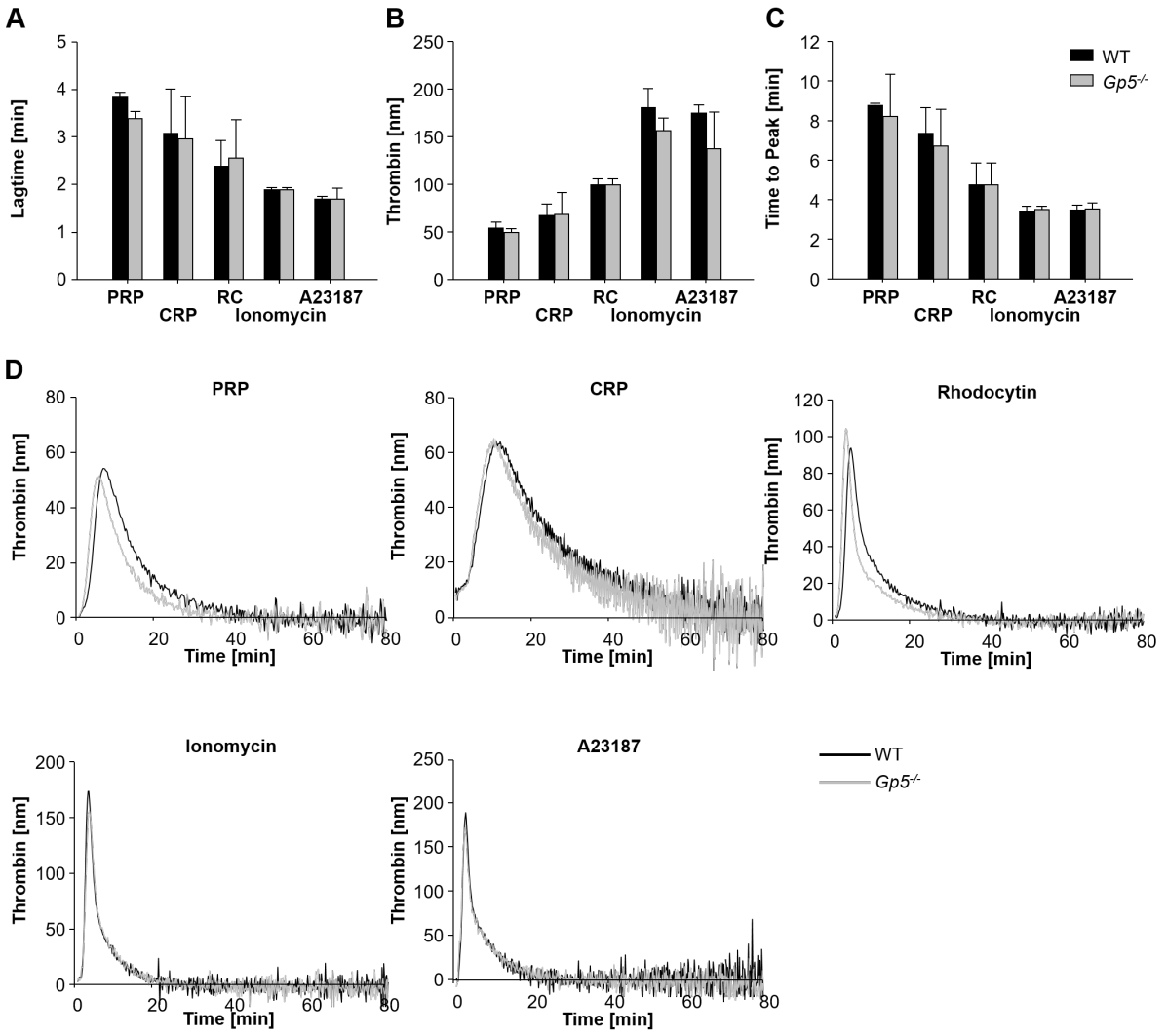

Figure 3-2: Unaltered thrombin generation in the absence of *Gp5*$^{-/-}$ on platelets. Citrate-anticoagulated platelet-rich plasma was left unstimulated (PRP) or activated by incubation with *collagen-related peptide* (CRP) (20 µg/ml), rhodocytin (1 µg/ml), ionomycin (10 µM) or A23187 (10 µM) for 10 min at 37°C. Thrombin generation was triggered with tissue factor/$CaCl_2$. Lagtime **(A)**, maximal thrombin concentration **(B)** and time to peak **(C)** were determined. **(D)** Representative thrombin generation curves. Values are depicted as mean ± SD (n=9).

3.1.3 GPIb-ligand interactions are not modulated in the absence of GPV

Initiation of thrombus formation requires platelet recruitment to the site of vascular damage. This process is mainly mediated by binding of GPIb to exposed vWF on the ECM, allowing platelet adhesion. To study a possibly role of GPV in this process, platelet-vWF interactions were investigated under static and flow conditions. Under static conditions, vWF- as well as fibronectin-binding to activated platelets was unaltered (Figure 3-3 A, B).

Since GPIb-signaling to a great extent depends on shear forces, flow adhesion studies were performed. A high shear rate of 1700 s^{-1} was used to ensure that platelet adhesion primarily

depends on GPIb [10]. In line with previous reports [135, 144], firm platelet adhesion to vWF and P-selectin, as well as the rolling velocity and accumulated rolling distance on vWF under flow were unaltered, but an increased rolling distance on P-selectin was observed in GPV-deficient platelets (Figure 3-3 C, D) indicating that GPIb-vWF interactions are not affected by the absence GPV.

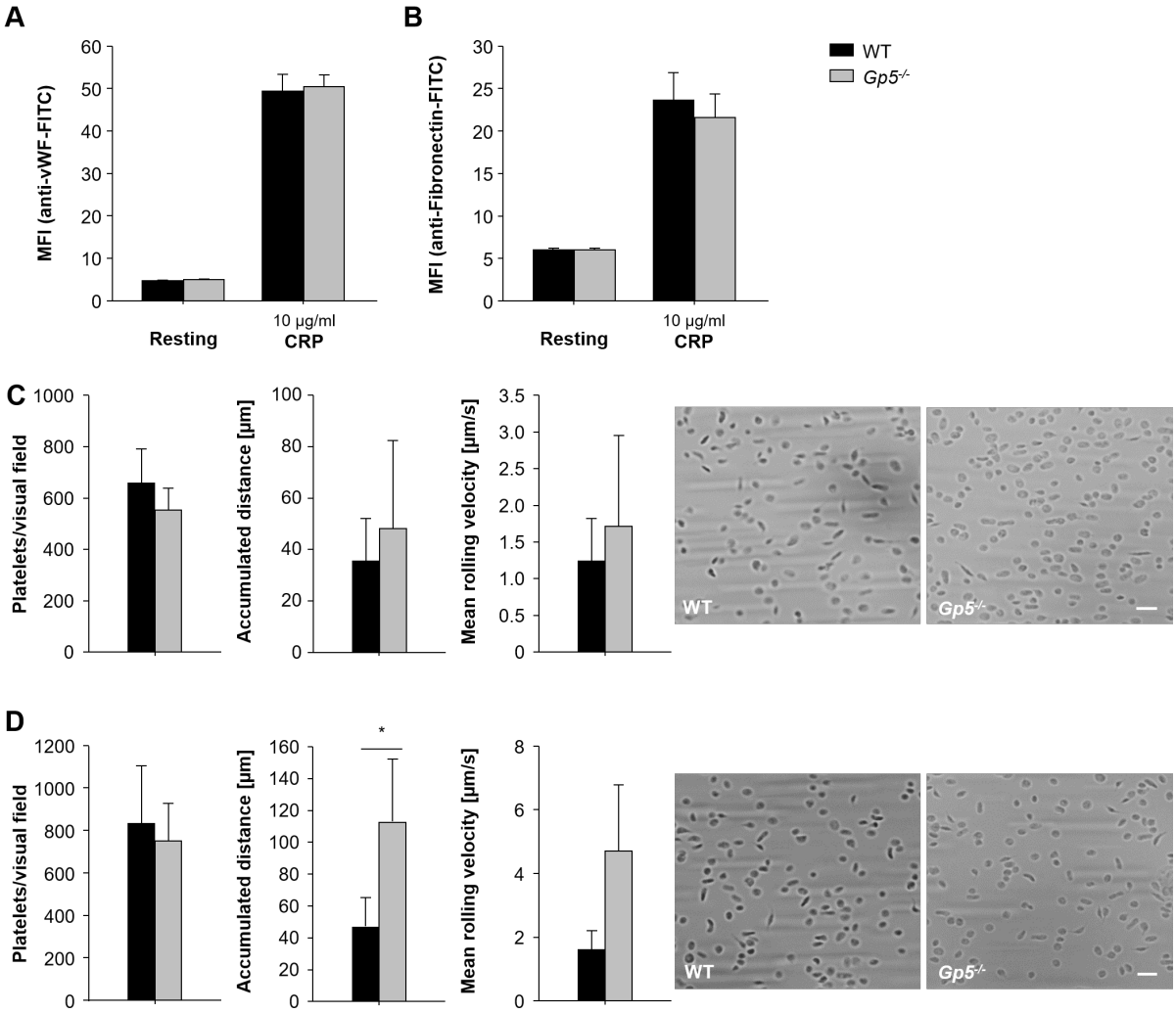

Figure 3-3: Unaltered adhesion to vWF and P-selectin under flow. Diluted whole blood was stimulated with CRP and vWF- **(A)** and anti-fibronectin- **(B)** binding to activated platelets was measured on a FACSCalibur. Data shown are mean fluorescence intensities (MFI) ± SD (n=4 mice per group; data are representative of three independent experiments). **(C, D)** Whole blood was perfused over a vWF- **(C)** or P-selectin-coated **(D)** surface at 1700 s^{-1} for 4 min and then washed with Tyrode's buffer for 4 min. Bar graphs display mean number of adhered platelets per visual field, the accumulated rolling distance over 30 s and the rolling velocity. 15 platelets per animal were tracked in time-lapse videos during washing over 30 s using Fiji and analyzed for their mean velocity, as well as the accumulated distance. Data shown are mean ± SD (n=5). Rest, resting; CRP, collagen-related peptide; vWF, von Willebrand factor. * $p<0.01$ as compared to WT values. Scale bar: 5 µm.

3.1.4 GPV-deficiency restores thrombus formation in the absence of GPVI and CLEC-2

It has been long established that lack or deficiency of GPVI or CLEC-2 protects from occlusive thrombus formation while only mildly prolonging bleeding times (see 1.4). However, the impact of GPV-deficiency on thrombosis has been discussed controversially in literature, reporting either a prothrombotic or antithrombotic tendency [135, 145, 206, 209, 243]. Previous studies in our group revealed a role of GPV in thrombus formation and showed in two different models of arterial thrombosis that GPV decelerates thrombus formation, independent of the expression of GPVI and α2, the two major collagen receptors on platelets [210]. Besides this, GPV-deficiency restored thrombus formation in the absence of the hemITAM receptor CLEC-2 after $FeCl_3$-induced injury of mesenteric arterioles [210].

In this study, it has been confirmed that GPV-deficiency restores thrombus formation in the absence of GPVI (Figure 3-4). For this, 100 µg anti-GPVI antibody (JAQ1) was injected intraperitoneally at day 7 and day 5 prior to the experiment, since it is known to deplete GPVI from the platelet surface, resulting in a GPVI-knockout like phenotype [67]. The antibody causes a transient thrombocytopenia with platelet counts returning to normal levels within 3 days, but platelets still lacking GPVI on their surface. Comparable to JAQ1 treatment, injection of the monoclonal anti-CLEC-2 antibody INU1 results in depletion of CLEC-2 from the platelet surface and a transient drop in platelet counts. Consequently, mice received 100 µg INU1 intraperitoneally at day 7 and day 5 prior to the experiment [80]. The efficiency of JAQ1- and INU1 treatment was confirmed by flow cytometry prior to each experiment.

In line with previous results on mesenteric arterioles after $FeCl_3$-induced thrombus formation, mice with a concomitant GPV- and CLEC-2-deficiency were able to form occlusive thrombi after mechanical injury of the abdominal aorta, indicating that lack of GPV restores thrombus formation in these mice (Figure 3-4).

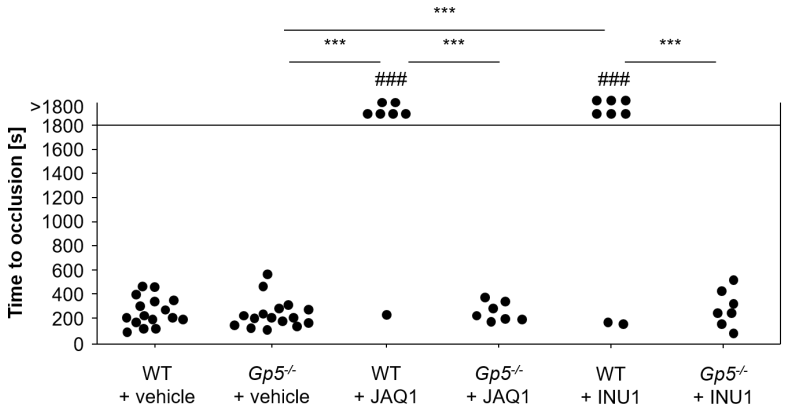

Figure 3-4: GPV-deficiency reverses protection from occlusive thrombus formation in the absence of GPVI and CLEC-2 in an aortic injury model. The abdominal aorta was mechanically injured by a single firm compression with a forceps and blood flow was monitored with a Doppler flowmeter. Time to final occlusion is shown. Each symbol represents one mouse. * $p<0.05$; ** $p<0.01$; *** $p<0.001$; ### $p<0.001$ as compared to WT mice.

3.1.5 Lack of GPV restores hemostasis in the absence of GPVI and CLEC-2

To study the role of GPV in hemostasis, 1 mm of the tail tip of GPVI- and CLEC-2-depleted mice in the absence or presence of GPV was cut and time to cessation of blood flow was assessed using a filter paper. This assay serves as an indicator of physiological blood clotting [244].

Combined treatment with JAQ1 and INU1 depleted both (hem)ITAM receptors from the platelet surface, which was confirmed by flow cytometry prior to the experiment (not shown). Preliminary data in our lab already showed slightly decreased tail bleeding times of GPV-single-deficient mice, indicating that GPV negatively regulates hemostasis. Like its role in thrombotic processes, lack of GPV also restored hemostatic function in the absence of GPVI and CLEC-2 [210]. This was confirmed in this thesis (Figure 3-5 A). Similar results were obtained for genetic CLEC-2/GPV-double-deficient mice. Increased tail bleeding times in megakaryocyte- and platelet-specific CLEC-2 knockout mice (referred to as *Clec-2*$^{-/-}$) were normalized to WT levels in the absence of GPV (Figure 3-5). Even more intriguingly, lack of GPV could also restore hemostasis in the absence of both (hem)ITAM receptors. GPVI-/CLEC-2-double-depleted mice had a severe hemostatic defect indicated by dramatically increased tail bleeding times. Only 4 out of 8 mice were able to arrest bleeding within the observation period. However, loss of both (hem)ITAM receptors did not alter tail bleeding times in *Gp5*$^{-/-}$ mice compared to untreated WT mice (Figure 3-5).

For these studies, constitutive GPV knockout mice were used, since GPV expression was described to be restricted to the megakaryocytic lineage [191]. Still, GPV bone marrow

chimeric mice were generated and subjected to a tail bleeding time experiment confirming that in the absence of GPV hemostasis was restored in GPVI-depleted mice (data not shown).

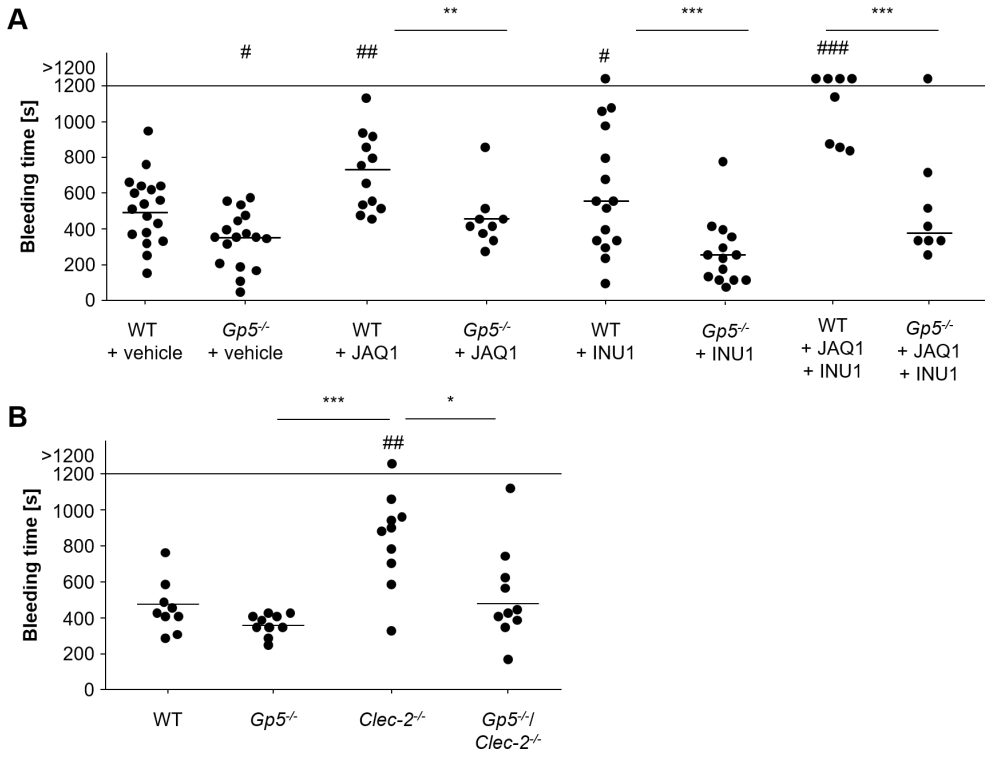

Figure 3-5: Lack of GPV restores the hemostatic function in the absence of GPVI and CLEC-2. 1 mm of the tail tip of each mouse was cut and time to cessation of blood flow was measured using a filter paper. Each symbol represents one animal. * p<0.05; ** p<0.01; *** p<0.001 as compared to the indicated group; # p<0.05; ## p<0.01 ### p<0.001 as compared to untreated WT mice.

In a next step, a potential effect of GPV-deficiency on hemostasis was assessed upon treatment with *acetylsalicylic acid* (ASA). ASA is a widely used antithrombotic agent, which interferes with TxA_2 production. While it is known to increase the risk of bleeding complications in humans [245, 246], treatment of mice with ASA had only mild effects on hemostasis and thrombosis in WT mice (Figure 3-6) [247-249]. Besides this, it was previously shown that TxA_2 is required for hemostasis in GPVI-deficient mice, since inhibition of TxA_2 by ASA severly compromised hemostasis in the absence of GPVI [247]. Mice were treated with a low dose of ASA (1 mg/kg) intravenously 1 h prior to experiments. This dose is the recommended treatment for prevention of cardiovascular diseases [250]. As described in literature [247], mice treated with ASA upon GPVI-depletion displayed prolonged bleeding times, which were significantly reduced in *Gp5*$^{-/-}$ mice with the same treatment (Figure 3-6).

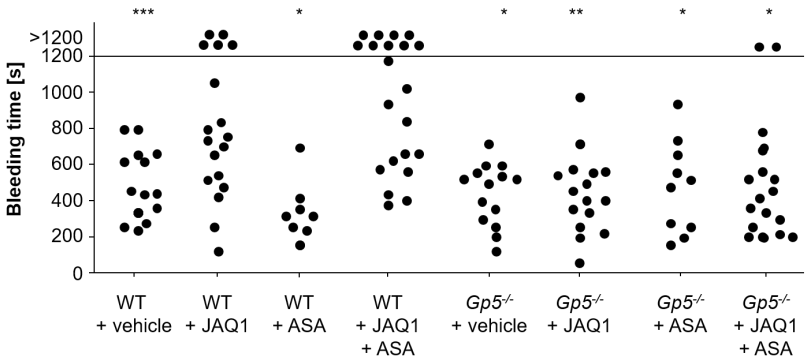

Figure 3-6: Lack of GPV restores the hemostatic function upon acetylsalicylic acid treatment in GPVI-depleted mice. 1 mm of the tail tip of each mouse was cut and time to cessation of blood flow was measured using a filter paper. Mice were treated with *acetylsalicylic acid* (ASA; 1 mg/kg i.v.) 1 h before the experiment. Each symbol represents one animal. * $p<0.05$; ** $p<0.01$; *** $p<0.001$ compared to JAQ1- and ASA-treated WT mice.

Together, these data establish GPV as an important modulator of hemostasis and thrombosis, since its deficiency can restore hemostatic function and thrombotic defects caused by isolated or combined lack of both activating (hem)ITAM receptors on platelets, GPVI and CLEC-2.

3.2 The anti-GPV antibody 89F12 reproduces the *Gp5*$^{-/-}$ phenotype

Monoclonal anti-GPV antibodies were previously generated in our lab [222] and screened for their ability to reproduce the *Gp5*$^{-/-}$ phenotype. The clone 89F12 was found to bind to the extracellular domain of GPV without affecting platelet count and size and the thrombin-mediated ectodomain shedding of the glycoprotein. Besides this, platelet activation upon thrombin stimulation was unaltered in the presence of 89F12 (data not shown). 89F12 reproduced the *Gp5*$^{-/-}$ phenotype in WT mice by reversing the thrombotic defect of GPVI-depleted animals (Figure 1-6). Fab-fragments of 89F12 had a comparable effect excluding a role of GPV dimerization in this process (Stegner *et al.,* unpublished). The role of 89F12 was studied in more detail in this thesis. 89F12 IgG was used for the experiments described.

3.2.1 89F12 has no effect on platelet aggregation, thrombus formation on collagen and thrombin generation

The role of 89F12 in platelet aggregation and platelet adhesion on collagen was studied. Incubation with 10 µg/ml 89F12 did not alter platelet aggregation in response to collagen or thrombin (Figure 3-7 A), in contrast to slightly increased aggregation responses upon thrombin stimulation in GPV-deficient mice. Consistently, 89F12 treatment had no effect on platelet adhesion and aggregate formation on collagen under flow at the indicated shear rates, an assay which is highly dependent on functional α2β1 integrins [247] (Figure 3-7 B, C).

In line with this, thrombin generation as assessed by time to initiation of thrombin generation, time to maximal thrombin generation and amount of maximal thrombin generation was also indistinguishable between 89F12-treated and control mice upon stimulation with CRP, convulxin, rhodocytin, or the Ca^{2+} ionophore ionomycin excluding a role of the 89F12-binding epitope in this process (data not shown). This was in line with the results obtained for *Gp5*$^{-/-}$ mice.

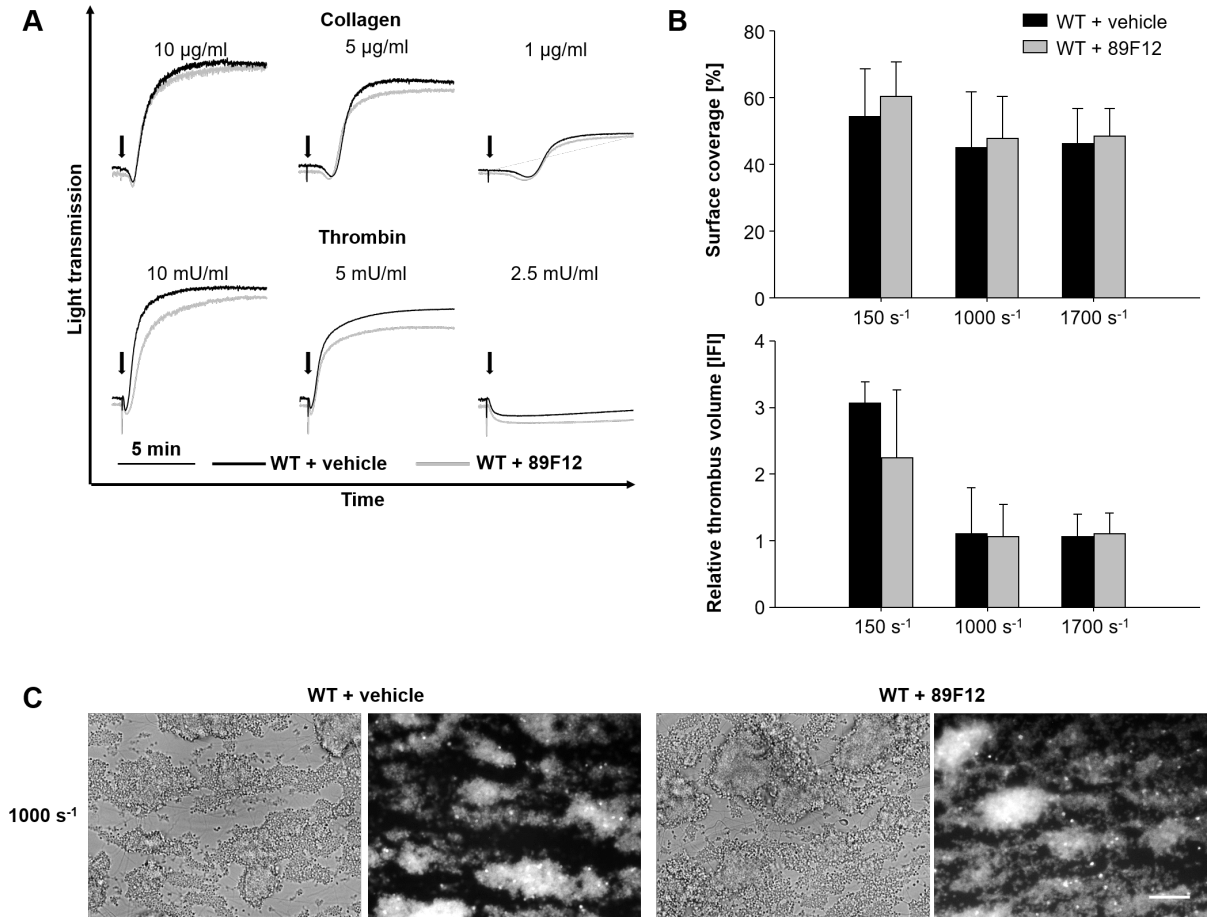

Figure 3-7: Unaltered aggregation, platelet adhesion and thrombus formation on collagen under flow after 89F12 treatment. (A) Washed platelets were incubated with 10 µg/ml 89F12 and then stimulated with the indicated agonists. Light transmission was recorded on an Apact four-channel aggregometer over 10 min. Representative aggregation traces of three individual experiments are shown. Arrows indicate platelet stimulation. **(B)** Whole blood was perfused over a collagen-coated (0.2 mg/ml) surface at the indicated shear rates after incubation with 10 µg/ml 89F12 for 5 min at 37°C and then washed with Tyrode's buffer for the same time period. Perfusion time was 10 min (150 s^{-1}) and 4 min (1000 and 1700 s^{-1}). **(C)** Representative images of brightfield and fluorescence microscopy. Scale bar: 25 µm. The bar graphs display mean values ± SD (n=5 mice each).

3.2.2 GPV blockade by 89F12 restores hemostasis in the absence of GPVI, CLEC-2 and Syk

In a next step, the ability of 89F12 to reproduce the *Gp5*$^{-/-}$ phenotype in hemostasis was tested. Therefore, mice were injected with JAQ1 or INU1 as described (3.1.4) to deplete GPVI and CLEC-2 and tail bleeding times were assessed.

Blockade of GPV by 89F12 in WT mice had no effect on hemostatic function (220 ±104 s in control and 153 ± 30 s in WT+89F12-mice). Lack of GPVI and CLEC-2 alone led to a severe bleeding phenotype, thereby confirming previous results [75]. As in thrombotic processes, GPV blockade by 89F12 could restore hemostasis in the absence of both activating (hem)ITAM

receptors (937 ± 357 s in WT+JAQ1+INU1 mice vs. 458 ± 266 s in WT+JAQ1+INU1+89F12 mice, p<0.01 compared to double-depleted mice) (Figure 3-8). These observations resembled the *Gp5*$^{-/-}$ phenotype (Figure 3-5 A).

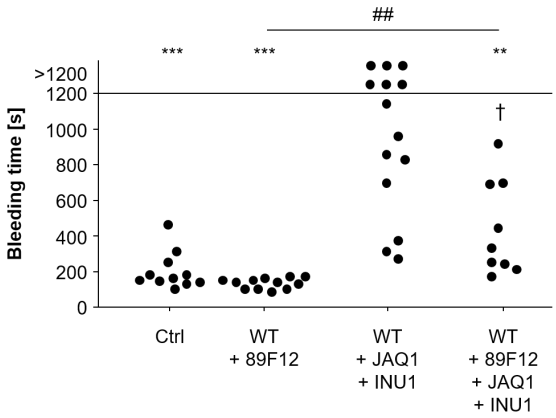

Figure 3-8: 89F12-mediated blockade of GPV reverses the hemostatic defect caused by the absence of the (hem)ITAM receptors GPVI and CLEC-2 and reproduces the GPV-knockout phenotype. 1 mm of the tail tip of each mouse was cut and time to cessation of blood flow was measured using a filter paper. Each symbol represents one animal. Each symbol represents one animal. * p<0.05; ** p<0.01; *** p<0.001 compared to WT+JAQ1+INU1 mice. † p<0.01 compared to control mice; ## p<0.01. In cases where mice were unable to arrest bleeding, Fisher's exact test was used to calculate p-values.

Since GPV blockade by 89F12 fully restored hemostatic function in the combined absence of GPVI and CLEC-2, this model was used to test whether GPV blockade could also reverse the effect of the absence of the *spleen tyrosine kinase* (Syk) in hemostasis and thrombosis. Syk is essential for downstream signaling of GPVI, CLEC-2 and FcγRIIA, the latter being only present on human, but not on murine platelets [54, 56]. Previous reports showed that *Syk*$^{fl/fl,\ Pf4\text{-}cre}$ mice have moderately prolonged bleeding times [251, 252], but arterial occlusive thrombus formation is abrogated in these mice [252]. Injection of 89F12 in *Syk*$^{fl/fl,\ Pf4\text{-}cre}$ mice led to tail bleeding times comparable to control mice. Likewise, in a model of arterial thrombosis 89F12 restored thrombus formation in the absence of Syk. This indicated that 89F12-mediated blockade of GPV can also restore hemostasis and thrombus formation downstream of (hem)ITAM receptors (Figure 3-9).

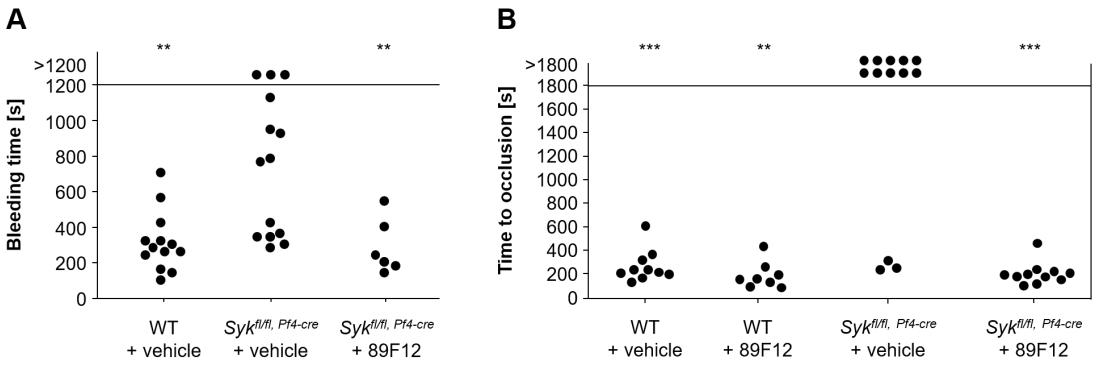

Figure 3-9: 89F12 restores hemostasis and thrombus formation in the absence of Syk. (A) 1 mm of the tail tip of each mouse was cut and time to cessation of blood flow was assessed using a filter paper. **(B)** The abdominal aorta was mechanically injured by a single firm compression with a forceps and blood flow was monitored with a Doppler flowmeter. Time to final occlusion is shown. Each symbol represents one individual mouse. * $p<0.05$; ** $p<0.01$; *** $p<0.001$ as compared to Syk-deficient mice.

3.2.3 89F12 restores hemostasis in the absence of RhoA, but not of Cdc42 or a combined lack of RhoA and Cdc42

A potential effect of GPV blockade on hemostasis was assessed in mice lacking the small GTPases RhoA [227] and Cdc42 [228], which are well known for regulating cytoskeletal rearrangements. Megakaryocyte- and platelet-specific RhoA and Cdc42 knockout mice both exhibit a macrothrombocytopenia and display different platelet defects [111, 253]. GPV was blocked by 89F12 and tail bleeding times in megakaryocyte- and platelet-specific RhoA and Cdc42 single- (further referred to as *RhoA*$^{-/-}$ and *Cdc42*$^{-/-}$) and double-(*RhoA*$^{-/-}$/*Cdc42*$^{-/-}$) deficient mice was assessed. In line with previous results, RhoA-deficient mice showed increased tail bleeding times [253] (Figure 3-10). Cdc42-deficiency also resulted in prolonged tail bleeding times, which confirms previous reports [111] (Figure 3-10). Surprisingly, 89F12 treatment of RhoA-deficient mice could restore hemostasis, leading to occlusion times comparable to control mice. In contrast, GPV blockade could not restore the hemostatic defect in the absence of Cdc42. In line with this, 89F12-mediated GPV blockade could also not restore the even more pronounced hemostatic defect of RhoA/Cdc42-double deficient animals (Figure 3-10). The fact that GPV-deficiency counterbalanced the absence of RhoA and restored hemostasis in the absence of RhoA, raised the question whether GPV serves as a master regulator of thrombus formation and hemostasis, which is not restricted to a compensatory mechanism on the (hem)ITAM signaling pathway.

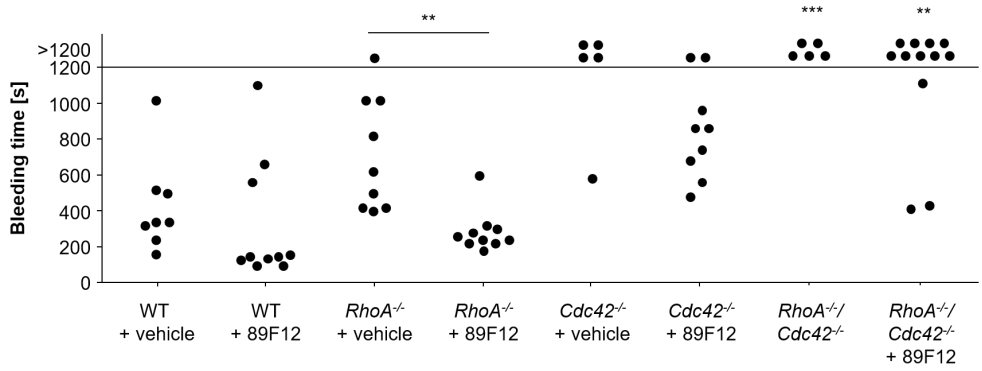

Figure 3-10: The hemostatic defect of RhoA-deficient mice is restored after GPV blockade, but 89F12 cannot overrule the hemostatic defect caused by lack of Cdc42 or combined lack of RhoA and Cdc42. 1 mm of the tail tip of each mouse was cut and time to cessation of blood flow was measured using a filter paper. Each symbol represents one animal. * p<0.05; ** p<0.01; *** p<0.001 compared to vehicle-treated WT mice. In cases where mice were unable to arrest bleeding, Fisher's exact test was used to calculate p-values.

3.2.4 89F12 does not restore hemostasis in the absence of functional GPIb, Talin, or Munc13-4

To assess a potential effect of GPV blockade on hemostasis in mice lacking functional GPIb, tail bleeding time in *Gp1ba-tg* mice was assessed. In these mice, the ectodomain of GPIbα is replaced by that of the human interleukin-4 receptor α (hIL4-Rα) (further referred to as *Gp1ba-tg*). The severe hemostatic defect in *Gp1ba-tg* mice (only 2 out of 14 mice ceased bleeding within the observation period) could not be restored by GPV blockade. All tested mice bled infinitely, indicating that 89F12 cannot counterbalance non-functional GPIb (Figure 3-11 A). This result is in line with previous data from our lab, showing that GPV-deficient mice cannot stop bleeding after p0p/B (anti-GPIb)-mediated GPIb blockade [210].

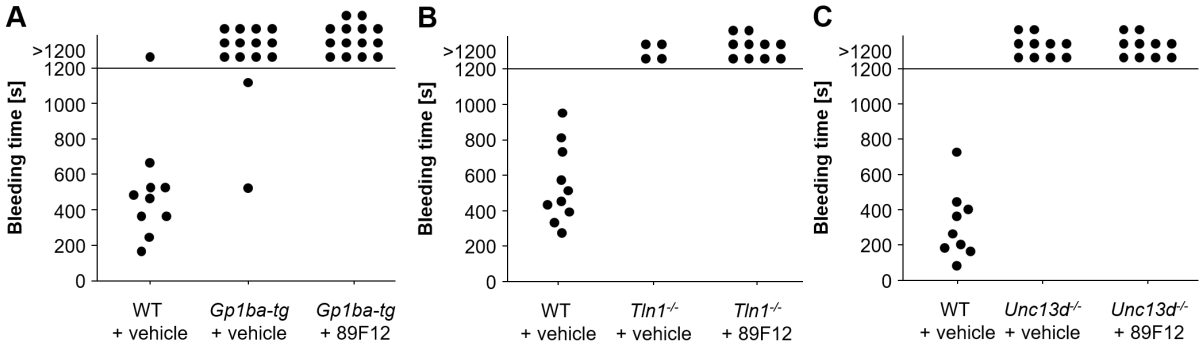

Figure 3-11: 89F12 cannot not restore hemostasis in the absence of functional GPIb, Talin or Munc13-4. 1 mm of the tail tip of each mouse was cut and time to cessation of blood flow was measured using a filter paper. Each symbol represents one animal. For all groups *** p<0.001 as compared to vehicle-treated WT mice. In cases where mice were unable to arrest bleeding, Fisher's exact test was used to calculate p-values.

Talin1 is essential for inside-out integrin activation and loss of talin1 in platelets abrogates integrin activation and platelet aggregation, which translates into abolished thrombus formation and severely defective hemostasis *in vivo* [229]. This was independent of 89F12-mediated blockade of GPV – none of the Talin1-deficient animals, independent of 89F12 treatment, did stop bleeding within the observation period (Figure 3-11 B). Similar results were obtained for 89F12-treated Munc14-3-deficient mice, which display an abolished platelet dense granule release and a reduced α-granule secretion, translating into infinite tail bleeding times [230, 254]. Independent of GPV blockade, all *Unc13d*$^{-/-}$ animals were unable to stop bleeding (Figure 3-11 C).

3.2.5 89F12-mediated GPV blockade lowers the minimum required platelet count for normal hemostasis

To maintain normal hemostasis, only very low platelet counts are necessary. A recent study from our lab showed that mice with a platelet count down to 10% of normal platelet counts (100 platelets/nl) have prolonged tail bleeding times, but are still able to arrest bleeding. Only mice with a platelet count lower than 2.5% of normal platelet counts showed infinite bleeding times [255]. In a next step, it was investigated whether 89F12 could lower the minimum platelet counts required to maintain normal hemostasis. To induce thrombocytopenia, platelets were depleted with an anti-GPIb antibody 12 h prior to the experiment. For this, 0.18 µg/g bodyweight antibody were injected to reach a final platelet count of 5-10% of WT levels. Platelet counts were determined by flow cytometry prior to each experiment. 89F12-mediated blockade of GPV significantly reduced the minimum platelet count required to maintain normal hemostasis after platelet depletion. 4 out of 5 mice with a platelet count of 5-10% arrested bleeding within the observation period after 89F12 treatment, whereas none of the platelet-depleted mice stopped bleeding (Figure 3-12). Comparable results were obtained for platelet-depleted *Gp5*$^{-/-}$ mice (data not shown).

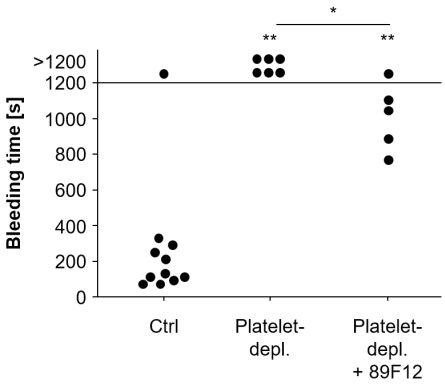

Figure 3-12: 89F12 lowers the platelet count required to maintain normal hemostasis. Mice were injected with 0.18 µg/g bodyweight platelet depletion antibody to induce thrombocytopenia 5-10% of normal counts. 1 mm of the tail tip of each mouse was cut and time to cessation of blood flow was assessed using a filter paper. Each symbol represents one animal. * $p<0.05$; ** $p<0.01$ as compared to control mice. In cases where mice were unable to arrest bleeding, Fisher's exact test was used to calculate p-values. Depicted is one of three independent experiments.

3.3 The newly generated monoclonal anti-mouse GPV antibody 5G2 partially reproduces the *Gp5*$^{-/-}$ phenotype

To further characterize the role of GPV, additional anti-mouse GPV antibodies were required. For this purpose, *Gp5*$^{-/-}$ mice were repeatedly immunized with washed WT mouse platelets, purified recombinant soluble murine GPV or immunoprecipitate from WT platelet lysates using the anti-GPV antibody 89H11. To generate hybridoma cells producing anti-GPV antibodies, the spleen of a repeatedly immunized mouse was isolated to obtain a single cell suspension und fused with mouse myeloma Ag14 cells by addition of PEG. However, the first four fusion approaches failed and no specific anti-mouse GPV antibodies were generated, hardly any antibody-producing clones grew (data not shown) probably because of very few feeder cells. For these fusions, feeder cells from C57B6/J mice were used. For further fusions, feeder cells from NMRI ex-breeder mice were used, which yielded considerably more feeder cells of better quality, and the number of antibody-producing clones increased. The fusion of two other mouse spleens after 5-6 rounds of immunization resulted in generation of antibody-producing hybridoma cells; approximately 800 hybridoma clones were obtained and screened for antibody production by flow cytometry. WT and *Gp5*$^{-/-}$ platelets were used to check for production of specific anti-mouse GPV antibodies. Hybridoma populations that produced antibodies directed against GPV were transferred into 24-well plates, polyclonal hybridomas were subcloned to generate monoclonal hybridoma populations and hybridoma populations were repeatedly tested by flow cytometry. Out of 8 polyclonal hybridoma clones, one hybridoma population in the end still produced monoclonal anti-GPV specific antibodies (clone 5G2) (Figure 3-13 A), whereas all other clones lost expression of the antibody or did not survive. As 5G2 stably expressed the antibody, the clone was cultured in RPMI/5% FCS medium and initially 13 mg of the antibody was purified.

Thereafter, the antibody 5G2 was further characterized. 5G2 specifically bound to GPV on WT platelets, since no 5G2 binding was observed in GPV-deficient platelets (Figure 3-13 A). The antibody did not crossreact with human platelets (data not shown). Further, it was tested on mouse platelet lysates by western blot. Neither under reducing nor non-reducing conditions, a specific band of the approximate size of GPV was detected in platelet lysates. In addition, the antibody did also not work in immunoprecipitation – neither from WT platelet lysates nor WT thrombin-induced platelet supernatant nor purified recombinant smGPV (data not shown).

The antibody 5G2 was again tested on both resting and activated platelets in flow cytometry, where it showed decreased binding upon stimulation with increasing thrombin concentrations indicating that the binding epitope of 5G2 is located within the cleaved/soluble GPV (data not shown).

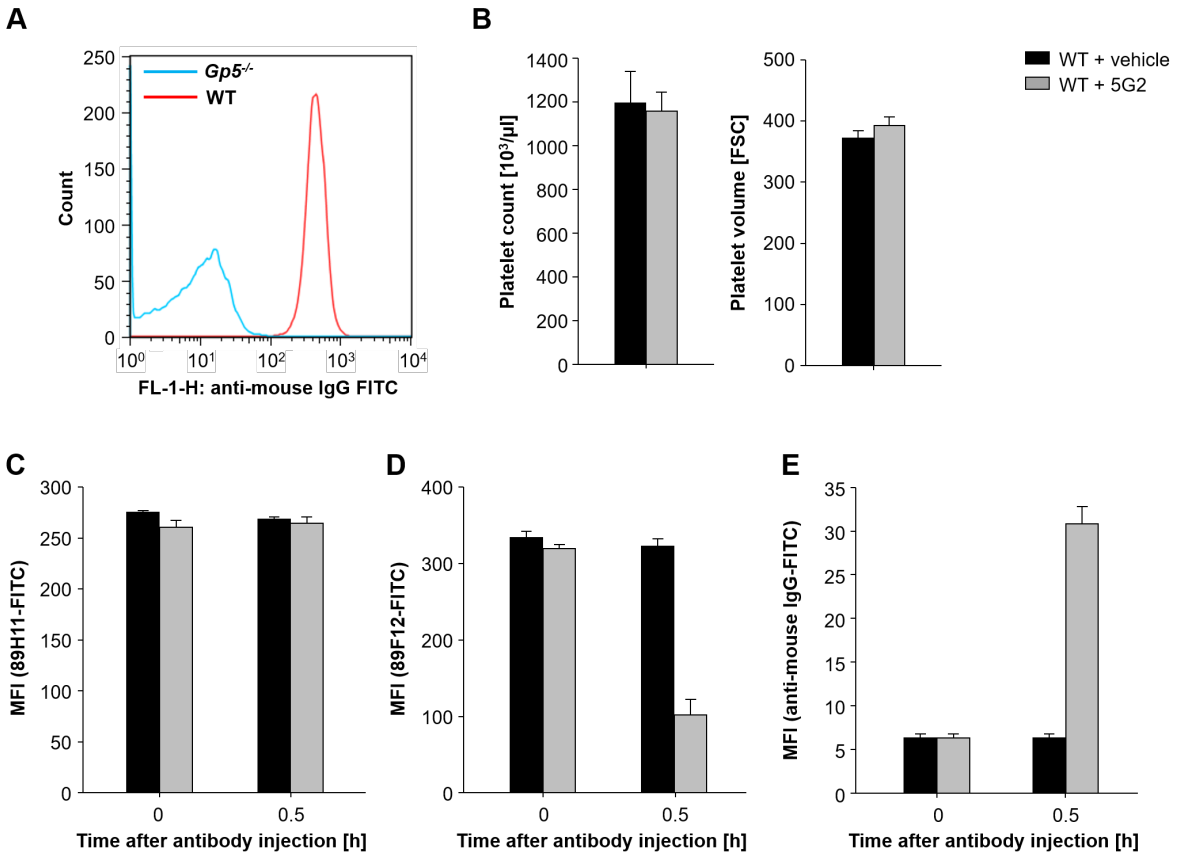

Figure 3-13: The monoclonal mouse anti-mouse GPV antibody 5G2 does not alter platelet count and size, but reduces binding of 89F12. (A) 5G2 binds to WT, but not to GPV-deficient platelets. WT and GPV-deficient platelets were incubated with 5G2 and washed. 5G2 binding was determined by flow cytometry using anti-mouse IgG FITC. **(B)** 5G2 has no effect on platelet count and size. Platelet count and size were determined 24 h after intravenous injection of 100 µg 5G2. Results are expressed as mean values ± SD for 5 mice per group. **(C-E)** Flow cytometric analysis of anti-GPV antibody binding after treatment with 100 µg 5G2. Blood was withdrawn 30 min after injection, stained with saturating amounts of FITC-labeled antibodies directed against GPV and analyzed on a FACSCalibur. Platelets were gated by their *forward and sideward scatter characteristics* (FSC and SSC). Unaltered expression of GPV **(C),** but reduced binding of 89F12 after 5G2 treatment **(D)**. **(E)** anti-mouse IgG confirms binding of the mouse anti-mouse 5G2 antibody to platelets. Results are expressed as mean values ± SD, n=5 mice per group. MFI, *mean fluorescence intensity*.

The effects of 5G2 IgG were also studied *in vivo*. For this, 100 µg/mouse 5G2 IgG was injected intravenously. Upon 5G2-injection, platelet count and size were unaltered for an observation period of 24 h (Figure 3-13 B), as well as expression of major glycoproteins on the platelet surface (data not shown). Most notably, expression of GPV on the platelet surface was not affected upon 5G2 treatment as indicated by indistinguishable mean fluorescence intensities for 89H11-FITC (Figure 3-13 C), but binding of 89F12-FITC to 5G2-opsonized platelets was reduced by approximately 50% as compared to not-opsonized vehicle-treated WT platelets (Figure 3-13 D), indicating that the binding epitopes of the two antibodies either partially overlap or that 5G2 indirectly hinders 89F12 binding to GPV.

The effect of 5G2 on platelet activation was studied in more detail. For this, blood was withdrawn 1 h after antibody injection (100 µg/mouse 5G2 i. v.) and then platelets were activated with the indicated agonists (Figure 3-14). 5G2-opsonized platelets displayed mildly increased αIIbβ3 integrin activation in response to intermediate and low thrombin concentrations and combined stimulation with ADP/U46619 and a slight reduction upon stimulation with high doses of CRP compared to control mice (Figure 3-14 A, B).

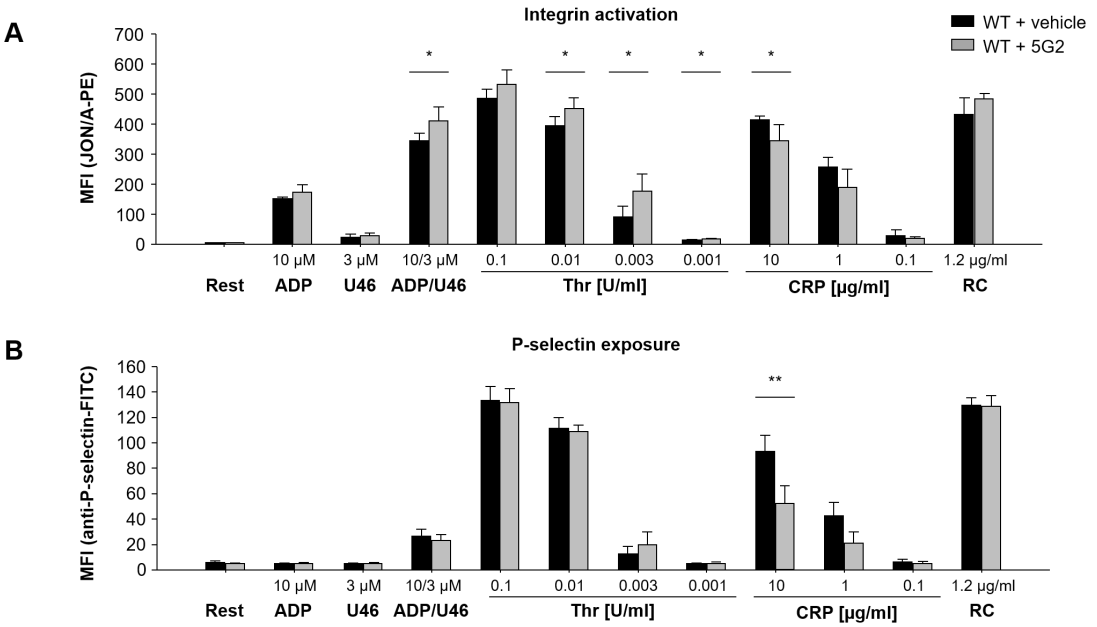

Figure 3-14: 5G2 only mildly affects platelet activation and degranulation. Mice were injected intravenously with 100 µg 5G2 and blood was withdrawn 1 h later. **(A, B)** Washed blood was activated with the indicated agonists in the presence of saturating amounts of JON/A-PE (activated αIIbβ3 integrin) **(A)** and anti-P-selectin-FITC **(B)** for 15 min. Platelets were gated by their *forward and sideward scatter characteristics* (FSC and SSC). 5G2 slightly enhances platelet activation upon stimulation with thrombin or a combination of ADP and U46619, but slightly reduces platelet activation and degranulation-dependent P-selectin exposure upon stimulation with high doses of CRP. Data shown are mean fluorescence intensities (MFI) ± SD (n=5 mice per group; data are representative of three independent experiments). Rest, resting; U46, U46619; Thr, thrombin; CRP, collagen-related peptide; RC, rhodocytin. * p<0.05; ** p<0.01 as compared to WT values**.**

These mild alterations in integrin activation and platelet degranulation did, however, not translate into altered aggregation responses. Aggregation studies upon 5G2 incubation *in vitro* were indistinguishable from vehicle-treated controls upon stimulation with collagen, CRP, convulxin, rhodocytin and thrombin (data not shown).

In a next step, the role of 5G2 was tested in *in vivo* thrombus formation and hemostasis. Since binding of 89F12 to GPV was reduced on 5G2-opsonized platelets, it was speculated whether 5G2 might be able to restore the hemostatic and thrombotic defects in the absence of GPVI. Therefore, mice were injected with JAQ1 as described (3.1.4) and tail bleeding times assessed.

Blockade of GPV by 5G2 had no effect on tail bleeding times in WT mice (486 ± 232 s in control and 306 ± 166 s in 5G2-treated mice). Lack of GPVI prolonged tail bleeding times, with 3 out of 10 mice not being able to arrest bleeding in the observation period. Surprisingly, GPV blockade by 5G2 could restore hemostasis in the absence of GPVI (938 ± 295 s in WT+JAQ1 mice vs. 408 ± 155 s in WT+JAQ1+5G2 mice, $p<0.001$ compared to JAQ1-treated WT mice) (Figure 3-15 A). These observations indicate that 5G2 can revert the hemostatic defect in GPVI-deficient mice, which is in line with results after 89F12 treatment.

Thrombus formation, studied in a model of mechanical injury of the abdominal aorta, was unaltered in 5G2-treated mice, but 5G2 partially restored thrombus formation in the absence of GPVI. While 10 out of 14 JAQ1-treated WT mice were protected from arterial occlusive thrombus formation, 12 out of 17 JAQ1/5G2-treated WT mice formed occlusive thrombi (Figure 3-15 B). Therefore, 5G2 at least partially restores arterial occlusive thrombus formation in the absence of GPVI, although the effect of 5G2 was more prominent in hemostasis. Overall, 5G2 reproduces the effect of 89F12 by compensating for the loss of the ITAM receptor GPVI in hemostasis and thrombosis.

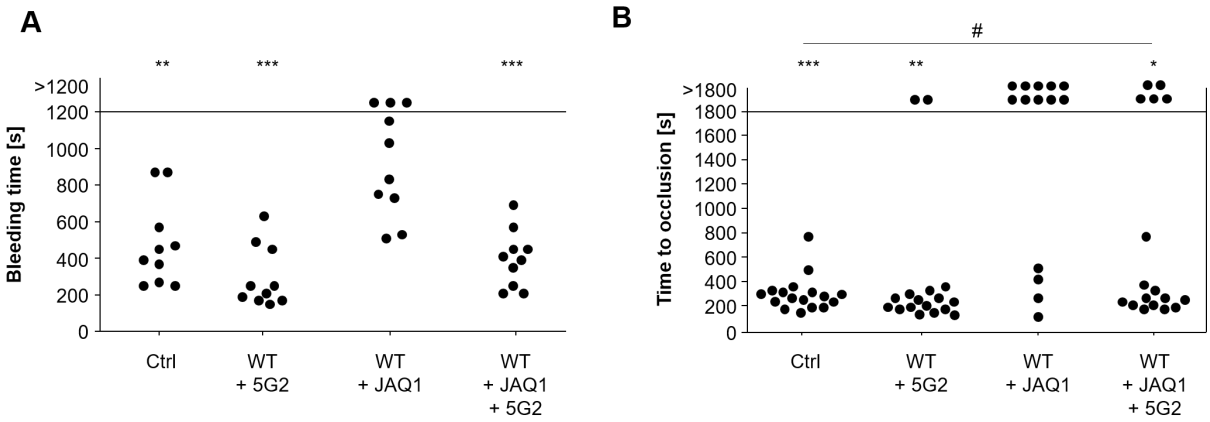

Figure 3-15: 5G2 partially phenocopies the effect of 89F12 *in vivo*. Mice were injected intravenously with 100 µg 5G2 IgG prior to the experiment. **(A)** 1 mm of the tail tip of each mouse was cut and time to cessation of blood flow was measured using a filter paper. **(B)** The abdominal aorta was mechanically injured by a single firm compression with a forceps and blood flow was monitored with a Doppler flowmeter. Time to final occlusion is shown. Each symbol represents one animal. * $p<0.05$; ** $p<0.01$; *** $p<0.001$ as compared to WT+JAQ1 mice. # $p<0.05$ as comared to control mice.

3.4 Mutation of the thrombin-cleavage site in GPV modulates thrombosis and hemostasis in the absence of (hem)ITAM receptors

GPV was shown to be a critical regulator of thrombosis and hemostasis. Since the anti-GPV antibody 89F12 reproduced the *Gp5*$^{-/-}$ phenotype, it could be concluded that the extracellular domain of GPV might be essential for its thrombus-modulating role. To shed new light on the relevance of the thrombin cleavage site *in vivo*, a mouse carrying a point mutation in the thrombin cleavage site was generated. Previously, the amino acids at position 476-477 were regarded as the potential thrombin cleavage site in mice with the sequence [187]:

5'-CCG GAT CCT CGC AGC CTG -3'
P D P R S L

In exon 2, CGC at position 1426 in the coding region was mutated to GCC leading to the amino acid mutation R476A (arginine to alanine) (Figure 3-16 A), which should prevent cleavage of GPV upon thrombin binding. Even upon platelet activation, when thrombin is present, GPV should not be cleaved from the platelet surface.

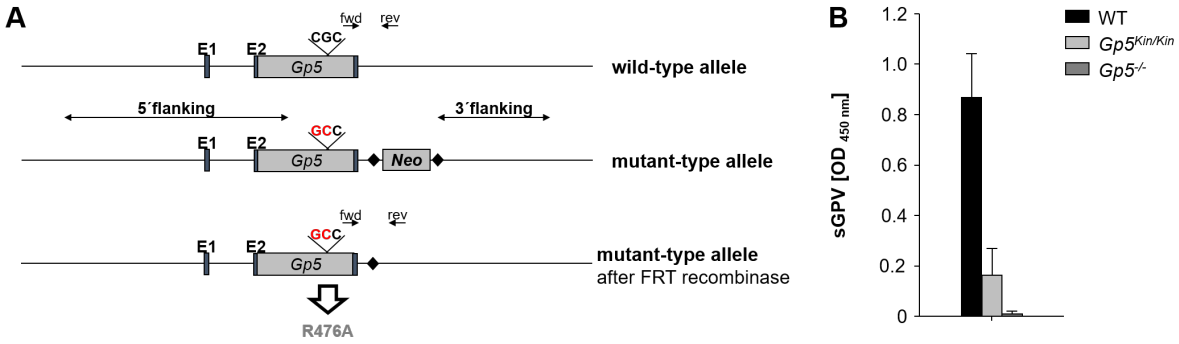

Figure 3-16: Generation of *Gp5*$^{Kin/Kin}$ mice. (A) Simplified targeting strategy. The point mutation R476A prevents cleavage of GPV by thrombin. **(B)** Plasma level of soluble GPV were determined using a GPV ELISA.

Under resting conditions, levels of soluble GPV (sGPV) in the plasma were significantly lower in *Gp5*$^{Kin/Kin}$ mice than in WT mice (Figure 3-16 B). To confirm the targeting strategy and prove that GPV was not cleaved from the platelet surface upon thrombin stimulation, washed platelets of WT and *Gp5*$^{Kin/Kin}$ mice were activated with thrombin or incubated with NEM (*N-ethylmaleimide*), the latter inducing GPV shedding by metalloproteinases; i.e. independently of thrombin [21], and the amount of sGPV in the supernatant as well as the receptor prevalence on the platelet surface were measured by ELISA and flow cytometry. Unstimulated, washed platelets (Figure 3-17 B, C) or supernatant of unstimulated, washed platelets (Figure 3-17 A)

were used to determine resting values. The amount of sGPV in the supernatant upon thrombin stimulation was greatly diminished in *Gp5*$^{Kin/Kin}$ samples compared to WT samples, confirming the targeting strategy.

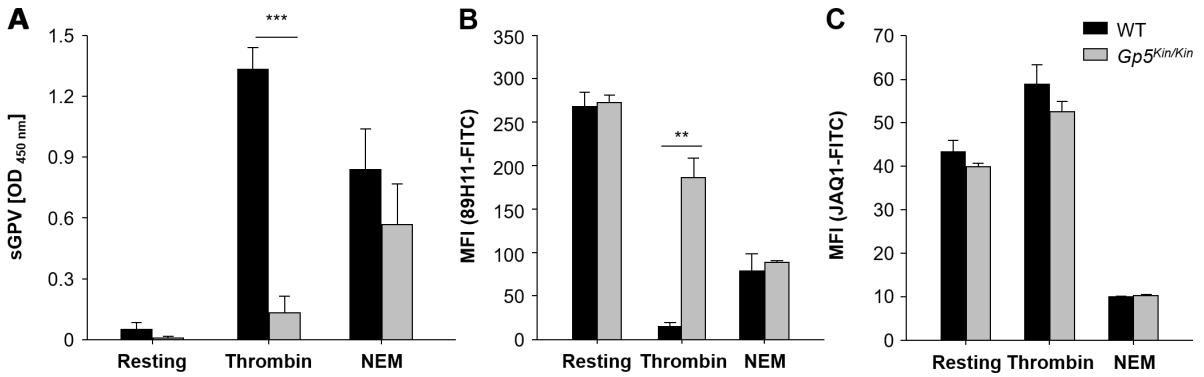

Figure 3-17: R476 point mutation renders GPV insensitive for thrombin-mediated cleavage. Washed platelets were left untreated or stimulated with 0.1 U/ml thrombin (in the presence of 40 µg/ml integrilin and 5 µM EGTA to prevent platelet aggregation) or 2 mM *N-ethylmaleimide* (NEM) for 15 min at 37°C. **(A)** sGPV concentration in the platelet supernatant was measured using a GPV ELISA. **(B, C)** Stimulated platelets were incubated with saturating amounts of fluorophore-conjugated antibodies for 15 min at RT and the surface expression of GPV and GPVI was immediately analyzed by flow cytometry.

Consistently, upon thrombin stimulation, flow cytometric analysis revealed markedly increased GPV levels on the platelet surface of *Gp5*$^{Kin/Kin}$ mice compared to WT mice. Of note, in *Gp5*$^{Kin/Kin}$ mice, a 20% reduction of GPV surface levels was observed upon thrombin stimulation compared to resting values. These experiments were also performed in the presence of the broad range matrix metalloproteinase inhibitor GM6001, since a role of ADAM17- (tumor necrosis factor-α-converting enzyme) dependent shedding of GPV was previously reported [256]. However, the slight reduction of GPV surface prevalence upon stimulation with thrombin was still detectable in the presence of GM6001 in *Gp5*$^{Kin/Kin}$ mice (data not shown). This reduction in GPV surface expression levels observed in the presence of GM6001 is due to internalization of the GPIb-V-IX complex [257]. Flow cytometric analysis revealed unaltered shedding of GPV induced by NEM in *Gp5*$^{Kin/Kin}$ mice compared to WT mice, which is in line with the results obtained by GPV ELISA (Figure 3-17 A, B). GPIX levels remained unchanged under all conditions confirming that the entire GPIb-IX-V complex is not downregulated from the cell surface, which is in line with previous reports [256] (data not shown). Downregulation of GPVI by NEM, but not thrombin served as control for metalloproteinase-dependent shedding [257] and occurred to the same extent in WT and *Gp5*$^{Kin/Kin}$ mice (Figure 3-17 C). Overall, these data confirmed that GPV is not cleaved in *Gp5*$^{Kin/Kin}$ mice upon thrombin stimulation.

3.4.1 Integrin activation and P-selectin exposure is slightly decreased upon CRP stimulation, but does not translate into altered platelet aggregation in *Gp5$^{Kin/Kin}$* mice

Platelet count and size (Table 3-1) as well as platelet life span (data not shown) were indistinguishable between WT and *Gp5$^{Kin/Kin}$* mice, indicating that the point mutation in the thrombin cleavage site does not affect platelet production or clearance.

Table 3-1: Analysis of platelet count, size and surface expression of glycoproteins in WT and *Gp5$^{Kin/Kin}$* mice. Mean platelet count and size were determined using a Sysmex cell counter. Surface expression of platelet glycoproteins was determined by flow cytometry. Diluted whole blood was stained with saturating amounts of FITC-labeled antibodies for 15 min at RT. Platelets were analyzed directly on a FACSCalibur. Results are expressed as mean values ± SD for at least 5 mice per group. MFI, *mean fluorescence intensity*. * p<0.05; ** p<0.01 as compared to WT values.

	WT	*Gp5$^{Kin/Kin}$*	
Count [10^3/µl]	860 ± 188	891 ± 183	
Size [fl]	5.5 ± 0.2	5.5 ± 0.2	
α-GPIb [MFI]	319 ± 18	319 ± 17	
α-GPV [MFI]	305 ± 14	303 ± 21	
α-GPIX [MFI]	504 ± 20	495 ± 33	
α-GPVI [MFI]	54 ± 4	53 ± 5	
α-β3 [MFI]	172 ± 30	154 ± 11	
α- αIIbβ3 [MFI]	409 ± 46	405 ± 44	
α-β1 [MFI]	122 ± 21	129 ± 9	
α- α2 [MFI]	55 ± 3	50 ± 4	**
α- α5 [MFI]	20 ± 3	30 ± 3	
α-CLEC-2 [MFI]	129 ± 19	119 ± 12	
α-CD9 [MFI]	985 ± 64	939 ± 83	
α-CD84 [MFI]	33 ± 6	30 ± 2	*

Expression levels of major platelet surface receptors as assessed by flow cytometry did not show significant alterations (Table 3-1) in *Gp5$^{Kin/Kin}$* mice. Of note, GPIb-V-IX surface expression levels were indistinguishable between mutant and WT platelets, indicating that the point mutation has no obvious effect on the complex composition.

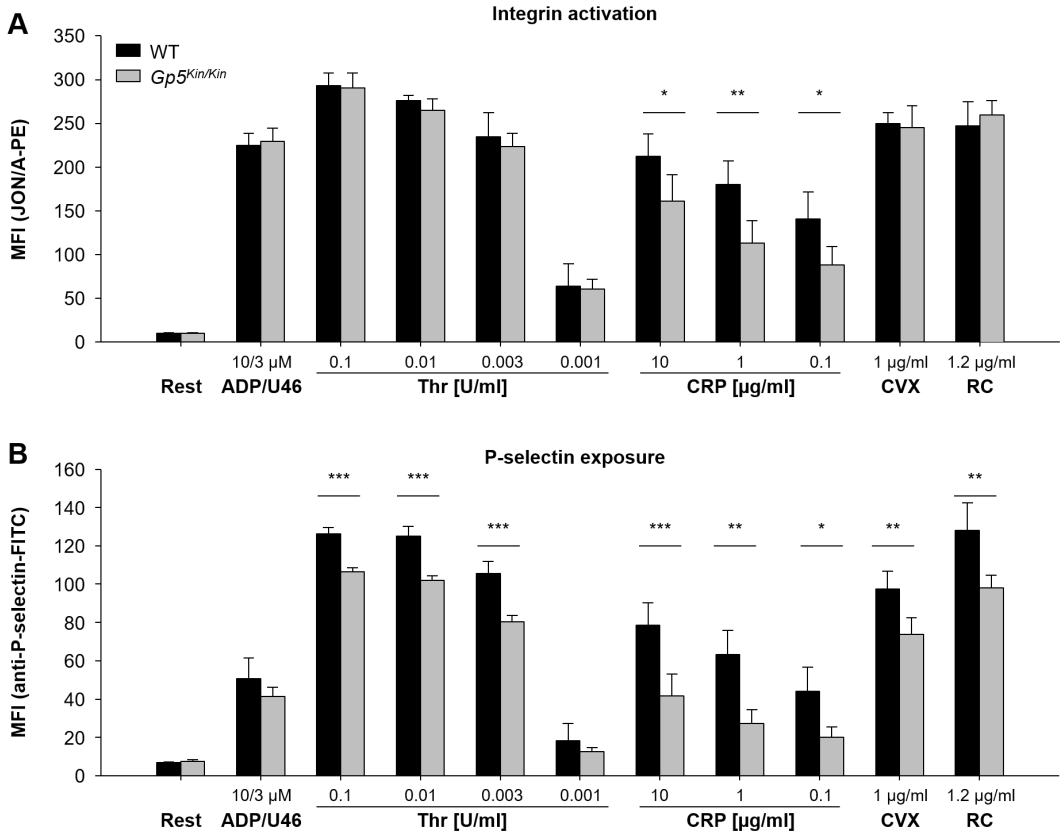

Figure 3-18: Mildly reduced responsiveness of *Gp5*$^{Kin/Kin}$ platelets upon CRP stimulation. (A, B) Washed blood was incubated for 15 min with the indicated agonists in the presence of saturating amounts of JON/A-PE (activated αIIbβ3 integrin) **(A)** and anti-P-selectin-FITC **(B)**. Platelets were gated by their *forward and sideward scatter characteristics* (FSC and SSC). Data shown are MFI ± SD (n=4 mice per group; the data are representative of 3 independent experiments). Rest, resting; U46, U46619; Thr, thrombin; CRP, collagen-related peptide; CVX, convulxin; RC, rhodocytin. * p<0.05; ** p<0.01; *** p<0.001 as compared to WT values.

Measurement of αIIbβ3 integrin activation revealed unaltered responses of *Gp5*$^{Kin/Kin}$ platelets upon stimulation with GPCR-coupled agonists (ADP + U46619, thrombin). Stimulation with CRP resulted in a mildly reduced integrin activation in *Gp5*$^{Kin/Kin}$ platelets, but in comparable integrin activation upon stimulation with CVX and rhodocytin (Figure 3-18 A). R476A point mutation caused slightly diminished degranulation-dependent P-selectin exposure in response to all tested agonists except for the combination of ADP + U46619 (Figure 3-18 B). However, aggregate formation upon stimulation with all tested agonists, including CRP, was unaltered in *Gp5*$^{Kin/Kin}$ platelets indicating that the observed platelet activation defects did not translate into a defective aggregation (Figure 3-19) and may therefore be of minor relevance.

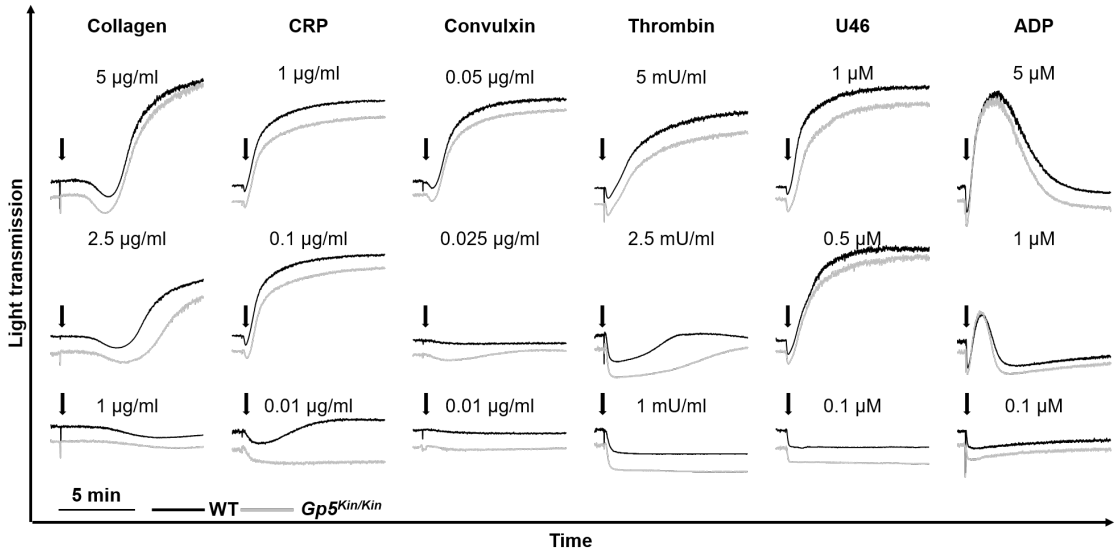

Figure 3-19: Unaltered aggregation of *Gp5*$^{Kin/Kin}$ platelets. Washed platelets were stimulated with the indicated agonists and light transmission was recorded on a Apact four-channel aggregometer over 10 min. Representative aggregation traces of at least 4 independent experiments are shown. U46, U46619; CRP, collagen-related peptide.

3.4.2 *Gp5*$^{Kin/Kin}$ mice display unaltered integrin αIIbβ3 outside-in signaling

To study integrin αIIbβ3 outside-in signaling and cytoskeletal remodeling, platelets were allowed to spread on a fibrinogen-coated surface. Like *Gp5*$^{-/-}$ platelets (data not shown), *Gp5*$^{Kin/Kin}$ platelets spread on fibrinogen to a similar extent and with similar kinetics as WT platelets (Figure 3-20 A, B). The integrin αIIbβ3 also plays a critical role in regulating clot retraction [81]. Upon ligand binding, clot retraction is mainly mediated by αIIbβ3 integrin and the cytoskeleton to consolidate thrombus formation *in vivo*. Clot formation was induced in WT and *Gp5*$^{Kin/Kin}$ *platelet rich plasma* (PRP) by stimulation with thrombin and addition of $CaCl_2$ and monitored over time. Consistently, clot retraction started 45 min after start of the experiment and was also unaltered in *Gp5*$^{Kin/Kin}$ mice (Figure 3-20 C, D), excluding an essential role of the thrombin cleavage site of GPV in cytoskeleton rearrangements and integrin αIIbβ3 outside-in signaling.

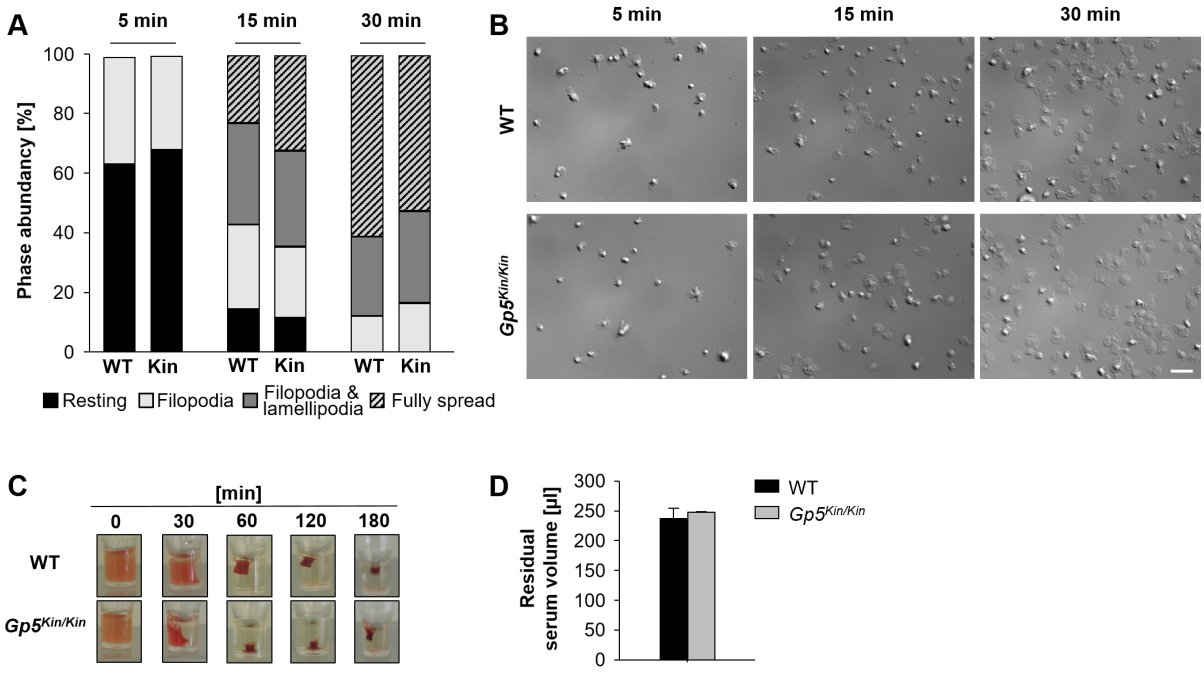

Figure 3-20: *Gp5*$^{Kin/Kin}$ platelets display unaltered spreading on fibrinogen. (A) Washed platelets from WT and *Gp5*$^{Kin/Kin}$ mice were allowed to adhere to immobilized human fibrinogen (100 µg/ml) in the presence of thrombin (0.01 U/ml). **(B)** Images were taken at the indicated time points and representative images are shown. Results indicate percentage of phase abundancy with: (1) round platelets; (2) filopodia; (3) filopodia and lamellipodia; (4) full spread platelets. Scale bar: 5 µm. **(C**) Clot formation was induced in PRP of WT and *Gp5*$^{Kin/Kin}$ mice with 4 U/ml thrombin and clot retraction was monitored over time. Representative images of the indicated time points are shown. **(D)** Residual serum volume after clot retraction. Data are shown as mean ± SD.

3.4.3 Thrombin-uncleavable GPV does not alter platelet adhesion on vWF or P-selectin under flow

In a next step, it was investigated whether a permanent presence of GPV on the platelet surface affects GPIb-ligand interactions. Upon CVX-mediated activation, binding of vWF to activated platelets was unaltered, however binding of fibronectin was reduced in mutant mice by 50% compared to WT mice under static conditions (Figure 3-21 A, B). Since GPIb ligand interactions are shear-dependent, flow adhesion experiments were performed at a high shear rate of 1700 s^{-1}. Firm platelet adhesion to vWF- (Figure 3-21 C) or P-selectin- (Figure 3-21 D) coated surfaces was unaltered in *Gp5*$^{Kin/Kin}$ mice, which is in line with data obtained from *Gp5*$^{-/-}$ mice (Figure 3-3), concluding that GPIb-ligand interactions under flow do not depend on the cleavage of GPV nor its presence on the platelet surface.

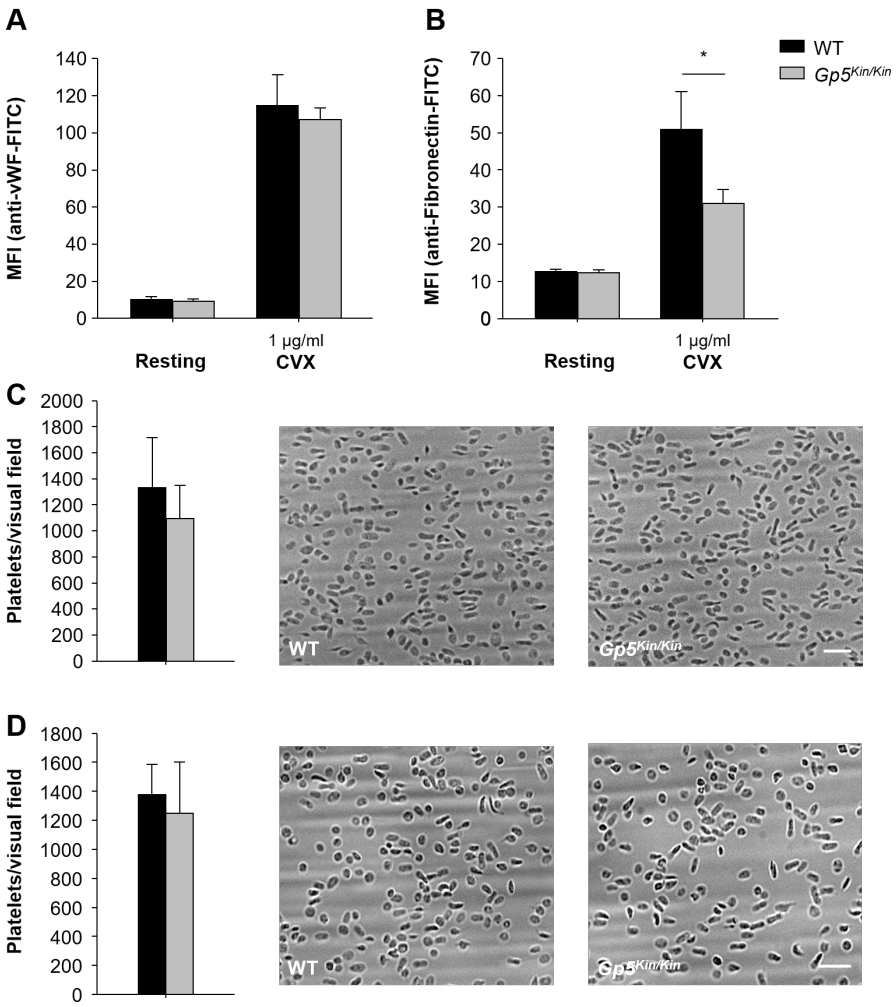

Figure 3-21: Reduced binding of fibronectin to *Gp5*$^{Kin/Kin}$ platelets, but unaltered binding of vWF and adhesion to vWF and P-selectin under flow. (A, B) Diluted whole blood was stimulated with CVX and stained with saturated amounts of anti-vWF FITC **(A)** and anti-fibronectin-FITC **(B)** and binding to activated platelets was measured on a FACSCalibur. Data shown are MFI ± SD (n=4 mice per group; the data are representative of three independent experiments). * $p<0.05$ as compared to WT values. **(C, D)** Whole blood was perfused over a vWF- **(C)** or P-selectin-coated **(D)** surface at 1700 s^{-1} for 4 min and then washed with Tyrode's buffer again for 4 min. The bar graphs display mean number of adherent platelets per visual field. Data shown are mean ± SD (n=5 mice each). Scale bar: 10 µm. CVX, convulxin; vWF, von Willebrand factor.

3.4.4 Increased thrombus formation of *Gp5*$^{Kin/Kin}$ platelets on collagen under flow

It has previously been shown that GPV-deficiency does not affect thrombus formation on collagen under flow and that the collagen-binding site on GPV is of minor relevance for platelet adhesion *in vitro* [135, 210]. To study the role of the thrombin-cleavage site of GPV on collagen under flow, whole blood perfusion experiments were performed at the indicated shear rates. While at a low shear rate of 150 s^{-1} thrombus formation was indistinguishable between *Gp5*$^{Kin/Kin}$ and WT mice, *Gp5*$^{Kin/Kin}$ mice displayed an enhanced surface coverage as well as

thrombus volume with increasing shear rates (Figure 3-22). In contrast, absence of GPV did not influence thrombus formation *in vitro* [210].

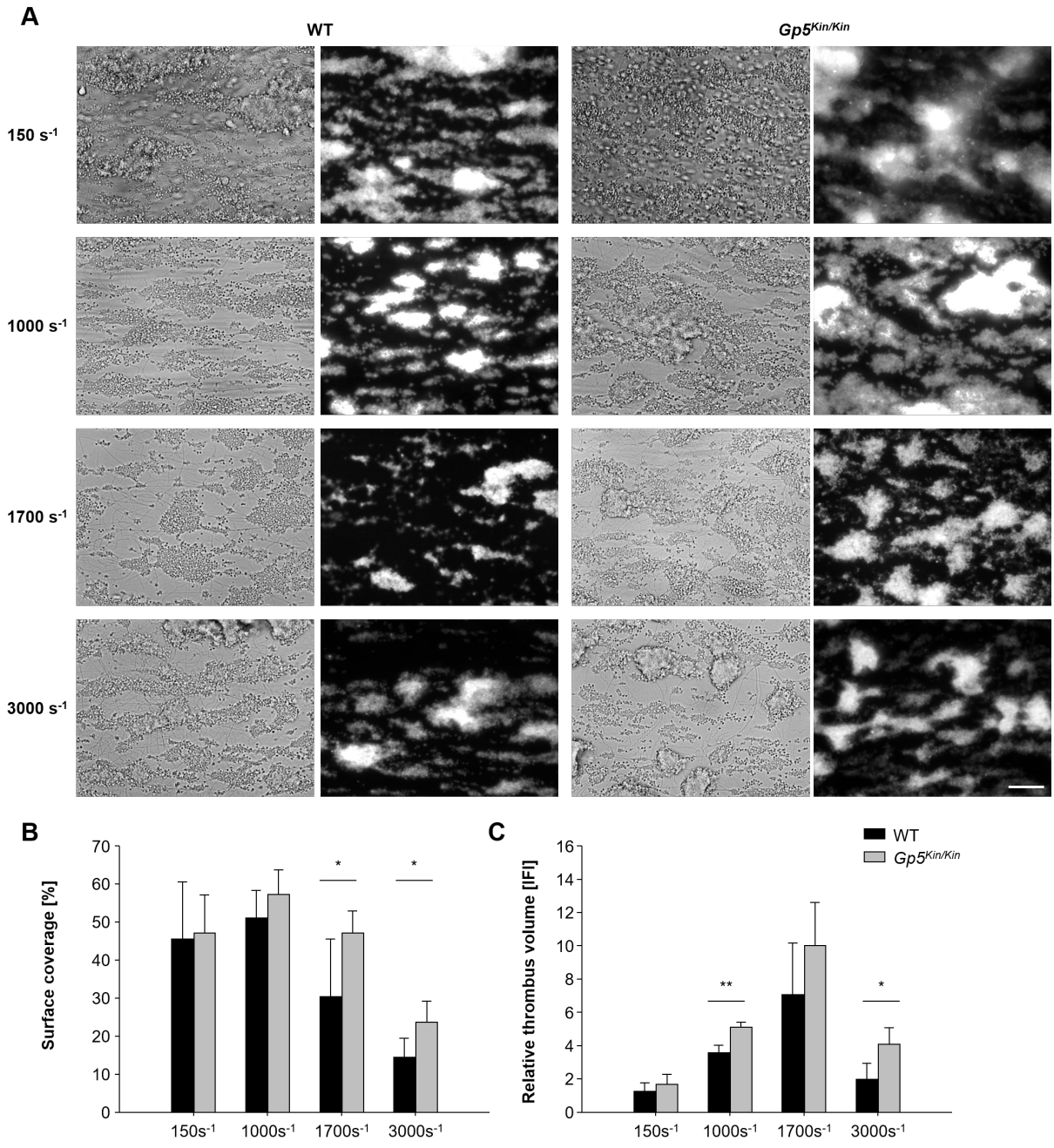

Figure 3-22: Thrombin-uncleavable GPV leads to enhanced adhesion and aggregate formation on collagen under flow. Whole blood was perfused over a collagen-coated (0.2 mg/ml) surface at the indicated shear rates and then washed with Tyrode's buffer for the same time period. Perfusion time was 10 min (150 s^{-1}), 4 min (1000 and 1700 s^{-1}) or 2 min (3000 s^{-1}). **(A)** Representative images of brightfield and fluorescence microscopy. Scale bar: 25 µm. **(B)** The bar graphs display mean values ± SD (n=5 mice each, 2 independent experiments). * $p<0.05$; ** $p<0.01$ as compared to WT values.

3.4.5 *Gp5*$^{Kin/Kin}$ platelets show unaltered procoagulant activity, but enhanced (hem)ITAM-dependent thrombin generation

PS exposure is a measure of procoagulant activity and occurs subsequent to sustained platelet activation and elevated cytosolic Ca^{2+} concentrations. For this, washed platelets were activated with GPCR- and (hem)ITAM-coupled agonists and PS exposure determined by annexin-A5 staining using flow cytometry was found to be unaltered in *Gp5*$^{Kin/Kin}$ mice (data not shown). To study procoagulant activity under flow, whole blood was perfused over a collagen-coated surface at a shear rate of 1000 s^{-1}. Comparable levels of procoagulant activity were found between mutant and WT mice (data not shown). Hence, it can be concluded that the increased reactivity of *Gp5*$^{Kin/Kin}$ platelets on collagen did not translate into enhanced procoagulant activity.

PS exposure plays a critical role in thrombin generation in PRP, which was subsequently studied in *Gp5*$^{Kin/Kin}$ mice. Point mutation of the thrombin cleavage site of GPV resulted in an elevated amount of totally produced thrombin upon stimulation with (hem)ITAM-specific agonists (Figure 3-23 D), but had no effect on the initiation of thrombin generation (Figure 3-23 A), maximal amount of newly generated thrombin (Figure 3-23 B) and time to maximal thrombin generation (Figure 3-23 C). The increased endogenous thrombin potential was rather caused by a delayed inhibition of thrombin generation in *Gp5*$^{Kin/Kin}$ mice upon stimulation with CRP or rhodocytin (Figure 3-23 E). This is partially in contrast to the unaltered PS exposure upon stimulation with (hem)ITAM-specific agonists, but may be consistent with the increased thrombus formation on collagen under flow. In addition, there is growing evidence that factors besides PS exposure trigger thrombin generation [258].

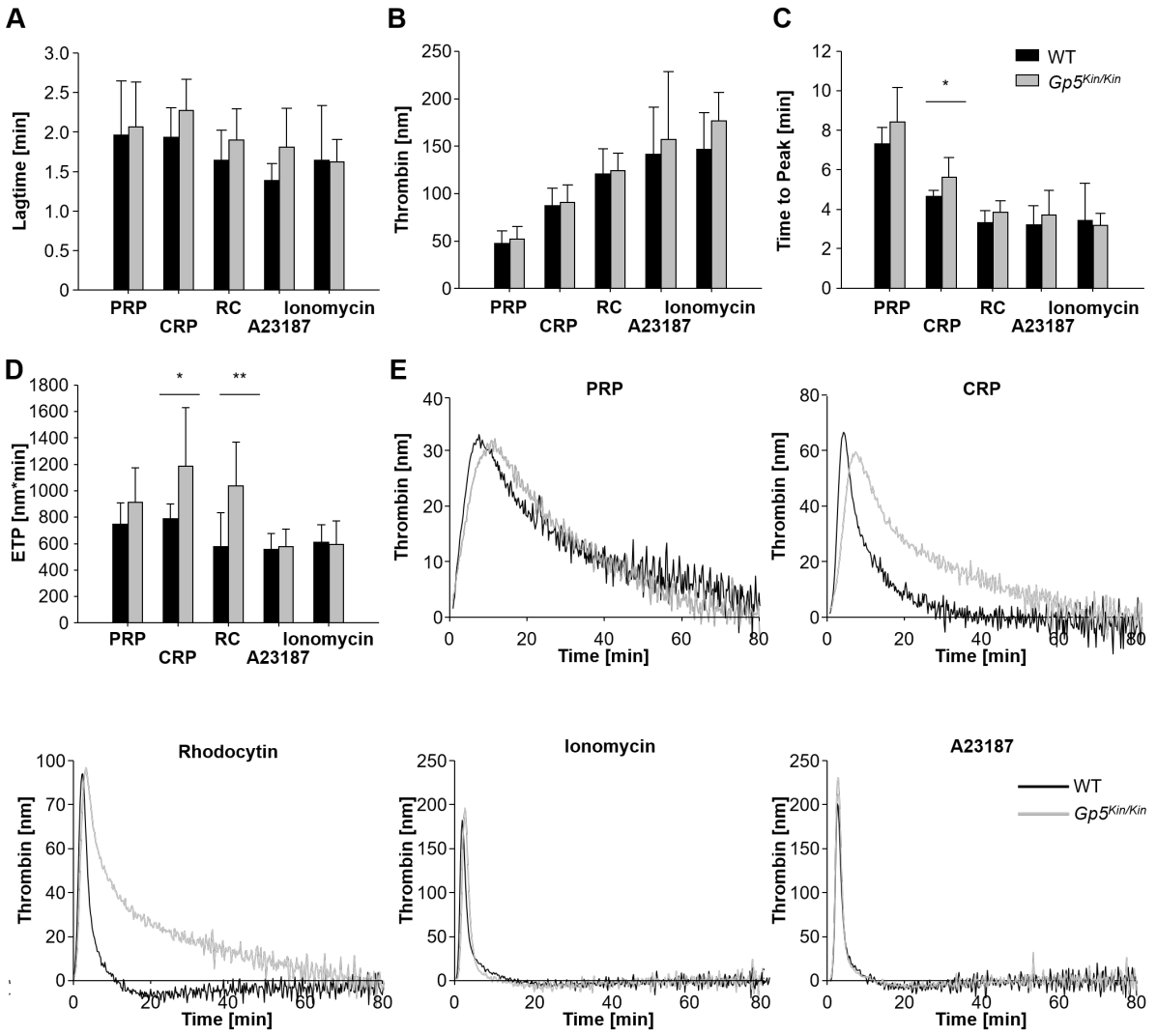

Figure 3-23: *Gp5*$^{Kin/Kin}$ platelets show enhanced (hem)ITAM-dependent thrombin generation. Citrate-anticoagulated platelet-rich plasma was left unstimulated (PRP) or activated by incubation with *collagen-related peptide* (CRP) (20 µg/ml), rhodocytin (1 µg/ml), A23187 (10 µM) or ionomycin (10 µM) for 10 min at 37°C. Thrombin generation was triggered with tissue factor/$CaCl_2$. Lagtime **(A)**, maximal thrombin concentration **(B),** time to peak **(C)** and *endogenous thrombin potential* (ETP) **(D)** were determined. **(E)** Representative thrombin generation curves. Values are mean ± SD (n=9). * p<0.05; ** p<0.01; *** p<0.001 as compared to WT values.

3.4.6 *Gp5*$^{Kin/Kin}$ mice reverse the hemostatic and thrombotic defect caused by lack of GPVI and CLEC-2

To study the *in vivo* relevance of the thrombin-cleavage site of GPV, *Gp5*$^{Kin/Kin}$ mice were subjected to a tail bleeding time assay. To this end, mice were again injected with JAQ1 or INU1 as described (3.1.4). Mutant mice displayed shortened bleeding times compared to WT mice (389 ± 186 s in WT mice vs. 232 ± 113 s in *Gp5*$^{Kin/Kin}$ mice, p<0.05) (Figure 3-24 A). Strikingly, *Gp5*$^{Kin/Kin}$ mice restored the hemostatic defect of GPVI-deficient or CLEC-2-deficient mice (Figure 3-24), resembling the *Gp5*$^{-/-}$ phenotype (Figure 3-5).

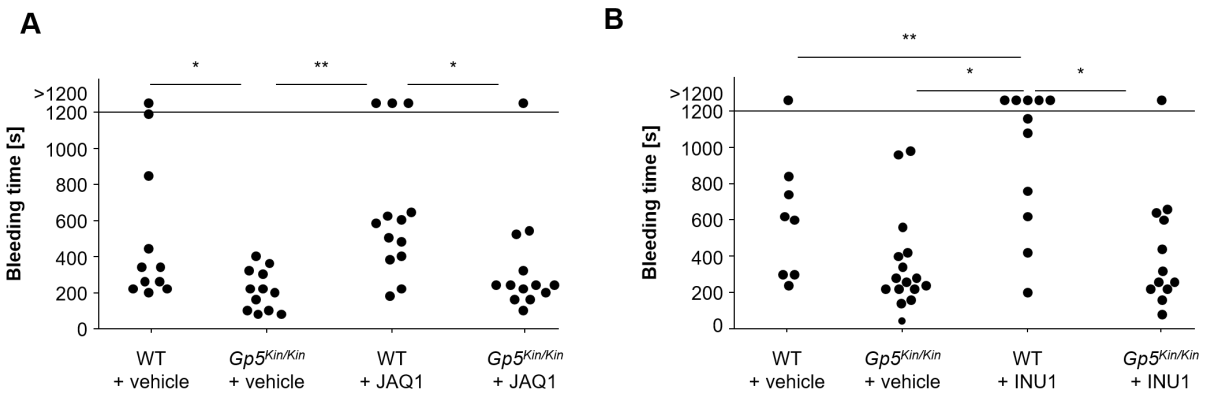

Figure 3-24: *Gp5*$^{Kin/Kin}$ mice phenocopy *Gp5*$^{-/-}$ mice and restore hemostasis in the absence of GPVI and CLEC-2. 1 mm of the tail tip of each mouse was cut and time to cessation of blood flow was measured using a filter paper. Each symbol represents one animal. * p<0.05; ** p<0.01.

In line with this, time to *in vivo* occlusive thrombus formation upon mechanical injury of the abdominal aorta was comparable between *Gp5*$^{Kin/Kin}$ and WT mice. Surprisingly, *Gp5*$^{Kin/Kin}$ mice maintained thrombus formation in the absence of GPVI and CLEC-2 leading to occlusion times comparable to WT mice (Figure 3-25 A).

In addition, platelet accumulation was studied after $FeCl_3$-induced injury of the mesenteric arterioles using intravital fluorescence microscopy. Time to beginning of thrombus formation was indistinguishable in mutant mice, independent of the expression of GPVI, whereas GPVI-depleted WT mice displayed a significant delay until beginning of thrombus formation (5.9 ± 3.1 min in vehicle-treated WT, 5.4 ± 2.6 min in vehicle-treated *Gp5*$^{Kin/Kin}$ mice, 7.2 ± 4.9 min in JAQ1-treated *Gp5*$^{Kin/Kin}$ mice (n.s.) versus 10.7 ± 6.1 min in JAQ1-treated WT mice, p<0.05 compared to WT and *Gp5*$^{Kin/Kin}$ mice). Consequently, time to occlusion was also unaltered in *Gp5*$^{Kin/Kin}$ mice as compared to WT mice. This was independent of the presence of GPVI, since GPVI-depleted *Gp5*$^{Kin/Kin}$ mice formed occlusive thrombi in a time comparable to WT mice, whereas most of JAQ1-treated WT mice were unable to form occlusive thrombi within the observation period (Figure 3-25 B). These results indicated that also mice with a point mutation rendering GPV uncleavable by thrombin can restore arterial thrombus formation in the absence of GPVI or CLEC-2 and thereby reproduce the *Gp5*$^{-/-}$ phenotype (Figure 3-4).

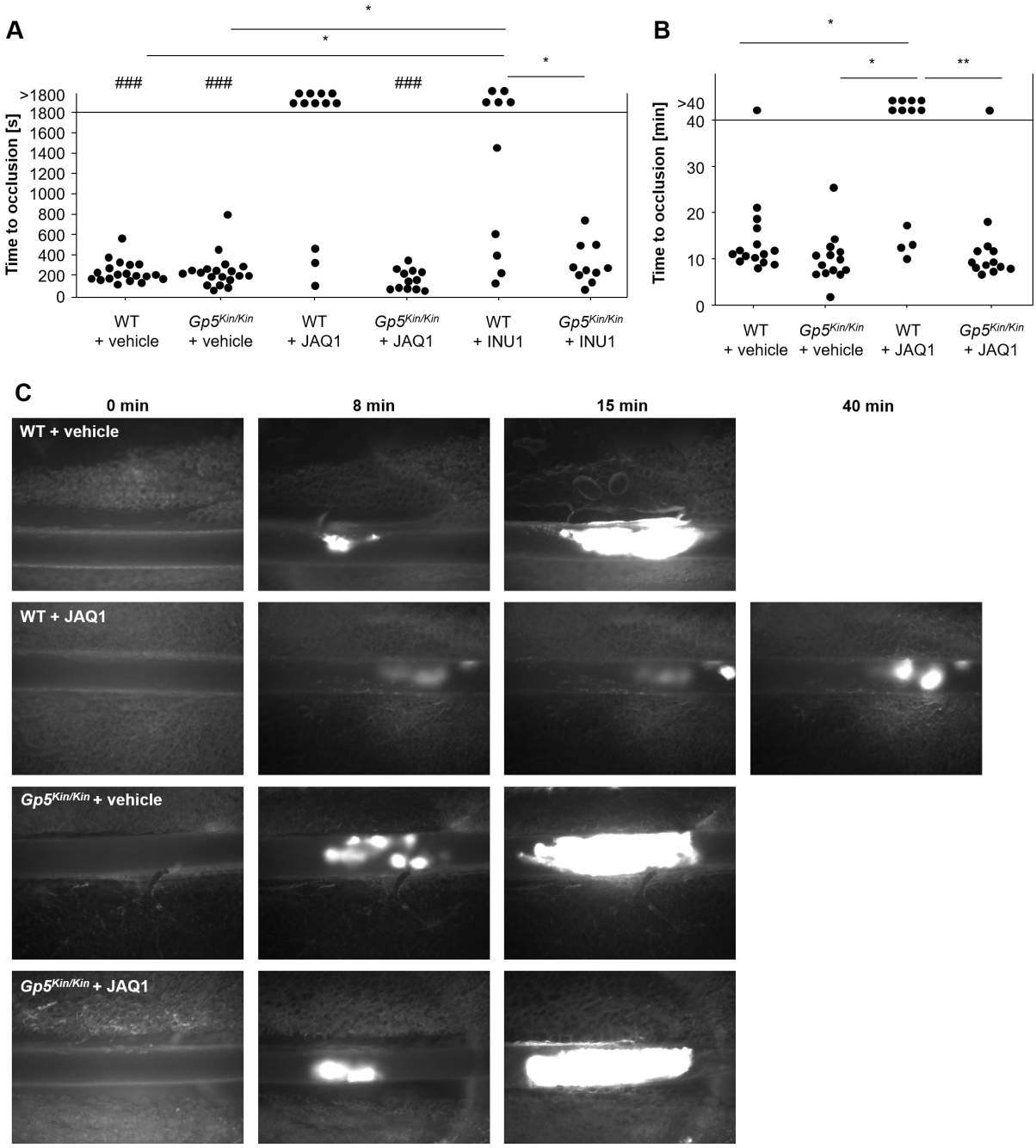

Figure 3-25: *Gp5*$^{Kin/Kin}$ mice phenocopy *Gp5*$^{-/-}$ mice and restore thrombus formation in the absence of GPVI and CLEC-2 in *in vivo* thrombosis models. (A) The abdominal aorta was mechanically injured by a single firm compression with a forceps and blood flow was monitored with a Doppler flowmeter. Time to final occlusion is shown. Each symbol represents one individual mouse. **(B, C)** Mesenteric arterioles were injured with 20% $FeCl_3$ and adhesion and thrombus formation of fluorescently-labeled platelets was monitored by intravital microscopy. Each dot represents one vessel. ### p<0.001, compared to JAQ1-treated WT mice; * p<0.05; ** p<0.01; *** p<0.001.

3.5 *Gp5*$^{hGp5/hGp5}$ mice display unaltered platelet activation, aggregation and thrombus formation on collagen

It was previously shown that GPV is dispensable for platelet function in thrombosis and hemostasis and GPV-deficiency only led to a slight thrombin hyperresponsiveness [144, 145, 210]. Most strikingly, the absence of GPV could restore thrombus formation and hemostasis in the absence of the two strong platelet-activating receptors GPVI and CLEC-2. The blocking anti-mouse GPV antibodies 89F12 and 5G2 reproduced the *Gp5*$^{-/-}$ phenotype by modulating thrombosis and hemostasis in the absence of GPVI and CLEC-2 in *in vivo* models. These results establish GPV as an important counter-regulator of (hem)ITAM signaling and are of high clinical relevance as they point to a potential treatment option under hemorrhagic or inflammatory conditions. However, GPV exhibits its thrombus-modulatory role only *in vivo*, but not in any tested *in vitro* condition. Therefore, an *in vivo* model to study human GPV is required to translate the findings on murine GPV to the human system.

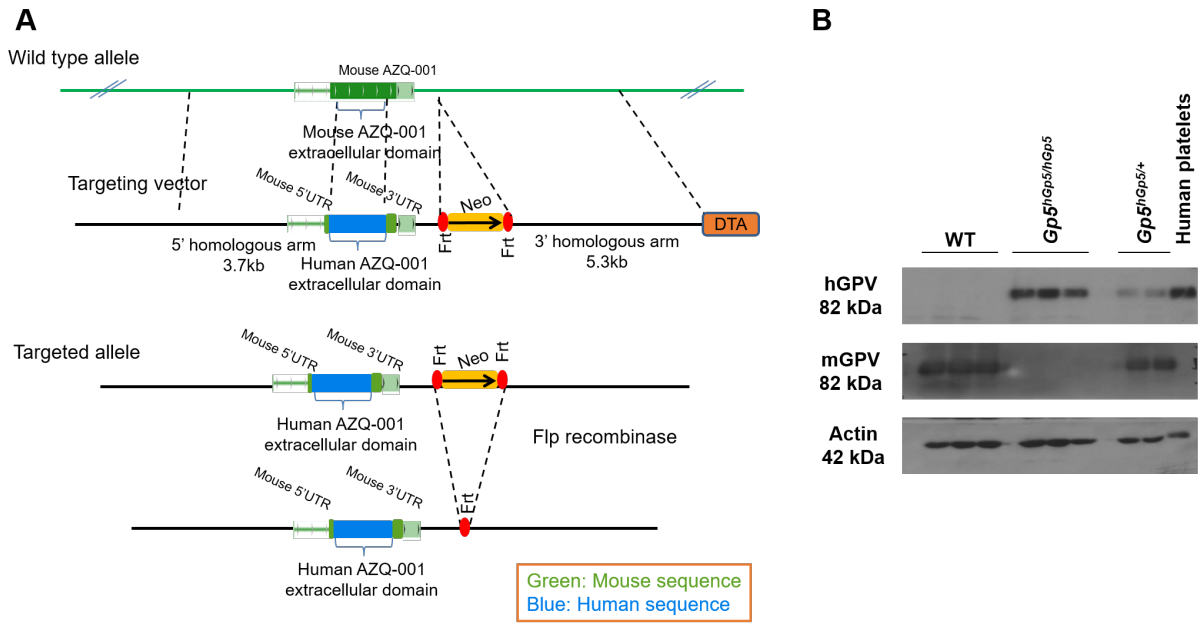

Figure 3-26: Generation of *Gp5*$^{hGp5/hGp5}$ mice. (A) Simplified targeting strategy. The extracellular domain of murine GPV was replaced by the extracellular domain of human GPV. **(B)** Confirmation of hGPV expression instead of mGPV in *Gp5*$^{hGp5/hGp5}$ mice by Western Blot.

Therefore, a humanized mouse line was generated where the extracellular domain of murine GPV (518 aa) was replaced by the extracellular domain of human GPV (519 aa). However, the intracellular and transmembrane domain were left as mouse protein to not interfere with the GPIb-V-IX complex assembly, since the interaction of the transmembrane domain of GPV and

GPIb is crucial for the correct expression and assembly of the whole complex (Prof. Renhao Li, personal communication). For this, 1.5 kb mouse *Gp5* genetic DNA, spanning from the 17th to 518th aa codon within in the second exon, was replaced with 1.5 kb human orthologous region. A Neo-cassette was inserted into the non-conserved regions downstream of mouse *Gp5* 3'UTR to minimize disruption of *Gp5* expression (Figure 3-26 A). The mouse line was generated in collaboration with Biocytogen. Heterozygous *Gp5*$^{hGp5/mGp5}$ mice were crossed with Flip-positive mice to remove the Neo-cassette. Expression of the human instead of the mouse extracellular domain of GPV was confirmed by Western blot analysis using anti-human and anti-mouse GPV antibodies, respectively, which both bind to the extracellular domain of GPV. While *Gp5*$^{hGp5/mGp5}$ mice expressed both proteins, the murine protein was absent in homozygous *Gp5*$^{hGp5/hGp5}$ mice (Figure 3-26 B).

Intercrossing of *Gp5*$^{hGp5/mGp5}$ mice yielded *Gp5*$^{hGp5/hGp5}$ mice in the expected Mendelian ratio. They showed normal growth, were fertile and appeared healthy (data not shown).

To study the consequences of the extracellular domain replacement by human GPV on the hematopoietic system, red blood cell, white blood cell as well as platelet count were determined and found to be unaltered in *Gp5*$^{hGp5/hGp5}$ mice, but the mean platelet volume was slightly increased. In consequence, surface expression of several platelet surface receptors was moderately elevated, including β3 and α5 integrins, CLEC-2 and CD84, however, GPVI surface expression was slightly reduced. Notably, the expression of the GPIb-IX complex was not affected by the replacement with human GPV, indicated by unaltered surface GPIb and GPIX levels (Table 3-2).

To test whether replacement of the mouse extracellular domain of GPV by human GPV affects platelet turnover, platelet life span was assessed as described previously (3.4.1). For this purpose, circulating platelets were labeled with a fluorescence-tagged anti-GPIX derivative. The life span of platelets with hGPV was indistinguishable from that in WT mice (data not shown), indicating that platelet production and clearing is not affected in mutant animals.

In a next step, agonist-induced αIIbβ3 integrin activation and degranulation-dependent P-selectin exposure were determined. Platelets of *Gp5*$^{hGp5/hGp5}$ and WT mice displayed a comparable integrin inside-out activation as well as P-selectin exposure in response to all tested agonists (Figure 3-27). Remarkably, platelet activation upon stimulation with intermediate and low concentrations of thrombin, which led to a mild hyperreactivity of GPV-deficient platelets, was unaltered in *Gp5*$^{hGp5/hGp5}$ mice indicating a comparable competition for thrombin by human and murine GPV.

Table 3-2: Analysis of platelet count, size and surface expression of glycoproteins in WT and *Gp5$^{hGp5/hGp5}$* mice. Mean platelet size, mean blood cell counts as well as hematocrit levels were determined using a Sysmex cell counter. Surface expression of platelet glycoproteins was determined by flow cytometry. Diluted whole blood was stained with saturating amounts of FITC-labeled antibodies for 15 min at RT. Platelets were analyzed directly on a FACSCalibur. Results are expressed as mean values ± SD for at least 5 mice per group. MFI, *mean fluorescence intensity*. * p<0.05; ** p<0.01; *** p<0.001 as compared to WT values.

	WT	***Gp5$^{hGp5/hGp5}$***	
Count [10^3/µl]	751 ± 95	704 ± 88	
Size [fl]	5.3 ± 0.1	5.8 ± 0.3	*
WBC [10^3/µl]	9.0 ± 2.1	7.9 ± 2.1	
RBC [10^6/µl]	7.8 ± 2.2	7.1 ± 1.4	
HCT [%]	42.1 ± 11.8	37.2 ± 7.3	
α-GPIb [MFI]	351 ± 14	394 ± 23	
α-mGPV [MFI]	470 ± 23	6 ± 2	***
α-GPIX [MFI]	472 ± 12	476 ± 13	
α-GPVI [MFI]	64 ± 1	57 ± 1	***
α-β3 [MFI]	384 ± 33	450 ± 23	**
α- αIIbβ3 [MFI]	560 ± 46	594 ± 50	
α- α2 [MFI]	73 ± 5	79 ± 6	
α- α5 [MFI]	57 ± 3	42 ± 1	***
α-CLEC-2 [MFI]	246 ± 7	273 ± 15	*
α-CD9 [MFI]	929 ± 67	995 ± 49	
α-CD84 [MFI]	38 ± 3	44 ± 2	**

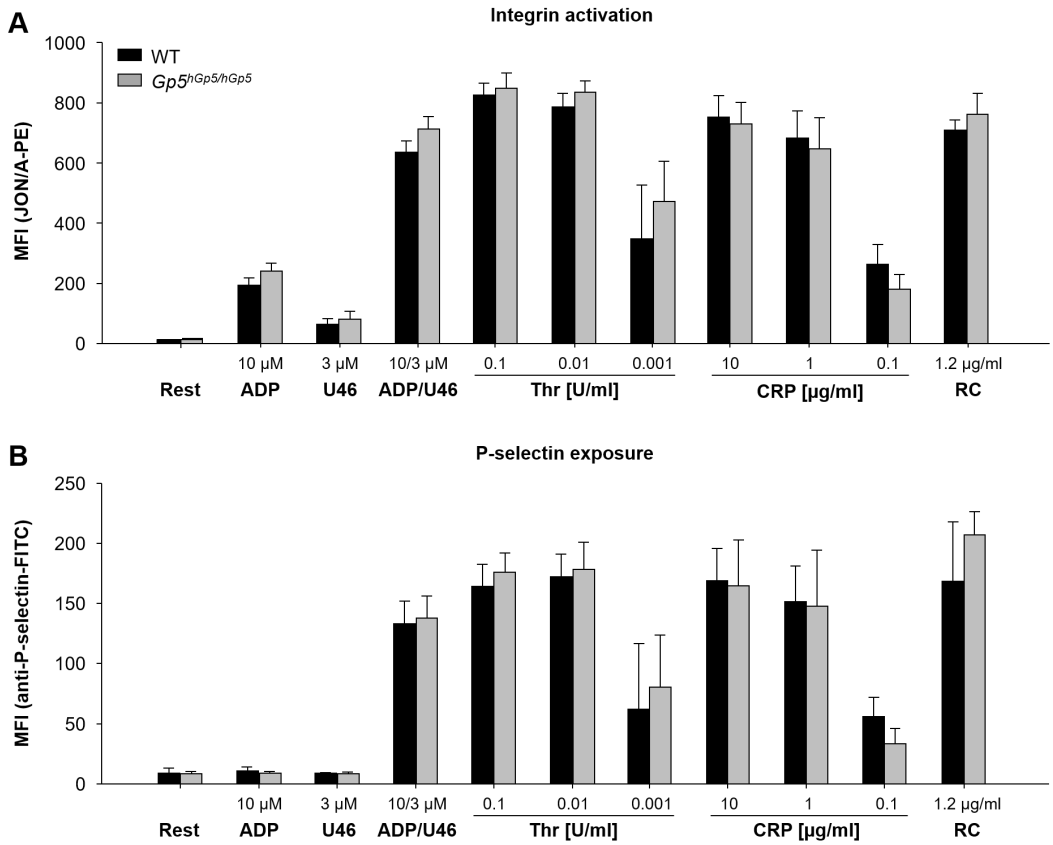

Figure 3-27: Platelet activation responses are comparable in *Gp5*$^{hGp5/hGp5}$ and WT mice. (A, B) Washed blood was stimulated with the indicated agonists in the presence of saturating amounts of JON/A-PE (activated αIIbβ3 integrin) **(A**) and anti-P-selectin-FITC **(B)** for 15 min. Platelets were gated by their *forward and sideward scatter characteristics* (FSC and SSC). Data shown are MFI ± SD (n=5 mice per group; 3 independent experiments). Rest, resting; U46, U46619; Thr, thrombin; CRP, collagen-related peptide; RC, rhodocytin.

In line with this, platelet aggregation was investigated in response to collagen, CRP and thrombin. None of the tested conditions revealed any differences in aggregation responses between *Gp5*$^{hGp5/hGp5}$ and WT mice (Figure 3-28 A).

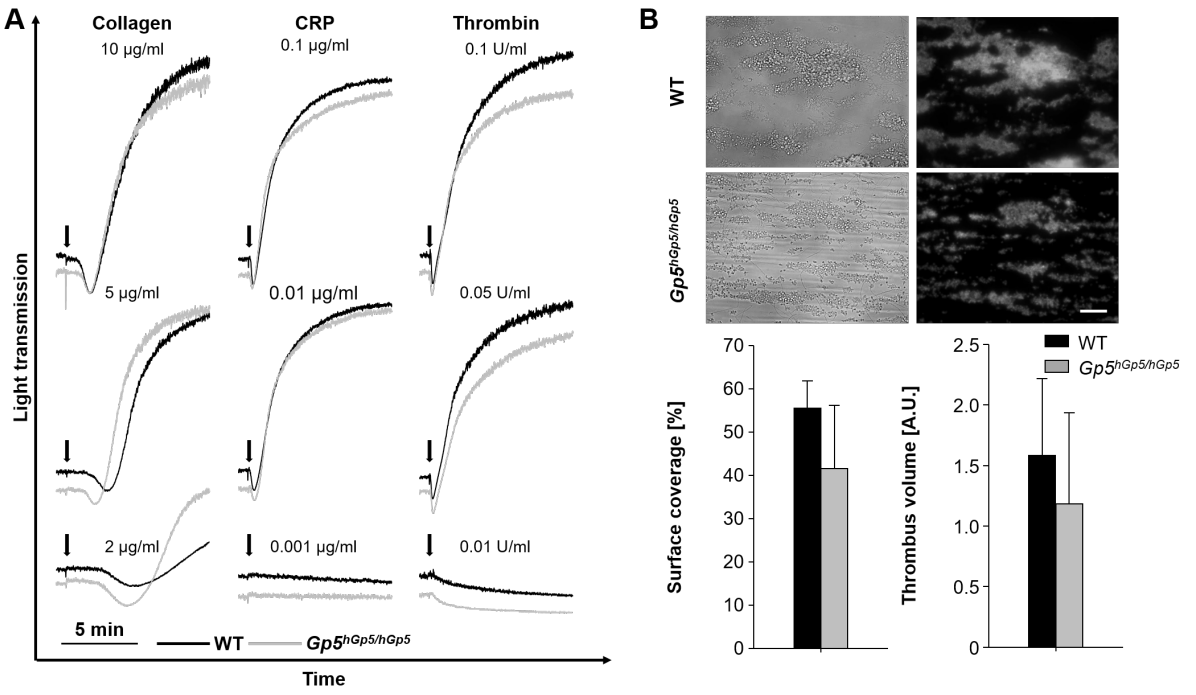

Figure 3-28: Neither platelet aggregation nor thrombus formation on collagen under flow is impaired in *Gp5*$^{hGp5/hGp5}$ platelets. (A) Washed platelets were activated with the indicated agonists. Light transmission was recorded on an Apact four-channel aggregometer over 10 min and calculated as arbitrary units with 100% transmission adjusted to platelet poor plasma. The results shown are representative of at least 3 independent experiments. Arrows indicate the time point of agonist addition. **(B)** Whole blood was perfused over a collagen-coated (0.2 mg/ml) surface at a shear rate of 1700 s^{-1} for 4 min and then washed with Tyrode's buffer for the same time period. Representative images of brightfield and fluorescence microscopy. Scale bar: 25 µm. The bar graphs display mean values ± SD (n=5 mice each, 2 independent experiments). CRP, collagen-related peptide.

To test the functional consequences of replacing the extracellular domain of murine GPV by human GPV under physiological conditions, platelet adhesion and thrombus formation on a collagen-coated surface were analyzed in a flow adhesion assay. At a high shear rate of 1700 s^{-1}, platelet adhesion and aggregate formation on collagen was indistinguishable between *Gp5*$^{hGp5/hGp5}$ and WT mice (Figure 3-28 B). Together, these results indicate that replacing the extracellular domain of murine GPV by human GPV does not affect major platelet functions *in vitro*, since the obtained results did not differ from those obtained with WT platelets. This renders this mouse line a valuable tool for further studies, e.g. to screen for newly produced anti-human GPV antibodies, to confirm a possible interaction of shGPV *in vivo* and later, to test and screen the efficacy of potential new antithrombotics based on the herein described mode of action of GPV.

3.6 Soluble murine GPV has an antithrombotic effect

Thrombin is the most potent physiological activator of platelets. During platelet activation upon vascular injury, thrombin is generated and triggers an amplification cascade leading to initiation of the coagulation cascade, further platelet activation and finally to the formation of a stable thrombus by converting fibrinogen to fibrin. Upon platelet activation, as soon as thrombin is present, GPV is cleaved releasing a soluble 69 kDa fragment (sGPV) into the plasma. It is known that this cleavage is not related to the physiological role of thrombin in platelet activation [46, 207], however, the physiological role of sGPV remained so far unknown. The results presented in this thesis on *Gp5*$^{-/-}$ and especially *Gp5*$^{Kin/Kin}$ mice indicate that GPV exerts its thrombus-modulating role independent of its thrombin cleavage site and therefore pointed to a regulatory role of soluble GPV in thrombus formation.

3.6.1 Expression and purification of smGPV

To study the role of smGPV, the extracellular domain of murine GPV (including the thrombin and the ADAM-cleavage sites) fused to a flag tag (Figure 3-29) was cloned into the pEZ-Mm02808-Lv203 vector and CHO-K1 cells were transduced with the lentiviral expression construct to obtain a stable cell line. Puromycin was used as selection antibiotic. The bicistronic pEZ-Mm02808-Lv203 vector also contains eGFP which is expressed together with GPV-EX. GFP fluorescence of CHO-GPV-EX cells confirmed expression of the vector (data not shown). Recombinant smGPV was secreted into the cell culture supernatant and could be detected in the supernatant of cultured cells by a GPV ELISA (Figure 3-30 A).

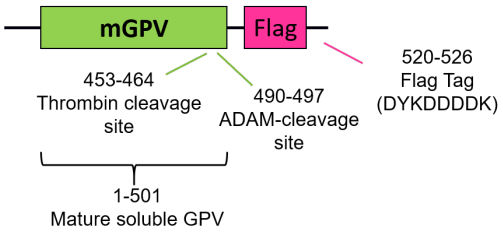

Figure 3-29: Recombinant soluble murine GPV. Simplified scheme of the extracellular domain of murine GPV. The protein contains the thrombin and the ADAM cleavage sites. To facilitate protein purification, a Flag tag was fused to the protein via a linker. ADAM, a disintegrin metalloprotease.

For purification, the cell culture supernatant was incubated with an anti-Flag M2 affinity gel allowing the binding of smGPV to the gel via its flag tag. The protein was then competitively eluted using flag-peptide. Purification of smGPV was assessed by Western blot using an anti-mGPV and an anti-Flag antibody (Figure 3-30 C). Besides this, the purified protein could be detected in a mGPV ELISA (Figure 3-30 D). Purity was checked by Coomassie staining (Figure

3-30 B). For further *in vitro* and *in vivo* studies, the purified protein was dialyzed against PBS and concentrated to approximately 1 mg/ml.

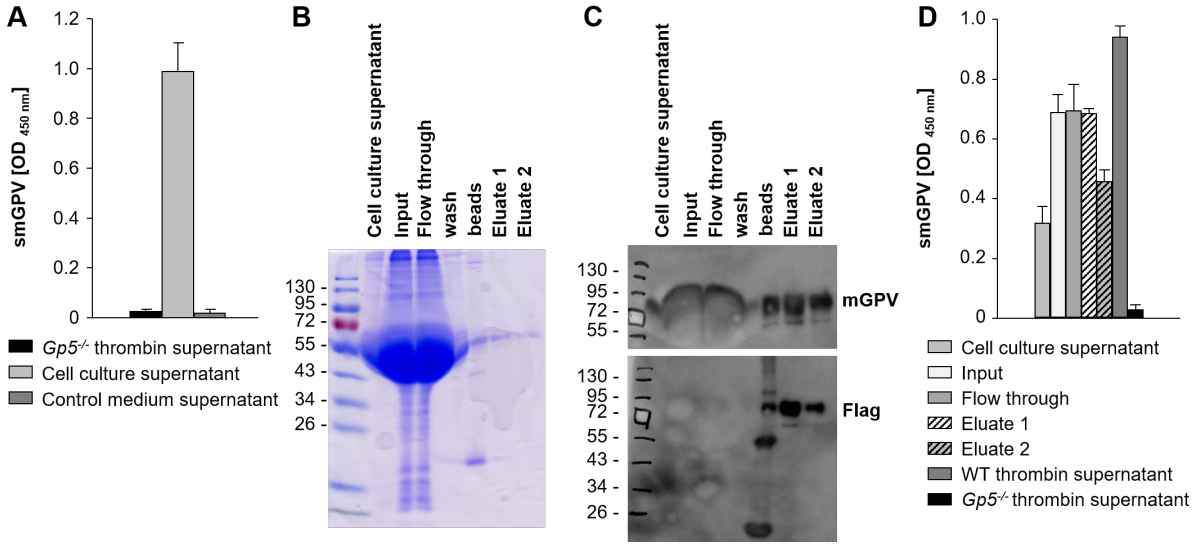

Figure 3-30: Expression and purification of soluble murine GPV. CHO-K1 cell line was stably transfected with the extracellular domain of murine GPV via a lentiviral approach. Therefore, the extracellular domain of GPV was cloned into the pEZ-Mm02808-Lv203 vector. **(A)** GPV ELISA of cell culture supernatant of CHO-GPV-EX cells. smGPV protein was secreted into the cell culture supernatant. **(B)** Coomassie staining and **(C)** Western blot were performed to validate purification of smGPV from cell culture supernatant with an anti-mouse GPV and an anti-Flag antibody. **(D)** GPV ELISA was used to validate purification of smGPV from cell culture supernatant.

3.6.2 smGPV does not alter platelet function *in vitro* under static conditions

Incubation of 10 µg/ml smGPV with washed whole blood did not cause any alteration in platelet count, but led to a very mild reduction in size as well as in the surface prevalence of GPIb, GPIX, αIIbβ3 and CD9 (data not shown). Injection of smGPV intravenously did also not affect platelet count (data not shown).

smGPV incubation *in vitro* did not influence agonist-induced αIIbβ3 integrin activation as well as degranulation-dependent P-selectin exposure upon stimulation with all tested agonists (data not shown). Consistently, aggregate formation in washed platelets (Figure 3-31 A), PRP (Figure 3-31 B) or whole blood (Figure 3-31 C) in response to all tested agonists was unaltered after incubation with smGPV compared to untreated WT controls (Figure 3-31). This indicates that smGPV does not affect platelet activation and aggregation under static conditions.

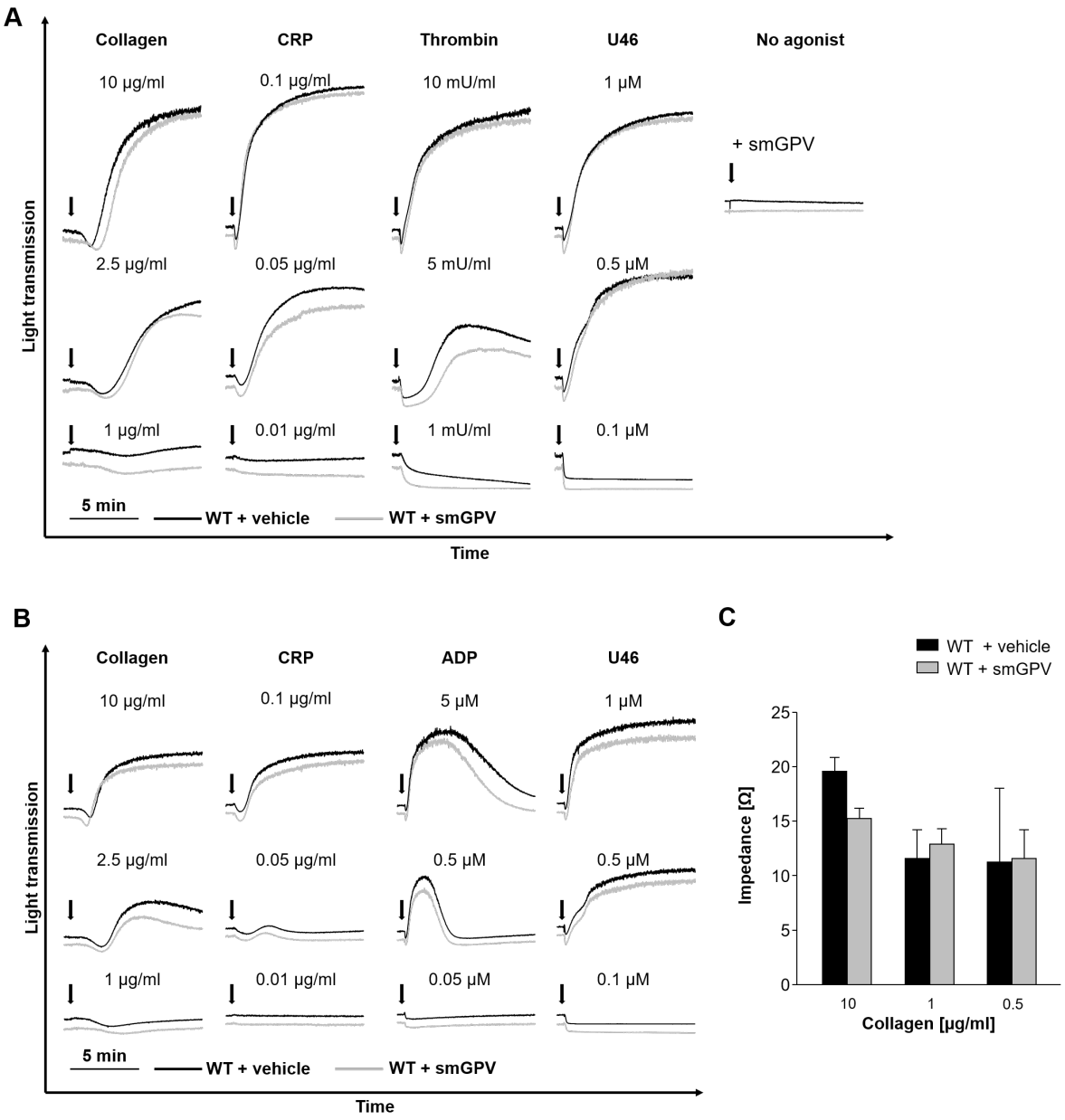

Figure 3-31: Platelet aggregation is not altered by exogenous smGPV. Washed platelets **(A),** PRP **(B)** and whole blood **(C)** were incubated with 10 µg/ml smGPV *in vitro* for 5 min at 37°C prior to stimulation with the indicated agonists. Light transmission was recorded on an Apact four-channel aggregometer (washed platelets, PRP) or on a Chrono-log whole blood aggregometer (whole blood) over 10 min. Traces represent light transmission over time, with PRP set as 0% and platelet poor plasma as 100% aggregation. The results are representative of at least 3 independent experiments. CRP, collagen-related peptide; Thr, thrombin; U46, U46619.

3.6.3 smGPV reduces thrombus formation on collagen under flow

Next, flow adhesion experiments were performed to study the role of smGPV under shear conditions. *In vitro,* platelet adhesion and thrombus formation on collagen was diminished in the presence of smGPV. The thrombus-reducing effect of smGPV was concentration-dependent, but shear rate-independent. While incubation with 10 µg smGPV was not sufficient

to alter thrombus formation, 20 µg smGPV caused a significant decrease in surface coverage as well as thrombus volume. The effect was even more pronounced after incubation with 40 µg smGPV, where thrombus formation was almost abrogated (Figure 3-32). Flow adhesion assays were performed at a low shear rate of 150 s^{-1} and 1000 s^{-1}, which model flow conditions in venules or large arteries, up to high shear rates of 1700 s^{-1} and 3000 s^{-1}, resembling shear stress in small arterioles [259]. After incubation with 20 µg smGPV, surface coverage and thrombus volume were diminished at all tested shear rates to a comparable extent (Figure 3-33). Together, *in vitro* incubation with smGPV reduced thrombus formation on collagen in a concentration-dependent, but shear rate-independent manner.

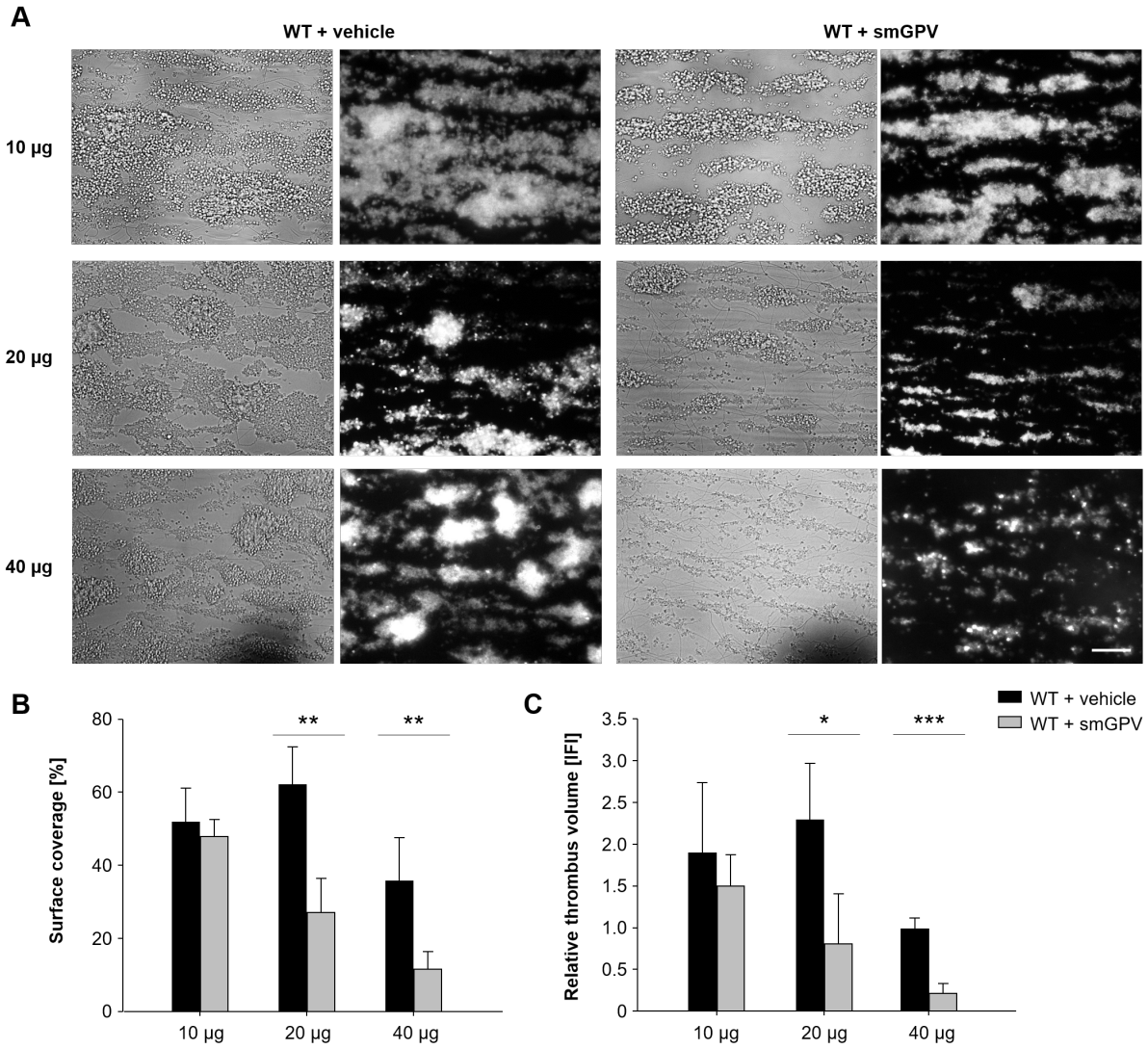

Figure 3-32: smGPV reduces platelet adhesion and thrombus formation on collagen under flow in a concentration-dependent manner. Heparinized whole blood was incubated with the indicated amount of smGPV *in vitro* for 5 min at 37°C in the presence of a Dylight 488-conjugated anti-GPIX derivative and perfused over a collagen-coated (0.2 mg/ml) surface at a shear rate of 1700 s^{-1} for 4 min and then washed with Tyrode's buffer for the same time period. **(A)** Representative images of brightfield and fluorescence microscopy. Scale bar: 25 µm. **(B)** The bar graphs display mean values ± SD (n=5 mice per group, 2 independent experiments per concentration). * p<0.05; ** p<0.01; *** p<0.001.

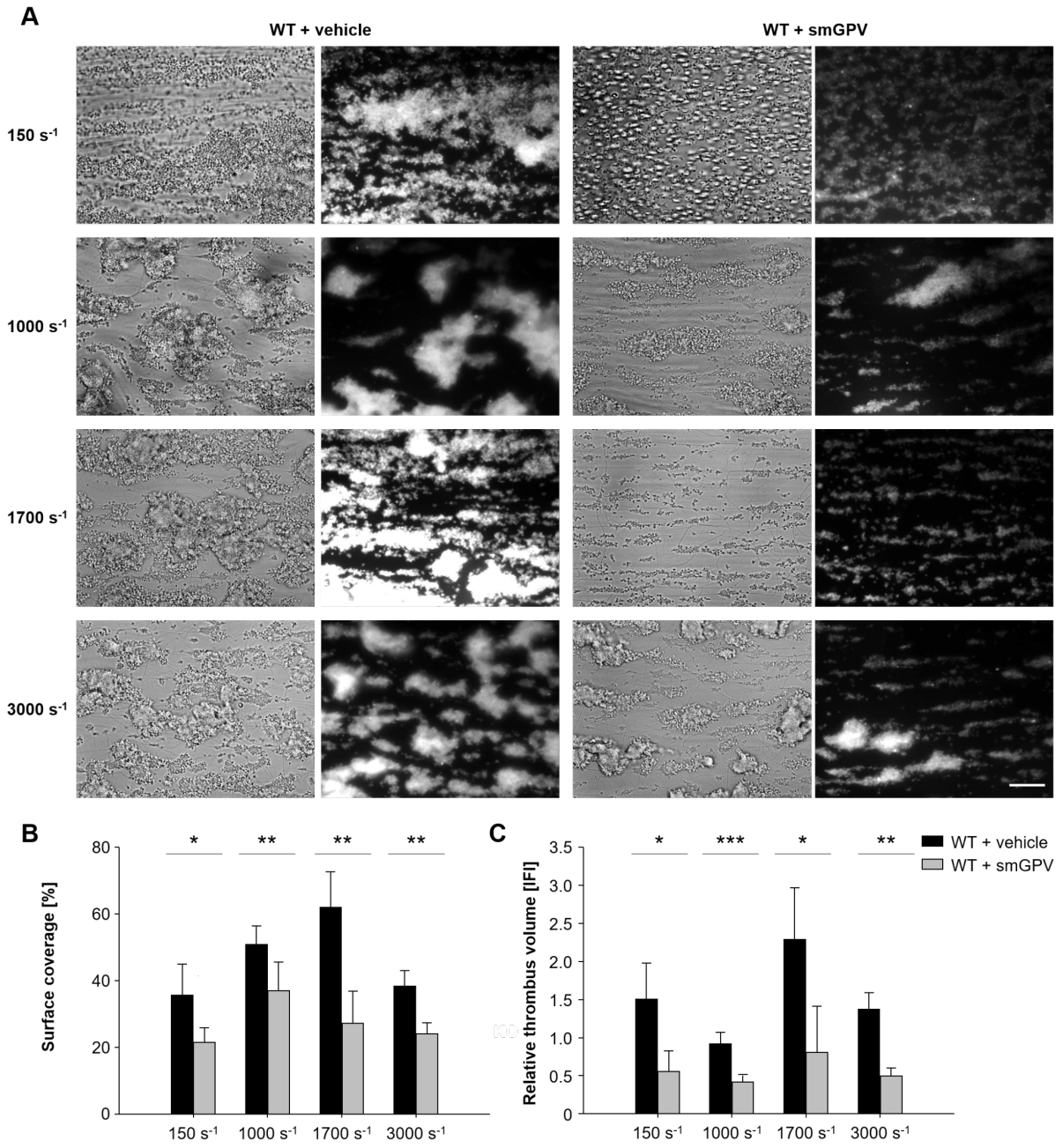

Figure 3-33: smGPV reduces platelet adhesion and thrombus formation on collagen under flow shear rate-independently. Heparinized whole blood was incubated with 20 µg smGPV *in vitro* for 5 min at 37°C in the presence of a Dylight 488-conjugated anti-GPIX derivative and perfused over a collagen-coated (0.2 mg/ml) surface at the indicated shear rates and then washed with Tyrode's buffer for the same time period. Perfusion time was 10 min (150 s^{-1}), 4 min (1000 and 1700 s^{-1}) or 2 min (3000 s^{-1}). **(A)** Representative images of brightfield and fluorescence microscopy. Scale bar: 25 µm. **(B)** The bar graphs display mean values ± SD (n=5 mice per group, 2 independent experiments per shear rate). * p<0.05; ** p<0.01; *** p<0.001.

The antithrombotic effect of smGPV was independent of the expression of GPV on the platelet surface, since 20 µg smGPV reduced thrombus formation in *Gp5*$^{-/-}$ mice to a comparable

extent as in WT animals (Figure 3-34 A, B). This excludes a direct interaction of smGPV with GPV on the platelet surface to exert its antithrombotic effect.

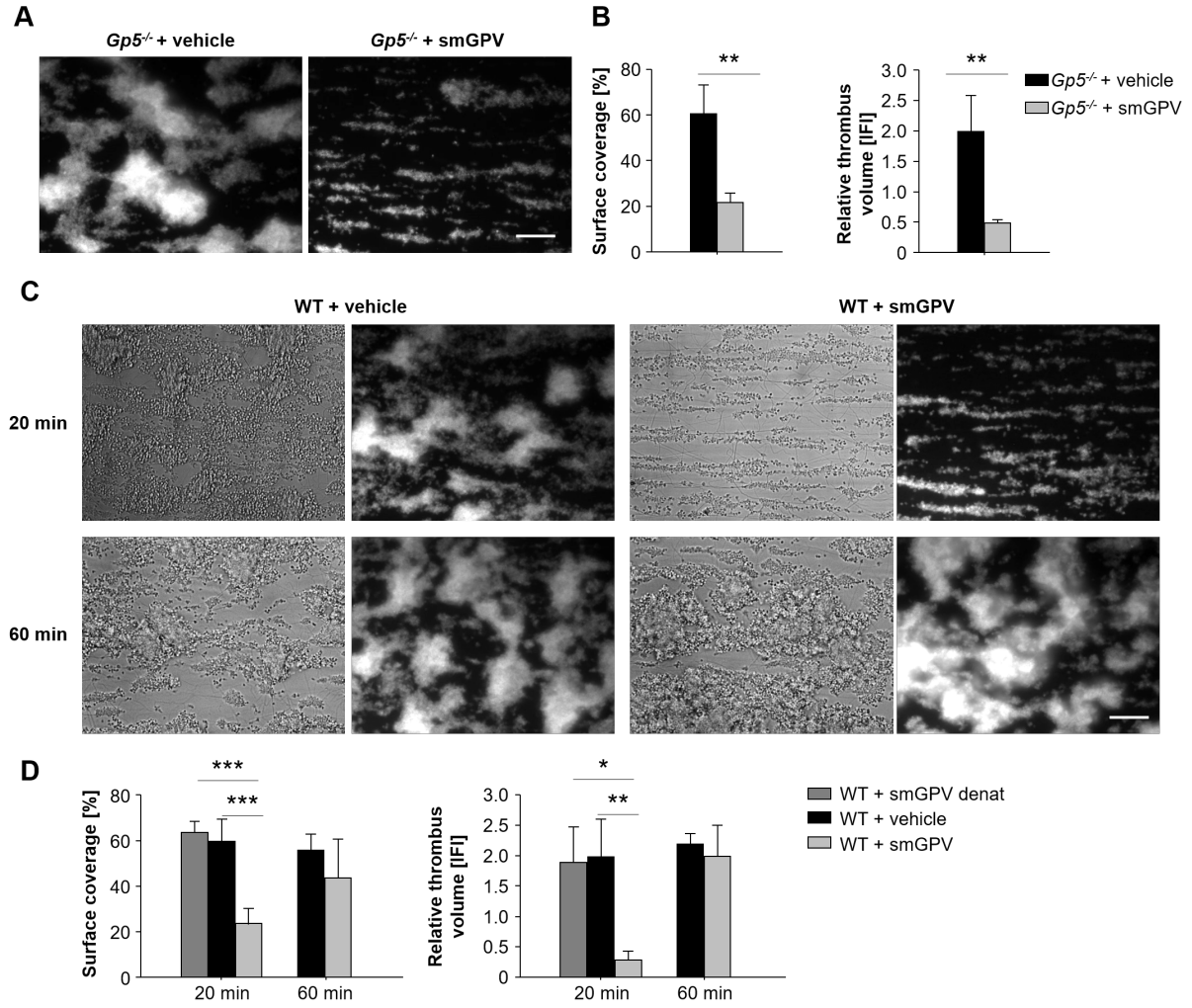

Figure 3-34: Thrombus-reducing effect of smGPV is independent of GPV expression on platelets and smGPV reduces thrombus formation on collagen *ex vivo*. (A, B) Heparinized whole blood was incubated with 20 µg smGPV *in vitro* for 5 min at 37°C in the presence of a Dylight 488-conjugated anti-GPIX derivative. Representative images of fluorescence microscopy. Scale bar: 25 µm. **(C, D)** Mice were injected with 20 µg smGPV intravenously and blood was withdrawn 20 or 60 min afterwards. Heparinized whole blood was incubated *in vitro* with a Dylight 488-conjugated anti-GPIX derivative for 5 min at 37°C and perfused over a collagen-coated (0.2 mg/ml) surface at a shear rate of 1700 s^{-1} for 4 min and then washed with Tyrode's buffer for the same time period. Representative images of brightfield and fluorescence microscopy. Scale bar: 25 µm. **(B, D)** The bar graphs display mean values ± SD (n=5 mice per group, 2 independent experiments). * p<0.05; ** p<0.01; *** p<0.001. smGPV denat: smGPV protein was denatured for 10 min at 95°C prior to the experiment.

So far, the effect of smGPV on platelet function was only studied under *in vitro* conditions. To investigate the effect of smGPV on thrombus formation under more physiological conditions, 20 µg smGPV was injected into mice and thrombus formation was determined *ex vivo*. 20 min after smGPV injection, blood was withdrawn and the flow adhesion experiment was performed immediately. Injection of smGPV led to a pronounced decrease in surface coverage and

thrombus volume. The extent was comparable to the obtained *in vitro* results, indicating that smGPV limits thrombus formation also *ex vivo*. As a control, boiled (95°C) smGPV was injected, which had no effect on thrombus formation compared to PBS-injected WT controls. However, the *in vivo* half-life of smGPV was rather short, since *ex vivo* thrombus formation assessed 1 h after injection of smGPV was indistinguishable between smGPV-treated mice and untreated controls (Figure 3-34 C, D).

While *Gp5*$^{Kin/Kin}$ mice *per se* displayed enhanced thrombus formation on collagen under flow (Figure 3-22), this was normalized to WT levels after smGPV incubation at a shear rate of 1000 s^{-1}. At 150 s^{-1}, where *Gp5*$^{Kin/Kin}$ mice were indistinguishable from WT mice, thrombus formation was reduced after smGPV incubation (Figure 3-35), confirming a strong antithrombotic activity of smGPV and indicating that the antithrombotic effect of smGPV is not altered by membrane GPV.

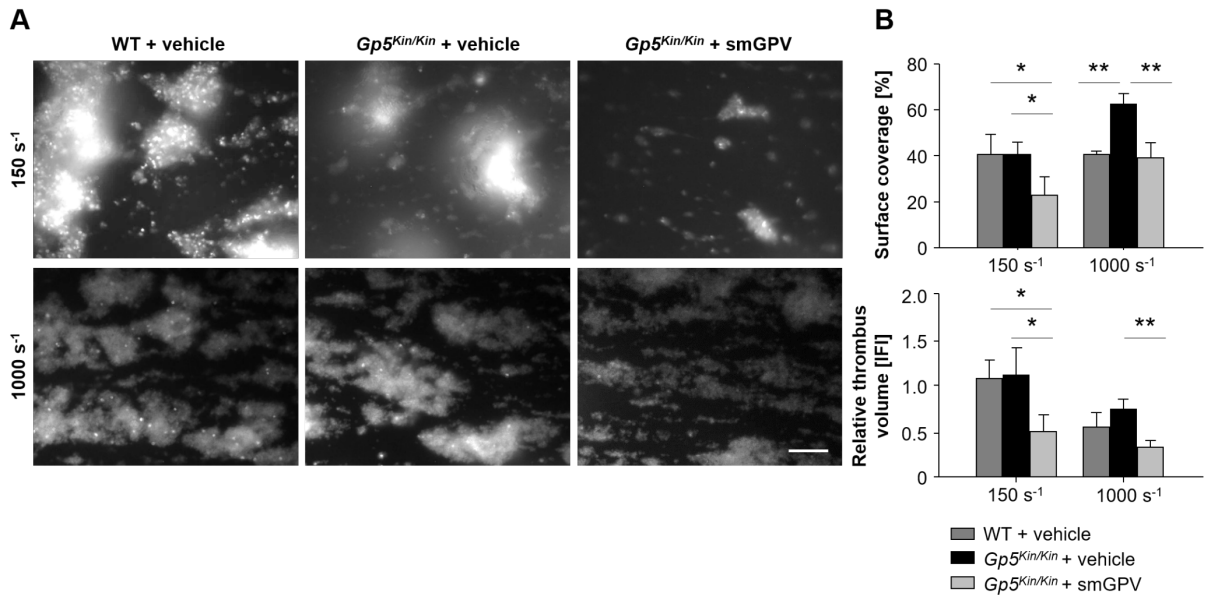

Figure 3-35: smGPV normalizes enhanced thrombus formation on collagen of *Gp5*$^{Kin/Kin}$ mice. Heparinized whole blood was incubated with 20 µg smGPV *in vitro* for 5 min at 37°C in the presence of a Dylight 488-conjugated anti-GPIX derivative and perfused over a collagen-coated (0.2 mg/ml) surface at a shear rate of 150 s^{-1} for 10 min or 1000 s^{-1} for 4 min, and then washed with Tyrode's buffer for the same time period. Representative images of fluorescence microscopy. Scale bar: 25 µm. The bar graphs display mean values ± SD (n=5 mice per group, 2 independent experiments). * p<0.05; ** p<0.01; *** p<0.001.

To evaluate the potential clinical relevance of sGPV as an antithrombotic agent, its effect was studied in human blood. Therefore, smGPV was incubated *in vitro* with blood from healthy volunteers (Ctrl) and always run in parallel to an untreated sample from the same donor to allow direct comparison. The fluorescent, cell permeant dye $DiOC_6$ was used to label human

platelets, since the above used anti-GPIX derivative does not bind to human platelets. The concentration of $DiOC_6$ needed for proper cell staining was titrated accurately prior to the experiment to avoid cell damage, since the dye is extremely phototoxic. Surface coverage and thrombus volume at a shear rate of 1000 s^{-1} was diminished in human blood after smGPV treatment (Figure 3-36), indicating that smGPV is a potential candidate for a novel antithrombotic agent.

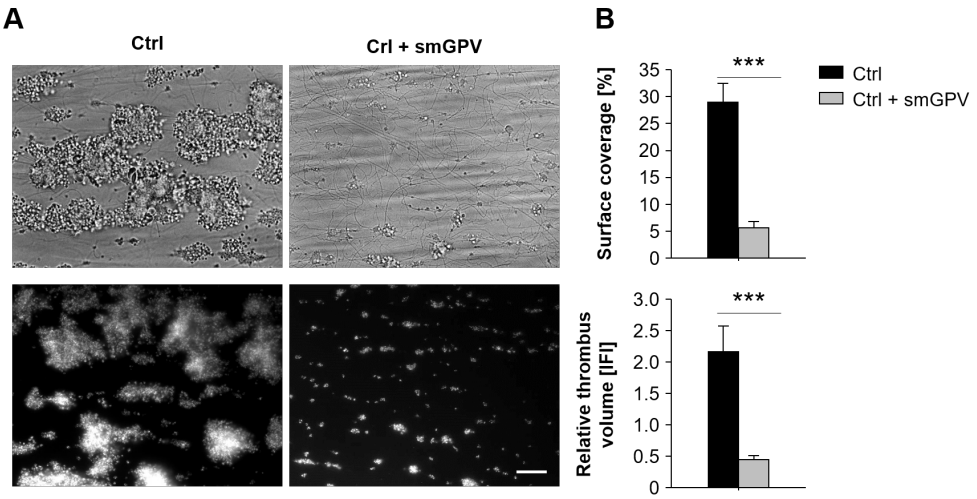

Figure 3-36: Thrombus-reducing effect of smGPV in human blood on collagen under flow. Heparinized whole blood from healthy volunteers (Ctrl) was incubated with 20 µg smGPV *in vitro* for 5 min at 37°C in the presence of 100 nM $DiOC_6$ and perfused over a collagen-coated (0.2 mg/ml) surface at a shear rate of 1000 s^{-1} for 4 min and then washed with Tyrode's buffer for the same time period. **(A)** Representative images of brightfield and fluorescence microscopy. Scale bar: 25 µm. **(B)** The bar graphs display mean values ± SD (n=5, 2 independent experiments). * p<0.05; ** p<0.01; *** p<0.001.

3.6.4 smGPV protects mice from occlusive thrombus formation without affecting tail bleeding time

To test the *in vivo* effect of smGPV on arterial thrombus formation, mice were injected with 20 µg smGPV directly before the experiment. Remarkably, thrombus formation was abolished after smGPV treatment in a model of mechanical injury of the abdominal aorta. smGPV-treated mice did not form occlusive thrombi within the observation period (Figure 3-37 B). Similar results were obtained in a second model of arterial thrombus formation. Here, platelet accumulation at sites of $FeCl_3$-induced mesenteric arteriole injury was determined using intravital fluorescence microscopy. Again, smGPV protected animals from arterial occlusive thrombus formation, since 9 out of 14 mice did not form stable thrombi within the observation period (Figure 3-37 C). Next, the hemostatic function in smGPV-treated mice was assessed. Unexpectedly, tail bleedings times were comparable between smGPV-injected mice and

vehicle-treated controls (Figure 3-37 A). These surprising results indicated that smGPV protects from arterial occlusive thrombus formation without affecting hemostasis.

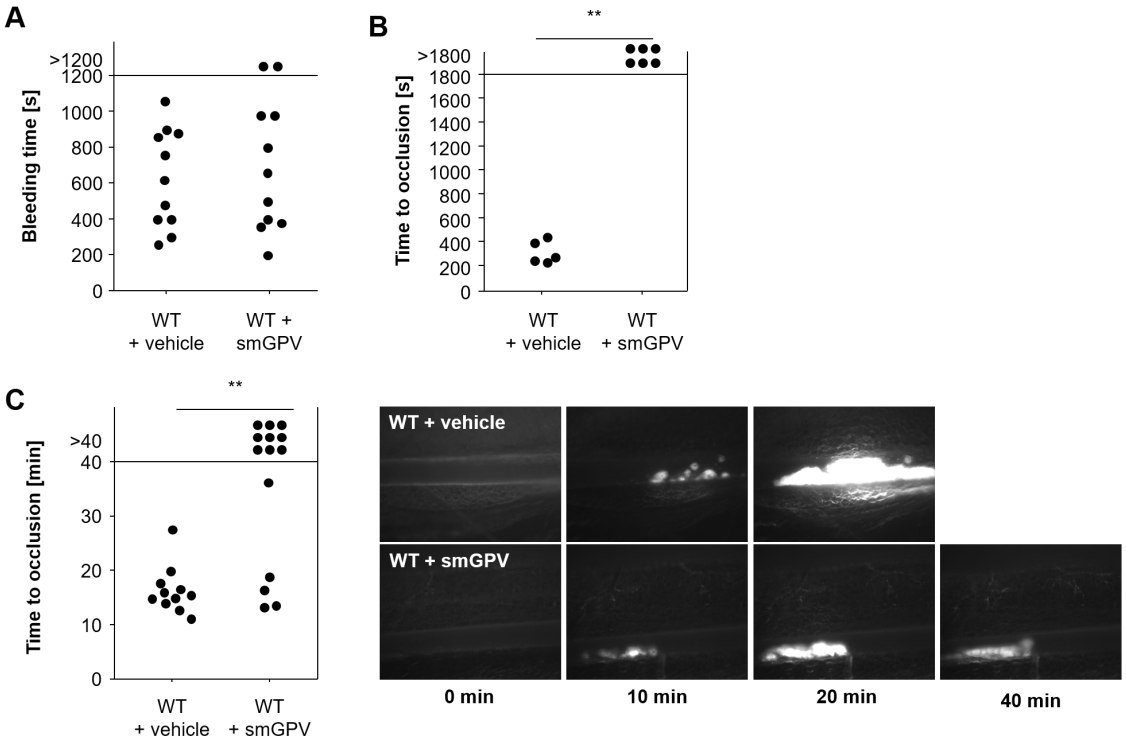

Figure 3-37: smGPV protects mice from arterial occlusive thrombus formation without affecting hemostasis. Mice were injected intravenously with 20 µg smGPV prior to the experiment. **(A)** 1 mm of the tail tip of each mouse was cut and time to cessation of blood flow was measured using a filter paper. Each symbol represents one animal. **(B)** The abdominal aorta was mechanically injured by a single firm compression with a forceps and blood flow was monitored with a Doppler flowmeter. Time to final occlusion is shown. Each symbol represents one individual mouse. **(C)** Mesenteric arterioles were injured with 20% $FeCl_3$ and adhesion and thrombus formation of fluorescently-labeled platelets was monitored by intravital microscopy. Each dot represents one vessel. * $p<0.05$; ** $p<0.01$.

3.6.5 89F12 reverses the thrombus-reducing effect of smGPV

The pronounced antithrombotic effect of smGPV in mouse as well as human blood was quite striking and could explain the phenotype of *Gp5*$^{-/-}$ and *Gp5*$^{Kin/Kin}$ mice. However, the mechanism underlying the antithrombotic effect of smGPV still remained unknown and was addressed in further experiments. The anti-GPV antibody 89F12 was shown to reverse the hemostatic and thrombotic defect caused by lack of the (hem)ITAM receptors GPVI and CLEC-2 (see 3.2). Consequently, 89F12 might bind to the epitope on GPV involved in GPV-ligand interactions. To test this, 89F12 Fab fragments were preincubated with smGPV and then added to the murine blood. While 89F12 Fab fragments alone did not modulate thrombus formation on collagen under flow, preincubation of smGPV with 89F12 Fab fragments abrogated the

thrombus-reducing effect of smGPV treatment (Figure 3-38) which indeed indicated that 89F12 blocks the epitope on smGPV involved in thrombus modulation.

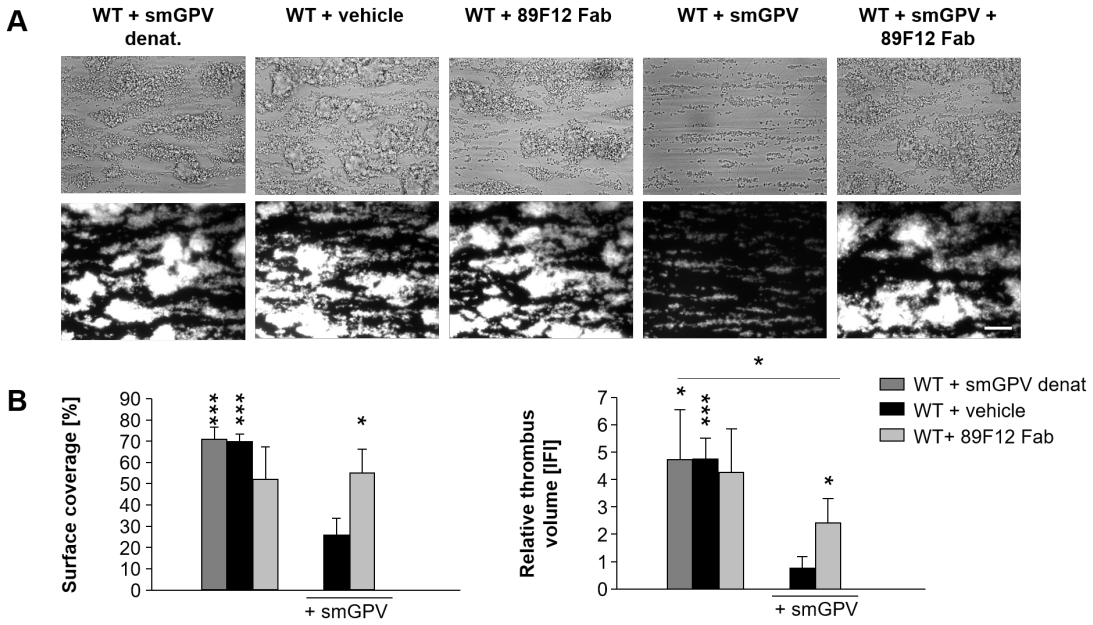

Figure 3-38: The anti-GPV antibody 89F12 reverses the thrombus-reducing effect of smGPV. Heparinized whole blood was incubated with 20 µg smGPV, 10 µg/ml 89F12 Fab alone or a combination of 20 µg smGPV and 10 µg/ml 89F12 Fab (mixed beforehand) *in vitro* for 5 min at 37°C in the presence of a Dylight 488-conjugated anti-GPIX derivative and perfused over a collagen-coated (0.2 mg/ml) surface at a shear rate of 1700 s^{-1} for 4 min and then washed with Tyrode's buffer for the same time period. **(A)** Representative images of brightfield and fluorescence microscopy. Scale bar: 25 µm. **(B)** The bar graphs display mean values ± SD (n=4 mice per group, 1 experiment). smGPV denat: smGPV protein was denatured for 10 min at 95°C prior to the experiment. * p<0.05; ** p<0.01; *** p<0.001, as compared to WT+smGPV.

3.6.6 Plasma factors are critical for the antithrombotic effect of smGPV

In a next step, it was tested whether plasma factors are critical for the thrombus-modulating effect of smGPV. For this, a plasma factor-free flow adhesion assay was established. Washed platelets, washed red blood cells, fibrinogen and Ca^{2+} were mixed at concentrations resembling those in whole blood perfusion assays. Red blood cells were necessary to force platelets to the wall of the flow chamber and thereby bringing them into contact with the coated collagen. Fibrinogen and Ca^{2+} were crucial to facilitate aggregate formation under flow. Overall, the surface coverage in this reconstituted flow adhesion assay was comparable to the whole blood perfusion assay. Incubation with smGPV still led to a reduction in surface coverage, albeit the effect was less pronounced than in the presence of plasma factors. However, the thrombus volume in the reconstituted flow chamber was unaltered after smGPV incubation (Figure 3-39). Comparable results were obtained with reconstituted *Gp5*$^{-/-}$ blood (data not

shown). These results indicate that smGPV requires plasma factors to exert its antithrombotic effect.

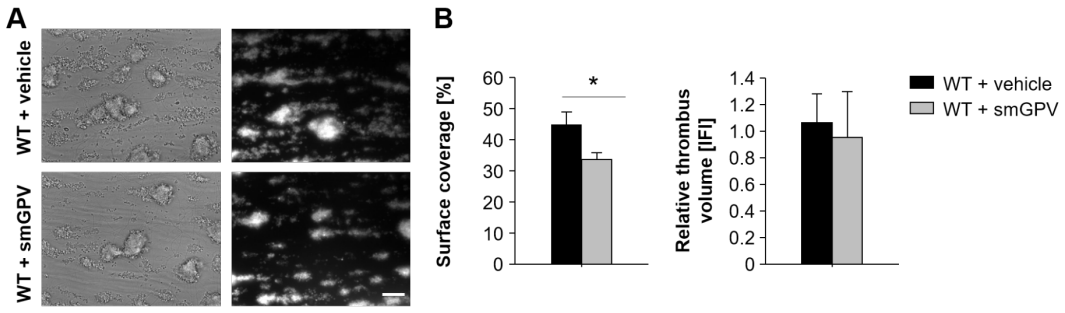

Figure 3-39: Plasma factors are critical for the thrombus-reducing effect of smGPV. Platelets and red blood cells were washed to remove all plasma components and afterwards reconstituted with fibrinogen and Ca^{2+}, which are critical to facilitate thrombus formation. The reconstituted blood was incubated with 20 µg smGPV *in vitro* in the presence of a Dylight 488-conjugated anti-GPIX derivative for 5 min at 37°C and perfused over a collagen-coated (0.2 mg/ml) surface at a shear rate of 1000 s^{-1} for 4 min and then washed with Tyrode's buffer for the same time period. **(A)** Representative images of brightfield and fluorescence microscopy. Scale bar: 25 µm. **(B)** The bar graphs display mean values ± SD (n=5 mice per group, 3 independent experiments). * p<0.05.

3.6.7 smGPV gets incorporated into the growing thrombus

To elucidate the mechanism underlying the thrombus-modulatory effect of smGPV, it was assessed whether smGPV directly binds to platelets. Several *in vitro* binding studies under static conditions were conducted, however they failed to give clear results (data not shown), since smGPV seemed to require shear flow conditions to exert its antithrombotic effect and probably also for its interaction with a postulated blood-borne ligand.

Flow adhesion assays with diluted whole blood were performed as described above and then the anti-GPV antibody 89H11 coupled to the fluorescent dye Alexa647 (A647) was perfused over the formed thrombi to stain GPV. *Gp5*$^{-/-}$ mice were used to exclusively stain the recombinant smGPV, but not endogenous GPV. While there was no 89H11 staining detectable in GPV-deficient blood, smGPV could be visualized in smGPV-treated *Gp5*$^{-/-}$ blood and was found primarily at the edges of platelet aggregates colocalizing with platelets (Figure 3-40 A) indicating that smGPV binds to platelets in growing thrombi.

Next, smGPV was coupled to a fluorophore (A647 or Dylight 488) to directly visualize smGPV and to allow its detection also *in vivo,* e.g. after thrombus formation, and in other mouse strains than *Gp5*$^{-/-}$ mice. However, smGPV-A647 or smGPV-Dylight 488 did not display the thrombus-reducing effect of smGPV. In addition, the staining pattern obtained from directly fluorophore-conjugated smGPV looked different to the previous described one: fluorophore-conjugated

smGPV bound to the collagen fibers coated on the cover slip (Figure 3-40 B). These results excluded the usage of fluorophore-conjugated smGPV for mechanistic assays. At this moment, it is unclear how labelling affects the bioactivity of smGPV. Unfortunately, there was no other possibility to distinguish between recombinant and endogenous smGPV *in vivo*.

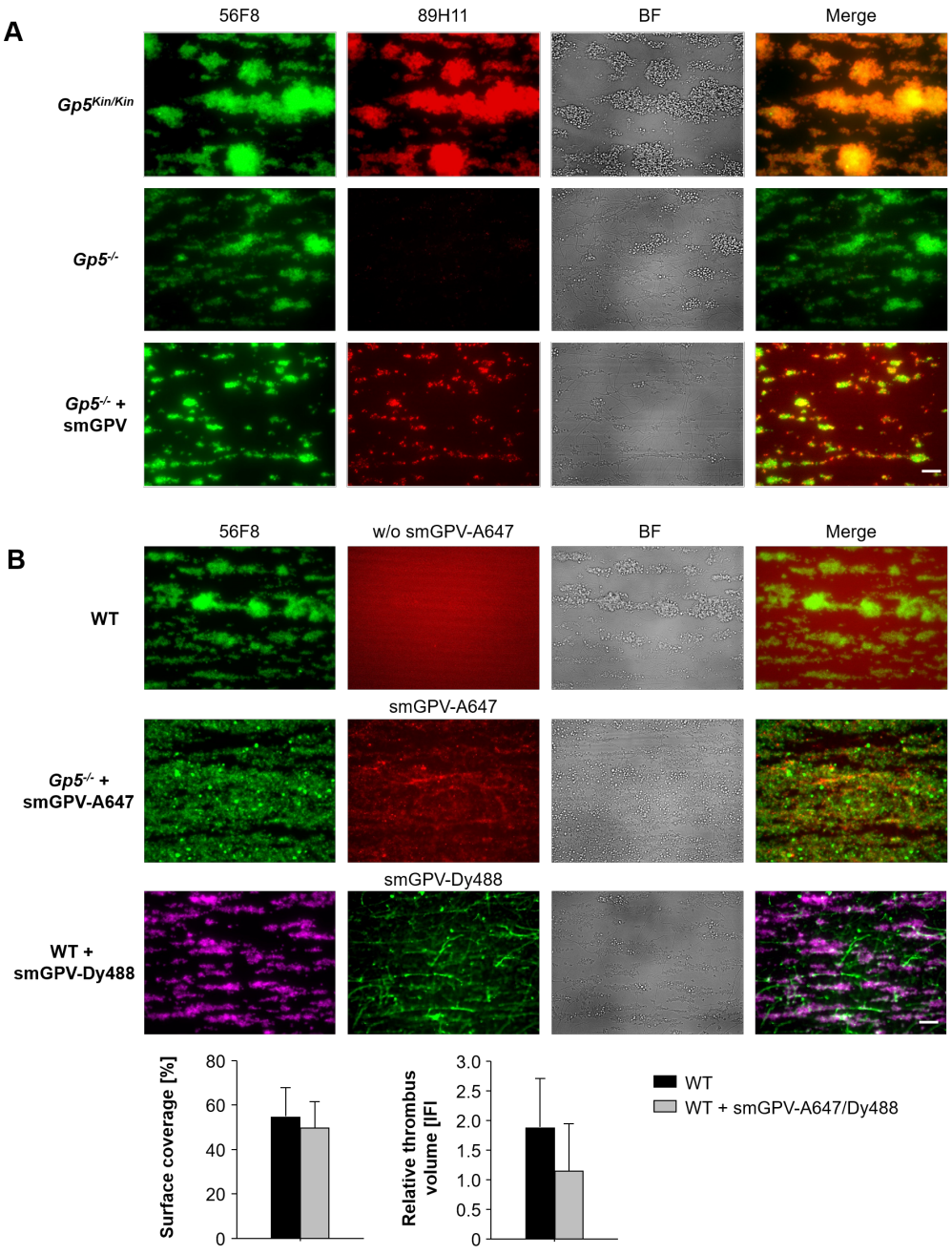

Figure 3-40: smGPV gets incorporated into the growing thrombus *in vitro* on collagen under flow. Heparinized whole blood was incubated with 20 µg smGPV *in vitro* for 5 min at 37°C in the presence of a Dylight 488-conjugated anti-GPIX derivative (green, lower panel: magenta) and perfused over a collagen-coated (0.2 mg/ml) surface at a shear rate of 1700 s^{-1} for 4 min and then washed with Tyrode's buffer for the same time period. **(A)** smGPV was stained with the A647-conjugated anti-GPV antibody 89H11 (red). **(B)** Direct coupling of smGPV to A647 (red) or Dylight 488 (green, lower panel) abolished the thrombus-reducing effect of smGPV. Representative fluorescence images of 5 mice per group. Scale bar: 20 µm. The bar graphs display mean values ± SD (2 independent experiments).

3.7 Soluble human GPV protects from arterial thrombosis

In parallel to the studies on smGPV, the effect of soluble human GPV (shGPV) on thrombus formation was investigated. Human and murine GPV share an amino acid sequence homology of 70% [128, 191]. However, it was so far unclear whether shGPV exhibits a comparable antithrombotic effect in human blood as it was described for smGPV.

For the initial studies, we kindly received a small amount of shGPV (extracellular domain aa 1-518) carrying a 10x His-tag, which was recombinantly produced in insect cells, from Prof. Renhao Li (Emory University, Atlanta, USA).

In addition, recombinant soluble human GPV was generated and purified in collaboration with CSL Behring (Marburg, Germany). In accordance with smGPV, the extracellular domain of human GPV (including the thrombin cleavage site) was fused to a human albumin tag, stably expressed in CHO-K1 cells and secreted into the cell culture supernatant (Figure 3-41 A). Fusion of albumin to shGPV resulted in a protein of approximately 120 kDa. The purified protein was tested by CSL Behring in a Coomassie staining as well as in Western blot using an anti-albumin antibody and an anti-human GPV antibody (Figure 3-41 D, E). So far, we obtained three batches shGPV-FP from CSL Behring. In addition, we also obtained shGPV without an albumin tag. Here, the albumin tag was cleaved off by thrombin (via the thrombin cleavage site of GPV). The cleaved product was purified using an anti-albumin column and a subsequent size exclusion chromatography of the flow through, resulting in a band for shGPV at approximately 64 kDa in Western blot analysis (Figure 3-41 C, E). Figure 3-41 C-E was kindly provided by CSL Behring. shGPV with the albumin tag will be referred to as shGPV-FP, whereas shGPV is the cleaved product. Recombinant shGPV-FP could be detected down to a concentration of 0.9 µg in Western blot using an anti-albumin and an anti-human GPV antibody and in an albumin ELISA down to a concentration of 0.1 µg/ml (Figure 3-41 F, G). Unfortunately, there was only a limited number of anti-human GPV antibodies commercially available, which did not work in a human GPV ELISA. Similar to the results obtained with smGPV, incubation of 10 µg/ml shGPV with washed whole blood did neither alter αIIbβ3 integrin activation nor degranulation-dependent P-selectin exposure in response to all tested agonists (data not shown).

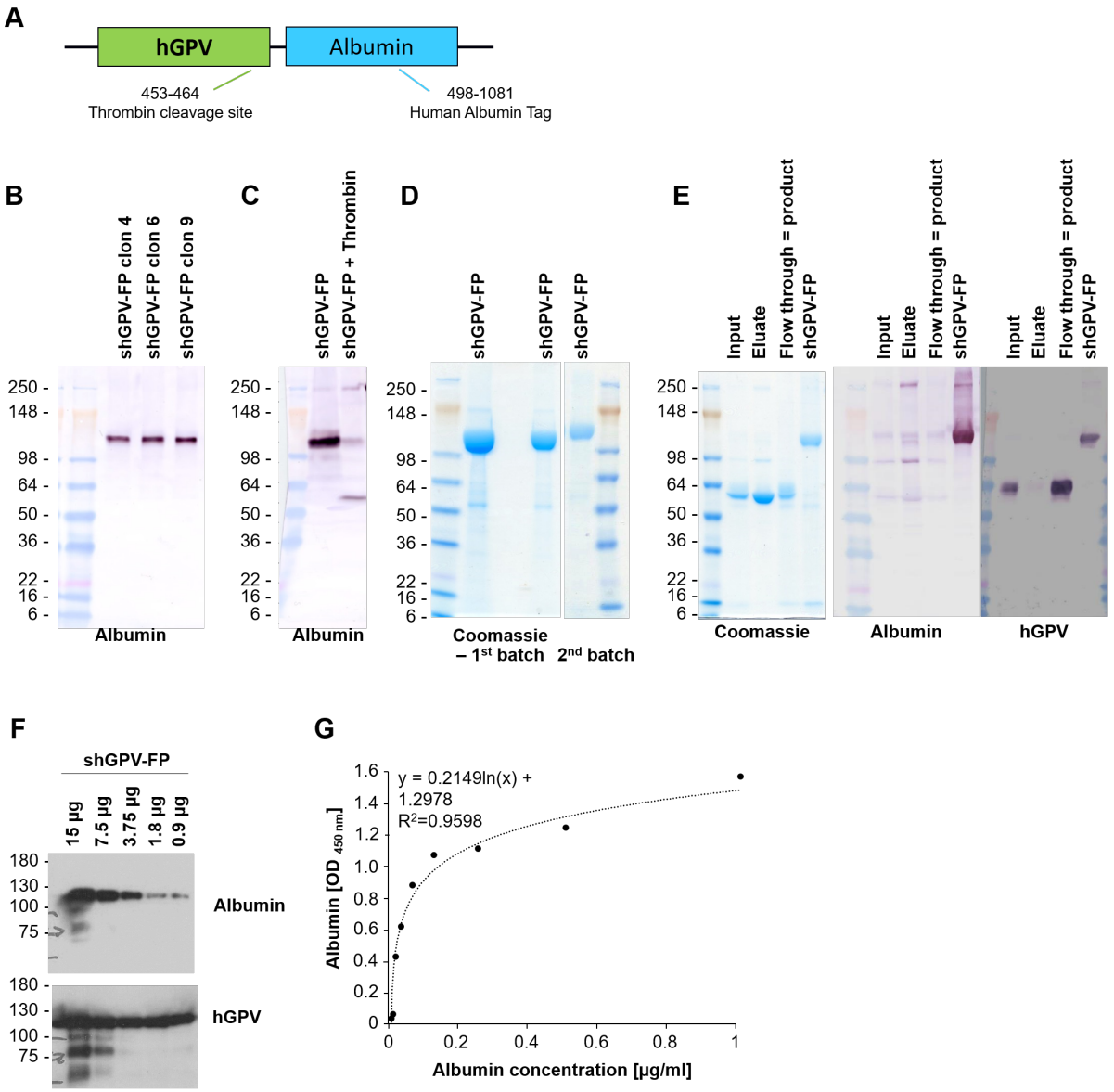

Figure 3-41: Recombinant soluble human GPV. (A) Simplified scheme of the extracellular domain of human GPV. The protein contains the thrombin and the ADAM cleavage site. A human albumin tag was fused to the protein via a linker (shGPV-FP). ADAM, a disintegrin metalloprotease. **(B)** Western Blot to validate fusion of shGPV to an albumin tag using an anti-albumin antibody. **(C)** The albumin tag was removed from shGPV by thrombin cleavage. Confirmation of the cleavable linker by western blot using an anti-albumin antibody. **(D)** Coomassie staining of batch 1 and 2 obtained from CSL Behring. **(E)** Coomassie staining and Western blot to verify cleavage and purification of batch 3 obtained from CSL Behring using an anti-albumin and an anti-human GPV antibody. Flow through = product = cleaved shGPV without albumin tag. shGPV-FP, shGPV with albumin tag. **(F)** Titration of shGPV-FP using an anti-albumin and an anti-human GPV antibody. **(G)** Detection of shGPV-FP using an albumin ELISA.

The two classical coagulation pathways serve as basis of the widely used standard methods to determine overall plasma coagulation in clinics (see 1.7). The Quick test along with its derived measure INR (*international normalized ratio*) is a measure of the extrinsic coagulation pathway by TF-FVIIa-initiated coagulation. The aPTT (*partial thromboplastin time*) determines the intrinsic coagulation pathway by FXII-triggered clotting. The effect of shGPV on the integrity

of plasma coagulation *in vitro* was assessed by determining the clinical parameters Quick, INR and aPTT in human blood. All three values were not affected by the presence of 10 µg/ml shGPV in human plasma (data not shown) indicating that shGPV has no influence on coagulation in the plasma of healthy volunteers.

Consistently, thrombin generation as assessed by the initiation of thrombin generation, maximal thrombin generation and time to maximal thrombin generation was comparable between shGPV-treated WT PRP and untreated PRP (data not shown). Altogether, shGPV – like smGPV – did not alter platelet activation or coagulation *in vitro*.

3.7.1 shGPV inhibits thrombus formation on collagen under flow

Thrombus formation on collagen under flow was markedly reduced upon treatment with smGPV *in vitro* or *ex vivo*. In a next step, it was investigated whether shGPV also exerts an inhibitory effect on platelet adhesion and aggregation on collagen under flow. In general, mean shear rates and wall shear stress are higher in mice than in humans [260, 261]. Therefore, flow adhesion experiments with human blood were performed at a shear rate of 150 s^{-1} (low), 500 s^{-1} (intermediate) and 1000 s^{-1} (high) [262]. shGPV-FP diminished thrombus formation in a concentration-dependent manner in human blood. 20 µg shGPV-FP (shGPV with albumin tag, 20 µg total protein equates approximately 10 µg shGPV) were sufficient to significantly reduce platelet adhesion and aggregate formation on collagen. This effect was even more pronounced after incubation with 40 µg or 80 µg shGPV-FP (Figure 3-42).

In contrast to smGPV, which diminished thrombus formation independently of the applied shear rate, shGPV-FP exerted its antithrombotic effect only at a high shear rate of 1000 s^{-1} in human blood, but not at a shear rate of 500 s^{-1} and 150 s^{-1} (Figure 3-43). Shear-dependency of shGPV was so far not studied in murine blood and that of smGPV not in human blood. It remained unknown whether the observed differences between smGPV and shGPV are due to the protein itself or due to differences in the hemorheology and hemodynamic shear stress of murine and human blood.

In line with these results, 40 µg shGPV without an albumin tag efficiently reduced thrombus formation on collagen in human blood (data not shown). These data showed that shGPV – like smGPV – is a potent thrombus-reducing agent *in vitro*.

In parallel to the studies with smGPV, the importance of plasma factors for the thrombus-modulatory role was also assessed for shGPV using the previously established flow adhesion assay (3.6.6). In reconstituted human blood, incubation with 40 µg shGPV-FP did not affect platelet adhesion and aggregate formation on collagen under flow (data not shown), indicating

that plasma factors are required for the antithrombotic effect of shGPV *in vitro*. This is in line with the results obtained for smGPV.

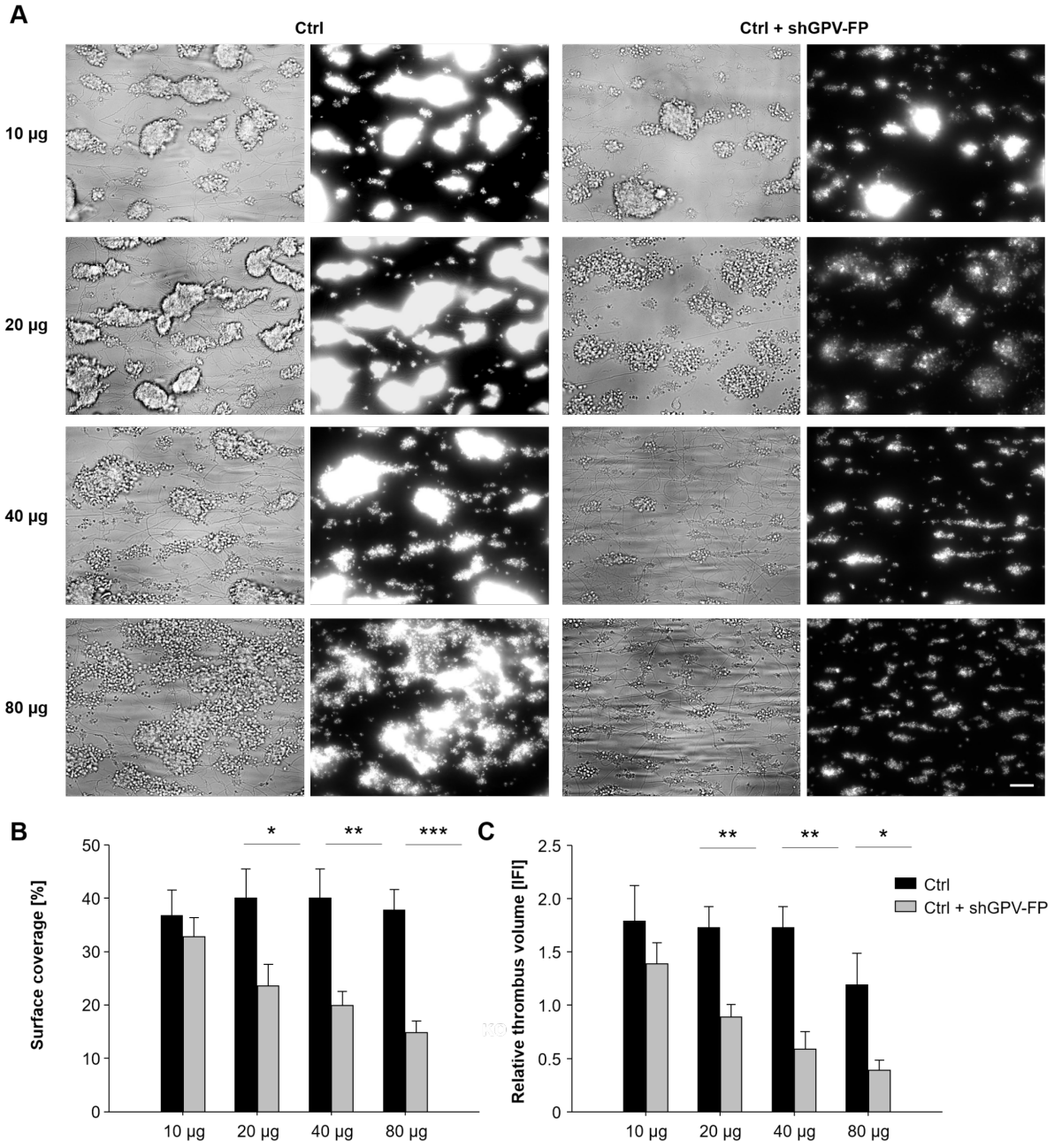

Figure 3-42: shGPV-FP reduces platelet adhesion and thrombus formation *in vitro* on collagen in a concentration-dependent manner. Whole blood from healthy human volunteers (Ctrl) was incubated with the indicated amount of shGPV-FP *in vitro* for 5 min at 37°C in the presence of 100 nM $DiOC_6$ and perfused over a collagen-coated (0.2 mg/ml) surface at a shear rate of 1000 s^{-1} for 4 min and then washed with Tyrode's buffer for the same time period. **(A)** Representative images of brightfield and fluorescence microscopy. Scale bar: 20 µm. **(B)** The bar graphs display the mean values ± SD (n=5, 2 independent experiments). * p<0.05; ** p<0.01; *** p<0.001 as compared to Ctrl values.

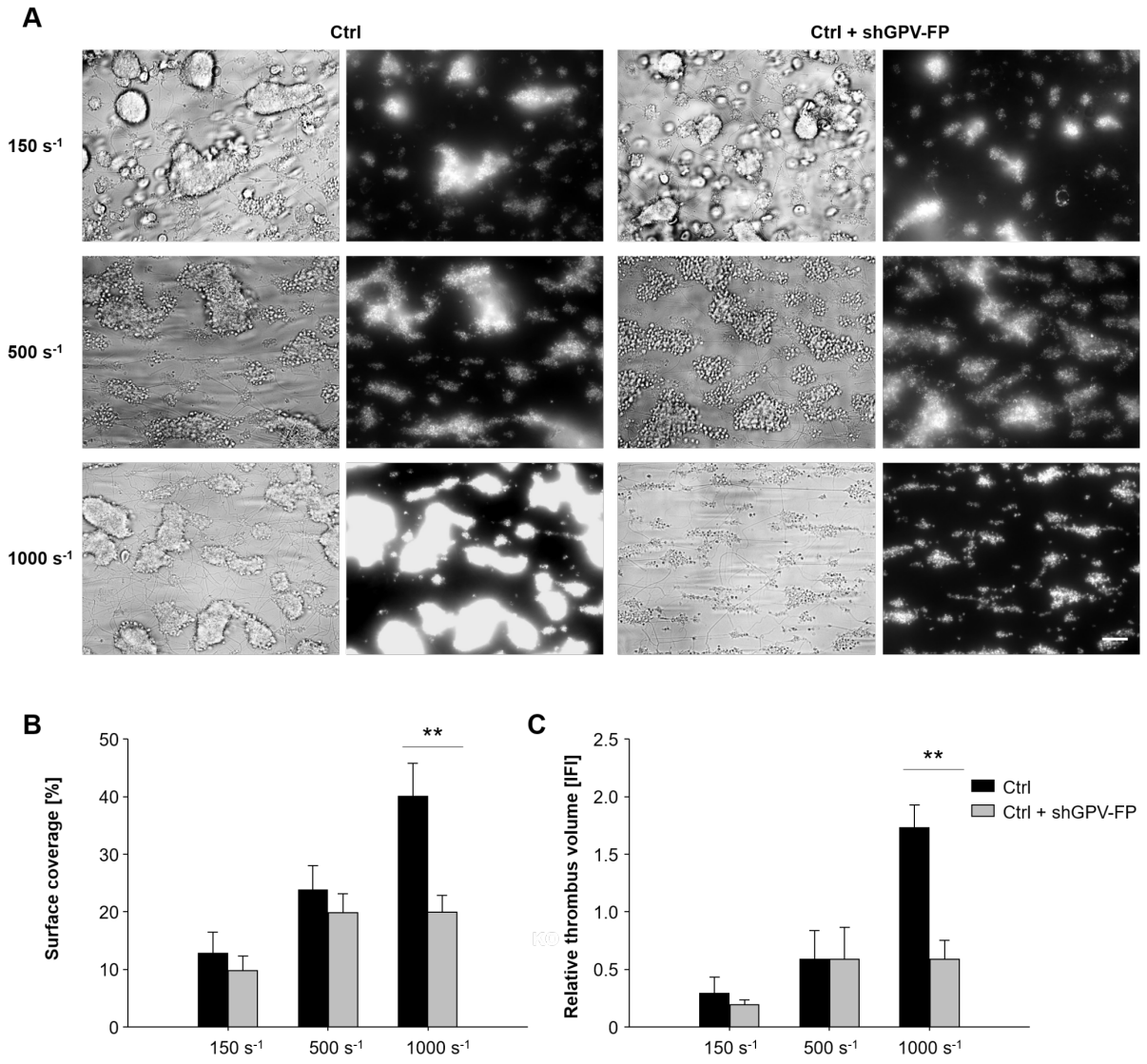

Figure 3-43: shGPV-FP reduces platelet adhesion and thrombus formation *in vitro* on collagen under flow shear rate-dependently. Whole blood from healthy human volunteers was incubated with 40 µg shGPV-FP *in vitro* for 5 min at 37°C in the presence of 100 nM $DiOC_6$ and perfused over a collagen-coated (0.2 mg/ml) surface at the indicated shear rates and then washed with Tyrode's buffer for the same time period. Perfusion time was 10 min (150 s^{-1}) or 4 min (500 and 1000 s^{-1}). **(A)** Representative images of brightfield and fluorescence microscopy. Scale bar: 20 µm. **(B)** The bar graphs display the mean values ± SD (n=5, 2 independent experiments). * $p<0.05$; ** $p<0.01$ as compared to Ctrl values.

Besides human blood, the effect of shGPV was also investigated in murine blood. For this purpose, shGPV with and without the albumin tag was incubated with murine blood *in vitro* prior to the experiment. Like in human blood, 40 µg shGPV abolished platelet aggregate formation very efficiently. 40 µg or 80 µg shGPV-FP reduced the surface coverage and thrombus volume significantly, but to a lesser extent than the cleaved protein (Figure 3-44).

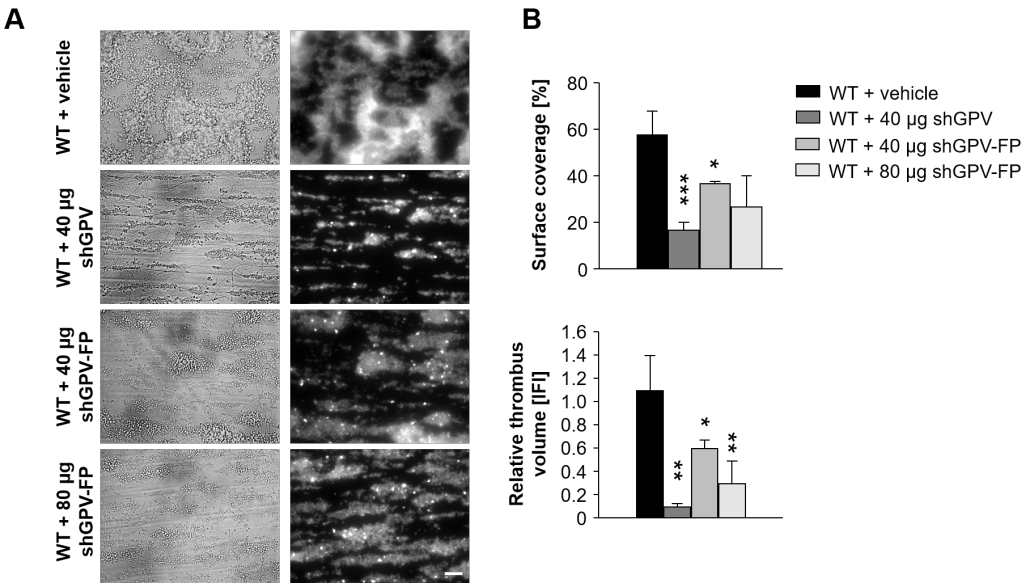

Figure 3-44: Thrombus-inhibiting effect of shGPV in murine blood *in vitro* on collagen under flow. Heparinized whole blood was incubated with the indicated amounts of shGPV and shGPV-FP *in vitro* for 5 min at 37°C in the presence of a Dylight 488-conjugated anti-GPIX derivative and perfused over a collagen-coated (0.2 mg/ml) surface at a shear rate of 1700 s^{-1} for 4 min and then washed with Tyrode's buffer for the same time period. **(A)** Representative images of brightfield and fluorescence microscopy. Scale bar: 20 µm. **(B)** The bar graphs display mean values ± SD (n=5 mice per group, 3 independent experiments). * p<0.05, ** p<0.01, *** p<0.001 as compared to WT values.

3.7.2 Abolished antithrombotic effect of fluorophore-conjugated shGPV

To identify interaction partners of sGPV, it is crucial to unravel the underlying mechanism of the thrombus-modulating effect of sGPV. Since, unfortunately, tools required to study human GPV such as ELISA and antibodies suitable for flow cytometry or immunofluorescence staining were limited or non-existent, shGPV was conjugated to a fluorophore to directly visualize the protein in flow adhesion assays and investigate whether it is bound by platelets or gets incorporated into the thrombus as observed for smGPV.

However, like for smGPV, direct conjugation of shGPV to Alexa 488 abrogated its antithrombotic effect in human as well as in murine blood (data not shown). Besides this, the staining pattern obtained by shGPV-A488 resembled staining of the coated collagen fibers indicating that shGPV-A488 might bind to collagen. These results were in line with data from studies with smGPV (3.6). Since flow adhesion studies were performed with diluted whole blood, it was also not possible to localize shGPV-FP via its albumin tag – it could not be distinguished between the endogenous human albumin and the recombinant human albumin. Furthermore, our anti-albumin antibodies were not specific for human albumin and cross-reacted with the mouse protein.

3.7.3 shGPV protects mice from occlusive thrombus formation without affecting tail bleeding time

In vitro, shGPV(-FP) reproduced the data obtained with smGPV. Consequently, we also tested the *in vivo* effect of shGPV in mice. To do so, mice were injected with 20 µg shGPV directly before the experiment. Comparable to smGPV, shGPV abolished occlusive thrombus formation in the mechanically injured abdominal aorta (14 out of 15 did not form occlusive thrombi within the observation period; Figure 3-45 B).

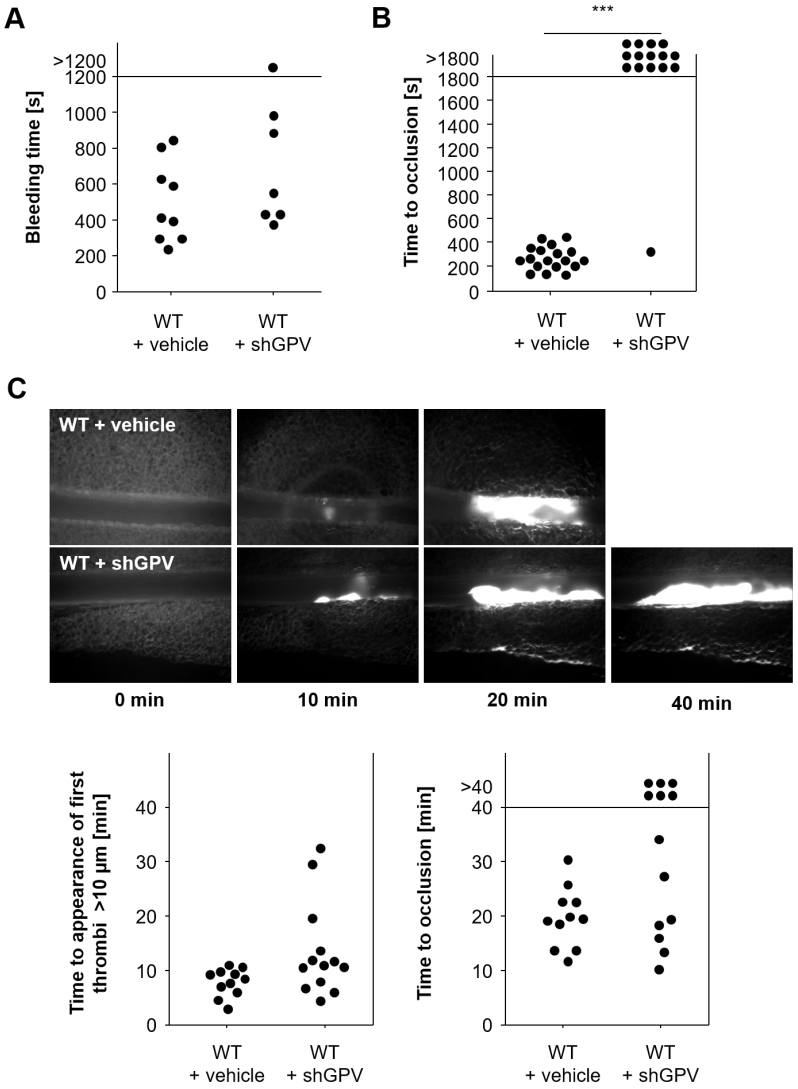

Figure 3-45: shGPV protects mice from arterial occlusive thrombus formation without affecting hemostasis. Mice were injected intravenously with 20 µg shGPV prior to the experiment. **(A)** 1 mm of the tail tip of each mouse was cut and time to cessation of blood flow was measured using a filter paper. Each symbol represents one animal. **(B)** The abdominal aorta was mechanically injured by a single firm compression with a forceps and blood flow was monitored with a Doppler flow-meter. Time to final occlusion is shown. Each symbol represents one individual mouse. **(C)** Mesenteric arterioles were injured with 20% $FeCl_3$ and adhesion and thrombus formation of fluorescently-labeled platelets was monitored by intravital microscopy. Each dot represents one vessel. shGPV was kindly provided by Prof. Renhao Li. * $p<0.05$; ** $p<0.01$; *** $p<0.001$.

In $FeCl_3$-injured mesenteric arterioles, half of the injured vessels remained patent, while a stable thrombus was formed in the other vessels upon injection of shGPV. Of note, there was no occlusive thrombus in the first analyzed arteriole per mouse in 4 out of 6 mice (Figure

3-45 C), suggesting that the half-life of shGPV is short and does not allow the analysis of more than one arteriole per mouse. In line with results obtained with smGPV, tail bleeding times of shGPV-treated mice were comparable to vehicle-treated controls (Figure 3-45 A), indicating that shGPV does not affect hemostasis. These *in vivo* studies on shGPV were performed with the protein kindly provided by Prof. Renhao Li.

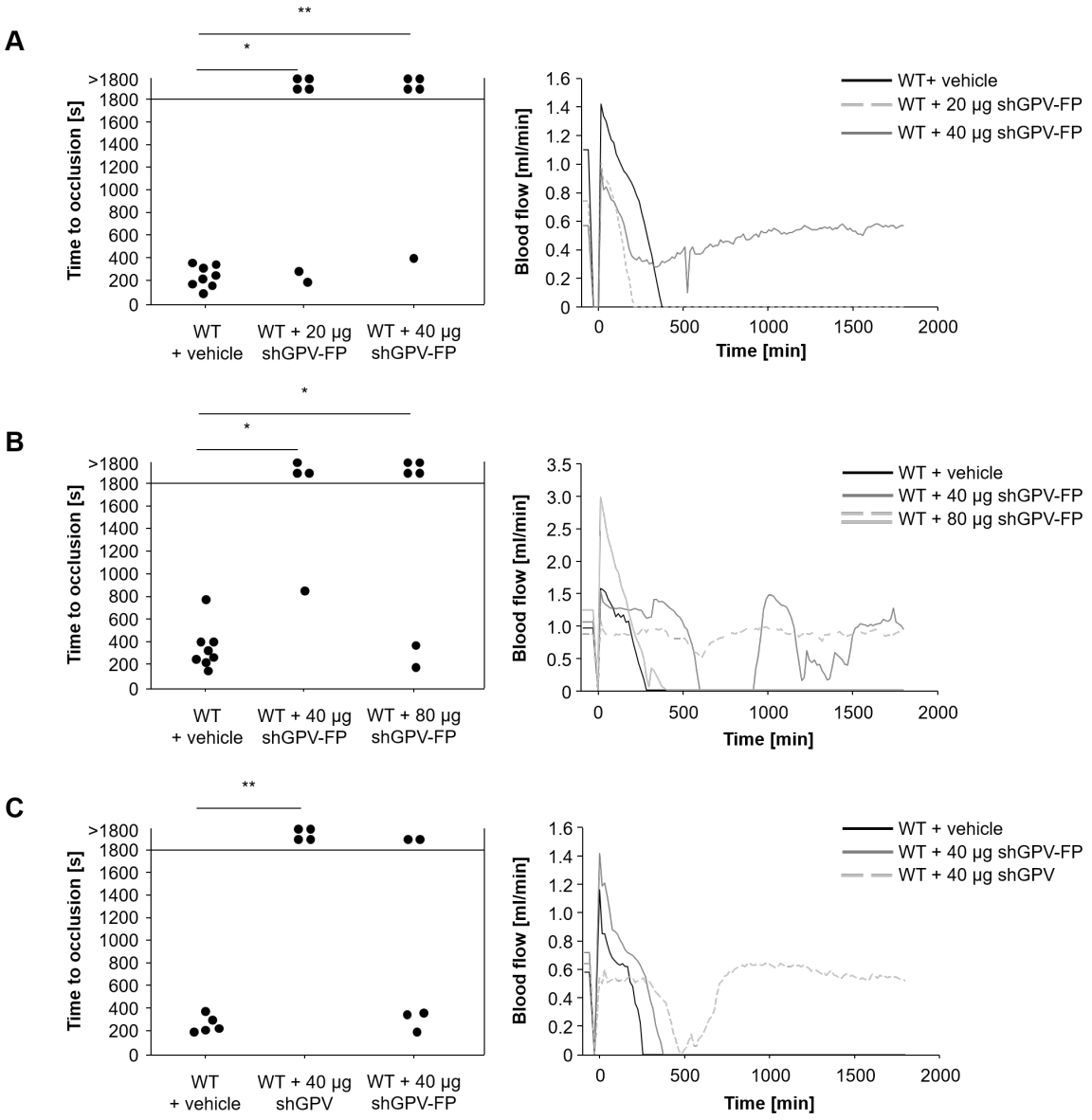

Figure 3-46: shGPV protects from arterial occlusive thrombus formation. Mice were injected intravenously with the indicated amount of shGPV prior to the experiment. **(A)** The abdominal aorta was mechanically injured by a single firm compression with a forceps and blood flow was monitored with a Doppler flowmeter. Time to final occlusion is shown. Each symbol represents one animal. **(A)** First batch shGPV, **(B)** second batch shGPV-FP, **(C)** third batch shGPV-FP. * p<0.05; ** p<0.01.

Besides this, the protein provided by CSL Behring was also tested for its ability to prevent thrombus formation *in vivo*. All three batches that were provided in the course of this thesis protected from arterial occlusive thrombus formation *in vivo* in a model of mechanical injury of the abdominal aorta, although the bioactivity of the three batches was variable. The first batch shGPV-FP potently prevented occlusive thrombus formation in mice at an amount of 20 µg. Occlusive thrombus formation was abrogated after treatment with 40 µg of the second batch shGPV-FP. However, mice injected with the second batch shGPV-FP frequently displayed embolization indicating that the formed thrombi were instable. The cleaved protein from the third batch obtained from CSL Behring also protected from occlusive thrombus formation, whereas 3 out of 5 mice formed occlusive thrombi after treatment with shGPV-FP, indicating that the third batch was even less bioactive (Figure 3-46). The reason for the variable bioactivity remains elusive and requires detailed further analysis.

The effect of shGPV on thrombo-inflammatory pathologies was tested in a model of focal cerebral ischemia in collaboration with Prof. Guido Stoll (Department of Neurology, University of Würzburg, Germany). Lack of GPV reverted the protection of GPVI-depleted mice in a model of ischemic stroke [210]. To study the effect of shGPV in a model of ischemic stroke, 20 µg shGPV were injected directly before the experiment (protein kindly provided by Prof. Renhao Li). Similar to the results obtained in *in vivo* thrombosis models, treatment with shGPV resulted in smaller infarct volumes after 1 h tMCAO (Figure 3-47).

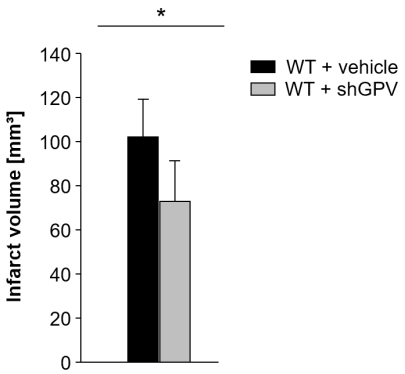

Figure 3-47: shGPV significantly reduces infarct volume after ischemic stroke. Mice were injected with 20 µg shGPV prior to the experiment. Brain infarct volumes after 60 min occlusion and 24 h reperfusion. Data are mean ± SD (n≥5 mice per group, 3 independent experiments). * $p<0.05$. Experiments were performed by Dr. Michael Schuhmann.

3.8 Protein kinase Cι/λ is dispensable for platelet function in thrombosis and hemostasis in mice

3.8.1 PKCι-deficiency has no effects on αIIbβ3 integrin inside-out activation, activation-dependent degranulation and platelet aggregate formation

Since constitutive PKCι/λ-deficient mice are not viable [118], mice with a platelet- and megakaryocyte-specific knockout (*Prkci*$^{fl/fl,\ Pf4\text{-}cre}$, further referred to as PKCι/λ KO) were generated and used together with WT littermates to analyze the role of PKCι/λ in platelets. PKCι/λ KO mice were born at normal Mendelian ratio, were viable and fertile and appeared overall healthy.

Table 3-3: Analysis of platelet count, size and surface expression of glycoproteins in WT and PKCι/λ KO mice. Mean platelet size and platelet counts were determined using a Sysmex cell counter. Surface expression of platelet glycoproteins was determined by flow cytometry. Diluted whole blood was stained with saturating amounts of FITC-labeled antibodies for 15 min at RT. Platelets were analyzed directly on a FACSCalibur. Results are expressed as mean values ± SD for at least 5 mice per group. MFI, *mean fluorescence intensity*. * p<0.05 as compared to WT values.

	WT	PKCι/λ KO	
Count [10^3/µl]	788 ± 67	872 ± 90	
Size [fl]	5.3 ± 0.1	5.3 ± 0.2	
α-GPIb [MFI]	210 ± 10	223 ± 12	
α-GPV [MFI]	247 ± 8	253 ± 12	
α-GPIX [MFI]	373 ± 4	375 ± 19	
α-GPVI [MFI]	38 ± 1	38 ± 2	
α-β3 [MFI]	176 ± 10	184 ± 13	
α- αIIbβ3 [MFI]	356 ± 30	344 ± 18	
α- α2 [MFI]	44 ± 1	45 ± 1	
α-β1 [MFI]	127 ± 9	116 ± 36	
α- α5 [MFI]	23 ± 1	23 ± 2	
α-CLEC-2 [MFI]	121 ± 9	114 ± 7	*
α-CD9 [MFI]	793 ± 16	767 ± 38	
α-CD84 [MFI]	27 ± 3	30 ± 5	

Gene targeting of *Prkcı* resulted in the complete absence of the protein in platelets (Figure 3-48 A). Besides this, the second atypical PKC isoform ζ could not be detected in mouse platelets neither by Western blot analysis nor by RT-PCR, independent of the expression of PKCı/λ (Figure 3-48 B, C). Platelet count, size and life span as well as surface abundance of major platelet glycoproteins were determined by flow cytometry and found to be unaffected by the loss of PKCı/λ in platelets and MKs (Table 3-3 and data not shown).

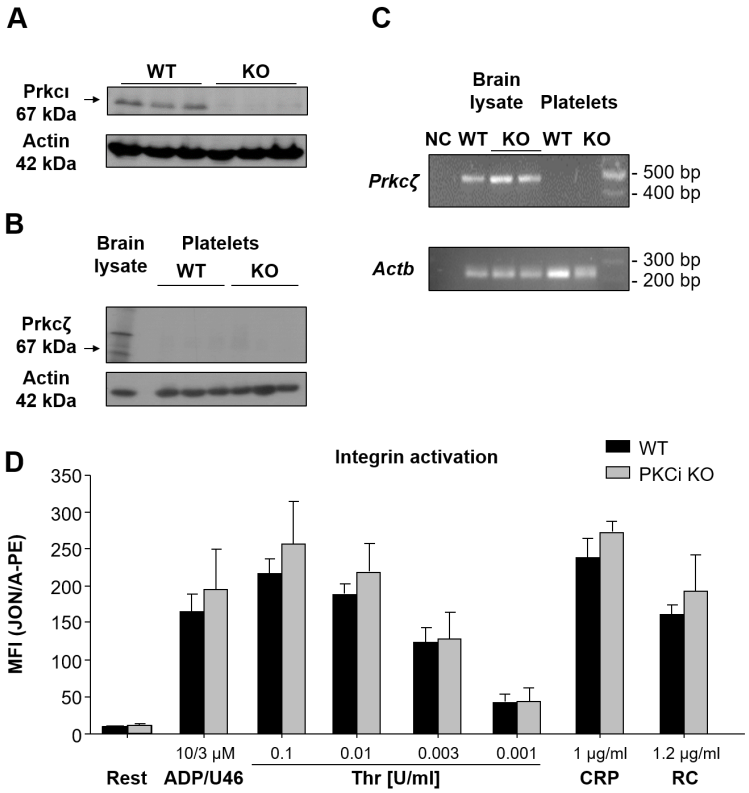

Figure 3-48: PKCı-deficiency has no effect on inside-out activation of platelet αIIbβ3 integrins. (A) PKCı expression was assessed by Western blot analysis. Actin served as a loading control. **(B)** PKCζ expression in platelet lysates was assessed by Western blot analysis. Actin served as a loading control. **(C)** Analysis of the presence of *Prkcz* mRNA in platelets. *Actin* mRNA served as positive control. cDNA free sample was used as negative control (NC). **(D)** Flow cytometric analyses of αIIbβ3 integrin activation (JON/A–PE) in response to the indicated agonists. Results are MFI ± SD, n=5, 3 independent experiments. Rest, resting; U46, U46619; Thr, thrombin; CRP, collagen-related peptide; RC, rhodocytin.

To clarify the role of PKCı/λ in integrin activation, integrin αIIbβ3 activation in response to different agonists was analyzed by flow cytometry. Stimulation of GPCRs with ADP, the thromboxane A_2 analogue U46619, a combination of both, or thrombin induced comparable integrin αIIbβ3 activation in WT and PKCı/λ-deficient platelets. Platelet activation in response to CRP and rhodocytin which activate the (hem)ITAM signaling pathway was also unaltered in the absence of PKCı/λ (Figure 3-48 D). Similar results were obtained for degranulation-dependent P-selectin exposure in response to all tested agonists (data not shown).

In line with unaltered agonist-induced integrin αIIbβ3 activation and degranulation, platelet aggregation was not affected by lack of PKCı/λ upon stimulation with any tested agonist (Figure 3-49). This also translated into an unaltered ATP secretion of PKCı/λ-deficient platelets in response to the tested agonists as assessed by luminoaggregometry (data not shown).

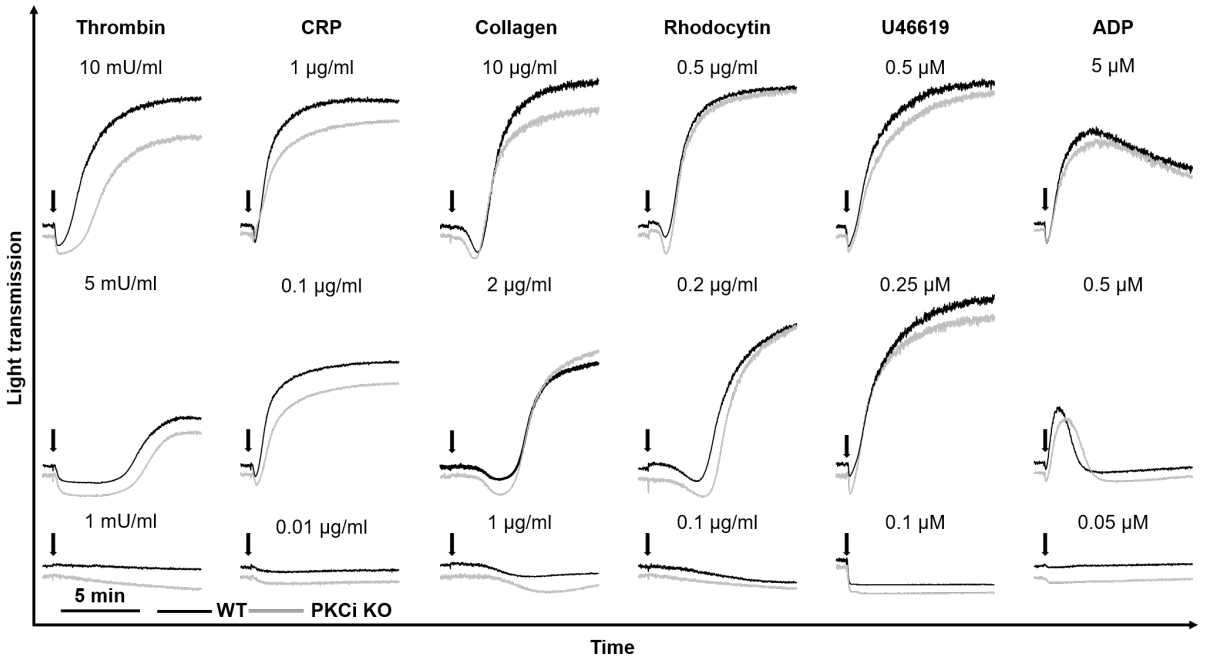

Figure 3-49: Unaltered platelet aggregation in PKCι-deficient mice. Washed platelets or platelet rich plasma (ADP) was stimulated with the indicated agonists, and light transmission was recorded with an Apact four-channel aggregometer. Representative aggregation traces of 3 individual experiments. CRP, collagen-related peptide.

3.8.2 PKCι/λ is dispensable for thrombus formation on collagen and platelet integrin outside-in signaling

Consistently, lack of PKCι/λ resulted in normal platelet adhesion, aggregate formation and thrombus volume *in vitro* on collagen under flow at a shear rate of 1700 s^{-1} (Figure 3-50 A, B) indicating that PKCι/λ is dispensable for platelet integrin inside-out signaling.

To investigate a potential role of PKCι/λ in integrin outside-in signaling, platelet spreading was analyzed. Ligand-occupied integrin αIIbβ3 mediates outside-in signaling, leading to cytoskeletal reorganization and platelet spreading [37]. The small Rho GTPases are known to be important mediators of cytoskeletal rearrangements [263]. Therefore, washed platelets were allowed to spread on a fibrinogen-coated surface *in vitro* after stimulation with thrombin (0.01 U/ml). PKCι/λ-deficient platelets formed filopodia and lamellipodia to the same extent and with similar kinetics as WT platelets (Figure 3-50 E, F). Therefore, PKCι/λ does not seem to influence reorganization of the actin cytoskeleton required for shape change and spreading. In line with this, clot retraction, a further assay to study integrin outside-in signaling, was not affected by lack of PKCι/λ in platelets (Figure 3-50 C, D). Thus, lack of PKCι/λ does not influence the ability of platelets to perform αIIbβ3-mediated adhesion on extracellular matrix proteins and changes in cytoskeleton organization do not depend on PKCι/λ.

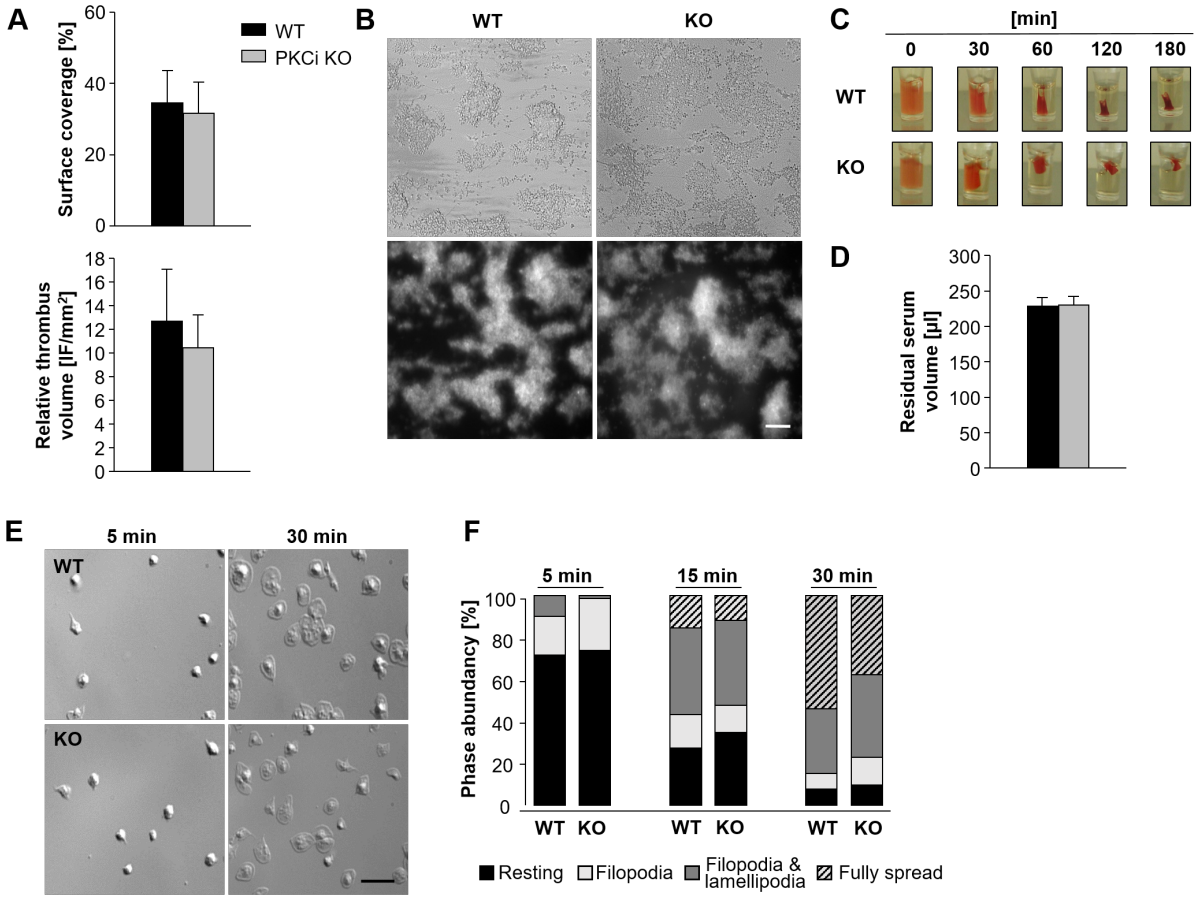

Figure 3-50: Lack of PKCι/λ has no influence on platelet adhesion to collagen, spreading on fibrinogen and platelet integrin outside-in signaling *in vitro*. (A) Adhesion and thrombus formation of platelets on collagen (0.2 mg/ml) was assessed in a flow adhesion assay at a shear rate of 1700 s^{-1} and with a perfusion time of 4 min. **(B)** Representative brightfield and fluorescent images. Scale bar: 25 µm. **(C, D)** Clot formation in PRP was induced by addition of thrombin (4 U/ml) and 20 mM $CaCl_2$ and clot retraction was monitored over time **(C). (D)** Residual volume of serum after clot retraction was measured. **(E, F)** Washed platelets of WT and PKCι/λ KO mice were allowed to spread on fibrinogen for up to 30 minutes after stimulation with 0.01 U/ml thrombin. **(E)** Representative images and **(F)** statistical evaluation of the percentage of spread platelets at different spreading stages are shown. Scale bar: 5 µm. Results are displayed as mean ± SD, n≥4, 3 independent experiments.

3.8.3 PKCι-deficient platelets display unaltered GPIb signaling

Next, the involvement of PKCι/λ in GPIb-mediated processes was evaluated. Upon vascular injury, vWF is exposed on the ECM and tethering of platelets to the ECM is mediated by GPIb-vWF interactions mainly under conditions of elevated shear. The adhesion to immobilized vWF under high shear rates was not affected by the absence of PKCι/λ. WT and PKCι/λ-deficient platelets attached and, in part, firmly adhered to the same extent and with similar kinetics as WT controls (Figure 3-51 A). Under static conditions, platelet adhesion to vWF upon blockade of integrin αIIbβ3 is triggered by a GPIb-specific signal resulting in shape change that is limited to contraction of cell body and filopodia formation [264]. Extent and kinetics of filopodia

formation were unaltered in the absence of PKCι/λ, indicating that GPIb-mediated signaling is intact in PKCι/λ-deficient platelets.

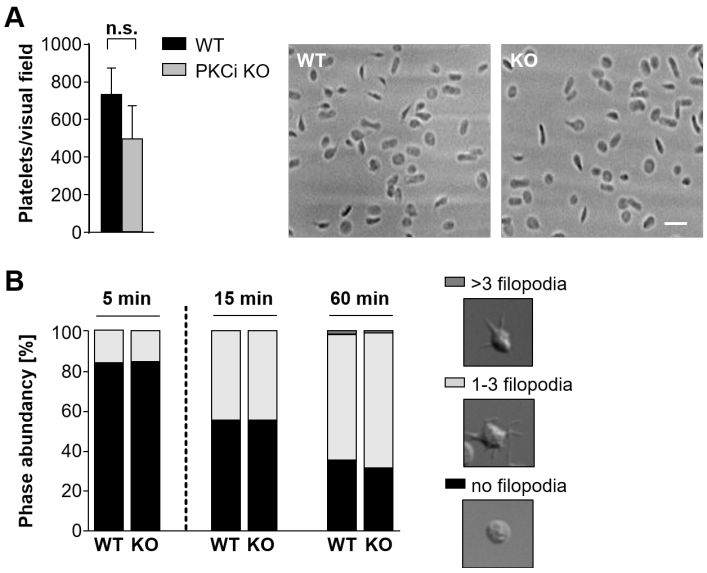

Figure 3-51: PKCι-deficient platelets display unaltered GPIb signaling. (A) Whole blood of WT and PKCι KO mice was perfused over a vWF-coated surface at a wall shear rate of 1700 s^{-1} for 4 min and the number of adherent platelets was quantified. Scale bar: 6.25 µm. Results are mean ± SD, n=5. **(B)** Washed platelets were treated with integrilin (60 µg/ml) and botrocetin (2 µg/ml) and allowed to adhere to vWF-coated cover slips. Filopodia formation was quantified according to the number of extensions per platelet at the indicated time points.

3.8.4 PKCι/λ is dispensable for *in vivo* thrombus formation

To study the *in vivo* relevance of platelet PKCι/λ, a tail bleeding time assay on filter paper was performed and revealed comparable results in WT and PKCι/λ-deficient mice indicating that PKCι/λ is not required to maintain hemostasis (Figure 3-52 A).

Thrombus formation *in vivo* was studied by intravital microscopy of $FeCl_3$-injured mesenteric arterioles of PKCι/λ-deficient and WT mice. Time to formation of occlusive stable thrombi was indistinguishable between both groups (Figure 3-52 B), which was in agreement with *in vitro* results. Overall, PKCι/λ is not required for proper platelet function *in vitro* and *in vivo* hemostasis and thrombus formation.

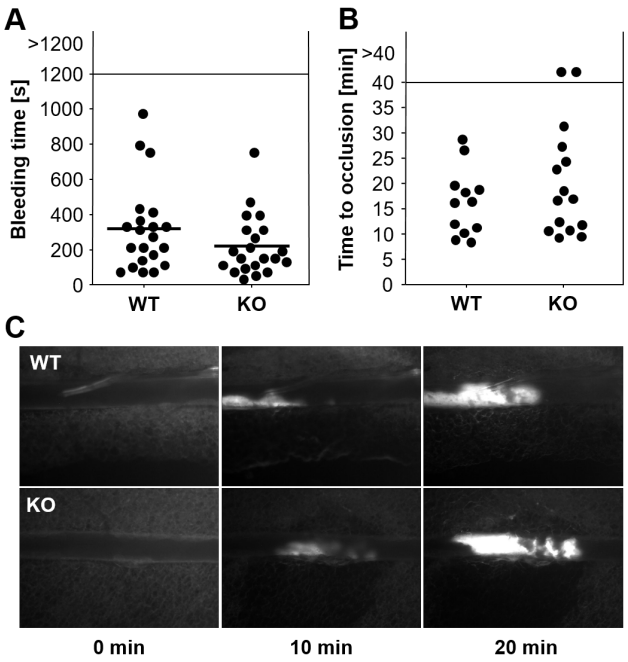

Figure 3-52: Unaltered *in vivo* thrombus formation in PKCι-deficient mice. (A) Tail bleeding times of WT and PKCι KO mice. 1 mm of the tail tip of each mouse was cut and time to cessation of blood flow was measured using a filter paper. Each symbol represents one animal. **(B, C**) Thrombus formation in small mesenteric arterioles was induced by topical application of 20% $FeCl_3$ and monitored by intravital microscopy via fluorescently-labeled platelets. Time to stable occlusion **(B**) and representative microscopic images **(C)** of WT and PKCι KO mice are shown. Each symbol represents one individual mouse.

4 Discussion

Platelet activation, aggregation, subsequent thrombus formation and coagulation at sites of vascular injury are critical to limit post-traumatic blood loss. Inherited gene defects causing impaired platelet activation or blood coagulation, ultimately leading to bleeding disorders [reviewed in 265] as well as acquired diseases accompanied by a severe thrombocytopenia, such as immune or heparin-induced thrombocytopenia, underline the relevance of platelets for maintenance of our circulatory system. Under pathological conditions, the tightly regulated steps of thrombus formation can overshoot, ultimately leading to complete vessel occlusion. Cardio- and cerebrovascular events, such as myocardial infarction and ischemic stroke, are major causes of death and disability worldwide. Anti-platelet agents (aspirin, clopidogrel, αIIbβ3 antagonists), which inhibit platelet function, have proven to be beneficial in the prevention of cardio- and cerebrovascular diseases [266]. However, established antithrombotic drugs are often associated with an elevated bleeding risk, can aggravate clinical outcome and therefore are often contraindicative. Therefore, currently available treatment options in acute ischemic disease states are limited. This emphasizes the necessity to identify novel pharmacological targets with a powerful yet safe antithrombotic profile. Detailed analysis of platelet activation and signaling pathways leading to thrombus formation has become an important field in cardiovascular research.

Thrombus formation is a complex, multistep process with several platelet adhesion and activation receptors and signaling molecules being involved. In recent years, the (hem)ITAM-bearing receptors GPVI and CLEC-2 have been identified as critical regulators of platelet activation and thrombus formation. Being critically involved in the initiation of thrombotic and thrombo-inflammatory signaling cascades, these receptors emerged as promising targets for novel anti-platelet drugs. However, their physiological role is not restricted to their involvement in primary hemostasis, but they also contribute to a plethora of (patho)physiological processes, including inflammation, atherosclerosis, tumor progression and lymphatic development, indicating that inference with (hem)ITAM signaling may lead to severe side-effects.

GPV has previously been identified as a mediator of thrombotic and hemostatic function [210], although only marginal effects were reported and the mode of action remains completely elusive. This thesis studied the role of GPV in thrombus formation using genetically modified mice, receptor blockade and recombinantly expressed, purified proteins. Surprisingly, these studies revealed a strong antithrombotic effect of soluble (thrombin-cleaved) GPV without affecting hemostatic function, establishing GPV as a master regulator of thrombus formation. Although data gained from studies using genetically modified mice cannot directly be transferred to humans, the findings presented in this thesis may serve as basis for the

generation of novel antithrombotic agents with a good safety profile for effective therapy of thromboembolic diseases.

4.1 *In vitro* studies on the functional role of GPV using *Gp5*$^{-/-}$ and *Gp5*$^{Kin/Kin}$ mice

This thesis focused on the investigation of the (patho-)physiological role of GPV. Extensive characterization of GPV-deficient mice, anti-GPV antibodies and mice with thrombin-uncleavable GPV revealed an unexpected role of GPV as modulator of platelet activation and thrombus formation and pointed to a critical antithrombotic function of soluble GPV. GPV-deficient mice as well as mice with a mutation rendering GPV uncleavable by thrombin restored the thrombotic and hemostatic defect caused by the absence of (hem)ITAM receptors. The fact that anti-GPV antibodies reproduced the GPV-knockout phenotype and soluble GPV had a strong antithrombotic effect establishes GPV as a key player in platelet physiology and might offer a novel treatment option for bleeding complications (anti-GPV antibodies) and thrombotic diseases (sGPV).

Platelets lacking GPV were overall functionally unaltered compared to WT platelets in *in vitro* settings. GPV-deficient mice showed a slightly increased platelet size, but unaltered platelet counts. In contrast, first descriptions of the two *Gp5*$^{-/-}$ mouse lines reported unaltered platelet size in the absence of GPV [144, 145]. Ramakrishnan *et al.* [145] described and Moog *et al.* [135] later confirmed a hyperreactivity of GPV-deficient platelets towards thrombin, which was not observed in the second *Gp5*$^{-/-}$ mouse line. Increased responsiveness of GPV-deficient platelets to thrombin was confirmed in our lab by flow cytometry and aggregation assays (Figure 3-1 and [210]) as well as in ATP release assays (data not shown). Initially, Ramakrishnan *et al.* ascribed the thrombin hyperresponsiveness to an unmasking of GPIb in the absence of GPV, contributing to thrombin signaling [243]. Today this hypothesis is believed to be overstated, since thrombin signaling in platelets is solely mediated via PARs [207] and thrombin binding to GPIb is not affected in the absence of GPV [206]. In fact, the absence of GPV as thrombin substrate leaves more thrombin available to activate platelets via PARs, which shifts the threshold required for platelet activation towards lower concentrations. This is also underlined by unaltered activation and aggregation responses of GPV-deficient platelets to PAR4-activating peptide (Figure 3-1 B). The activation response to all other agonists except for collagen was indistinguishable between GPV-deficient and WT platelets, which is also in line with previous reports [144, 145]. The role of GPV in collagen responses has already been extensively studied, revealing partially redundant, but overall minor functions of the collagen receptors α2β1 and GPV in collagen-induced aggregation [210].

The results presented in this thesis identify GPV as critical regulator of thrombosis and hemostasis and point to a possible role of the extracellular domain of GPV in these processes. GPV is efficiently downregulated by thrombin, leading to the assumption that this downregulation is critically involved in thrombotic and thrombo-inflammatory processes. So far, the *in vivo* relevance of the thrombin cleavage of GPV remains unknown. To shed new light on the relevance of the thrombin cleavage site *in vivo*, a mouse carrying a point mutation (R476A) in the thrombin cleavage site was generated, rendering GPV insensitive to thrombin cleavage. In these mice, GPV is not cleaved upon thrombin stimulation leading to permanent presence of the glycoprotein on the platelet surface. This was confirmed by an ELISA measuring cleaved GPV and by flow cytometric analysis of GPV surface levels upon thrombin stimulation (Figure 3-16 and Figure 3-17). As expected, the point mutation does not affect ADAM-dependent shedding of GPV, since stimulation with NEM, which induces metalloproteinase-dependent shedding, resulted in lowered GPV surface prevalence as well as increased levels of cleaved GPV. Of note, a reduction of approximately 20% of GPV surface prevalence levels was detected in *Gp5*$^{Kin/Kin}$ mice upon thrombin stimulation compared to resting controls. To exclude GPV shedding by ADAM17 [256] as probable reason for reduced GPV levels, experiments were also conducted in the presence of the broad matrix metalloproteinase inhibitor GM6001. However, a slight reduction of GPV surface expression levels was still detectable in the presence of the inhibitor. This receptor downregulation is due to internalization of the GPIb-V-IX complex [257].

Gp5$^{Kin/Kin}$ mice displayed normal platelet count, size and life span, and the permanent presence of GPV did also not alter the composition of the GPIb-V-IX complex. Unlike GPV-deficient mice, *Gp5*$^{Kin/Kin}$ mice displayed reduced αIIbβ3 integrin activation and aggregation upon CRP stimulation, but showed unaltered responses upon stimulation with convulxin. These differences in GPVI-dependent platelet activation might be due to a different GPVI-binding affinity of both agonists, which is much higher for convulxin than for CRP [267, 268]. In *Gp5*$^{Kin/Kin}$ mice, degranulation-dependent P-selectin exposure was overall reduced in response to all agonists and this reduction was most pronounced for the (hem)ITAM-dependent agonists CRP, convulxin and rhodocytin. Further studies are required to investigate whether reduced P-selectin exposure is due to a reduced total P-selectin content or whether this is a degranulation-specific effect.

GPV is dispensable for integrin αIIbβ3 outside-in signaling and cytoskeletal remodeling, since clot retraction and spreading on fibrinogen occurred to a similar extent and with similar kinetics in GPV-deficient and *Gp5*$^{Kin/Kin}$ platelets compared to respective controls.

While an additive effect of GPV- and α2-deficiency was previously reported in aggregation responses [210], there was no effect of GPV-deficiency in a whole blood perfusion system on

collagen, indicating that GPV is of minor relevance for platelet adhesion under flow conditions, further supporting the idea that GPV enhances GPVI-collagen interactions especially under static conditions [210]. In contrast, GPV mutant platelets displayed increasingly enhanced thrombus formation on collagen under flow with increasing shear rates. This raises the question of a shear-dependent involvement of GPV in thrombus formation with enhanced GPV-collagen interactions in *Gp5*$^{Kin/Kin}$ mice. It could also be speculated whether permanent presence of GPV facilitates GPVI-collagen interactions at high shear rates and thereby mediates firm platelet adhesion, thus supporting enhanced thrombus formation, while in WT mice GPV is cleaved due to the presence of low amounts of thrombin, thereby explaining the lack of a phenotype in GPV-deficient platelets. However, this hypothesis requires further investigation.

Initial results on the thrombus-modulatory role of GPV postulated that it may act as a regulator of platelet reactivity or procoagulant activity *in vivo* and that GPV may interact with an unknown ligand, modulating thrombosis and hemostasis. In this thesis, GPV was found to be dispensable for agonist-induced procoagulant activity in platelets measured by PS exposure under static and flow conditions in GPV-deficient and *Gp5*$^{Kin/Kin}$ platelets. However, increased TF-induced thrombin generation was observed *in vitro* in mutant PRP (Figure 3-23), yet it was unaltered in GPV-deficient PRP (Figure 3-2). Thrombin generation appeared to be independent of PS exposure on the platelet surface. In line with this, it has previously been shown that thrombin generation does not directly correlate with PS exposure on the platelet membrane and that platelets contribute to thrombin generation through a yet unknown mechanism besides PS exposure [269]. An increased overall amount of produced thrombin caused increased thrombin generation in *Gp5*$^{Kin/Kin}$ mice, while start and propagation phase, measured by lagtime, time to peak and maximal thrombin generation, were unaltered. In fact, increased thrombin generation is caused by delayed inhibition of thrombin generation (Figure 3-23). The reason for delayed inactivation of thrombin generation in mutant mice is still unknown. It can only be speculated whether it is caused by permanent presence of GPV on the platelet surface, which in turn may delay the inhibition process or whether ratio or activity of plasma factors are altered. Circulating protease inhibitors, among those the potent inhibitors antithrombin (inhibits FIX, FX and thrombin) and *tissue factor pathway inhibitor* (TFPI) (acting primarily on FX), as well as the protein C/S pathway are effective negative regulators of coagulation [219] and may be altered in mutant mice.

Platelet adhesion at sites of vascular injury is mainly mediated by binding of GPIb to exposed vWF on the ECM. It was further investigated whether lack or permanent presence of GPV on the platelet surface might support or prevent interactions of GPIb-IX with one of its ligands, which would account for the observed thrombus-modulating effects. GPIb is known to bind to

multiple ligands, among them vWF, thrombin, P-selectin, Mac-1, FXI, FXII, HMWK and protein C [155]. As reviewed in [210], it is unlikely that FXI, FXII and HMWK contribute to the observed effects of GPV-deficiency, since they are dispensable for hemostasis. GPIb-vWF interaction were unaltered under static and flow conditions in GPV-deficient as well as *Gp5*$^{Kin/Kin}$ platelets (Figure 3-3 and Figure 3-21). This is in line with previous reports [135, 144]. Under static conditions, botrocetin-induced platelet aggregation [144] as well as binding of botrocetin to activated vWF [145] is not affected by lack of GPV. However, despite unaltered αIIbβ3 integrin activation in response to convulxin, fibronectin binding to activated platelets was diminished in *Gp5*$^{Kin/Kin}$ mice compared to WT controls (Figure 3-21), while being unaltered in the absence of GPV (Figure 3-3). This could be due to several reasons. All experiments were performed in diluted whole blood. Therefore, binding of fibronectin originating from plasma and fibronectin secreted from activated platelets cannot be distinguished. Further research is required to clarify the underlying processes using different platelet agonists and platelet preparations (washed blood, PRP, washed platelets).

P-selectin has been postulated as a possible candidate to explain the *Gp5*$^{-/-}$ phenotype [210], since P-selectin is involved in thrombosis [270] and lack of P-selectin causes prolonged tail bleeding times [271]. Absence of GPV and thrombin-uncleavable GPV, however, did not affect platelet adhesion to P-selectin under flow (Figure 3-3 and Figure 3-21) except for a slightly elevated rolling distance. Together, these results exclude P-selectin as the major interaction partner of GPV.

Overall, GPV or its cleavage, as demonstrated by studies using *Gp5*$^{-/-}$ and *Gp5*$^{Kin/Kin}$ mice, is of minor relevance for platelet function *in vitro,* since *Gp5*$^{Kin/Kin}$ mice are to a large extent comparable to GPV-deficient mice, except for increased thrombus formation on collagen under flow, delayed inhibition of thrombin generation and the absence of thrombin hyperreactivity. The minor role of the thrombin cleavage site *in vitro* does not explain the observed *Gp5*$^{-/-}$ phenotype. *In vitro*, the minor relevance of GPV is further underlined by studies using the GPV blocking antibodies 89F12 or 5G2, which do not influence platelet reactivity and thrombus formation under *in vitro* conditions.

4.2 *In vivo* studies on the functional role of GPV in thrombosis and hemostasis using *Gp5*$^{-/-}$ and *Gp5*$^{Kin/Kin}$ mice and antibody-mediated blockade of GPV

Previously, an unexpected role of GPV as regulator of *in vivo* hemostasis, thrombus formation and thrombo-inflammatory brain infarction has been identified in our lab [210]. In previously

published reports, the role of GPV in thrombus formation was discussed contradictory, showing either a pro- or antithrombotic phenotype of GPV-deficient mice [135, 209]. These differences were ascribed to variations in severity of the injury and to differences in the genetic background of the mice [206]. Recent results from our group displayed a mild prothrombotic phenotype of GPV-deficient mice ([210] and Figure 3-4). Analyzing the effect of a double-deficiency of the collagen receptors α2β1 and GPV regarding a potential functional redundancy of both receptors in *in vivo* thrombosis models showed surprising results. Lack of both receptors did not lead to an additive effect - like in aggregation assays, but double-deficient mice reflected the *Gp5*$^{-/-}$ phenotype [210]. Unexpectedly, GPV-deficiency also reversed the hemostatic (Figure 3-5 and [210]) as well as thrombotic (Figure 3-4 and [210]) defect in the absence of the major collagen receptor GPVI. Deficiency or depletion of GPVI *per se* is known to protect from thrombosis [73, 182, 272] and GPV-deficiency reverses this effect. In genetic knockout mice double-deficient for the two collagen receptors GPV and GPVI, lack of GPV reversed the hemostatic and thrombotic defect in the absence of GPVI in *in vivo* thrombosis and hemostasis models. However, the *Gp6*$^{-/-}$ phenotype predominated in *in vitro* assays (data not shown), indicating that lack of GPV reverses thrombotic and hemostatic defects caused by lack of GPVI – independent of whether GPVI-deficiency was induced by antibodies or by gene inactivation.

In addition, lack of GPV restored thrombus formation and hemostasis in absence of the hemITAM receptor CLEC-2 (Figure 3-4, Figure 3-5 and [210]). Deficiency or depletion of CLEC-2 is associated with unaltered initial adhesion of platelets to the injured vessel wall, but the formed thrombi are unstable, translating into variable, yet prolonged bleeding times and pronounced protection from arterial thrombus formation [80]. In the absence of GPV, CLEC-2-deficient mice formed stable thrombi and bleeding ceased in a time comparable to WT mice without frequent emboli. Furthermore, lack of GPV restored hemostasis and reversed protection from arterial occlusive thrombus formation not only in mice deficient of GPVI or CLEC-2, but also in mice double-deficient for GPVI and CLEC-2 (Figure 3-4 and Figure 3-5).

Due to this unexpected role of GPV in thrombosis and hemostasis, in-house generated anti-GPV antibodies were screened for their ability to reproduce the *Gp5*$^{-/-}$ phenotype in WT mice. In line with previous reports [273, 274], some anti-GPV antibodies (e.g. clone 89H11) induce thrombocytopenia, which renders them unsuitable for *in vivo* studies (data not shown). One of our in-house generated monoclonal anti-GPV antibodies - clone 89F12 - was found to reproduce the *Gp5*$^{-/-}$ phenotype. It binds to the extracellular domain of GPV without affecting platelet count and thrombin-mediated cleavage of GPV (Beck, Stegner *et al.,* unpublished). While 89F12 had no effect on *in vitro* platelet function (see 3.2) and single treatment of WT mice with 89F12 did not alter hemostasis, it efficiently restored hemostatic function in absence of both (hem)ITAM receptors GPVI and CLEC-2 (Figure 3-8). This compensatory effect was

comparable to that observed in GPV-deficient mice (Figure 3-5), confirming 89F12 to be a suitable antibody to study further effects of GPV on other signaling pathways besides (hem)ITAM. Furthermore, these results indicate that the extracellular domain of GPV is essential for its functional role in thrombosis and hemostasis. Since Fab fragments of 89F12 exhibit the same effect (Beck, Stegner *et al*., unpublished), a role of GPV dimerization can be excluded in this process.

This thrombus-modulating effect of GPV is thought to be specific for (hem)ITAM receptors, since GPV-deficiency did not restore defective thrombus formation after blockade of GPIb-vWF interaction or in absence of FXII [210]. Circumventing the time-consuming breeding of double-deficient animals, 89F12-mediated blockade of GPV was used to assess the role of GPV as master regulator of thrombosis and hemostasis in more detail. These experiments showed that the thrombus-modulatory effect of GPV is not only limited to (hem)ITAM receptors. Syk, located downstream of GPVI and CLEC-2, is essential for arterial occlusive thrombus formation and proper hemostasis [252]. The protective effect of Syk-deficiency was fully reversed by blockade of GPV (Figure 3-9). This suggests that lack of GPV does not only restore thrombotic defects in the absence of (hem)ITAM surface receptors, but also reverses thrombus formation in absence of (hem)ITAM-related downstream signaling molecules. Surprisingly, GPV acts even more generally as a master regulator of *in vivo* thrombosis and hemostasis, since 89F12 restored hemostatic function in absence of RhoA, which is stimulated by G_q- and $G_{12/13}$-coupled receptors (Figure 3-10). Deficiency of RhoA in megakaryocytes and platelets is associated with platelet activation defects, translating into protection from arterial occlusive thrombus formation and increased bleeding times [253]. In contrast, deficiency of both small RhoGTPases RhoA and Cdc42 resulted in infinite bleeding times independent of GPV blockade. 89F12 treatment did not have any effect on hemostatic function in these mice. However, previous studies in our lab showed that RhoA/Cdc42 double-deficient mice suffer from severe macrothrombocytopenia with approximately 20% of normal platelet counts and circulating platelets exhibiting multiple platelet activation defects. Taken this into consideration, it is not surprising that blockade of GPV alone cannot reverse these multiple platelet defects.

Similarly, blockade of GPV had no influence on impaired hemostasis in *Gp1ba-tg* as well as Talin1- or Munc13-4-deficient mice, which showed infinite bleeding times independent of GPV blockade (Figure 3-11). Results obtained with *Gp1ba-tg* are in line with a previous report indicating that GPV-deficiency cannot reverse the effect of non-functional GPIb-vWF interaction in thrombus formation [210]. In conclusion, initial platelet adhesion, activation and degranulation are critical requirements for proper hemostasis. Deficiencies interfering with one of these major steps cannot be reversed by blocking GPV alone.

In addition, GPV-deficiency significantly shortened tail bleeding times in ASA-treated mice upon GPVI-depletion (Figure 3-6). In contrast to humans, ASA treatment alone only mildly affects hemostasis in WT mice [247-249]. However, in the absence of GPVI the TxA_2-mediated activation pathway becomes crucial, which manifests in markedly prolonged tail bleeding times in ASA-treated mice upon GPVI-depletion [247], suggesting that safe anti-GPV treatment in patients concomitantly taking aspirin at antithrombotic, analgetic, or antiphlogistic dosages might reduce bleeding risk and that anti-GPV treatment could be beneficial in situations of bleeding complications of these patients.

Similarly, 89F12 treatment lowered the minimum platelet count required to maintain proper hemostasis (Figure 3-12). Mice with 10% of normal platelet counts have prolonged tail bleeding times, but are still able to arrest bleeding [255]. Thrombocytopenia occurs frequently in humans. It can be caused by medical treatment or by different mechanisms in the context of a variety of pathologies, such as immune thrombocytopenia (ITP) or bacterial or viral infections. These results suggest that anti-GPV treatment could be helpful in acute thrombocytopenic situations to protect from life-threatening bleeding complications.

In addition to 89F12, the monoclonal mouse anti-mouse GPV antibody 5G2 was generated in the course of this thesis. Like 89F12, it binds to the extracellular domain of GPV without affecting platelet count or thrombin-induced ectodomain shedding or any other tested platelet function *in vitro* (Figure 3-13 and Figure 3-14). Surprisingly, injection of 5G2 *in vivo* reproduced the 89F12/*Gp5*$^{-/-}$ phenotype by reversing the hemostatic and thrombotic defect in absence of GPVI (Figure 3-15). Partially overlapping binding epitopes of 5G2 and 89F12 (Figure 3-13) may be a reason for comparable *in vivo* effects. It is speculative that both, 5G2 and 89F12, bind to the same epitope on GPV critically involved in GPV-ligand interactions, thus preventing GPV-ligand interactions by blocking the binding site for the ligand. Unfortunately, both the structure of GPV and binding epitopes of both antibodies await identification, which would facilitate identification of a GPV ligand.

The effect of GPV could be broadened from a specific (hem)ITAM-related to a more general thrombus-modulatory role, however, the underlying mechanism still remains elusive. *In vivo* studies on *Gp5*$^{Kin/Kin}$ mice revealed that thrombin cleavage of GPV is of minor relevance at first sight, since *Gp5*$^{Kin/Kin}$ mice *per se* displayed unaltered occlusion times in models of arterial thrombus formation and hemostasis (Figure 3-24 and Figure 3-25). More detailed analysis revealed that *Gp5*$^{Kin/Kin}$ mice reproduced the *Gp5*$^{-/-}$ phenotype: Mutant mice reversed the hemostatic defect of GPVI- or CLEC-2-depleted mice, restoring hemostasis (Figure 3-24). Comparable results were obtained in two models of arterial occlusive thrombus formation and *Gp5*$^{Kin/Kin}$ mice reversed the protection of GPVI- or CLEC-2-depleted mice (Figure 3-25). These results indicate that the thrombus-modulating role of GPV depends on thrombin-mediated

cleavage, since mice with complete absence of the receptor as well as mice with a mutation rendering GPV uncleavable by thrombin exhibited the same phenotype.

4.3 Soluble GPV as a potential antithrombotic agent

The results presented in this thesis point to a central regulatory role of GPV in *in vivo* thrombus formation and hemostasis with a specific importance of thrombin-induced cleavage of GPV. This led to the hypothesis that thrombin-cleaved soluble GPV may modulate thrombus formation. To study the effects of soluble GPV on thrombosis and hemostasis, recombinant smGPV coupled to a Flag tag was generated and purified in our lab, recombinant shGPV coupled to a human albumin tag was provided by CSL Behring.

Indeed, smGPV and shGPV effectively prevented occlusive thrombus formation in two models of arterial thrombosis, without affecting hemostatic function (Figure 3-37, Figure 3-45 and Figure 3-46). Preliminary data also pointed to a protective effect of shGPV in ischemic stroke (Figure 3-47). The *in vivo* results indicate that sGPV is a strong antithrombotic agent, whose physiological role is both temporally and locally restricted at sites of vascular injury where it limits platelet activatory responses.

However, *in vitro* under static conditions, neither smGPV nor shGPV did have any effect on platelet function or coagulation: αIIbβ3 integrin activation, degranulation-dependent P-selectin exposure, platelet aggregation in washed platelet, PRP and whole blood (Figure 3-31), as well as thrombin generation and coagulation measured by QUICK and aPTT were unaltered, indicating that sGPV is of minor relevance for platelet function under static conditions.

Ex vivo and *in vitro* flow adhesion assays on collagen reproduced the antithrombotic effect of smGPV and shGPV observed in *in vivo* thrombosis assays. smGPV and shGPV diminished thrombus formation in murine and human blood dose-dependently, with 20 µg of the protein being sufficient to significantly reduce thrombus formation in mouse and human blood (Figure 3-32 and Figure 3-43).

As mentioned above, the antithrombotic effect of sGPV was observed *in vitro* only under flow conditions. smGPV exhibited its antithrombotic effect independent of the applied shear rate (Figure 3-33), however, the antithrombotic effect of shGPV depended on the applied shear rate and was only detectable at a high shear rate of 1000 s^{-1}, but not at lower shear rates (Figure 3-43). These results indicate that the thrombus-modulating effect of sGPV critically requires flow conditions, leading to the assumption that it probably depends on shear-induced unfolding of either sGPV or its ligand. This discrepancy between a shear rate-independent effect of smGPV and a shear rate-dependent effect of shGPV could be due to several reasons.

The studies on shear rate-dependency have only been conducted in murine blood for smGPV and in human blood for shGPV. Taken into consideration that mean shear rates and wall shear stress are higher in mice than in humans [260, 261], the observed differences may originate from a (I) different behavior of shGPV and smGPV, (II) different rheology of human blood compared to murine blood or (III) a complete distinct mechanism in the human system compared to the mouse system. To further clarify whether the observed shear rate-dependency is an effect inherent in sGPV or rather in blood, experiments with smGPV in human blood and vice versa need to be conducted at different shear rates. At high shear rates (human blood: 1000 s^{-1}; murine blood: 1700 s^{-1}), smGPV and shGPV were tested in human blood and murine blood, respectively (Figure 3-36 and Figure 3-45). Both showed a strong antithrombotic effect, suggesting that the antithrombotic effect of sGPV *per se* is not species-specific, but rather of general nature and will probably allow translation of mechanistic results obtained in murine models to the human vascular system. Regarding the clinical relevance of sGPV as a potential new antithrombotic agent, translation from murine models to the human vascular system is critical, since tools to study shGPV are limited and direct proof of the mechanism underlying the antithrombotic effect *in vivo* would not be possible in humans.

Furthermore, half-life of smGPV *in vivo* is rather short. *Ex vivo* flow adhesion experiments showed a pronounced antithrombotic effect of smGPV 20 min after smGPV injection, however, the antithrombotic effect of smGPV had vanished 60 min after smGPV injection. The short half-life observed *in vivo* is in line with a calculated half-life of 0.8 h by ProtParam based on the amino acid sequence of GPV. Regarding a potential application of sGPV as antithrombotic agent, a longer *in vivo* half-life of the protein would be necessary. There are several strategies available to prolong the plasma half-life of proteins with improved pharmacokinetic profiles while simultaneously preserving bioactivity of the protein. Albumin and IgG are often used to prolong plasma half-life [275]. Albumin has a long half-life of 17-19 days [276], is highly abundant in plasma and can significantly increase the *in vivo* half-life of fusion proteins [277-279]. For this purpose, human albumin was fused to shGPV, however, the half-life of shGPV-FP in plasma has not yet been studied.

sGPV does not require interaction with GPV on the platelet surface to exert its antithrombotic effect, since reduction of thrombus formation after sGPV treatment was comparable between GPV-deficient and WT mice (Figure 3-34). smGPV even overruled the *Gp5*$^{Kin/Kin}$ phenotype in thrombus formation on collagen under flow and normalized the enhanced thrombus formation in *Gp5*$^{Kin/Kin}$ mice back to untreated WT levels at an intermediate shear rate. At low shear, where *Gp5*$^{Kin/Kin}$ mice form thrombi indistinguishable from untreated WT mice, smGPV even further reduced thrombus formation. These data underline the strong antithrombotic effect of sGPV. These striking observations could also explain the *Gp5*$^{-/-}$ and *Gp5*$^{Kin/Kin}$ phenotypes

described in this thesis. Both mouse lines lack sGPV, whereas it is released in WT mice as soon as thrombin is present. Therefore, it is tempting to speculate that lack of antithrombotic sGPV overrules thrombotic or hemostatic defects e.g. in the absence of (hem)ITAM receptors, while initial platelet adhesion and activation are prerequisites of proper thrombus formation and cannot be compensated by sGPV alone. Understanding the mechanism underlying the antithrombotic effect of sGPV requires the identification of its ligand(s).

As discussed earlier, shear stress seems to be a prerequisite for the antithrombotic activity of sGPV. So far, no static *in vitro* assay has been identified which can reproduce the observed effects of sGPV. This renders the search for a binding partner of sGPV more challenging, since classical immunoprecipitation and pulldown experiments to identify interaction partners are typically not performed under conditions of shear flow. Nevertheless, immunoprecipitation experiments using plasma, PRP or washed platelets were carried out, but did not lead to clear results. In addition, pulldown experiments after flow adhesion runs have so far failed to give clear results and require further optimization.

It has been speculated that the anti-GPV antibody 89F12 binds to the epitope on GPV that is involved in GPV-ligand interactions, thus preventing this activity. Indeed, preincubation of 89F12 with smGPV abolished the antithrombotic effect of smGPV (Figure 3-38), presumably by preventing GPV-ligand interactions.

smGPV gets incorporated into the growing thrombus, since it was stained on thrombi colocalizing with platelets in flow adhesion assays (Figure 3-40 A). smGPV was primarily found at the edges of platelets, however, this localization should be considered with caution. smGPV was stained with an anti-GPV antibody after thrombus formation, possibly preventing the antibody from reaching the thrombus core to stain sGPV. In addition, plasma factors are crucial for the antithrombotic effect of sGPV, since the thrombus-modulating effect of smGPV was abrogated in the absence of plasma factors (Figure 3-39 and data not shown). Further studies will concentrate on staining smGPV in a reconstituted flow chamber. This could add insight into whether (I) smGPV still binds to platelets in the absence of plasma factors without exerting its antithrombotic effect, (II) the antithrombotic effect is due to an indirect interaction of smGPV with platelets or (III) binding to platelets is directly linked to inhibition of thrombus formation.

It is likely that a sGPV ligand is expressed either in the plasma or on the surface of activated platelets, mediating an indirect interaction with plasma factors. Potential candidates for ligands of sGPV include - besides others - vWF, fibronectin, thrombospondin or laminins. Since smGPV did exert its thrombus-reducing effect only *in vitro* under flow or *in vivo*, but not *in vitro* under static conditions, we speculated whether GPV binds to vWF. vWF has a key role in coagulation as carrier for FVIII and is essential for primary hemostasis by binding to exposed

collagen on the ECM upon vascular injury and by mediating tethering of platelets via GPIb. Besides this, vWF is shear-dependently unfolded and activated. It has previously been shown that platelet-derived vWF is not essential for hemostasis and thrombosis, but promotes ischemic stroke [280]. In *in vivo* thrombosis models, *vWF*$^{-/-}$ mice can form thrombi, although with a persistent flow channel [281], but are protected from ischemic stroke [184]. Nevertheless, it appears rather unlikely that vWF is the ligand responsible for the GPV phenotype, since (I) GPIb-vWF interactions are unaltered in the absence of GPV [144, 210], (II) GPV-deficiency cannot reverse the effect of non-functional GPIb-vWF interaction in thrombus formation [210] and (III) smGPV incubation *in vitro* does not affect platelet adhesion on vWF (data not shown).

Fibronectin has long been proposed to be involved in thrombosis and hemostasis, but its exact role in these processes is controversial [282]. Plasma fibronectin (pFN) is involved in multiple steps of hemostasis and thrombosis and its effect depends on the presence of fibrin, where pFN supports hemostasis and thrombosis. However, in the absence of fibrin(ogen) pFN inhibits platelet aggregation. This self-limiting mechanism may prevent platelet aggregation at the outer shell of the thrombus [283] (Figure 4-1). In addition to pFn, cellular fibronectin (cFN) is found to be prothrombotic and may contribute to increased thrombosis risk under certain disease conditions [284]. In combination, this renders fibronectin a possible candidate to explain the antithrombotic effect of smGPV.

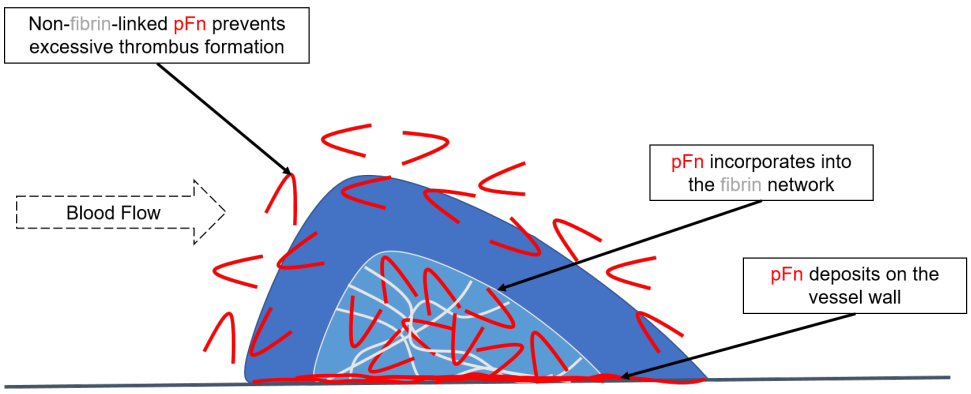

Figure 4-1: Schematic model of plasma fibronectin maintaining the balance between thrombosis and hemostasis. Plasma fibronectin (pFN) deposits quickly on the injured vessel wall. Platelets accumulate on the deposited pFN and release pFN from α-granules. In the inner core of the thrombus, pFN is crosslinked with fibrin, promoting platelet aggregation. However, on the outer shell of the thrombus where fibrin is almost absent, non-fibrin-linked pFN prevents platelet aggregation and thereby limits thrombus growth. Modified from: Wang, Ni 2016 [285].

Another possible candidate to interact with GPV is thrombospondin-1 that is stored in α-granules and released from platelets upon activation. Besides this, it is also synthesized by

various cells, among those endothelial cells and monocytes, and incorporated into the ECM. Once released from platelets, it is incorporated into the growing thrombus and can bind to several receptors on the platelet surface (e.g. CD36, GPIb-V-IX complex, CD47) as well as to various plasma proteins including fibrinogen, vWF, plasminogen and TFPI [286]. Conflicting *in vitro* and *in vivo* data – depending on the source of thrombospondin-1, its interaction partners and its conformation – make a statement regarding its role in platelet aggregation difficult, but indicate that thrombospondin-1 is involved in thrombus stability [287-289].

Laminins are major components of the basement membrane and platelets express many receptors which can bind laminins, including $\alpha_6\beta_1$, GPVI and the GPIb-IX/vWF axis. Various laminin isoforms are expressed in the vascular wall and support platelet adhesion and activation under arterial shear conditions. Deficiency of integrin $\alpha_6\beta_1$ protects from arterial thrombosis, but does not affect hemostasis [290], making it more unlikely that laminins contribute to the effects of GPV.

At sites of vascular injury, sGPV is cleaved from the platelet surface by locally produced thrombin and is released locally and temporally limited during thrombus formation, resulting in GPV-deficient platelets. Under physiological conditions, lack of sGPV *per se* affects thrombotic or hemostatic processes only to a small extent – as shown in GPV-deficient or *Gp5*$^{Kin/Kin}$ mice. However, when administered in excessive amounts, sGPV shows a strong antithrombotic effect *in vivo* without negatively affecting hemostasis. Although the underlying mechanism remains elusive, the results are very promising and potentially of high clinical relevance. sGPV potently inhibits thrombus formation, while it does not affect hemostasis. These data indicate that sGPV treatment results in efficient and safe protection from pathological thrombus formation in different vascular beds without causing major bleeding complications, strongly suggesting that sGPV might become a novel, safe antithrombotic agent.

The effect of sGPV on thrombo-inflammation so far is unknown. Initial results point to a protective effect of sGPV by reducing infarct volumes in a tMCAO model. In this study, sGPV was administered before tMCAO, which reflects a prophylactic treatment. The therapeutic effect of sGPV has not yet been studied. The tMCAO model is well-established to study ischemia-reperfusion injury, which often occurs after successful recanalization of occluded cerebral arteries, and reflects critical aspects of thrombectomy in patients. sGPV treatment at the time of reperfusion would reflect a therapeutic setting in clinical situations, where a patient undergoes successful thrombectomy with additional treatment with an antithrombotic agent.

A potential use of sGPV as long-term prophylactic treatment may be limited by its short plasma half-life and its corresponding time-dependent antithrombotic effect, which could be circumvented by modification of the protein as discussed. Still, sGPV might be a potent drug

for short-term therapy for patients with a high thrombotic risk in acute clinical settings, such as heart surgeries or to prevent secondary infarctions often occurring shortly after primary transient ischemic attacks.

Besides this, anti-GPV antibodies can antagonize the antithrombotic effect of sGPV and mimic a GPV-deficiency. Since anti-GPV treatment lowered the minimum platelet count required to maintain proper hemostasis (Figure 3-12), it can be helpful in acute thrombocytopenic situations to protect from life-threatening bleeding complications. Besides this, anti-GPV treatment can be clinically relevant to prevent hemorrhages during inflammation especially under conditions of limited (hem)ITAM signaling. (hem)ITAM signaling is critical to secure vascular integrity, since the risk for inflammatory bleeding is increased in the absence of GPVI or CLEC-2 [86]. Assuming a similar compensatory effect of GPV-deficiency under inflammatory conditions as in thrombotic processes, GPV blockade would be beneficial to prevent hemorrhages under limited (hem)ITAM signaling. Additionally, it could be of high clinical relevance in prevention of intracranial hemorrhage (ICH). Primary ICH, bleeding into the brain subsequent to rupture of a weakened blood vessel, is an acutely life-threatening disease state often caused by hypertension or hyperglycemia and represents a leading cause of stroke, particularly since effective treatment options for acute ICH are missing [291]. Plasma kallikrein is a key player in hyperglycemia-induced ICH: it binds and blocks GPVI binding sites of collagen, thereby preventing platelet activation via GPVI. This is enhanced in the presence of high glucose concentrations. GPVI stimulation by administration of CRP reduced hematoma expansion, demonstrating that GPVI stimulation is beneficial [292]. Therefore, GPV blockade which compensates for decreased GPVI signaling would probably be similarly effective.

Still, caution is required when translating data from mice to humans. First *in vitro* results on sGPV in human blood are promising, but further experiments on the role of GPV in human diseases are required. The newly generated humanized GPV mouse model provides an interesting tool, especially for *in vivo* studies to evaluate antithrombotic and antihemostatic GPV compounds and to screen newly generated anti-human GPV antibodies for their ability to reproduce the phenotype of the anti-mouse GPV antibodies 89F12 and 5G2.

4.4 PKCι/λ is dispensable for platelet function in thrombosis and hemostasis

Platelet- and megakaryocyte-specific PKCι/λ knockout mice were used to assess the role of this aPKC in platelet function *in vitro* and *in vivo*. PKC isoforms, including isoforms alpha, epsilon, delta, theta and eta [97, 98], were previously shown to play critical roles in regulating

various aspects of platelet activation and function. However, little is known about atypical PKC isoforms and in particular PKCι/λ has never been studied in platelets before. PKCι/λ is an effector of Cdc42 and Rac1 in other cell types [106], and constitutive knockout of PKCι/λ is embryonically lethal [117, 118].

Recent studies by our group identified the GTPases RhoA and Cdc42 as important regulators of MK polarization and subsequent release of platelets into the vessel lumen [122]. GPIb- or Cdc42-deficiency results in defective MK polarization, translating into impaired transendothelial platelet release. Similarly to Cdc42-deficient MKs, loss of PKCι/λ in MKs affects their localization and polarization with less MKs being in direct contact with the bone marrow vasculature [122]. These data demonstrate (i) that PKCι/λ is expressed in MKs and platelets, and (ii) that loss of this protein has functional consequences, at least in MKs.

Platelet count, size and life span were not affected by the absence of PKCι/λ (Table 3-3) which, however, contrasts findings in GPIb- [124] or Cdc42-deficient [111] mice, as these mice suffer from macrothrombocytopenia and exhibit a reduced platelet life span. Additionally, this indicates that PKCι/λ contributes to Cdc42-signaling, but does not affect the entire Cdc42-signaling in MKs.

Rac1$^{-/-}$ platelets display a general defect in (hem)ITAM signaling and reduced platelet activation upon stimulation with low doses of thrombin [20, 109, 293]. Absence of Cdc42 results in enhanced platelet degranulation [111] and aPKCs have been demonstrated to modulate secretion [294]. Surprisingly, we observed no difference in platelet activation or degranulation between PKCι/λ-deficient and WT platelets (Figure 3-48) indicating that PKCι/λ is not essential for platelet degranulation.

The gold compound aurothiomalate (ATM) is a specific PKCι/λ inhibitor that is used in clinics as an antirheumatic agent and reported to be a potent inhibitor of oncogenic PKCι/λ [295, 296]. It binds PKCι/λ and blocks activation of PKCι-Par6-Rac1-Pak-Mek 1,2-Erk 1,2 signaling pathway. Therefore, the effect of ATM on platelet integrin αIIbβ3 activation and platelet degranulation was assessed. ATM treatment resulted in decreased, but not abolished αIIbβ3 activation and P-selectin exposure in response to low doses of thrombin and CRP in both PKCι/λ-deficient and WT platelets (data not shown). Therefore, it is speculated that ATM exhibits unspecific side effects and off-target effects, but does not influence platelet activation in a PKCι/λ-dependent manner. Overall, this confirms that PKCι/λ is dispensable for integrin inside-out activation. Comparable results were obtained for platelet aggregation and adhesion to collagen under flow. In contrast to aggregation, spreading on fibrinogen is dependent on integrin outside-in signaling. *Rac1*$^{-/-}$ and *Cdc42/Rac1*$^{-/-}$ platelets showed pronounced spreading defects on fibrinogen and *Cdc42*$^{-/-}$ platelets on vWF, as they failed to develop filopodia on this

substrate [109-111]. Given the role of PKCι/λ in rearrangement of the cytoskeleton [294], a similar defect was expected for PKCι/λ-deficient platelets. However, PKCι/λ KO platelets did not show any alterations in spreading on fibrinogen in comparison to WT platelets (Figure 3-50). Consequently, stress fiber formation assessed in spread platelets by confocal microscopy was not affected by lack of PKCι/λ (data not shown). Even more surprisingly, GPIb-signaling was not impaired in PKCι/λ-deficient platelets (Figure 3-51), despite the fact that absence of PKCι/λ resembles the phenotype of Cdc42-deficiency with respect to GPIb-triggered MK polarization [122]. In line with this, PKCι/λ activity assessed by measuring phosphorylation of threonine 410 and 555 was unaltered in the absence of Cdc42 upon platelet stimulation with thrombin. Consistent with the *in vitro* results obtained, hemostasis and experimental thrombus formation were unaltered in the absence of PKCι/λ *in vivo*.

The effect of PKCι/λ-deficiency on its downstream signaling in platelets is largely unknown. PKCι/λ interacts with and activates several proteins, among them Par6, epithelial cell transforming sequence 2 oncogene (ECT2), interleukin-1 receptor-associated kinase 1 (IRAK1), lethal giant larvae homolog 1 (LLGL1), which are not expressed in platelets. Potential downstream molecules which are expressed in platelets are ezrin, partitioning defective 3 homolog (Par3) or GAPDH, however, experimental evidence for interactions in platelets is lacking. Thus, it is difficult to assess downstream signaling of PKCι/λ in platelets.

Lack of a phenotype in the absence of PKCι/λ suggests that loss of its function is compensated by the second aPKC isoform PKCζ. While PKCζ is expressed in human platelets [297], albeit in very low copy numbers [298], PKCζ was not expressed in murine platelets – neither on mRNA nor on protein level (Figure 3-48 and [299]), which might be due to species-specific differences. Likewise, PKCι/λ has not been detected in proteomic studies using human platelets [300, 301]. Therefore, it appears likely that PKCζ is the aPKC in human and PKCι/λ the aPKC in murine platelets. It is also unlikely that other conventional or novel PKC isoforms compensate for the absence of PKCι/λ, since the ‘mode of activation’ as well as the physiological role in platelets differs substantially between the different classes of PKC isoforms [97, 302]. This is further underlined by unaltered expression levels of different PKC isoforms assessed by qPCR analysis (data not shown). Thus, the only PKC isoform which could potentially compensate for the loss of PKCι/λ is PKCζ which is, however, not expressed in murine platelets.

A possible, yet not proven explanation for unaltered platelet function in PKCι/λ-deficient mice could be that functional relevance of PKCι/λ is restricted to MKs, regulating their localization and transendothelial platelet biogenesis [122]. This thesis clearly shows that PKCι/λ, the only aPKC in murine platelets, has no non-redundant functions in classic platelet physiology.

4.5 Concluding remarks and future plans

The role of GPV as a regulator of thrombosis and hemostasis was further settled and expanded in this thesis. While previous results point to a specific (hem)ITAM-dependent modulatory role of GPV, this thesis establishes a more generalized role of GPV as a master regulator mediating thrombotic and hemostatic processes.

However, further experimental data are required to elucidate the principal mechanism of the thrombus-modulatory role of GPV. First hints that sGPV is incorporated into the growing thrombus and that plasma factors are crucial, are provided in this thesis, but identification of an interaction partner of GPV is fundamental.

On the other hand, the results on the anti-GPV antibody 89F12 clearly show that blockade of GPV by 89F12 phenocopies GPV-deficient mice and can restore thrombus formation and hemostasis in the absence of crucial platelet surface receptors as well as signaling molecules. Blockade of GPV thereby exerts the same effects as GPV-deficiency. Furthermore, 89F12 lowers the minimum platelet count required to maintain normal hemostasis, implying the use of 89F12 as a coagulant in treatment of hemorrhagic conditions during inflammation or as probably beneficial application in acute treatment of severely thrombocytopenic patients or after acute blood loss/trauma.

For clinical translation of these findings, anti-human GPV antibodies are critically required. Commercially available anti-human GPV antibodies are limited. Therefore, the generation of anti-human GPV antibodies was already started in our laboratory and at the moment, sub-cloning of two mouse anti-human and several rat anti-human GPV antibodies is ongoing. These antibodies will not only be screened for their ability to reproduce the 89F12 phenotype in the herein described *Gp5*$^{hGp5/hGp5}$ mouse line, but will rather provide a valuable tool box to study hGPV.

5 References

1 Jackson SP. Arterial thrombosis—insidious, unpredictable and deadly. *Nature medicine*. 2011; **17**: 1423.

2 http://www.who.int/mediacentre/factsheets/fs317/en/.

3 Lozano R, Naghavi M, Foreman K, Lim S, Shibuya K, Aboyans V, Abraham J, Adair T, Aggarwal R, Ahn SY, Alvarado M, Anderson HR, Anderson LM, Andrews KG, Atkinson C, Baddour LM, Barker-Collo S, Bartels DH, Bell ML, Benjamin EJ, Bennett D, Bhalla K, Bikbov B, Bin Abdulhak A, Birbeck G, Blyth F, Bolliger I, Boufous S, Bucello C, Burch M, Burney P, Carapetis J, Chen H, Chou D, Chugh SS, Coffeng LE, Colan SD, Colquhoun S, Colson KE, Condon J, Connor MD, Cooper LT, Corriere M, Cortinovis M, de Vaccaro KC, Couser W, Cowie BC, Criqui MH, Cross M, Dabhadkar KC, Dahodwala N, De Leo D, Degenhardt L, Delossantos A, Denenberg J, Des Jarlais DC, Dharmaratne SD, Dorsey ER, Driscoll T, Duber H, Ebel B, Erwin PJ, Espindola P, Ezzati M, Feigin V, Flaxman AD, Forouzanfar MH, Fowkes FG, Franklin R, Fransen M, Freeman MK, Gabriel SE, Gakidou E, Gaspari F, Gillum RF, Gonzalez-Medina D, Halasa YA, Haring D, Harrison JE, Havmoeller R, Hay RJ, Hoen B, Hotez PJ, Hoy D, Jacobsen KH, James SL, Jasrasaria R, Jayaraman S, Johns N, Karthikeyan G, Kassebaum N, Keren A, Khoo JP, Knowlton LM, Kobusingye O, Koranteng A, Krishnamurthi R, Lipnick M, Lipshultz SE, Ohno SL, Mabweijano J, MacIntyre MF, Mallinger L, March L, Marks GB, Marks R, Matsumori A, Matzopoulos R, Mayosi BM, McAnulty JH, McDermott MM, McGrath J, Mensah GA, Merriman TR, Michaud C, Miller M, Miller TR, Mock C, Mocumbi AO, Mokdad AA, Moran A, Mulholland K, Nair MN, Naldi L, Narayan KM, Nasseri K, Norman P, O'Donnell M, Omer SB, Ortblad K, Osborne R, Ozgediz D, Pahari B, Pandian JD, Rivero AP, Padilla RP, Perez-Ruiz F, Perico N, Phillips D, Pierce K, Pope CA, 3rd, Porrini E, Pourmalek F, Raju M, Ranganathan D, Rehm JT, Rein DB, Remuzzi G, Rivara FP, Roberts T, De Leon FR, Rosenfeld LC, Rushton L, Sacco RL, Salomon JA, Sampson U, Sanman E, Schwebel DC, Segui-Gomez M, Shepard DS, Singh D, Singleton J, Sliwa K, Smith E, Steer A, Taylor JA, Thomas B, Tleyjeh IM, Towbin JA, Truelsen T, Undurraga EA, Venketasubramanian N, Vijayakumar L, Vos T, Wagner GR, Wang M, Wang W, Watt K, Weinstock MA, Weintraub R, Wilkinson JD, Woolf AD, Wulf S, Yeh PH, Yip P, Zabetian A, Zheng ZJ, Lopez AD, Murray CJ, AlMazroa MA, Memish ZA. Global and regional mortality from 235 causes of death for 20 age groups in 1990 and 2010: a systematic analysis for the Global Burden of Disease Study 2010. *Lancet*. 2012; **380**: 2095-128.

4 Heuschmann P, Busse O, Wagner M, Endres M, Villringer A, Röther J, Kolominsky-Rabas P, Berger K, Schlaganfall-Hilfe fdKSdDSGsdSD. Schlaganfallhäufigkeit und Versorgung von Schlaganfallpatienten in Deutschland - Frequency and Care of Stroke in Germany. *Akt Neurol* 2010; **37**: 333-40.

5 Ward A, Payne KA, Caro JJ, Heuschmann PU, Kolominsky-Rabas PL. Care needs and economic consequences after acute ischemic stroke: the Erlangen Stroke Project. *Eur J Neurol*. 2005; **12**: 264-7.

6 Jauch EC, Saver JL, Adams HP, Jr., Bruno A, Connors JJ, Demaerschalk BM, Khatri P, McMullan PW, Jr., Qureshi AI, Rosenfield K, Scott PA, Summers DR, Wang DZ, Wintermark M, Yonas H, American Heart Association Stroke C, Council on Cardiovascular N, Council on Peripheral Vascular D, Council on Clinical C. Guidelines for the early management of patients with acute ischemic stroke: a guideline for healthcare professionals from the American Heart Association/American Stroke Association. *Stroke; a journal of cerebral circulation*. 2013; **44**: 870-947.

7 Gerczuk PZ, Kloner RA. An update on cardioprotection: a review of the latest adjunctive therapies to limit myocardial infarction size in clinical trials. *Journal of the American College of Cardiology*. 2012; **59**: 969-78.

8 Soares BP, Tong E, Hom J, Cheng SC, Bredno J, Boussel L, Smith WS, Wintermark M. Reperfusion is a more accurate predictor of follow-up infarct volume than recanalization: a proof of concept using CT in acute ischemic stroke patients. *Stroke; a journal of cerebral circulation*. 2010; **41**: e34-40.

9 Eltzschig HK, Eckle T. Ischemia and reperfusion—from mechanism to translation. *Nature medicine*. 2011; **17**: 1391.

10 Morgenstern E. The formation of compound granules from different types of secretory organelles in human platelets (dense granules and alpha-granules). A cryofixation/-substitution study using serial sections. *European journal of cell biology*. 1995; **68**: 183-90.

11 Ault KA, Knowles C. In vivo biotinylation demonstrates that reticulated platelets are the youngest platelets in circulation. *Experimental hematology*. 1995; **23**: 996-1001.

12 Hartwig J, Italiano J, Jr. The birth of the platelet. *Journal of thrombosis and haemostasis*. 2003; **1**: 1580-6.

13 Grozovsky R, Hoffmeister KM, Falet H. Novel clearance mechanisms of platelets. *Current opinion in hematology*. 2010; **17**: 585-9.

14 Chang Y, Bluteau D, Debili N, Vainchenker W. From hematopoietic stem cells to platelets. *Journal of Thrombosis and Haemostasis*. 2007; **5**: 318-27.

15 Italiano JE, Jr., Lecine P, Shivdasani RA, Hartwig JH. Blood platelets are assembled principally at the ends of proplatelet processes produced by differentiated megakaryocytes. *The Journal of cell biology*. 1999; **147**: 1299-312.

16 Junt T, Schulze H, Chen Z, Massberg S, Goerge T, Krueger A, Wagner DD, Graf T, Italiano JE, Shivdasani RA, von Andrian UH. Dynamic Visualization of Thrombopoiesis Within Bone Marrow. *Science*. 2007; **317**: 1767-70.

17 Stegner D, vanEeuwijk JMM, Angay O, Gorelashvili MG, Semeniak D, Pinnecker J, Schmithausen P, Meyer I, Friedrich M, Dütting S, Brede C, Beilhack A, Schulze H, Nieswandt B, Heinze KG. Thrombopoiesis is spatially regulated by the bone marrow vasculature. *Nature Communications*. 2017; **8**: 127.

18 Davì G, Patrono C. Platelet Activation and Atherothrombosis. *New England Journal of Medicine*. 2007; **357**: 2482-94.

19 Nieswandt B, Pleines I, Bender M. Platelet adhesion and activation mechanisms in arterial thrombosis and ischaemic stroke. *Journal of Thrombosis and Haemostasis*. 2011; **9**: 92-104.

20 Varga-Szabo D, Pleines I, Nieswandt B. Cell adhesion mechanisms in platelets. *Arteriosclerosis, thrombosis, and vascular biology*. 2008; **28**: 403-12.

21 Andrews RK, Karunakaran D, Gardiner EE, Berndt MC. Platelet Receptor Proteolysis. *A Mechanism for Downregulating Platelet Reactivity*. 2007; **27**: 1511-20.

22 Jenne CN, Kubes P. Platelets in inflammation and infection. *Platelets*. 2015; **26**: 286-92.

23 Nurden AT, Nurden P, Sanchez M, Andia I, Anitua E. Platelets and wound healing. *Front Biosci*. 2008; **13**: 3532-48.

24 Stegner D, Dütting S, Nieswandt B. Mechanistic explanation for platelet contribution to cancer metastasis. *Thrombosis research*. 2014; **133**: S149-S57.

25 White JG. Interaction of Membrane Systems in Blood Platelets. *The American journal of pathology*. 1972; **66**: 295-312.

26 Thon JN, Italiano JE. Platelets: production, morphology and ultrastructure. *Handb Exp Pharmacol*. 2012: 3-22.

27 Flaumenhaft R. Molecular basis of platelet granule secretion. *Arteriosclerosis, thrombosis, and vascular biology*. 2003; **23**: 1152-60.

28 Harrison P, Cramer EM. Platelet alpha-granules. *Blood reviews*. 1993; **7**: 52-62.

29 Rendu F, Brohard-Bohn B. The platelet release reaction: granules' constituents, secretion and functions. *Platelets*. 2001; **12**: 261-73.

30 Savage B, Saldivar E, Ruggeri ZM. Initiation of platelet adhesion by arrest onto fibrinogen or translocation on von Willebrand factor. *Cell*. 1996; **84**: 289-97.

31 Savage B, Almus-Jacobs F, Ruggeri ZM. Specific Synergy of Multiple Substrate–Receptor Interactions in Platelet Thrombus Formation under Flow. *Cell*. 1998; **94**: 657-66.

32 Ruggeri ZM. Von Willebrand factor, platelets and endothelial cell interactions. *Journal of Thrombosis and Haemostasis*. 2003; **1**: 1335-42.

33 Moroi M, Jung SM, Nomura S, Sekiguchi S, Ordinas A, Diaz-Ricart M. Analysis of the involvement of the von Willebrand factor-glycoprotein Ib interaction in platelet adhesion to a collagen-coated surface under flow conditions. *Blood*. 1997; **90**: 4413-24.

34 Nieswandt B, Watson SP. Platelet-collagen interaction: is GPVI the central receptor? *Blood*. 2003; **102**: 449-61.

35 Dütting S, Bender M, Nieswandt B. Platelet GPVI: a target for antithrombotic therapy?! *Trends Pharmacol Sci.* 2012; **33**: 583-90.

36 Offermanns S. Activation of platelet function through G protein-coupled receptors. *Circulation research*. 2006; **99**: 1293-304.

37 Shattil SJ, Newman PJ. Integrins: dynamic scaffolds for adhesion and signaling in platelets. *Blood*. 2004; **104**: 1606-15.

38 Varga-Szabo D, Braun A, Nieswandt B. Calcium signaling in platelets. *Journal of Thrombosis and Haemostasis*. 2009; **7**: 1057-66.

39 Clemetson KJ. Platelet activation: signal transduction via membrane receptors. *Thromb Haemost*. 1995; **74**: 111-6.

40 Stegner D, Nieswandt B. Platelet receptor signaling in thrombus formation. *Journal of molecular medicine*. 2011; **89**: 109-21.

41 Nieswandt B, Aktas B, Moers A, Sachs UJH. Platelets in atherothrombosis: lessons from mouse models. *Journal of Thrombosis and Haemostasis*. 2005; **3**: 1725-36.

42 Bergmeier W, Hynes RO. Extracellular matrix proteins in hemostasis and thrombosis. *Cold Spring Harb Perspect Biol*. 2012; **4**.

43 Braun A, Vogtle T, Varga-Szabo D, Nieswandt B. STIM and Orai in hemostasis and thrombosis. *Front Biosci (Landmark Ed)*. 2011; **16**: 2144-60.

44 Fox JE. The platelet cytoskeleton. *Thromb Haemost*. 1993; **70**: 884-93.

45 Coughlin SR. Thrombin signalling and protease-activated receptors. *Nature*. 2000; **407**: 258-64.

46 Kahn ML, Nakanishi-Matsui M, Shapiro MJ, Ishihara H, Coughlin SR. Protease-activated receptors 1 and 4 mediate activation of human platelets by thrombin. *JClinInvest*. 1999; **103**: 879-87.

47 Nakanishi-Matsui M, Zheng YW, Sulciner DJ, Weiss EJ, Ludeman MJ, Coughlin SR. PAR3 is a cofactor for PAR4 activation by thrombin. *Nature*. 2000; **404**: 609-13.

48 Sambrano GR, Weiss EJ, Zheng YW, Huang W, Coughlin SR. Role of thrombin signalling in platelets in haemostasis and thrombosis. *Nature*. 2001; **413**: 74-8.

49 Offermanns S, Toombs CF, Hu YH, Simon MI. Defective platelet activation in G alpha(q)-deficient mice. *Nature*. 1997; **389**: 183-6.

50 Cantley LC. The phosphoinositide 3-kinase pathway. *Science*. 2002; **296**: 1655-7.

51 Mikelis CM, Simaan M, Ando K, Fukuhara S, Sakurai A, Amornphimoltham P, Masedunskas A, Weigert R, Chavakis T, Adams RH, Offermanns S, Mochizuki N, Zheng Y, Gutkind JS. RhoA and ROCK mediate histamine-induced vascular leakage and anaphylactic shock. *Nature Communications*. 2015; **6**: 6725.

52 Sánchez-Fernández G, Cabezudo S, García-Hoz C, Benincá C, Aragay AM, Mayor F, Ribas C. Gαq signalling: The new and the old. *Cellular signalling*. 2014; **26**: 833-48.

53 Underhill DM, Goodridge HS. The many faces of ITAMs. *Trends Immunol*. 2007; **28**: 66-73.

54 Stegner D, Haining EJ, Nieswandt B. Targeting Glycoprotein VI and the Immunoreceptor Tyrosine-Based Activation Motif Signaling Pathway. *Arteriosclerosis, thrombosis, and vascular biology*. 2014; **34**: 1615-20.

55 Watson SP, Herbert JM, Pollitt AY. GPVI and CLEC-2 in hemostasis and vascular integrity. *Journal of thrombosis and haemostasis*. 2010; **8**: 1456-67.

56 Lorenz V, Stegner D, Stritt S, Vögtle T, Kiefer F, Witke W, Schymeinsky J, Watson SP, Walzog B, Nieswandt B. Targeted downregulation of platelet CLEC-2 occurs through Syk-independent internalization. *Blood*. 2015; **125**: 4069-77.

57 Spalton JC, Mori J, Pollitt AY, Hughes CE, Eble JA, Watson SP. The novel Syk inhibitor R406 reveals mechanistic differences in the initiation of GPVI and CLEC-2 signaling in platelets. *Journal of thrombosis and haemostasis*. 2009; **7**: 1192-9.

58 Clemetson JM, Polgar J, Magnenat E, Wells TN, Clemetson KJ. The platelet collagen receptor glycoprotein VI is a member of the immunoglobulin superfamily closely related to FcalphaR and the natural killer receptors. *The Journal of biological chemistry*. 1999; **274**: 29019-24.

59 Gibbins JM, Okuma M, Farndale R, Barnes M, Watson SP. Glycoprotein VI is the collagen receptor in platelets which underlies tyrosine phosphorylation of the Fc receptor gamma-chain. *FEBS letters*. 1997; **413**: 255-9.

60 Nieswandt B, Bergmeier W, Schulte V, Rackebrandt K, Gessner JE, Zirngibl H. Expression and function of the mouse collagen receptor glycoprotein VI is strictly dependent on its association with the FcRgamma chain. *The Journal of biological chemistry*. 2000; **275**: 23998-4002.

61 Andrews RK, Suzuki-Inoue K, Shen Y, Tulasne D, Watson SP, Berndt MC. Interaction of calmodulin with the cytoplasmic domain of platelet glycoprotein VI. *Blood*. 2002; **99**: 4219-21.

62 Gardiner EE, Arthur JF, Kahn ML, Berndt MC, Andrews RK. Regulation of platelet membrane levels of glycoprotein VI by a platelet-derived metalloproteinase. *Blood*. 2004; **104**: 3611-7.

63 Suzuki-Inoue K, Tulasne D, Shen Y, Bori-Sanz T, Inoue O, Jung SM, Moroi M, Andrews RK, Berndt MC, Watson SP. Association of Fyn and Lyn with the proline-rich domain of glycoprotein VI regulates intracellular signaling. *The Journal of biological chemistry*. 2002; **277**: 21561-6.

64 Jandrot-Perrus M, Lagrue AH, Okuma M, Bon C. Adhesion and activation of human platelets induced by convulxin involve glycoprotein VI and integrin alpha2beta1. *The Journal of biological chemistry*. 1997; **272**: 27035-41.

65 Mammadova-Bach E, Ollivier V, Loyau S, Schaff M, Dumont B, Favier R, Freyburger G, Latger-Cannard V, Nieswandt B, Gachet C, Mangin PH, Jandrot-Perrus M. Platelet glycoprotein VI binds to polymerized fibrin and promotes thrombin generation. *Blood*. 2015; **126**: 683-91.

66 Alshehri OM, Hughes CE, Montague S, Watson SK, Frampton J, Bender M, Watson SP. Fibrin activates GPVI in human and mouse platelets. *Blood*. 2015; **126**: 1601-8.

67 Nieswandt B, Schulte V, Bergmeier W, Mokhtari-Nejad R, Rackebrandt K, Cazenave JP, Ohlmann P, Gachet C, Zirngibl H. Long-term antithrombotic protection by in vivo depletion of platelet glycoprotein VI in mice. *Journal of Experimental Medicine*. 2001; **193**: 459-69.

68 Schulte V, Rabie T, Prostredna M, Aktas B, Gruner S, Nieswandt B. Targeting of the collagen-binding site on glycoprotein VI is not essential for in vivo depletion of the receptor. *Blood*. 2003; **101**: 3948-52.

69 Stegner D, Popp M, Lorenz V, Wax JK, Gessner JE, Nieswandt B. FcgammaRIIB on liver sinusoidal endothelial cells is essential for antibody-induced GPVI ectodomain shedding in mice. *Blood*. 2016; **128**: 862-5.

70 Rabie T, Varga-Szabo D, Bender M, Pozgaj R, Lanza F, Saito T, Watson SP, Nieswandt B. Diverging signaling events control the pathway of GPVI down-regulation in vivo. *Blood*. 2007; **110**: 529-35.

71 Bender M, Hofmann S, Stegner D, Chalaris A, Bosl M, Braun A, Scheller J, Rose-John S, Nieswandt B. Differentially regulated GPVI ectodomain shedding by multiple platelet-expressed proteinases. *Blood*. 2010; **116**: 3347-55.

72 Induruwa I, Jung SM, Warburton EA. Beyond antiplatelets: The role of glycoprotein VI in ischemic stroke. *Int J Stroke*. 2016; **11**: 618-25.

73 Bender M, Hagedorn I, Nieswandt B. Genetic and antibody-induced glycoprotein VI deficiency equally protects mice from mechanically and FeCl3-induced thrombosis. *Journal of Thrombosis and Haemostasis*. 2011; **9**: 1423-6.

74 Pachel C, Mathes D, Arias-Loza AP, Heitzmann W, Nordbeck P, Deppermann C, Lorenz V, Hofmann U, Nieswandt B, Frantz S. Inhibition of Platelet GPVI Protects Against Myocardial Ischemia-Reperfusion Injury. *Arteriosclerosis, thrombosis, and vascular biology*. 2016; **36**: 629-35.

75 Bender M, May F, Lorenz V, Thielmann I, Hagedorn I, Finney BA, Vögtle T, Remer K, Braun A, Bösl M, Watson SP, Nieswandt B. Combined In Vivo Depletion of Glycoprotein VI and C-Type Lectin-Like Receptor 2 Severely Compromises Hemostasis and Abrogates Arterial Thrombosis in Mice. *Arteriosclerosis, thrombosis, and vascular biology*. 2013; **33**: 926-34.

76 Vögtle T, Cherpokova D, Bender M, Nieswandt B. Targeting platelet receptors in thrombotic and thrombo-inflammatory disorders. *Hämostaseologie*. 2015; **35**: 235-43.

77 Gitz E, Pollitt AY, Gitz-Francois JJ, Alshehri O, Mori J, Montague S, Nash GB, Douglas MR, Gardiner EE, Andrews RK, Buckley CD, Harrison P, Watson SP. CLEC-2 expression is maintained on activated platelets and on platelet microparticles. *Blood*. 2014; **124**: 2262-70.

78 Suzuki-Inoue K, Fuller GL, Garcia A, Eble JA, Pohlmann S, Inoue O, Gartner TK, Hughan SC, Pearce AC, Laing GD, Theakston RD, Schweighoffer E, Zitzmann N,

Morita T, Tybulewicz VL, Ozaki Y, Watson SP. A novel Syk-dependent mechanism of platelet activation by the C-type lectin receptor CLEC-2. *Blood*. 2006; **107**: 542-9.

79 Suzuki-Inoue K, Osada M, Ozaki Y. Physiologic and pathophysiologic roles of interaction between C-type lectin-like receptor 2 and podoplanin: partners from in utero to adulthood. *Journal of thrombosis and haemostasis*. 2017; **15**: 219-29.

80 May F, Hagedorn I, Pleines I, Bender M, Vogtle T, Eble J, Elvers M, Nieswandt B. CLEC-2 is an essential platelet-activating receptor in hemostasis and thrombosis. *Blood*. 2009; **114**: 3464-72.

81 Suzuki-Inoue K, Kato Y, Inoue O, Kaneko MK, Mishima K, Yatomi Y, Yamazaki Y, Narimatsu H, Ozaki Y. Involvement of the Snake Toxin Receptor CLEC-2, in Podoplanin-mediated Platelet Activation, by Cancer Cells. *Journal of Biological Chemistry*. 2007; **282**: 25993-6001.

82 Suzuki-Inoue K, Inoue O, Ding G, Nishimura S, Hokamura K, Eto K, Kashiwagi H, Tomiyama Y, Yatomi Y, Umemura K, Shin Y, Hirashima M, Ozaki Y. Essential in vivo roles of the C-type lectin receptor CLEC-2: embryonic/neonatal lethality of CLEC-2-deficient mice by blood/lymphatic misconnections and impaired thrombus formation of CLEC-2-deficient platelets. *The Journal of biological chemistry*. 2010; **285**: 24494-507.

83 Hughes CE, Navarro-Nunez L, Finney BA, Mourao-Sa D, Pollitt AY, Watson SP. CLEC-2 is not required for platelet aggregation at arteriolar shear. *Journal of thrombosis and haemostasis*. 2010; **8**: 2328-32.

84 Bertozzi CC, Schmaier AA, Mericko P, Hess PR, Zou Z, Chen M, Chen CY, Xu B, Lu MM, Zhou D, Sebzda E, Santore MT, Merianos DJ, Stadtfeld M, Flake AW, Graf T, Skoda R, Maltzman JS, Koretzky GA, Kahn ML. Platelets regulate lymphatic vascular development through CLEC-2-SLP-76 signaling. *Blood*. 2010; **116**: 661-70.

85 Finney BA, Schweighoffer E, Navarro-Núñez L, Bénézech C, Barone F, Hughes CE, Langan SA, Lowe KL, Pollitt AY, Mourao-Sa D, Sheardown S, Nash GB, Smithers N, Reis e Sousa C, Tybulewicz VLJ, Watson SP. CLEC-2 and Syk in the megakaryocytic/platelet lineage are essential for development. *Blood*. 2012; **119**: 1747-56.

86 Boulaftali Y, Hess PR, Getz TM, Cholka A, Stolla M, Mackman N, Owens AP, Ware J, Kahn ML, Bergmeier W. Platelet ITAM signaling is critical for vascular integrity in inflammation. *The Journal of Clinical Investigation*. 2013; **123**: 908-16.

87 Boulaftali Y, Hess PR, Kahn ML, Bergmeier W. Platelet Immunoreceptor Tyrosine-Based Activation Motif (ITAM) Signaling and Vascular Integrity. *Circulation research*. 2014; **114**: 1174-84.

88 Herzog BH, Fu J, Wilson SJ, Hess PR, Sen A, McDaniel JM, Pan Y, Sheng M, Yago T, Silasi-Mansat R, McGee S, May F, Nieswandt B, Morris AJ, Lupu F, Coughlin SR, McEver RP, Chen H, Kahn ML, Xia L. Podoplanin maintains high endothelial venule integrity by interacting with platelet CLEC-2. *Nature*. 2013; **502**: 105-9.

89 Hess PR, Rawnsley DR, Jakus Z, Yang Y, Sweet DT, Fu J, Herzog B, Lu M, Nieswandt B, Oliver G, Makinen T, Xia L, Kahn ML. Platelets mediate lymphovenous hemostasis to maintain blood-lymphatic separation throughout life. *The Journal of clinical investigation*. 2014; **124**: 273-84.

90 Suzuki-Inoue K. CLEC-2/podoplanin and thromboinflammation. *Blood*. 2017; **129**: 1896-8.

91 Suzuki-Inoue K, Tsukiji N, Shirai T, Osada M, Inoue O, Ozaki Y. Platelet CLEC-2: Roles Beyond Hemostasis. *Seminars in thrombosis and hemostasis*. 2017.

92 Suzuki-Inoue K, Inoue O, Ozaki Y. Novel platelet activation receptor CLEC-2: from discovery to prospects. *Journal of thrombosis and haemostasis*. 2011; **9 Suppl 1**: 44-55.

93 Lee RH, Bergmeier W. Platelet immunoreceptor tyrosine-based activation motif (ITAM) and hemITAM signaling and vascular integrity in inflammation and development. *Journal of Thrombosis and Haemostasis*. 2016; **14**: 645-54.

94 Haining EJ, Cherpokova D, Wolf K, Becker IC, Beck S, Eble JA, Stegner D, Watson SP, Nieswandt B. CLEC 2 contributes to hemostasis independently of classical hemITAM signaling in mice. *Blood*. 2017.

95 Rosse C, Linch M, Kermorgant S, Cameron AJM, Boeckeler K, Parker PJ. PKC and the control of localized signal dynamics. *Nat Rev Mol Cell Biol*. 2010; **11**: 103-12.

96 Hoque M, Rentero C, Cairns R, Tebar F, Enrich C, Grewal T. Annexins — Scaffolds modulating PKC localization and signaling. *Cellular signalling*. 2014; **26**: 1213-25.

97 Harper MT, Poole AW. Diverse functions of protein kinase C isoforms in platelet activation and thrombus formation. *Journal of Thrombosis and Haemostasis*. 2010; **8**: 454-62.

98 Heemskerk JW, Harper MT, Cosemans JM, Poole AW. Unravelling the different functions of protein kinase C isoforms in platelets. *FEBS letters*. 2011; **585**: 1711-6.

99 Hall KJ, Harper MT, Gilio K, Cosemans JM, Heemskerk JWM, Poole AW. Genetic Analysis of the Role of Protein Kinase Cθ in Platelet Function and Thrombus Formation. *PloS one*. 2008; **3**: e3277.

100 Pears CJ, Thornber K, Auger JM, Hughes CE, Grygielska B, Protty MB, Pearce AC, Watson SP. Differential Roles of the PKC Novel Isoforms, PKCδ and PKCε, in Mouse and Human Platelets. *PloS one*. 2008; **3**: e3793.

101 Bynagari YS, Nagy B, Tuluc F, Bhavaraju K, Kim S, Vijayan KV, Kunapuli SP. Mechanism of Activation and Functional Role of Protein Kinase Cη in Human Platelets. *Journal of Biological Chemistry*. 2009; **284**: 13413-21.

102 Nagy B, Bhavaraju K, Getz T, Bynagari YS, Kim S, Kunapuli SP. Impaired activation of platelets lacking protein kinase C-θ isoform. *Blood*. 2009; **113**: 2557-67.

103 Murugappan S, Tuluc F, Dorsam RT, Shankar H, Kunapuli SP. Differential Role of Protein Kinase Cδ Isoform in Agonist-induced Dense Granule Secretion in Human Platelets. *Journal of Biological Chemistry*. 2004; **279**: 2360-7.

104 Buensuceso CS, Obergfell A, Soriani A, Eto K, Kiosses WB, Arias-Salgado EG, Kawakami T, Shattil SJ. Regulation of Outside-in Signaling in Platelets by Integrin-associated Protein Kinase Cβ. *Journal of Biological Chemistry*. 2005; **280**: 644-53.

105 Lin D, Edwards AS, Fawcett JP, Mbamalu G, Scott JD, Pawson T. A mammalian PAR-3-PAR-6 complex implicated in Cdc42/Rac1 and aPKC signalling and cell polarity. *Nat Cell Biol*. 2000; **2**: 540-7.

106 Iden S, Collard JG. Crosstalk between small GTPases and polarity proteins in cell polarization. *Nat Rev Mol Cell Biol*. 2008; **9**: 846-59.

107 Nobes CD, Hall A. Rho, Rac, and Cdc42 GTPases regulate the assembly of multimolecular focal complexes associated with actin stress fibers, lamellipodia, and filopodia. *Cell*. 1995; **81**: 53-62.

108 Chang J-C, Chang H-H, Lin C-T, Lo SJ. The integrin α6β1 modulation of PI3K and Cdc42 activities induces dynamic filopodium formation in human platelets. *Journal of Biomedical Science*. 2005; **12**: 881-98.

109 McCarty OJT, Larson MK, Auger JM, Kalia N, Atkinson BT, Pearce AC, Ruf S, Henderson RB, Tybulewicz VLJ, Machesky LM, Watson SP. Rac1 Is Essential for Platelet Lamellipodia Formation and Aggregate Stability under Flow. *Journal of Biological Chemistry*. 2005; **280**: 39474-84.

110 Pleines I, Dütting S, Cherpokova D, Eckly A, Meyer I, Morowski M, Krohne G, Schulze H, Gachet C, Debili N, Brakebusch C, Nieswandt B. Defective tubulin organization and proplatelet formation in murine megakaryocytes lacking Rac1 and Cdc42. *Blood*. 2013; **122**: 3178-87.

111 Pleines I, Eckly A, Elvers M, Hagedorn I, Eliautou S, Bender M, Wu X, Lanza F, Gachet C, Brakebusch C, Nieswandt B. Multiple alterations of platelet functions dominated by increased secretion in mice lacking Cdc42 in platelets. *Blood*. 2010; **115**: 3364-73.

112 Pleines I, Elvers M, Strehl A, Pozgajova M, Varga-Szabo D, May F, Chrostek-Grashoff A, Brakebusch C, Nieswandt B. Rac1 is essential for phospholipase C-γ2 activation in platelets. *Pflügers Archiv - European Journal of Physiology*. 2009; **457**: 1173-85.

113 Horikoshi Y, Suzuki A, Yamanaka T, Sasaki K, Mizuno K, Sawada H, Yonemura S, Ohno S. Interaction between PAR-3 and the aPKC–PAR-6 complex is indispensable for apical domain development of epithelial cells. *Journal of Cell Science*. 2009; **122**: 1595-606.

114 Welchman DP, Mathies LD, Ahringer J. Similar requirements for CDC-42 and the PAR-3/PAR-6/PKC-3 complex in diverse cell types. *Developmental biology*. 2007; **305**: 347-57.

115 Nakanishi H, Brewer KA, Exton JH. Activation of the zeta isozyme of protein kinase C by phosphatidylinositol 3,4,5-trisphosphate. *The Journal of biological chemistry*. 1993; **268**: 13-6.

116 Wooten MW, Seibenhener ML, Neidigh KBW, Vandenplas ML. Mapping of Atypical Protein Kinase C within the Nerve Growth Factor Signaling Cascade: Relationship to Differentiation and Survival of PC12 Cells. *Molecular and cellular biology*. 2000; **20**: 4494-504.

117 Soloff RS, Katayama C, Lin MY, Feramisco JR, Hedrick SM. Targeted Deletion of Protein Kinase C λ Reveals a Distribution of Functions between the Two Atypical Protein Kinase C Isoforms. *The Journal of Immunology*. 2004; **173**: 3250-60.

118 Seidl S, Braun U, Roos N, Li S, Lüdtke THW, Kispert A, Leitges M. Phenotypical Analysis of Atypical PKCs In Vivo Function Display a Compensatory System at Mouse Embryonic Day 7.5. *PloS one*. 2013; **8**: e62756.

119 Martin P, Duran A, Minguet S, Gaspar ML, Diaz-Meco MT, Rennert P, Leitges M, Moscat J. Role of ζPKC in B-cell signaling and function. *The EMBO Journal*. 2002; **21**: 4049-57.

120 Leitges M, Sanz L, Martin P, Duran A, Braun U, García JF, Camacho F, Diaz-Meco MaT, Rennert PD, Moscat J. Targeted Disruption of the ζPKC Gene Results in the Impairment of the NF-κB Pathway. *Molecular cell*. 2001; **8**: 771-80.

121 Yang J-Q, Leitges M, Duran A, Diaz-Meco MT, Moscat J. Loss of PKCλ/ι impairs Th2 establishment and allergic airway inflammation in vivo. *Proceedings of the National Academy of Sciences*. 2009; **106**: 1099-104.

122 Dütting S, Gaits-Iacovoni F, Stegner D, Popp M, Antkowiak A, van Eeuwijk JMM, Nurden P, Stritt S, Heib T, Aurbach K, Angay O, Cherpokova D, Heinz N, Baig AA, Gorelashvili MG, Gerner F, Heinze KG, Ware J, Krohne G, Ruggeri ZM, Nurden AT, Schulze H, Modlich U, Pleines I, Brakebusch C, Nieswandt B. A Cdc42/RhoA regulatory circuit downstream of glycoprotein Ib guides transendothelial platelet biogenesis. 2017; **8**: 15838.

123 Qi Y, Liu J, Wu X, Brakebusch C, Leitges M, Han Y, Corbett SA, Lowry SF, Graham AM, Li S. Cdc42 Controls Vascular Network Assembly Through Protein Kinase Cı During Embryonic Vasculogenesis. *Arteriosclerosis, thrombosis, and vascular biology*. 2011; **31**: 1861-70.

124 Ware J, Russell S, Ruggeri ZM. Generation and rescue of a murine model of platelet dysfunction: The Bernard-Soulier syndrome. *Proceedings of the National Academy of Sciences*. 2000; **97**: 2803-8.

125 Jain S, Zuka M, Liu J, Russell S, Dent J, Guerrero JA, Forsyth J, Maruszak B, Gartner TK, Felding-Habermann B, Ware J. Platelet glycoprotein Ib alpha supports experimental lung metastasis. *Proceedings of the National Academy of Sciences of the United States of America*. 2007; **104**: 9024-8.

126 Corken A, Russell S, Dent J, Post SR, Ware J. Platelet glycoprotein Ib-IX as a regulator of systemic inflammation. *Arteriosclerosis, thrombosis, and vascular biology*. 2014; **34**: 996-1001.

127 Bergmeier W, Piffath CL, Goerge T, Cifuni SM, Ruggeri ZM, Ware J, Wagner DD. The role of platelet adhesion receptor GPIbalpha far exceeds that of its main ligand, von Willebrand factor, in arterial thrombosis. *ProcNatlAcadSciUSA*. 2006; **103**: 16900-5.

128 Katsutani S, Fujimoto TT, Noda M, Shimomura T, Takafuta T, Kimura A, Fujimura K. Cloning and characterization of the gene encoding the murine glycoprotein V: the conserved thrombin-cleavable protein on platelet surface. *Thrombosis research*. 1998; **92**: 43-51.

129 Luo SZ, Mo X, Afshar-Kharghan V, Srinivasan S, Lopez JA, Li R. Glycoprotein Ibalpha forms disulfide bonds with 2 glycoprotein Ibbeta subunits in the resting platelet. *Blood*. 2007; **109**: 603-9.

130 Lopez JA, Andrews RK, Afshar-Kharghan V, Berndt MC. Bernard-Soulier syndrome. *Blood*. 1998; **91**: 4397-418.

131 Phillips DR, Agin PP. Platelet plasma membrane glycoproteins. Evidence for the presence of nonequivalent disulfide bonds using nonreduced-reduced two-dimensional gel electrophoresis. *The Journal of biological chemistry*. 1977; **252**: 2121-6.

132 Du X, Beutler L, Ruan C, Castaldi PA, Berndt MC. Glycoprotein Ib and glycoprotein IX are fully complexed in the intact platelet membrane. *Blood*. 1987; **69**: 1524-7.

133 Li R, Emsley J. The Organizing Principle of Platelet Glycoprotein Ib-IX-V Complex. *Journal of thrombosis and haemostasis*. 2013; **11**: 605-14.

134 Mo X, Liu L, Lopez JA, Li R. Transmembrane domains are critical to the interaction between platelet glycoprotein V and glycoprotein Ib-IX complex. *Journal of thrombosis and haemostasis*. 2012; **10**: 1875-86.

135 Moog S, Mangin P, Lenain N, Strassel C, Ravanat C, Schuhler S, Freund M, Santer M, Kahn M, Nieswandt B, Gachet C, Cazenave JP, Lanza F. Platelet glycoprotein V binds to collagen and participates in platelet adhesion and aggregation. *Blood*. 2001; **98**: 1038-46.

136 Li CQ, Dong JF, Lanza F, Sanan DA, Sae-Tung G, Lopez JA. Expression of platelet glycoprotein (GP) V in heterologous cells and evidence for its association with GP Ib alpha in forming a GP Ib-IX-V complex on the cell surface. *The Journal of biological chemistry*. 1995; **270**: 16302-7.

137 Andrews RK, Gardiner EE, Shen Y, Whisstock JC, Berndt MC. Glycoprotein Ib-IX-V. *The international journal of biochemistry & cell biology*. 2003; **35**: 1170-4.

138 Arthur JF, Gardiner EE, Matzaris M, Taylor SG, Wijeyewickrema L, Ozaki Y, Kahn ML, Andrews RK, Berndt MC. Glycoprotein VI is associated with GPIb-IX-V on the

membrane of resting and activated platelets. *Thrombosis and Haemostasis*. 2005; **93**: 716-28.

139 Sullam PM, Hyun WC, Szollosi J, Dong J, Foss WM, Lopez JA. Physical proximity and functional interplay of the glycoprotein Ib-IX-V complex and the Fc receptor FcgammaRIIA on the platelet plasma membrane. *The Journal of biological chemistry*. 1998; **273**: 5331-6.

140 White TC, Berny MA, Tucker EI, Urbanus RT, de Groot PG, Fernandez JA, Griffin JH, Gruber A, McCarty OJ. Protein C supports platelet binding and activation under flow: role of glycoprotein Ib and apolipoprotein E receptor 2. *Journal of thrombosis and haemostasis*. 2008; **6**: 995-1002.

141 Bernard J, Soulier JP. Sur une nouvelle variété de dystrophie thrombocytaire-hémorragipare congeénitale. *Sem Hop*. 1948; **24**: 3217-23.

142 Nurden AT, Caen JP. Specific roles for platelet surface glycoproteins in platelet function. *Nature*. 1975; **255**: 720-2.

143 Kato K, Martinez C, Russell S, Nurden P, Nurden A, Fiering S, Ware J. Genetic deletion of mouse platelet glycoprotein Ibbeta produces a Bernard-Soulier phenotype with increased alpha-granule size. *Blood*. 2004; **104**: 2339-44.

144 Kahn ML, Diacovo TG, Bainton DF, Lanza F, Trejo J, Coughlin SR. Glycoprotein V-deficient platelets have undiminished thrombin responsiveness and Do not exhibit a Bernard-Soulier phenotype. *Blood*. 1999; **94**: 4112-21.

145 Ramakrishnan V, Reeves PS, DeGuzman F, Deshpande U, Ministri-Madrid K, DuBridge RB, Phillips DR. Increased thrombin responsiveness in platelets from mice lacking glycoprotein V. *Proceedings of the National Academy of Sciences of the United States of America*. 1999; **96**: 13336-41.

146 Clemetson KJ. A short history of platelet glycoprotein Ib complex. *Thromb Haemost*. 2007; **98**: 63-8.

147 Du X. Signaling and regulation of the platelet glycoprotein Ib-IX-V complex. *Curr Opin Hematol*. 2007; **14**: 262-9.

148 Moake JL, Turner NA, Stathopoulos NA, Nolasco L, Hellums JD. Shear-induced platelet aggregation can be mediated by vWF released from platelets, as well as by exogenous large or unusually large vWF multimers, requires adenosine diphosphate, and is resistant to aspirin. *Blood*. 1988; **71**: 1366-74.

149 Romo GM, Dong JF, Schade AJ, Gardiner EE, Kansas GS, Li CQ, McIntire LV, Berndt MC, Lopez JA. The glycoprotein Ib-IX-V complex is a platelet counterreceptor for P-selectin. *The Journal of experimental medicine*. 1999; **190**: 803-14.

150 Simon DI, Chen Z, Xu H, Li CQ, Dong J, McIntire LV, Ballantyne CM, Zhang L, Furman MI, Berndt MC, Lopez JA. Platelet glycoprotein ibalpha is a counterreceptor for the leukocyte integrin Mac-1 (CD11b/CD18). *The Journal of experimental medicine*. 2000; **192**: 193-204.

151 Baglia FA, Badellino KO, Li CQ, Lopez JA, Walsh PN. Factor XI binding to the platelet glycoprotein Ib-IX-V complex promotes factor XI activation by thrombin. *The Journal of biological chemistry*. 2002; **277**: 1662-8.

152 Bradford HN, Dela Cadena RA, Kunapuli SP, Dong J-F, López JA, Colman RW. Human Kininogens Regulate Thrombin Binding to Platelets Through the Glycoprotein Ib-IX-V Complex. *Blood*. 1997; **90**: 1508-15.

153 Bradford HN, Pixley RA, Colman RW. Human factor XII binding to the glycoprotein Ib-IX-V complex inhibits thrombin-induced platelet aggregation. *The Journal of biological chemistry*. 2000; **275**: 22756-63.

154 Joseph K, Nakazawa Y, Bahou WF, Ghebrehiwet B, Kaplan AP. Platelet glycoprotein Ib: a zinc-dependent binding protein for the heavy chain of high-molecular-weight kininogen. *Mol Med*. 1999; **5**: 555-63.

155 Ruggeri ZM, Zarpellon A, Roberts JR, Mc Clintock RA, Jing H, Mendolicchio GL. Unravelling the mechanism and significance of thrombin binding to platelet glycoprotein Ib. *Thromb Haemost*. 2010; **104**: 894-902.

156 Lu Q, Navdaev A, Clemetson JM, Clemetson KJ. Snake venom C-type lectins interacting with platelet receptors. Structure-function relationships and effects on haemostasis. *Toxicon*. 2005; **45**: 1089-98.

157 Andrews RK, Harris SJ, McNally T, Berndt MC. Binding of purified 14-3-3 zeta signaling protein to discrete amino acid sequences within the cytoplasmic domain of the platelet membrane glycoprotein Ib-IX-V complex. *Biochemistry*. 1998; **37**: 638-47.

158 Calverley DC, Kavanagh TJ, Roth GJ. Human signaling protein 14-3-3zeta interacts with platelet glycoprotein Ib subunits Ibalpha and Ibbeta. *Blood*. 1998; **91**: 1295-303.

159 Strassel C, Moog S, Baas MJ, Cazenave JP, Lanza F. Biosynthesis of platelet glycoprotein V expressed as a single subunit or in association with GPIb-IX. *European journal of biochemistry / FEBS*. 2004; **271**: 3671-7.

160 Andrews RK, Fox JE. Interaction of purified actin-binding protein with the platelet membrane glycoprotein Ib-IX complex. *The Journal of biological chemistry*. 1991; **266**: 7144-7.

161 Munday AD, Berndt MC, Mitchell CA. Phosphoinositide 3-kinase forms a complex with platelet membrane glycoprotein Ib-IX-V complex and 14-3-3zeta. *Blood*. 2000; **96**: 577-84.

162 Du X, Fox JE, Pei S. Identification of a binding sequence for the 14-3-3 protein within the cytoplasmic domain of the adhesion receptor, platelet glycoprotein Ib alpha. *The Journal of biological chemistry*. 1996; **271**: 7362-7.

163 Dai K, Bodnar R, Berndt MC, Du X. A critical role for 14-3-3zeta protein in regulating the VWF binding function of platelet glycoprotein Ib-IX and its therapeutic implications. *Blood*. 2005; **106**: 1975-81.

164 Andrews RK, Munday AD, Mitchell CA, Berndt MC. Interaction of calmodulin with the cytoplasmic domain of the platelet membrane glycoprotein Ib-IX-V complex. *Blood*. 2001; **98**: 681-7.

165 Bergmeier W, Piffath CL, Cheng G, Dole VS, Zhang Y, von Andrian UH, Wagner DD. Tumor necrosis factor-alpha-converting enzyme (ADAM17) mediates GPIbalpha shedding from platelets in vitro and in vivo. *Circulation research*. 2004; **95**: 677-83.

166 Maxwell MJ, Westein E, Nesbitt WS, Giuliano S, Dopheide SM, Jackson SP. Identification of a 2-stage platelet aggregation process mediating shear-dependent thrombus formation. *Blood*. 2007; **109**: 566-76.

167 Ruggeri ZM, Orje JN, Habermann R, Federici AB, Reininger AJ. Activation-independent platelet adhesion and aggregation under elevated shear stress. *Blood*. 2006; **108**: 1903-10.

168 Nesbitt WS, Westein E, Tovar-Lopez FJ, Tolouei E, Mitchell A, Fu J, Carberry J, Fouras A, Jackson SP. A shear gradient-dependent platelet aggregation mechanism drives thrombus formation. *Nature medicine*. 2009; **15**: 665-73.

169 Ozaki Y, Asazuma N, Suzuki-Inoue K, Berndt MC. Platelet GPIb-IX-V-dependent signaling. *Journal of thrombosis and haemostasis*. 2005; **3**: 1745-51.

170 Ruggeri ZM, Mendolicchio GL. Adhesion mechanisms in platelet function. *Circulation Research*. 2007; **100**: 1673-85.

171 Howard MA, Firkin BG. Ristocetin--a new tool in the investigation of platelet aggregation. *Thromb Diath Haemorrh*. 1971; **26**: 362-9.

172 Brinkhous KM, Read MS, Fricke WA, Wagner RH. Botrocetin (venom coagglutinin): reaction with a broad spectrum of multimeric forms of factor VIII macromolecular complex. *Proceedings of the National Academy of Sciences of the United States of America*. 1983; **80**: 1463-6.

173 Rathore V, Stapleton MA, Hillery CA, Montgomery RR, Nichols TC, Merricks EP, Newman DK, Newman PJ. PECAM-1 negatively regulates GPIb/V/IX signaling in murine platelets. *Blood*. 2003; **102**: 3658-64.

174 Liu J, Fitzgerald ME, Berndt MC, Jackson CW, Gartner TK. Bruton tyrosine kinase is essential for botrocetin/VWF-induced signaling and GPIb-dependent thrombus formation in vivo. *Blood*. 2006; **108**: 2596-603.

175 Yin H, Liu J, Li Z, Berndt MC, Lowell CA, Du X. Src family tyrosine kinase Lyn mediates VWF/GPIb-IX-induced platelet activation via the cGMP signaling pathway. *Blood*. 2008; **112**: 1139-46.

176 Canobbio I, Balduini C, Torti M. Signalling through the platelet glycoprotein Ib-V-IX complex. *Cell Signal*. 2004; **16**: 1329-44.

177 Ozaki Y, Asazuma N, Suzuki-Inoue K, Berndt MC. Platelet GPIb-IX-V-dependent signaling. *Journal of thrombosis and haemostasis*. 2005; **3**: 1745-51.

178 Wu Y, Suzuki-Inoue K, Satoh K, Asazuma N, Yatomi Y, Berndt MC, Ozaki Y. Role of Fc receptor gamma-chain in platelet glycoprotein Ib-mediated signaling. *Blood*. 2001; **97**: 3836-45.

179 Kasirer-Friede A, Cozzi MR, Mazzucato M, De ML, Ruggeri ZM, Shattil SJ. Signaling through GP Ib-IX-V activates alpha IIb beta 3 independently of other receptors. *Blood*. 2004; **103**: 3403-11.

180 Wu Y, Asazuma N, Satoh K, Yatomi Y, Takafuta T, Berndt MC, Ozaki Y. Interaction between von Willebrand factor and glycoprotein Ib activates Src kinase in human platelets: role of phosphoinositide 3-kinase. *Blood*. 2003; **101**: 3469-76.

181 Kasirer-Friede A, Moran B, Nagrampa-Orje J, Swanson K, Ruggeri ZM, Schraven B, Neel BG, Koretzky G, Shattil SJ. ADAP is required for normal alphaIIbbeta3 activation by VWF/GP Ib-IX-V and other agonists. *Blood*. 2007; **109**: 1018-25.

182 Massberg S, Gawaz M, Gruner S, Schulte V, Konrad I, Zohlnhofer D, Heinzmann U, Nieswandt B. A crucial role of glycoprotein VI for platelet recruitment to the injured arterial wall in vivo. *The Journal of experimental medicine*. 2003; **197**: 41-9.

183 Kleinschnitz C, Pozgajova M, Pham M, Bendszus M, Nieswandt B, Stoll G. Targeting platelets in acute experimental stroke: impact of glycoprotein Ib, VI, and IIb/IIIa blockade on infarct size, functional outcome, and intracranial bleeding. *Circulation*. 2007; **115**: 2323-30.

184 Kleinschnitz C, De Meyer SF, Schwarz T, Austinat M, Vanhoorelbeke K, Nieswandt B, Deckmyn H, Stoll G. Deficiency of von Willebrand factor protects mice from ischemic stroke. *Blood*. 2009; **113**: 3600-3.

185 Kraft P, Schuhmann MK, Fluri F, Lorenz K, Zernecke A, Stoll G, Nieswandt B, Kleinschnitz C. Efficacy and Safety of Platelet Glycoprotein Receptor Blockade in Aged and Comorbid Mice With Acute Experimental Stroke. *Stroke; a journal of cerebral circulation*. 2015; **46**: 3502-6.

186 Stoll G, Kleinschnitz C, Nieswandt B. The role of glycoprotein Ibalpha and von Willebrand factor interaction in stroke development. *Hamostaseologie*. 2010; **30**: 136-8.

187 Ravanat C, Morales M, Azorsa DO, Moog S, Schuhler S, Grunert P, Loew D, Van Dorsselaer A, Cazenave JP, Lanza F. Gene cloning of rat and mouse platelet glycoprotein V: identification of megakaryocyte-specific promoters and demonstration of functional thrombin cleavage. *Blood*. 1997; **89**: 3253-62.

188 Yagi M, Edelhoff S, Disteche CM, Roth GJ. Human platelet glycoproteins V and IX: mapping of two leucine-rich glycoprotein genes to chromosome 3 and analysis of structures. *Biochemistry*. 1995; **34**: 16132-7.

189 Wenger RH, Kieffer N, Wicki AN, Clemetson KJ. Structure of the human blood platelet membrane glycoprotein Ib alpha gene. *Biochemical and biophysical research communications*. 1988; **156**: 389-95.

190 Hickey MJ, Roth GJ. Characterization of the gene encoding human platelet glycoprotein IX. *The Journal of biological chemistry*. 1993; **268**: 3438-43.

191 Lanza F, Morales M, Delasalle C, Cazenave JP, Clemetson KJ, Shimomura T, Phillips DR. Cloning and Characterization of the Gene Encoding the Human Platelet Glycoprotein-V - a Member of the Leucine-Rich Glycoprotein Family Cleaved during Thrombin-Induced Platelet Activation. *Journal of Biological Chemistry*. 1993; **268**: 20801-7.

192 Roth GJ, Church TA, McMullen BA, Williams SA. Human platelet glycoprotein V: a surface leucine-rich glycoprotein related to adhesion. *Biochemical and biophysical research communications*. 1990; **170**: 153-61.

193 Shimomura T, Fujimura K, Maehama S, Takemoto M, Oda K, Fujimoto T, Oyama R, Suzuki M, Ichihara-Tanaka K, Titani K, et al. Rapid purification and characterization of human platelet glycoprotein V: the amino acid sequence contains leucine-rich repetitive modules as in glycoprotein Ib. *Blood*. 1990; **75**: 2349-56.

194 Takafuta T, Fujimura K, Kawano H, Noda M, Fujimoto T, Oda K, Shimomura T, Kuramoto A. Expression of platelet membrane glycoprotein V in human megakaryocytes and megakaryocytic cell lines: a study using a novel monoclonal antibody against GPV. *Thromb Haemost*. 1994; **72**: 762-9.

195 Modderman PW, Admiraal LG, Sonnenberg A, von dem Borne AE. Glycoproteins V and Ib-IX form a noncovalent complex in the platelet membrane. *The Journal of biological chemistry*. 1992; **267**: 364-9.

196 Dong JF, Gao S, Lopez JA. Synthesis, assembly, and intracellular transport of the platelet glycoprotein Ib-IX-V complex. *The Journal of biological chemistry*. 1998; **273**: 31449-54.

197 Fredrickson BJ, Dong JF, McIntire LV, Lopez JA. Shear-dependent rolling on von Willebrand factor of mammalian cells expressing the platelet glycoprotein Ib-IX-V complex. *Blood*. 1998; **92**: 3684-93.

198 Azorsa DO, Moog S, Ravanat C, Schuhler S, Follea G, Cazenave JP, Lanza F. Measurement of GPV released by activated platelets using a sensitive immunocapture ELISA--its use to follow platelet storage in transfusion. *Thromb Haemost*. 1999; **81**: 131-8.

199 Aleil B, Kessler L, Meyer N, Wiesel M-L, Simeoni J, Cazenave J-P, Pinget M, Gachet C, Lanza F. Plasma levels of soluble platelet glycoprotein V are linked to fasting blood glucose in patients with type 2 diabetes. *Thrombosis and Haemostasis*. 2008; **100**: 713-5.

200 Aleil B, Meyer N, Wolff V, Kientz D, Wiesel M-L, Gachet C, Cazenave J-P, Lanza F. Plasma glycoprotein V levels in the general population: Normal distribution, associated parameters and implications for clinical studies. *Thrombosis and Haemostasis*. 2006; **96**: 505-11.

201 Wolff V, Aleil B, Giroud M, Lorenzini JL, Meyer N, Wiesel ML, Cazenave JP, Lanza F. Soluble platelet glycoprotein V is a marker of thrombosis in patients with ischemic stroke. *Stroke; a journal of cerebral circulation*. 2005; **36**: e17-9.

202 Blann AD, Lanza F, Galajda P, Gurney D, Moog S, Cazenave JP, Lip GYH. Increased Platelet Glycoprotein V Levels in Patients with Coronary and Peripheral Atherosclerosis The Influence of Aspirin and Cigarette Smoking. *Thrombosis and Haemostasis*. 2001; **86**: 777-83.

203 Atalar E, Haznedaroglu IC, Kilic H, Ozer N, Coskun S, Ozturk E, Aksoyek S, Ovunc K, Kirazli S, Ozmen F. Increased soluble glycoprotein V concentration during the acute onset of unstable angina pectoris in association with chronic cigarette smoking. *Platelets*. 2005; **16**: 329-33.

204 Ravanat C, Freund M, Mangin P, Azorsa DO, Schwartz C, Moog S, Schuhler S, Dambach J, Cazenave JP, Lanza F. GPV is a marker of in vivo platelet activation--study in a rat thrombosis model. *Thromb Haemost*. 2000; **83**: 327-33.

205 Aktas B, Pozgajova M, Bergmeier W, Sunnarborg S, Offermanns S, Lee D, Wagner DD, Nieswandt B. Aspirin induces platelet receptor shedding via ADAM17 (TACE). *The Journal of biological chemistry*. 2005; **280**: 39716-22.

206 Nonne C, Hechler B, Cazenave JP, Gachet C, Lanza F. Reassessment of in vivo thrombus formation in glycoprotein V deficient mice backcrossed on a C57Bl/6 strain. *Journal of Thrombosis and Haemostasis*. 2008; **6**: 210-2.

207 Kahn ML, Zheng YW, Huang W, Bigornia V, Zeng D, Moff S, Farese RV, Jr., Tam C, Coughlin SR. A dual thrombin receptor system for platelet activation. *Nature*. 1998; **394**: 690-4.

208 Hamilton JR, Cornelissen I, Coughlin SR. Impaired hemostasis and protection against thrombosis in protease-activated receptor 4-deficient mice is due to lack of thrombin signaling in platelets. *Journal of thrombosis and haemostasis*. 2004; **2**: 1429-35.

209 Ni H, Ramakrishnan V, Ruggeri ZM, Papalia JM, Phillips DR, Wagner DD. Increased thrombogenesis and embolus formation in mice lacking glycoprotein V. *Blood*. 2001; **98**: 368-73.

210 Stegner D. Novel aspects of platelet signaling and of the pathogenesis of immune thrombocytopenia. *Doctoral thesis*. 2011.

211 Colman R. Hemostasis and thrombosis: basic principles and clinical practice. *Philadelphia: Lippincott Williams & Wilkins*. 2006; **5 th ed**: 1827.

212 Mackman N, Tilley RE, Key NS. Role of the extrinsic pathway of blood coagulation in hemostasis and thrombosis. *Arteriosclerosis, thrombosis, and vascular biology*. 2007; **27**: 1687-93.

213 Krishnaswamy S, Nesheim ME, Pryzdial EL, Mann KG. Assembly of prothrombinase complex. *Methods Enzymol*. 1993; **222**: 260-80.

214 Heemskerk JW, Kuijpers MJ, Munnix IC, Siljander PR. Platelet collagen receptors and coagulation. A characteristic platelet response as possible target for antithrombotic treatment. *Trends in Cardiovascular Medicine*. 2005; **15**: 86-92.

215 Lentz BR. Exposure of platelet membrane phosphatidylserine regulates blood coagulation. *Prog Lipid Res*. 2003; **42**: 423-38.

216 Heemskerk JW, Mattheij NJ, Cosemans JM. Platelet-based coagulation: different populations, different functions. *Journal of thrombosis and haemostasis*. 2012.

217 Muller F, Mutch NJ, Schenk WA, Smith SA, Esterl L, Spronk HM, Schmidbauer S, Gahl WA, Morrissey JH, Renne T. Platelet polyphosphates are proinflammatory and procoagulant mediators in vivo. *Cell*. 2009; **139**: 1143-56.

218 Kannemeier C, Shibamiya A, Nakazawa F, Trusheim H, Ruppert C, Markart P, Song Y, Tzima E, Kennerknecht E, Niepmann M, von Bruehl ML, Sedding D, Massberg S, Gunther A, Engelmann B, Preissner KT. Extracellular RNA constitutes a natural procoagulant cofactor in blood coagulation. *Proceedings of the National Academy of Sciences of the United States of America*. 2007; **104**: 6388-93.

219 Versteeg HH, Heemskerk JW, Levi M, Reitsma PH. New fundamentals in hemostasis. *Physiological reviews*. 2013; **93**: 327-58.

220 Macfarlane RG. An Enzyme Cascade in the Blood Clotting Mechanism, and Its Function as a Biochemical Amplifier. *Nature*. 1964; **202**: 498-9.

221 Stritt S, Wolf K, Lorenz V, Vögtle T, Gupta S, Bösl MR, Nieswandt B. Rap1-GTP–interacting adaptor molecule (RIAM) is dispensable for platelet integrin activation and function in mice. *Blood*. 2015; **125**: 219-22.

222 Nieswandt B, Bergmeier W, Rackebrandt K, Gessner JE, Zirngibl H. Identification of critical antigen-specific mechanisms in the development of immune thrombocytopenic purpura in mice. *Blood*. 2000; **96**: 2520-7.

223 Hofmann S, Vögtle T, Bender M, Rose-John S, Nieswandt B. The SLAM family member CD84 is regulated by ADAM10 and calpain in platelets. *Journal of thrombosis and haemostasis*. 2012; **10**: 2581-92.

224 Bergmeier W, Schulte V, Brockhoff G, Bier U, Zirngibl H, Nieswandt B. Flow cytometric detection of activated mouse integrin alphaIIbbeta3 with a novel monoclonal antibody. *Cytometry*. 2002; **48**: 80-6.

225 Shida Y, Rydz N, Stegner D, Brown C, Mewburn J, Sponagle K, Danisment O, Crawford B, Vidal B, Hegadorn CA, Pruss CM, Nieswandt B, Lillicrap D. Analysis of the role of von Willebrand factor, platelet glycoprotein VI-, and α2β1-mediated collagen binding in thrombus formation. *Blood*. 2014; **124**: 1799-807.

226 Nieswandt B, Echtenacher B, Wachs F-P, Schröder J, Gessner JE, Schmidt RE, Grau GE, Männel DN. Acute Systemic Reaction and Lung Alterations Induced by an Antiplatelet Integrin gpIIb/IIIa Antibody in Mice. *Blood*. 1999; **94**: 684-93.

227 Jackson B, Peyrollier K, Pedersen E, Basse A, Karlsson R, Wang Z, Lefever T, Ochsenbein AM, Schmidt G, Aktories K, Stanley A, Quondamatteo F, Ladwein M, Rottner K, van Hengel J, Brakebusch C. RhoA is dispensable for skin development, but crucial for contraction and directed migration of keratinocytes. *Molecular Biology of the Cell*. 2011; **22**: 593-605.

228 Wu X, Quondamatteo F, Lefever T, Czuchra A, Meyer H, Chrostek A, Paus R, Langbein L, Brakebusch C. Cdc42 controls progenitor cell differentiation and beta-catenin turnover in skin. *Genes Dev*. 2006; **20**: 571-85.

229 Nieswandt B, Moser M, Pleines I, Varga-Szabo D, Monkley S, Critchley D, Fässler R. Loss of talin1 in platelets abrogates integrin activation, platelet aggregation, and thrombus formation in vitro and in vivo. *The Journal of experimental medicine*. 2007; **204**: 3113-8.

230 Stegner D, Deppermann C, Kraft P, Morowski M, Kleinschnitz C, Stoll G, Nieswandt B. Munc13-4-mediated secretion is essential for infarct progression but not intracranial

hemostasis in acute stroke. *Journal of Thrombosis and Haemostasis*. 2013; **11**: 1430-3.

231 Ye J, Coulouris G, Zaretskaya I, Cutcutache I, Rozen S, Madden TL. Primer-BLAST: A tool to design target-specific primers for polymerase chain reaction. *BMC Bioinformatics*. 2012; **13**: 134.

232 Hemker HC, Beguin S. Thrombin generation in plasma: its assessment via the endogenous thrombin potential. *Thromb Haemost*. 1995; **74**: 134-8.

233 Hemker HC, Giesen P, Al Dieri R, Regnault V, de Smedt E, Wagenvoord R, Lecompte T, Beguin S. Calibrated automated thrombin generation measurement in clotting plasma. *Pathophysiology of haemostasis and thrombosis*. 2003; **33**: 4-15.

234 Carpenter AE, Jones TR, Lamprecht MR, Clarke C, Kang IH, Friman O, Guertin DA, Chang JH, Lindquist RA, Moffat J, Golland P, Sabatini DM. CellProfiler: image analysis software for identifying and quantifying cell phenotypes. *Genome Biology*. 2006; **7**: R100.

235 Kamentsky L, Jones TR, Fraser A, Bray M-A, Logan DJ, Madden KL, Ljosa V, Rueden C, Eliceiri KW, Carpenter AE. Improved structure, function and compatibility for CellProfiler: modular high-throughput image analysis software. *Bioinformatics*. 2011; **27**: 1179-80.

236 Dirnagl U. Bench to bedside: the quest for quality in experimental stroke research. *J Cereb Blood Flow Metab*. 2006; **26**: 1465-78.

237 Braeuninger S, Kleinschnitz C, Nieswandt B, Stoll G. Focal Cerebral Ischemia. In: Gibbins JM, Mahaut-Smith MP, eds. *Platelets and Megakaryocytes: Volume 3, Additional Protocols and Perspectives*. New York, NY: Springer New York, 2012, 29-42.

238 Bederson JB, Pitts LH, Tsuji M, Nishimura MC, Davis RL, Bartkowski H. Rat middle cerebral artery occlusion: evaluation of the model and development of a neurologic examination. *Stroke*. 1986; **17**: 472-6.

239 Moran PM, Higgins LS, Cordell B, Moser PC. Age-related learning deficits in transgenic mice expressing the 751-amino acid isoform of human beta-amyloid precursor protein. *Proc Natl Acad Sci U S A*. 1995; **92**: 5341-5.

240 Swanson RA, Morton MT, Tsao-Wu G, Savalos RA, Davidson C, Sharp FR. A semiautomated method for measuring brain infarct volume. *J Cereb Blood Flow Metab*. 1990; **10**: 290-3.

241 Ravanat C, Strassel C, Hechler B, Schuhler S, Chicanne G, Payrastre B, Gachet C, Lanza F. A central role of GPIb-IX in the procoagulant function of platelets that is independent of the 45-kDa GPIbalpha N-terminal extracellular domain. *Blood*. 2010; **116**: 1157-64.

242 Zwaal RF, Schroit AJ. Pathophysiologic implications of membrane phospholipid asymmetry in blood cells. *Blood*. 1997; **89**: 1121-32.

243 Ramakrishnan V, DeGuzman F, Bao M, Hall SW, Leung LL, Phillips DR. A thrombin receptor function for platelet glycoprotein Ib-IX unmasked by cleavage of glycoprotein V. *Proceedings of the National Academy of Sciences of the United States of America*. 2001; **98**: 1823-8.

244 Rodgers RP, Levin J. A critical reappraisal of the bleeding time. *Semin Thromb Hemost*. 1990; **16**: 1-20.

245 De Berardis G, Lucisano G, D'Ettorre A, et al. Association of aspirin use with major bleeding in patients with and without diabetes. *JAMA*. 2012; **307**: 2286-94.

246 Li L, Geraghty OC, Mehta Z, Rothwell PM. Age-specific risks, severity, time course, and outcome of bleeding on long-term antiplatelet treatment after vascular events: a population-based cohort study. *The Lancet*. **390**: 490-9.

247 Gruner S, Prostredna M, Aktas B, Moers A, Schulte V, Krieg T, Offermanns S, Eckes B, Nieswandt B. Anti-glycoprotein VI treatment severely compromises hemostasis in mice with reduced alpha2beta1 levels or concomitant aspirin therapy. *Circulation*. 2004; **110**: 2946-51.

248 Kawamura Y, Takahari Y, Tamura N, Eguchi Y, Urano T, Ishida H, Goto S. Imaging of structural changes in endothelial cells and thrombus formation at the site of FeCl(3)-induced injuries in mice cremasteric arteries. *J Atheroscler Thromb*. 2009; **16**: 807-14.

249 Dütting S, Vögtle T, Morowski M, Schiessl S, Schäfer CM, Watson SK, Hughes CE, Ackermann JA, Radtke D, Hermanns HM, Watson SP, Nitschke L, Nieswandt B. Growth Factor Receptor–Bound Protein 2 Contributes to (Hem)Immunoreceptor Tyrosine-Based Activation Motif–Mediated Signaling in Platelets. *Circulation research*. 2014; **114**: 444-53.

250 Campbell CL, Smyth S, Montalescot G, Steinhubl SR. Aspirin dose for the prevention of cardiovascular disease: A systematic review. *JAMA*. 2007; **297**: 2018-24.

251 Law DA, Nannizzi-Alaimo L, Ministri K, Hughes PE, Forsyth J, Turner M, Shattil SJ, Ginsberg MH, Tybulewicz VLJ, Phillips DR. Genetic and Pharmacological Analyses of Syk Function in alphaIIbbeta3 Signaling in Platelets. *Blood*. 1999; **93**: 2645-52.

252 van Eeuwijk JMM, Stegner D, Lamb DJ, Kraft P, Beck S, Thielmann I, Kiefer F, Walzog B, Stoll G, Nieswandt B. The Novel Oral Syk Inhibitor, BI1002494, Protects Mice From Arterial Thrombosis and Thromboinflammatory Brain Infarction. *Arteriosclerosis, Thrombosis, and Vascular Biology*. 2016; **36**: 1247-53.

253 Pleines I, Hagedorn I, Gupta S, May F, Chakarova L, van Hengel J, Offermanns S, Krohne G, Kleinschnitz C, Brakebusch C, Nieswandt B. Megakaryocyte-specific RhoA deficiency causes macrothrombocytopenia and defective platelet activation in hemostasis and thrombosis. *Blood*. 2012; **119**: 1054-63.

254 Ren Q, Wimmer C, Chicka MC, Ye S, Ren Y, Hughson FM, Whiteheart SW. Munc13-4 is a limiting factor in the pathway required for platelet granule release and hemostasis. *Blood*. 2010; **116**: 869-77.

255 Morowski M, Vögtle T, Kraft P, Kleinschnitz C, Stoll G, Nieswandt B. Only severe thrombocytopenia results in bleeding and defective thrombus formation in mice. *Blood*. 2013; **121**: 4938-47.

256 Rabie T, Strehl A, Ludwig A, Nieswandt B. Evidence for a role of ADAM17 (TACE) in the regulation of platelet glycoprotein V. *The Journal of biological chemistry*. 2005; **280**: 14462-8.

257 Bergmeier W, Rabie T, Strehl A, Piffath CL, Prostredna M, Wagner DD, Nieswandt B. GPVI down-regulation in murine platelets through metalloproteinase-dependent shedding. *Thrombosis and Haemostasis*. 2004; **91**: 951-8.

258 Monroe DM, Hoffman M, Roberts HR. Platelets and Thrombin Generation. *Arteriosclerosis, thrombosis, and vascular biology*. 2002; **22**: 1381-9.

259 Bluestein D, Niu L, Schoephoerster R, Dewanjee M. Fluid mechanics of arterial stenosis: relationship to the development of mural thrombus. *Ann Biomed Eng*. 1997; **25**: 344-56.

260 Greve JM, Les AS, Tang BT, Draney Blomme MT, Wilson NM, Dalman RL, Pelc NJ, Taylor CA. Allometric scaling of wall shear stress from mice to humans: quantification

using cine phase-contrast MRI and computational fluid dynamics. *American Journal of Physiology - Heart and Circulatory Physiology*. 2006; **291**: H1700-H8.

261 Suo J, Ferrara DE, Sorescu D, Guldberg RE, Taylor WR, Giddens DP. Hemodynamic Shear Stresses in Mouse Aortas. *Implications for Atherogenesis*. 2007; **27**: 346-51.

262 Sakariassen K, Orning L, Turitto V. The impact of blood shear rate on arterial thrombus formation. *Future Science OA*. 2015; **1**.

263 Jaffe AB, Hall A. Rho GTPases: biochemistry and biology. *Annu Rev Cell Dev Biol*. 2005; **21**: 247-69.

264 Yuan Y, Kulkarni S, Ulsemer P, Cranmer SL, Yap CL, Nesbitt WS, Harper I, Mistry N, Dopheide SM, Hughan SC, Williamson D, de la Salle C, Salem HH, Lanza F, Jackson SP. The von Willebrand Factor-Glycoprotein Ib/V/IX Interaction Induces Actin Polymerization and Cytoskeletal Reorganization in Rolling Platelets and Glycoprotein Ib/V/IX-transfected Cells. *Journal of Biological Chemistry*. 1999; **274**: 36241-51.

265 Brown DL. Congenital bleeding disorders. *Curr Probl Pediatr Adolesc Health Care*. 2005; **35**: 38-62.

266 Michelson AD. Antiplatelet therapies for the treatment of cardiovascular disease. *Nat Rev Drug Discov*. 2010; **9**: 154-69.

267 Snell DC, Schulte V, Jarvis GE, Arase K, Sakurai D, Saito T, Watson SP, Nieswandt B. Differential effects of reduced glycoprotein VI levels on activation of murine platelets by glycoprotein VI ligands. *Biochemical Journal*. 2002; **368**: 293-300.

268 Horii K, Brooks MT, Herr AB. Convulxin Forms a Dimer in Solution and Can Bind Eight Copies of Glycoprotein VI: Implications for Platelet Activation. *Biochemistry*. 2009; **48**: 2907-14.

269 Sumner WT, Monroe DM, Hoffman M. Variability in platelet procoagulant activity in healthy volunteers. *Thrombosis research*. 1996; **81**: 533-43.

270 Cambien B, Wagner DD. A new role in hemostasis for the adhesion receptor P-selectin. *Trends Mol Med*. 2004; **10**: 179-86.

271 Subramaniam M, Frenette PS, Saffaripour S, Johnson RC, Hynes RO, Wagner DD. Defects in hemostasis in P-selectin-deficient mice. *Blood*. 1996; **87**: 1238-42.

272 Konstantinides S, Ware J, Marchese P, mus-Jacobs F, Loskutoff DJ, Ruggeri ZM. Distinct antithrombotic consequences of platelet glycoprotein Ibalpha and VI deficiency in a mouse model of arterial thrombosis. *Journal of thrombosis and haemostasis*. 2006; **4**: 2014-21.

273 Joutsi-Korhonen L, Javela K, Hormila P, Kekomaki R. Glycoprotein V-specific platelet-associated antibodies in thrombocytopenic patients. *Clinical and laboratory haematology*. 2001; **23**: 307-12.

274 Garner SF, Campbell K, Metcalfe P, Keidan J, Huiskes E, Dong JF, Lopez JA, Ouwehand WH. Glycoprotein V: the predominant target antigen in gold-induced autoimmune thrombocytopenia. *Blood*. 2002; **100**: 344-6.

275 Weimer T, Wormsbächer W, Kronthaler U, Lang W, Liebing U, Schulte S. Prolonged in-vivo half-life of factor VIIa by fusion to albumin. *Thrombosis and Haemostasis*. 2008; **99**: 659-67.

276 Sterling K. The turnover rate of serum albumin in man as measured by I(131)-tagged albumin. *Journal of Clinical Investigation*. 1951; **30**: 1228-37.

277 Schulte S. Use of albumin fusion technology to prolong the half-life of recombinant factor VIIa. *Thrombosis research*. 2008; **122**: S14-S9.

278 Schulte S, Weimer T, Wormsbaecher W, Kronthaler U, Groener A, Lang W, Liebing U. Prolonged In-Vivo Half-Life of FVIIa by Fusion to Albumin. *Blood*. 2007; **110**: 3142-.

279 Sheffield WP, Smith IJ, Syed S, Bhakta V. Prolonged in vivo anticoagulant activity of a hirudin-albumin fusion protein secreted from Pichia pastoris. *Blood coagulation & fibrinolysis : an international journal in haemostasis and thrombosis*. 2001; **12**: 433-43.

280 Verhenne S, Denorme F, Libbrecht S, Vandenbulcke A, Pareyn I, Deckmyn H, Lambrecht A, Nieswandt B, Kleinschnitz C, Vanhoorelbeke K, De Meyer SF. Platelet-derived VWF is not essential for normal thrombosis and hemostasis but fosters ischemic stroke injury in mice. *Blood*. 2015; **126**: 1715-22.

281 Ni H, Denis CV, Subbarao S, Degen JL, Sato TN, Hynes RO, Wagner DD. Persistence of platelet thrombus formation in arterioles of mice lacking both von Willebrand factor and fibrinogen. *The Journal of Clinical Investigation*. 2000; **106**: 385-92.

282 Ni H. Unveiling the new face of fibronectin in thrombosis and hemostasis. *Journal of thrombosis and haemostasis*. 2006; **4**: 940-2.

283 Wang Y, Reheman A, Spring CM, Kalantari J, Marshall AH, Wolberg AS, Gross PL, Weitz JI, Rand ML, Mosher DF, Freedman J, Ni H. Plasma fibronectin supports hemostasis and regulates thrombosis. *The Journal of clinical investigation*. 2014; **124**: 4281-93.

284 Maurer E, Schaff M, Receveur N, Bourdon C, Mercier L, Nieswandt B, Dubois C, Jandrot-Perrus M, Goetz JG, Lanza F, Gachet C, Mangin PH. Fibrillar cellular fibronectin supports efficient platelet aggregation and procoagulant activity. *Thromb Haemost*. 2015; **114**: 1175-88.

285 Wang Y, Ni H. Fibronectin maintains the balance between hemostasis and thrombosis. *Cellular and molecular life sciences : CMLS*. 2016; **73**: 3265-77.

286 Jurk K, Clemetson KJ, de Groot PG, Brodde MF, Steiner M, Savion N, Varon D, Sixma JJ, Van Aken H, Kehrel BE. Thrombospondin-1 mediates platelet adhesion at high shear via glycoprotein Ib (GPIb): an alternative/backup mechanism to von Willebrand factor. *FASEB journal : official publication of the Federation of American Societies for Experimental Biology*. 2003; **17**: 1490-2.

287 Bonnefoy A, Moura R, Hoylaerts MF. Thrombospondins: from structure to therapeutics. *Cellular and Molecular Life Sciences*. 2008; **65**: 713.

288 Kuijpers MJ, de Witt S, Nergiz-Unal R, van Kruchten R, Korporaal SJ, Verhamme P, Febbraio M, Tjwa M, Voshol PJ, Hoylaerts MF, Cosemans JM, Heemskerk JW. Supporting roles of platelet thrombospondin-1 and CD36 in thrombus formation on collagen. *Arteriosclerosis, thrombosis, and vascular biology*. 2014; **34**: 1187-92.

289 Prakash P, Kulkarni PP, Chauhan AK. Thrombospondin 1 requires von Willebrand factor to modulate arterial thrombosis in mice. *Blood*. 2015; **125**: 399-406.

290 Schaff M, Tang C, Maurer E, Bourdon C, Receveur N, Eckly A, Hechler B, Arnold C, de Arcangelis A, Nieswandt B, Denis CV, Lefebvre O, Georges-Labouesse E, Gachet C, Lanza F, Mangin PH. Integrin α₆β₁ Is the Main Receptor for Vascular Laminins and Plays a Role in Platelet Adhesion, Activation, and Arterial Thrombosis. *Circulation*. 2013; **128**: 541-52.

291 Qureshi AI, Mendelow AD, Hanley DF. Intracerebral haemorrhage. *Lancet*. 2009; **373**: 1632-44.

292 Liu J, Gao BB, Clermont AC, Blair P, Chilcote TJ, Sinha S, Flaumenhaft R, Feener EP. Hyperglycemia-induced cerebral hematoma expansion is mediated by plasma kallikrein. *Nat Med*. 2011; **17**: 206-10.

293 Dütting S, Heidenreich J, Cherpokova D, Amin E, Zhang SC, Ahmadian MR, Brakebusch C, Nieswandt B. Critical off-target effects of the widely used Rac1 inhibitors NSC23766 and EHT1864 in mouse platelets. *Journal of Thrombosis and Haemostasis*. 2015; **13**: 827-38.

294 Tisdale EJ, Azizi F, Artalejo CR. Rab2 Utilizes Glyceraldehyde-3-phosphate Dehydrogenase and Protein Kinase Cı to Associate with Microtubules and to Recruit Dynein. *Journal of Biological Chemistry*. 2009; **284**: 5876-84.

295 Mansfield AS, Fields AP, Jatoi A, Qi Y, Adjei AA, Erlichman C, Molina JR. Phase I dose escalation study of the PKCı inhibitor aurothiomalate for advanced non-small cell lung cancer, ovarian cancer and pancreatic cancer. *Anti-cancer drugs*. 2013; **24**: 1079-83.

296 Erdogan E, Lamark T, Stallings-Mann M, Jamieson L, Pellechia M, Thompson EA, Johansen T, Fields AP. Aurothiomalate Inhibits Transformed Growth by Targeting the PB1 Domain of Protein Kinase Cı. *Journal of Biological Chemistry*. 2006; **281**: 28450-9.

297 Mayanglambam A, Bhavanasi D, Vijayan KV, Kunapuli SP. Differential dephosphorylation of the Protein Kinase C-zeta (PKCζ) in an integrin αIIbβ3-dependent manner in platelets. *Biochemical pharmacology*. 2011; **82**: 505-13.

298 Burkhart JM, Vaudel M, Gambaryan S, Radau S, Walter U, Martens L, Geiger J, Sickmann A, Zahedi RP. The first comprehensive and quantitative analysis of human platelet protein composition allows the comparative analysis of structural and functional pathways. *Blood*. 2012; **120**: e73.

299 Zeiler M, Moser M, Mann M. Copy Number Analysis of the Murine Platelet Proteome Spanning the Complete Abundance Range. *Molecular & Cellular Proteomics*. 2014; **13**: 3435-45.

300 Burkhart JM, Vaudel M, Gambaryan S, Radau S, Walter U, Martens L, Geiger J, Sickmann A, Zahedi RP. The first comprehensive and quantitative analysis of human platelet protein composition allows the comparative analysis of structural and functional pathways. *Blood*. 2012; **120**: e73-e82.

301 Solari FA, Mattheij NJ, Burkhart JM, Swieringa F, Collins PW, Cosemans JM, Sickmann A, Heemskerk JW, Zahedi RP. Combined Quantification of the Global Proteome, Phosphoproteome, and Proteolytic Cleavage to Characterize Altered Platelet Functions in the Human Scott Syndrome. *Mol Cell Proteomics*. 2016; **15**: 3154-69.

302 Mellor H, Parker PJ. The extended protein kinase C superfamily. *Biochemical Journal*. 1998; **332**: 281-92.

6 Appendix

6.1 Abbreviations

AA	Amino acid
AC	Adenylyl cyclase
ADAM	A disintegrin and metalloproteinase
ADP	Adenosine diphosphate
ATP	Adenosine triphosphate
BM	Bone marrow
BSA	Bovine serum albumin
BSS	Bernard-Soulier syndrome
Ca^{2+}	Calcium
CD	Cluster of differentiation
CLEC-2	C-type lectin receptor 2
CRP	Collagen-related peptide
CVD	Cardiovascular disease
d	Day
DAG	Diacylglycerol
DIC	Differential interference contrast
DKO	Double knockout
DMEM	Dulbecco’s modified Eagle's medium
DMSO	Dimethyl sulfoxide
DTS	Dense tubular system
ECL	Enhanced chemiluminescence
ECM	Extracellular matrix
EDTA	Ethylenediaminetetraacetate
EGTA	Ethyleneglycoltetraacetate
ELISA	Enzyme-linked immunosorbent assay

ER	Endoplasmic reticulum
F	Coagulation factor
FACS	Fluorescence-activated cell sorting
FcR	Fc receptor
FCS	Fetal calf serum
FITC	Fluorescein isothiocyanate
FN	Fibronectin
FSC	Forward scatter
g	Gravity
GEF	Guanine nucleotide exchange factor
GP	Glycoprotein
GPCR	G protein-coupled receptors
GTP	Guanosine-5-triphosphate
GTPase	Guanosine-5-triphosphatase
h	Hour
HEPES	4-(2-hydroxyethyl)-1-piperazineethanesulfonic acid
HMWK	High-molecular weight kininogen
HRP	Horseradish peroxidase
i.p.	Intraperitoneal(ly)
i.v.	Intravenous(ly)
Ig	Immunoglobulin
IP	Immunoprecipitation
IP_3	Inositol-1,4,5-trisphosphate
IP_3R	IP_3 receptor
ITAM	Immunoreceptor tyrosine-based activating motif
ITP	Immune thrombocytopenia
kDa	Kilodalton
KO	Knockout

LAT	Linker of activated T cells
LRR	Leucine-rich repeat
MFI	Mean fluorescence intensity
MI	Myocardial infarction
min	Minute
MK	Megakaryocyte
MOPS	3-(N-morpholino) propanesulfonic
n.s.	Not significant
OCS	Open canalicular system
o/n	Over night
PAGE	Polyacrylamide gel electrophoresis
PAR	Protease-activated receptor
PBS	Phosphate-buffered saline
PCR	Polymerase chain reaction
PDGF	Platelet derived growth factor
PE	Phycoerythrin
PF4	Platelet factor 4
PGI_2	Prostacyclin
PI3K	Phosphoinositide-3-kinase
PIP_2	Phosphatidylinositol-4,5-bisphosphate
PIP_3	Phosphatidylinositol-3,4,5-triphosphate
PKC	Protein kinase C
PL	Phospholipase
polyP	Polyphosphates
PRP	Platelet-rich plasma
PS	Phosphatidylserine
PVDF	Polyvinylidene difluoride
RBC	Red blood cells

Rho	Ras homolog gene family
Rpm	Rounds per minute
RT	Room temperature; in case of RT-PCR, RT indicates reverse transcription
Rt-PA	Recombinant tissue plasminogen activator
SDS	Sodium dodecyl sulfate
SFK	Src family kinases
SH2	Src homology domain 2
shGPV	Soluble human GPV
SLP-76	SH2 domain containing leukocyte protein of 76 kDa
smGPV	Soluble murine GPV
SOCE	Store-operated calcium entry
SSC	Sideward scatter
STIM	Stromal interaction molecule
Syk	Spleen tyrosine kinase
TBS	TRIS-buffered saline
TF	Tissue factor
TFPI	Tissue factor pathway inhibitor
TMB	3,3,5,5-tetramethylbenzidine
tMCAO	Transient middle cerebral artery occlusion
TP	Thromboxane A_2 receptor
TPO	Thrombopoietin
TRIS	Tris(hydroxymethyl)aminomethane
TTC	2,3,5-triphenyltetrazolium chloride
TxA_2	Thromboxane A_2
vWF	Von Willebrand factor
WT	Wildtype

6.2 Acknowledgments

The work presented here was accomplished at the Institute of Experimental Biomedicine I, University Hospital and Rudolf Virchow Center for Experimental Biomedicine, University of Würzburg, Germany, in the group of Prof. Bernhard Nieswandt between October 2013 and April 2018. The results on PKCι/λ summarized in this thesis have been published.

Many persons supported me throughout my PhD studies, whom I would like to thank for their help:

- Prof. Bernhard Nieswandt for giving me the opportunity to perform my PhD thesis in his laboratory, for his enthusiasm, constant support, encouragement, critical and valuable scientific input and basing my scientific network and career.
- The members of my thesis committee: Prof. Guido Stoll and Prof. Johan W. M. Heemskerk for critical discussion, helpful suggestions and reviewing this thesis.
- Dr. David Stegner for his critical and valuable scientific input, for his commitment to our joint projects, for inspiration, constant support and friendship.
- Dr. Julia Preu for fruitful collaboration.
- Prof. Harald Schulze, Dr. Sebastian Dütting, Dr. Elmina Mammadova-Bach, Dr. Georgi Manukjan and Dr. Irina Pleines for valuable discussions and critical input.
- Dr. Peter Kraft and Dr. Michael Schuhmann for their support with tMCAO analyses.
- The technicians, especially Juliana Goldmann and Stefanie Hartmann, for excellent technical support.
- The Bio-Imaging Center for good collaboration and providing technical infrastructure.
- Dr. Dr. Katharina Remer and all animal caretakers, especially Azer Achmedov, Marie Blum, Mario Müller, Wolfgang Radel and Valentina Zemskova in the animal facilities at the RVZ and ZEMM, for their excellent work.
- The secretaries, Elke Hauck and Kerstin Siegmann, for their organizational support.
- All external collaboration partners not mentioned by name for the fruitful collaboration and for giving me insights into new research fields.
- All current members of the Nieswandt lab for sharing their knowledge, their support, the excellent working atmosphere, many fun moments besides work and especially Inga, Isi, Julia, Julia and Vanessa for carefully proofreading this thesis.
- My former colleagues and especially Viola, Deya, Judith, Simon, Michael and Carsten for their great scientific and social encouragement and great memories.
- My parents and my sister, who always supported and encouraged me.
- Finally, I would like to thank my husband Hanno for his support, patience and love.

6.3 Publications

6.3.1 Articles

Stritt S, **Beck S**, Becker IC, Vögtle T, Hakala M, Heinze KG, Du X, Bender M, Braun A, Lappalainen P, Nieswandt B. Twinfilin2a is a regulator of platelet reactivity and turnover in mice. Blood. 2017 Jul. pii: blood-2017-02-770768.

Haining EJ, Cherpokova D, Wolf K, Becker IC, **Beck S**, Eble JA, Stegner D, Watson SP, Nieswandt B. CLEC2 contributes to hemostasis independently of classical hemITAM signaling in mice. Blood. 2017 Aug. pii: blood-2017-03-771907.

Beck S, Leitges M, Stegner D. Protein kinase Cι/λ is dispensable for platelet function in thrombosis and hemostasis in mice. Cell Signal. 2017 Oct;38:223-229.

Deppermann C, Kraft P, Volz J, Schuhmann MK, **Beck S**, Wolf K, Stegner D, Stoll G, Nieswandt B. Platelet secretion is crucial to prevent bleeding in the ischemic brain but not in the inflamed skin or lung in mice. Blood. 2017 Mar;129(12):1702-1706.

Baig AA, Haining EJ, Geuss E, **Beck S**, Swieringa F, Wanitchakool P, Schuhmann MK, Stegner D, Kunzelmann K, Kleinschnitz C, Heemskerk JW, Braun A, Nieswandt B. TMEM16F-mediated platelet membrane phospholipid scrambling is criticl for hemostasis and thrombosis but not thromboinflammation in mice. Brief Report. ATVB. 2016 Nov;36(11):2152-2157.

Van Eeuwijk JMM, Stegner D, Lamb DJ, Kraft P, **Beck S**, Thielmann I, Kiefer F, Walzog B, Stoll G, Nieswandt B. The novel oral Syk inhibitor, Bl1002494, protects mice from arterial thrombosis and thromboinflammatory brain infarction. ATVB. 2016 Jun;36(6):1247-53.

Dütting S, Vögtle T, Morowski M, **Schiessl S**, Schäfer CM, Watson SK, Hughes CE, Ackermann JA, Radtke D, Hermanns HM, Watson SP, Nitschke L, Nieswandt B. Growth factor receptor-bound protein 2 contributes to (hem)immunoreceptor tyrosine-based activation motif-mediated signaling in platelets. Circ Res. 2014 Jan;114(3):444-453.

6.3.2 Oral Presentations

GPV is a central regulator of hemostasis, thrombosis and thrombo-inflammatory brain infarction in mice. XXVth Congress of the International Society on Thrombosis and Hemostasis, June 2015, Toronto (Canada) (ISTH 2015 Young Investigator Award).

GPV is a central regulator of hemostasis, thrombosis and thrombo-inflammatory brain infarction in mice. 1st European Congress on Thrombosis and Haemostasis, September 2016, The Hague (The Netherlands).

GPV is a central regulator of hemostasis, thrombosis and thrombo-inflammatory brain infarction in mice. Eureka! XIth International Symposium organized by the Students of the Graduate School of Life Sciences, October 2016, Würzburg (Germany)

Profilin 1 is a central regulator of integrin turnover and function in mouse platelets. XXVIth Congress of the International Society on Thrombosis and Hemostasis, July 2017, Berlin (Germany) (ISTH 2017 Young Investigator Award).

6.3.3 Poster Presentations

Soluble GPV dampens hemostasis. 9th International Symposium of the Graduate School of Life Science: EUREKA!, 2014, Würzburg, Germany

GPV is a central regulator of hemostasis, thrombosis and thrombo-inflammatory brain infarction in mice. 10th International Symposium of the Graduate School of Life Science: EUREKA!, 2015, Würzburg, Germany

Analysis of cellular regulation of platelet adhesion receptors in thrombosis and hemostasis. Joint Symposium of SFB688 and DZHI, 2017, Würzburg, Germany

6.3.4 Patents

Glycoprotein V inhibitors for use as coagulants (WO 2017/109180 A1, #EP3184544A1, published 29.06.2017)

Soluble GPV for treating thrombotic diseases (WO 2017/109212 A1, #EP3184149A1, published 29.06.2017)

6.4 Curriculum Vitae

6.5 Affidavit

I hereby confirm that my thesis entitled “The role of platelet glycoprotein V in thrombosis and hemostasis: *in vitro* and *in vivo* studies in mice” is the result of my own work. I did not receive any help or support from commercial consultants. All sources and/or materials applied are listed and specified in the thesis.

Furthermore, I confirm that this thesis has not yet been submitted as part of another examination process neither in identical nor in similar form.

Würzburg, April 2018 _____

Sarah Beck

6.6 Eidesstattliche Erklärung

Hiermit erkläre ich an Eides statt, die Dissertation „Die Rolle des Thrombozytenrezeptors Glykoprotein V in Thrombose und Hämostase: *in vitro* und *in vivo* Studien in Mäusen“ eigenständig, d.h. insbesondere selbstständig und ohne Hilfe eines kommerziellen Promotionsberaters, angefertigt und keine anderen als die von mir angegebenen Quellen und Hilfsmittel verwendet zu haben.

Ich erkläre außerdem, dass die Dissertation weder in gleicher noch in ähnlicher Form bereits in einem anderen Prüfungsverfahren vorgelegen hat.

Würzburg, April 2018 _____

Sarah Beck